



Norwegian University of
Science and Technology

Design of a Portable Reverse Osmosis System

Thea Karlsen Løken

Master of Energy and Environmental Engineering

Submission date: June 2016

Supervisor: Ole Gunnar Dahlhaug, EPT

Co-supervisor: Torbjørn K. Nielsen, EPT
Pål-Tore Storli, EPT

Norwegian University of Science and Technology
Department of Energy and Process Engineering

EPT-M-2016-83

MASTEROPPGAVEfor
Thea Karlsen Løken
Våren 2016**Produksjon av rent vann vha reversert osmose**
*Production of clean water with a reversed osmosis system***Bakgrunn og målsetting**

Rent vann er en knapp ressurs i mange deler av verden. Det gjør at produksjon av rent vann ved hjelp av teknologi er nødvendig. En av de ledende teknologiene for produksjon av rent vann er reversert osmose. I et reversert osmose system føres vann med høyt innhold av uønskede partikler gjennom en membran som holder igjen de uønskede partiklene, og lar rent vann passere. Vannet føres inn på membranen med høyt trykk, rent vann med lavt trykk passerer, og restvann med høyt trykk og høy konsentrasjon av partikler føres ut. Energien som kreves til denne prosessen utgjør en stor del av kostnaden på det ferdige vannet. Ved å utnytte trykenergien i restvannet kan energiforbruket reduseres betraktelig.

Mål

Design av et reversert osmose system som er lett å transportere til katastrofeområder.

Oppgaven bearbeides ut fra følgende punkter

1. Gjennomføre litteraturstudie på følgende:
 - a. Design av Turgo turbiner
 - b. Design av stempelpumper
2. Lære å benytte softwaren Ansys for CFD-analyser
3. Designe fire systemer som gir nødvendig trykk og energi gjenvinning vha:
 - a. Sentrifugalpumpe og Turgo turbin
 - b. Stempelpumpe og Turgo turbin
 - c. Stempelpumper
 - d. Stempelpumpe uten bruk av energi gjenvinning
4. Evaluer hvilket system som vil være det mest praktiske for formålet
5. Utarbeid tegninger for hele systemet
6. Dersom det blir tid skal studenten gjennomføre numeriske analyser av:
 - a. CFD-analyse av strømmingen i Turgo turbinen
 - b. CFD-analyse av strømmingen i stempelpumpen

Senest 14 dager etter utlevering av oppgaven skal kandidaten levere/sende instituttet en detaljert fremdrift- og eventuelt forsøksplan for oppgaven til evaluering og eventuelt diskusjon med faglig ansvarlig/veiledere. Detaljer ved eventuell utførelse av dataprogrammer skal avtales nærmere i samråd med faglig ansvarlig.

Besvarelsen redigeres mest mulig som en forskningsrapport med et sammendrag både på norsk og engelsk, konklusjon, litteraturliste, innholdsfortegnelse etc. Ved utarbeidelsen av teksten skal kandidaten legge vekt på å gjøre teksten oversiktlig og velskrevet. Med henblikk på lesning av besvarelsen er det viktig at de nødvendige henvisninger for korresponderende steder i tekst, tabeller og figurer anføres på begge steder. Ved bedømmelsen legges det stor vekt på at resultatene er grundig bearbeidet, at de oppstilles tabellarisk og/eller grafisk på en oversiktlig måte, og at de er diskutert utførlig.

Alle benyttede kilder, også muntlige opplysninger, skal oppgis på fullstendig måte. For tidsskrifter og bøker oppgis forfatter, tittel, årgang, sidetall og eventuelt figurnummer.

Det forutsettes at kandidaten tar initiativ til og holder nødvendig kontakt med faglærer og veileder(e). Kandidaten skal rette seg etter de reglementer og retningslinjer som gjelder ved alle (andre) fagmiljøer som kandidaten har kontakt med gjennom sin utførelse av oppgaven, samt etter eventuelle pålegg fra Institutt for energi- og prosesssteknikk.

Risikovurdering av kandidatens arbeid skal gjennomføres i henhold til instituttets prosedyrer. Risikovurderingen skal dokumenteres og inngå som del av besvarelsen. Hendelser relatert til kandidatens arbeid med uheldig innvirkning på helse, miljø eller sikkerhet, skal dokumenteres og inngå som en del av besvarelsen. Hvis dokumentasjonen på risikovurderingen utgjør veldig mange sider, leveres den fulle versjonen elektronisk til veileder og et utdrag inkluderes i besvarelsen.

I henhold til "Utfyllende regler til studieforskriften for teknologistudiet/sivilingeniørstudiet" ved NTNU § 20, forbeholder instituttet seg retten til å benytte alle resultater og data til undervisnings- og forskningsformål, samt til fremtidige publikasjoner.

Besvarelsen leveres digitalt i DAIM. Et faglig sammendrag med oppgavens tittel, kandidatens navn, veileders navn, årstall, instituttnavn, og NTNUs logo og navn, leveres til instituttet som en separat pdf-fil. Etter avtale leveres besvarelse og evt. annet materiale til veileder i digitalt format.

- Arbeid i laboratorium (vannkraftlaboratoriet, strømningsteknisk, varmeteknisk)
 Feltarbeid

NTNU, Institutt for energi- og prosesssteknikk, 11. januar 2016



Olav Bolland
Instituttleder



Ole Gunnar Dahlhaug
Faglig ansvarlig/veileder

Medveiledere:

- Torbjørn K. Nielsen torbjorn.nielsen@ntnu.no
- Pål-Tore Storli pal-tore.storli@ntnu.no

Preface

This work is a master's thesis written at Department of Energy and Process Engineering at the Norwegian University of Science and Technology. The work of the thesis was carried out during the spring semester of 2016. The theme of the thesis is the design of a portable and lightweight reverse osmosis system for production of drinking water.

I would like to thank Professor Ole Gunnar Dahlhaug for guidance, and the students and PhD Candidates at the Waterpower Laboratory for inspiration and support. I would especially like to thank Stian Solvik, who always has a good idea when needed. I would also like to thank Julia Navarsete at Waterbox4Life Norway AS, for the idea behind this master's thesis and her enthusiasm and help. The last person I would like to thank is Jostein Sandvik, for taking the time to teach me all about the possibilities of energy recovery.

Thea Karlsen Løken

Trondheim, June 10th, 2016

Abstract

The motivation for this thesis was to design a reverse osmosis system that is small, lightweight, durable and easy to transport. The intended application area of the system is to secure the supply of clean drinking water in remote parts of the world where infrastructure is lacking, or in areas struck by natural disasters. Reverse osmosis is a leading water treatment technology. In a reverse osmosis system, pressurized feedwater is forced through a membrane, and low pressure permeate and high pressure concentrate exits. The energy consumption of the process is a key factor that influences the production cost of the water. By utilizing the energy of the exiting high pressure concentrate, the energy consumption of the process can be significantly reduced.

The primary focus of this thesis was the high pressure pump supplying the feedwater to the system and the energy recovery device utilizing the pressure energy of the exiting concentrate. These components and their influence on the performance of the entire system was to be evaluated by looking at four different solutions. The first solution comprises a high pressure centrifugal pump and a Turgo turbine energy recovery device coupled together on the same shaft. The second solution comprises a high pressure reciprocating pump and a Turgo turbine energy recovery device coupled together on the same shaft. The third solution comprises a high pressure reciprocating pump without any energy recovery device. The fourth and final solution comprises a reciprocating pump with integrated energy recovery. After investigating all four solutions the most practical solution for the given application area was decided, and a prototype of the entire system was constructed using the computer-aided design software Autodesk Inventor.

The most practical solution for the system is believed to be the reciprocating pump with integrated energy recovery. It is believed that the energy savings can be as high as 43 percent when using this solution. The reason for choosing the reciprocating pump over the centrifugal pump is that a reciprocating pump is much better suited for applications of high pressure

and low flow rate. The centrifugal pump could not be designed without considerable hydraulic losses. The design of the Turgo turbine was however successful, and it was found that the energy savings by implementing the Turgo turbine as an energy recovery device could be as high as 41 percent. The drawback of the Turgo turbine is that it will increase the size of the system compared to a reciprocating pump with integrated energy recovery. The efficiency of the Turgo turbine will also depend more closely on available head. The reciprocating pump without energy recovery will only reduce the size and complexity of the system slightly, and the recommended solution for the system is therefore the reciprocating pump with integrated energy recovery.

To further validate the assumptions made on the efficiency of the reciprocating pump with integrated energy recovery, a Computational Fluid Dynamics analysis should be performed. Due to time limitations this was however not performed in this master's thesis, and is therefore suggested as further work.

Sammendrag

Motivasjonen for denne masteroppgaven var å designe et system som benytter teknologien reversert osmose til å produsere drikkevann. Målet var å designe et lett, lite og robust system som enkelt kan transporteres. Systemet skal kunne benyttes i katastrofeområder og i andre deler av verden hvor infrastruktur er manglende eller fraværende. Reversert osmose er en av de ledende teknologiene på verdensbasis for produksjon av drikkevann. I et reversert osmosesystem føres vann med høyt innhold av uønskede partikler gjennom en membran som holder igjen de uønskede partiklene, og lar rent vann passere. Det urene vannet føres inn på membranen med høyt trykk, rent vann med lavt trykk passerer, og restvann med høyt trykk og høy konsentrasjon av partikler føres ut av systemet. Energien som kreves under denne prosessen utgjør en stor del av kostnaden på det ferdige vannet. Ved å utnytte trykkenergien til restvannet kan energiforbruket reduseres betraktelig.

Hovedfokuset i denne masteroppgaven har vært pumpa som trykksetter tilførselsvannet og enheten som gjenvinner trykkenergien i restvannet. Disse komponentene og deres innvirkning på ytelsen til hele systemet skulle evalueres ved å vurdere fire forskjellige løsninger. Den første løsningen består av en sentrifugalpumpe og en Turgoturbin. Den andre løsningen består av en stempelpumpe og en Turgoturbin. I både første og andre løsning er pumpa og turbinen koblet på samme aksling, slik at energien gjenvunnet i turbinen direkte bidrar til å redusere energien som kreves for å drive pumpa. Den tredje løsningen består av en stempelpumpe uten noen form for energigjenvinning. Den fjerde og siste løsningen består av en stempelpumpe med integrert energigjenvinning. Etter å ha undersøkt alle fire løsninger, skulle den mest praktiske løsningen for systemet bestemmes. En modell av hele systemet ble konstruert med designprogramvaren Autodesk Inventor.

Den mest praktiske løsningen for systemet antas å være en stempelpumpe med integrert energigjenvinning. Ved å benytte en slik løsning er det grunn til å tro at energibesparelsen kan bli så mye som 43 prosent. Grunnen til

å velge en stempelpumpe over en sentrifugalpumpe er at stempelpumpa er mye bedre egnet for systemer som krever høyt trykk og lav volumstrøm. Det var ikke mulig å designe en sentrifugalpumpe uten store hydrauliske tap. Designet av Turgoturbinen anses som vellykket, og det antas at energibesparelsen ved å benytte denne til energigjenvinning kan bli opp mot 41 prosent. Bakdelen ved å benytte Turgoturbinen til energigjenvinning er at størrelsen på systemet vil øke i forhold til å benytte en stempelpumpe med integrert energigjenvinning. Virkningsgraden til Turgoturbinen er også mye nærere knyttet opp mot tilgjengelig trykk. Ved å benytte en stempelpumpe uten energigjenvinning vil størrelsen og kompleksiteten på systemet kun reduseres litt. Den anbefalte løsningen for systemet er derfor stempelpumpa med integrert energigjenvinning.

For å validere antakelsene gjort om virkningsgraden til stempelpumpa med integrert energigjenvinning, burde det vært gjort en CFD analyse. På grunn av tidsbegrensninger ble dette ikke gjort i arbeidet med denne masteroppgaven, og det er derfor foreslått som videre arbeid.

Contents

List of Figures

List of Tables

Nomenclature

1	Introduction	1
2	Background and History	3
3	Theory	5
3.1	Reverse Osmosis	5
3.1.1	Energy Recovery Devices	7
3.2	The Centrifugal and the Reciprocating Pump	12
3.2.1	Classification of Pumps	12
3.2.2	The Centrifugal Pump	13
3.2.3	The Reciprocating Pump	24
3.2.4	Comparison between the Reciprocating and the Centrifugal pump	44
3.3	The Turgo Turbine	45
3.3.1	Energy Conversion	48
3.3.2	Jet Inlet Angle	51
3.3.3	Shape of Buckets	51
3.3.4	Number of Buckets	52
3.3.5	Parameters Influencing the Efficiency	53
4	System Design	55
4.1	The Centrifugal Pump and the Turgo Turbine	57
4.1.1	Design of the Centrifugal Pump	57
4.1.2	Design of the Turgo Turbine	76
4.2	The Reciprocating Pump and the Turgo Turbine	86
4.2.1	About the System	86
4.2.2	About the Measurements	88

4.2.3	Measurement Results	89
4.2.4	Uncertainty Analysis	93
4.2.5	Discussion of the Results	95
4.2.6	Suggestions on Improvement	95
4.2.7	Concluding Remarks on the Measurements	96
4.3	The Reciprocating Pump without Energy Recovery	97
4.3.1	Design of the Reciprocating Pump	97
4.4	The Reciprocating Pump with Integrated Energy Recovery .	107
4.4.1	Size of Concentrate Pressure Chambers	109
4.4.2	Camshafts and Check Valves	109
4.4.3	Safety Relief Valve	110
4.5	Energy savings	112
4.6	System Drive Mechanism	113
4.7	Reverse Osmosis System	113
5	Discussion and Conclusion	117
6	Further Work	121
	Appendices	129
A	Turgo Drawing	131
B	Centrifugal Pump Drawings	135
C	Reciprocating Pump without Energy Recovery Drawings	153
D	Reciprocating Pump with Integrated Energy Recovery Drawings	161
E	Reverse Osmosis System	179
F	Reverse Osmosis System Components	185
G	Risk Assessment	196

List of Figures

3.1	Sketch showing the working principle of osmosis (left) and reverse osmosis (right) [11].	5
3.2	The main components of a reverse osmosis system. The feedwater is pressurized through a high pressure pump (HPP).	6
3.3	RO system configuration including a turbine. The feedwater is pressurized through a high pressure pump (HPP).	8
3.4	Turbocharger [17].	9
3.5	RO system configuration including positive displacement energy recovery device. Parts of the feedwater is pressurized through a high pressure pump (HPP), and the other part is pressurized in an energy recovery device and rejoins the rest of the feed stream through a booster pump (Booster).	10
3.6	Schematics of a pressure exchanger. Arrows indicate flow direction and pressure. Red color for concentrate, blue for feedwater, high pressure white arrow, low pressure transparent arrow. [1]	11
3.7	Schematics of a work exchanger [13].	12
3.8	Impeller geometry as a function of flow and head [6].	14
3.9	Simple sketch of a single stage centrifugal pump. Axial view to the left, and radial view to the right [5].	15
3.10	Velocity diagrams at inlet and outlet of a radial centrifugal impeller. An axial view of the impeller is given in the upper left corner and radial view of the impeller is given in the lower left corner [6].	16
3.11	A cutaway of a multistage pump with 5 stages connected in series [14].	19
3.12	Principal sketch of a centrifugal pumping system with lower and upper reservoir [25].	23
3.13	Sketch showing the basic geometry of a single-acting reciprocating piston pump.	24
3.14	Sketch showing the basic geometry of a double-acting reciprocating pump [7].	26

3.15	Model drawing of a triplex single-acting piston pump [35].	28
3.16	Wing valve assembly. [29]	29
3.17	A sketch showing the geometry of one single-acting cylinder in a reciprocating pump [29].	31
3.18	The piston velocity pattern during one full revolution of the crankshaft.	32
3.19	The flow rate in one cylinder of a reciprocating pump during one full revolution of the crankshaft.	33
3.20	The piston velocity generates varying flow rate and thus varying frictional pressure loss or frictional pressure pulsations. Valid for a single-cylinder reciprocating pump.	34
3.21	The shape of the discharge flow pattern in a triplex single-acting pump during one full revolution of the crankshaft.	36
3.22	The velocity and acceleration of the piston during one stroke.	37
3.23	The friction and acceleration pressure in the suction and discharge pipe.	38
3.24	Pump inlet pressure trace. Pulsations due to acceleration are denoted SA, pulsations due to frictional pressure drop are denoted SV, and waterhammer due to the opening of the valve are denoted SO. Note how acceleration pressure overwhelms the friction pressure [29].	40
3.25	Typical suction system with suction lift, z	41
3.26	Suction pressure trace for the same pump without (upper) and with (lower) suction stabilizer. The upper pressure trace shows a typical cavitation waveform, where the downward pressure spikes have rounded bottoms. The lower pressure trace with suction stabilizer shows that the pressure spikes have lower amplitude and no rounded bottoms. The low-frequency cycles over which the high frequency is imposed, are the remnant of pump rotation-generated cycles [29].	43
3.27	Photos of a Turgo turbine (a) and a Pelton turbine (b) [10].	47
3.28	Difference in direction of water flow between the Pelton (left) and Turgo (right) turbines [19].	48
3.29	Velocity diagrams at inlet and outlet of Turgo bucket [27].	49
4.1	Radial view of an impeller blade of single curvature, slightly extended forward [25].	59
4.2	Radial view of an impeller blade of single curvature, slightly extended forward [25].	65
4.3	Pump characteristic for the standard design.	67
4.4	Shape of the standard impeller, model constructed in Autodesk Inventor.	73

4.5	Shape of the adjusted impeller, model constructed in Autodesk Inventor.	74
4.6	Cutaway of the casing containing the seven pump stages of the standard design, model constructed in Autodesk Inventor.	75
4.7	Cutaway of the casing containing the seven pump stages of the adjusted design, model constructed in Autodesk Inventor.	75
4.8	Radial view of the velocity diagrams at inlet and outlet of the Turgo bucket [2].	77
4.9	Axial view of the Turgo runner.	79
4.10	Radial view of the Turgo runner. Angles between the bucket positions from the axial view.	81
4.11	Dimensions of the Turgo bucket. Width B, length L and depth H is indicated.	82
4.12	Axial view of the Turgo runner. Relative velocity vector at point of bucket where jet is incident.	83
4.13	Model of the designed Turgo turbine.	85
4.14	Sketch showing the working principle of the Waterbox. An electric motor drives a high pressure pump (HHP) coupled to the same shaft as a Pelton turbine. The feedwater is forced through the membrane and the products are low pressure freshwater (permeate) and high pressure concentrate. The concentrate leaves the system directly or is directed through the Pelton turbine where the hydraulic energy is converted to mechanical energy.	87
4.15	Sketch showing the measurement setup for the reverse osmosis system Waterbox. The alternating current supply is denoted AC. The current supplied to the electric motor and the voltage over the motor was measured by a power analyzer. Pressure was measured at the locations denoted P1, P2 and P3, and the flow rate was measured at the location denoted Q.	88
4.16	The measurement setup for the <i>PM3000A Power Analyzer</i>	89
4.17	Measured power consumption with and without the turbine as part of the system. Each of the curves represent the mean value of three measurements done with continuous operation of the system.	90
4.18	Measured power savings when operating the turbine as part of the system. The curve is based on the mean values in figure 4.17.	91
4.19	Measured efficiency for the Pelton turbine. The curve is based on the difference in the mean power consumption with and without the turbine compared to the available hydraulic power.	92

4.20	Measured power consumption with and without the turbine as part of the system. Each of the curves represents the mean value of three measurements done with continuous operation of the system. The vertical lines represent the uncertainty of the efficiency measurements.	94
4.21	Sketch showing the connecting rod, crosshead and crankshaft forces. The force on the piston F_p is transferred to the connecting rod and crosshead. F_p is therefore the vector sum of F_{ch} and F_{cr}	100
4.22	Model of the designed reciprocating pump without energy recovery.	106
4.23	Model of the designed reciprocating pump with energy recovery.	111
4.24	Model of the designed reciprocating pump with energy recovery.	114

List of Tables

4.1	Flow and head specifications.	56
4.2	Assumed pump efficiencies	58
4.3	Checking for cavitation at impeller inlet	61
4.4	Specification basis and inlet and outlet values for impeller and return passage for both pump designs	69
4.5	Point by point method determining the blade shape for the standard design impeller [25].	71
4.6	Point by point method determining the blade shape for the standard design return vane [25].	71
4.7	Point by point method determining the blade shape for the adjusted design impeller [25].	72
4.8	Point by point method determining the blade shape for the adjusted design return vane [25].	72
4.9	Main dimensions and physical properties of the Turgo design.	84
4.10	Uncertainty analysis.	94
4.11	Maximum forces on crosshead and connecting rod.	100
4.12	Main dimensions and physical properties of the reciprocating pump design.	103
4.13	Estimated energy savings for systems with energy recovery. .	112

Nomenclature

List of Abbreviations

BEP Best Efficiency Point

CFD Computational Fluid Dynamics

ERD Energy Recovery Device

NPSH Net Positive Suction Head

NPSHA Net Positive Suction Head Available

NPSHR Net Positive Suction Head Required

RO Reverse Osmosis

TCP Total Cylinder Pressure

UCLA University of California, Los Angeles

WHO World Health Organization

Subscripts

m meridional component

u circumferential or peripheral component

Constants

g gravitational constant 9.81m/s^2

Greek Letters

α angle between absolute and peripheral velocity \circ

β	angle between relative and peripheral velocity	o
β	angle of inclination of blade	o
β''	constructional angle of blade	o
δ	angle of incidence	o
η_h	hydraulic efficiency	—
η_m	mechanical efficiency	—
η_p	total pump efficiency	—
η_v	volumetric efficiency	—
ω	angular velocity	rad s ⁻¹
ϕ	angle traveled by bucket when in contact with water	o
ϕ	constriction coefficient	—
ψ	angle traveled by bucket when water travels angle 2ϕ	o
ρ	density	kg m ⁻³
σ_f	fatigue limit	N m ⁻²
σ_y	yield limit	N m ⁻²
τ	torsional stress	N m ⁻²
θ	crank angle	o
θ	maximum distance between buckets	o
ζ	resistance coefficient	—

List of Symbols

ΔH	pressure rise in meter water column	m
Δh	pressure loss loss due to friction in meter water column	m
A	area	m ²
a	acceleration	m s ⁻²

a	speed of sound	m s^{-1}
a_d	discharge acceleration	m s^{-2}
A_p	area of piston	m^2
a_p	instantaneous piston acceleration	m s^{-2}
a_s	suction acceleration	m s^{-2}
A_{pr}	area of piston rod	m^2
b	width	m
c	absolute velocity	m s^{-1}
C_p	Pfleiderer correction factor for slip	—
D	diameter	m
D	displacement	m^3
d	diameter	m
d_d	diameter of discharge pipe	m
d_s	diameter of suction pipe	m
d_{pr}	diameter of piston rod	m
F	force	N
f	Darcy's coefficient of friction	—
f	frequency	Hz
F_p	force on piston	N
H	pressure head in meter water column	m
h	osmotic pressure	Pa
H_a	acceleration pressure in meter water column	m
H_f	pressure loss due to friction in meter water column	m
H_n	available pressure in meter water column	m

H_s	absolute static pressure at connection between suction pipe and cylinder in meter water column	m
H_{atm}	atmospheric pressure in meter water column	m
H_{va}	vapor pressure of fluid in meter water column	m
I_{RMS}	effective value of current	A
L	length	m
L_c	connecting rod length	m
m	mass	kg
n	rotational speed	rpm
n_q	specific speed	$m^{3/4}s^{-1/2}$ rpm
P	power	W
p	pressure	Pa
p_d	discharge pressure	Pa
p_{dp}	differential pressure acting on piston	Pa
P_{sh}	shaft input power	W
Q	volume flow rate	$m^3 s^{-1}$
Q'	volume flow rate including leakage losses	$m^3 s^{-1}$
r	radius	m
s	blade thickness	m
S_f	safety factor	—
s_u	blade thickness projected on the circumference	m
T	torque	Nm
t	circumferential pitch of blades	m
t	time	s

u	peripheral velocity	m s^{-1}
v	velocity	m s^{-1}
v_d	discharge velocity	m s^{-1}
v_p	instantaneous piston velocity	m s^{-1}
v_s	suction velocity	m s^{-1}
V_{RMS}	effective value of voltage	V
w	relative velocity	m s^{-1}
z	elevation between pump inlet and suction	m
Z_b	number of buckets	—
Z_i	number of impeller blades	—
Z_p	number of pole pairs per phase in electric motor	—
Z_r	number of blades in return passage	—

1 Introduction

”We’d empty half the hospital beds in the world if we just gave people clean water.” These are the words of a very inspirational man by the name of Dean Kamen [24]. His words are supported by the World Health Organization (WHO) who in 2014 confirmed that at least 1.9 billion people rely on unimproved or contaminated water [33]. WHO also states that access to safe drinking water is essential to health and a basic human right [32].

In areas where clean water is a scarce resource, water treatment technologies are essential. Kamen, well known as the man behind the Segway personal transportation device, has designed a small and portable water treatment system that goes by the name of the *Slingshot Water Purifier*. The system is the size of a dorm fridge. The technology behind the *Slingshot* is vapor compression distillation. Water is heated in a boiling chamber, the vapor is collected and compressed, and the superheated vapor is condensed in a heat exchanger between the incoming and outgoing water. The energy required to heat the incoming water is thus reduced at the same time as the superheated vapor is condensed.

Being able to produce an efficient water purification system is one thing. Distributing it to the parts of the world where it is needed is another. Kamen managed to distribute his *Slingshot* in a very clever manner. He approached the Coca-Cola Company which has one of the best developed distribution systems in the world. Together, Coca-Cola and Kamen announced that they would place up to 2000 units around Africa, Asia and Latin America within the end of 2015 [24].

The objective of this thesis is to design a small scale water treatment system. The intended application area of the system is to secure the supply of clean water in remote parts of the world where infrastructure is lacking, and in areas struck by natural disasters. For this reason, the system is designed to be lightweight, small, durable and easy to transport. The system is however based on a different technology than Kamens *Slingshot*, namely reverse osmosis. Reverse osmosis is a leading water treatment technology worldwide, both for small and large scale applications. Reverse osmosis,

although an energy intensive process, is known to be less energy intensive than vapor compression distillation. This is because the energy required to pressurize the water in a reverse osmosis system is less than the energy required to vaporize water [15].

In a reverse osmosis system, pressurized feedwater is forced through a membrane. The products of the process are low pressure freshwater called permeate and high pressure reject water called concentrate. The process is very energy intensive, and the energy cost could represent up to 50 percent of the final cost of the water product [34]. By utilizing the energy of the exiting high pressure concentrate, the energy consumption of the process can be significantly reduced.

The primary focus of this thesis is the high pressure pump supplying the feed water to the system and the energy recovery device utilizing the high pressure energy of the exiting concentrate. These components and their influence on the performance of the entire system is to be evaluated by looking at three different solutions. The first solution comprises a high pressure centrifugal pump and a Turgo turbine energy recovery device coupled together on the same shaft. The second solution comprises a high pressure reciprocating pump and a Turgo turbine energy recovery device coupled together on the same shaft. The third solution comprises a high pressure reciprocating pump without any energy recovery device. The fourth and final solution comprises a reciprocating pump with integrated energy recovery. After investigating all four solutions the most practical solution for the given application area is decided.

This report will have the following structure. First a short background and history on the reverse osmosis technology is given. Then the theory on reverse osmosis, the centrifugal pump, the reciprocating pump, and the Turgo turbine is covered, together with their respective working principles. With the theory in mind, the design procedure and results are covered in detail. Finally the optimal solution for the reverse osmosis system is discussed and presented, and further work is suggested.

2 Background and History

This section is taken from the project thesis written in the fall of 2015 by Løken [26].

Desalination is a water treatment technology applied to recover freshwater from sea and brackish waters with a high concentration of dissolved solids. In the early 1950s, the predominating technologies were based on thermal energy [21], like thermal flash evaporation. With thermal flash evaporation the feedwater is evaporated, the evaporated water is collected, and the remaining concentrate returned to the sea. The energy requirement for this process is independent of the salt content [39], but the process is extremely energy intensive.

A significant breakthrough in desalination technology was made in 1959, when researchers at the University of California (UCLA) demonstrated the process known as reverse osmosis (RO). Reverse osmosis is not a thermal process like thermal flash evaporation, but a membrane process. Samuel Yuster and two of his students at UCLA, Sidney Loeb and Srinivasa Sourirajan, were able to produce a synthetic RO membrane from cellulose acetate polymer. The membrane was capable of rejecting salty water and passing freshwater at acceptable pressures and flow rates.

The first commercial RO plant producing pure water began operation in 1965 in Coalinga, California. The Coalinga plant produced pure water from brackish water. Producing freshwater from seawater is a more challenging task, seeing as the salt content of seawater is roughly ten times that of brackish water. Nevertheless, research progressed rapidly, and today freshwater is produced from seawater at large scale through reverse osmosis [18]. The working principle of reverse osmosis is reviewed in more detail in section 3.1.

3 Theory

3.1 Reverse Osmosis

Parts of this section is taken from the project thesis *Desalination of Water by Reverse Osmosis* written in the fall of 2015 by Løken [26].

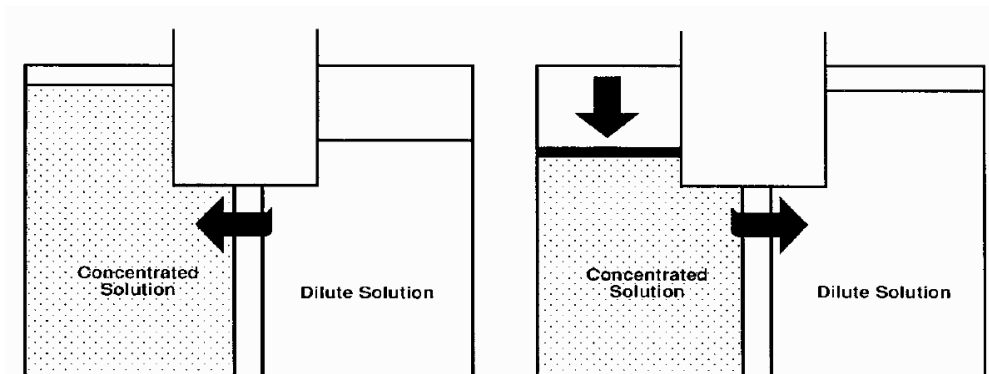


Figure 3.1: Sketch showing the working principle of osmosis (left) and reverse osmosis (right) [11].

Osmosis is a natural process that plays an important role in the metabolism of humans, plants and animals. Osmosis equalizes the difference in concentration of a solute between two solutions. If seawater and freshwater are separated by a semi-permeable membrane (meaning that only specific particles may travel through), the freshwater will travel through the membrane and tend to dilute the seawater, lowering the salt concentration on this side. This process will continue until the osmotic pressure is reached on the seawater side, and freshwater can no longer travel through the membrane.

Reverse osmosis is the opposite process of osmosis, i.e., the water is forced in the opposite direction by applying an external pressure greater than the osmotic pressure. This is the working principle when producing drinking

water from seawater or brackish water. By applying an external pressure greater than the osmotic pressure of the saline waters, freshwater can be forced through a membrane while the unwanted particles remain. The energy requirement, i.e., the external pressure required, depends on the salt content of the feedwater, in contrast to the energy requirement for thermal flash evaporation.

Due to remarkable improvements in membrane technology and energy consumption, reverse osmosis is today a leading desalination technology. It is used worldwide in both small and large scale applications [21].

A simple sketch showing the main components of a reverse osmosis system is given in figure 3.2.

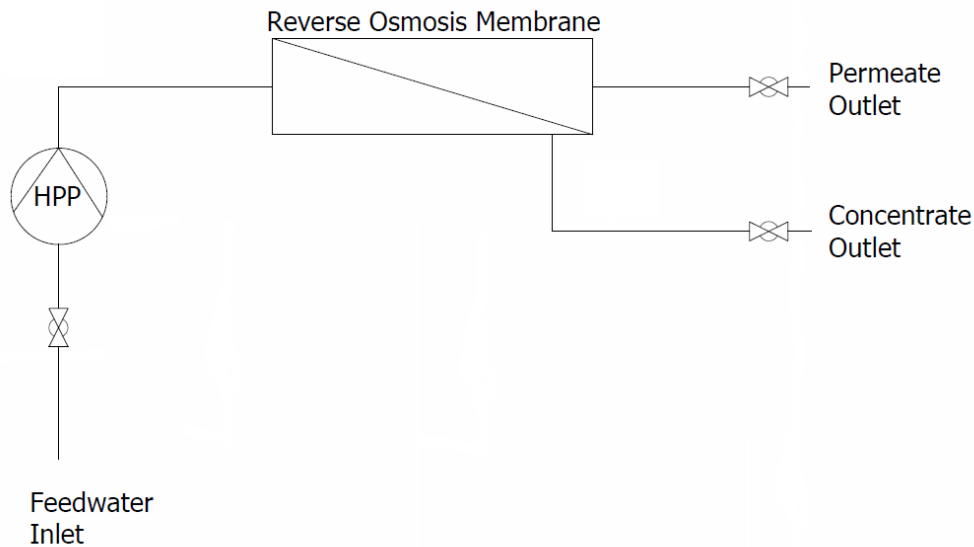


Figure 3.2: The main components of a reverse osmosis system. The feedwater is pressurized through a high pressure pump (HPP).

The feedwater enters the membrane at high pressure, and low pressure freshwater and high pressure concentrate exits. The amount of freshwater produced depends on the recovery ratio of the membrane, defined as the volume of freshwater produced per unit volume of feedwater. The recovery ratio for seawater is in the range of 40 - 70 percent [20]. The sea or brackish water, here on out referred to as the feedwater, must be applied a pressure exceeding that of the osmotic pressure to force freshwater through the membrane. For seawater this pressure is in the range of 65 to 75 bar [39], and for brackish water in the range of 15 to 40 bar.

The energy consumption is a key factor that influences the production cost

of freshwater produced by reverse osmosis. Typically 50 - 75 percent of the energy consumed by seawater RO desalination plants is used to drive the motors for the high pressure feed pumps [21]. The energy consumption can be reduced by improving the membrane technology, and by utilizing the high pressure of the exiting concentrate stream in energy recovery devices (ERD).

3.1.1 Energy Recovery Devices

The first energy recovery devices were turbines, utilized in RO systems since the early eighties. In a paper published in the international journal *Desalination* in 1981 [43], Woodcock suggests that the Pelton turbine can be used to convert the kinetic energy of the concentrate jet to rotating mechanical energy which again can drive an electric generator. Woodcock also suggests that the turbine might be coupled directly to the shaft of the feedwater pump to reduce the electrical input to the motor. The simplicity as well as the flat efficiency curve of the Pelton turbine is emphasized, making it well suited to operate at flows outside the best efficiency point (BEP). A compact unit comprising a pump and a turbine on the same shaft was featured in the journal *World Pumps* in 2000, manufactured by Sulzer Roteq [39]. The application area for the system was geographical regions with dry climates and towns and villages located in remote areas.

Today, energy recovery devices can be classified as turbine types or positive displacement types. The turbine based ERDs include Francis turbines, Pelton turbines and hydraulic turbochargers. The positive displacement types are pressure exchangers or work exchangers. The positive displacement types can achieve a higher energy recovery efficiency, up to 90 - 95 percent, and is a promising technology. However, the turbine type recovery devices, with efficiencies ranging from 50 to 90 percent, are the most common devices utilized due to mechanical simplicity, higher process uptime and operational flexibility [21].

3.1.1.1 Turbine Energy Recovery Devices

The turbine energy recovery device converts the kinetic energy of the concentrate jet exiting the nozzle to rotating mechanical energy. When the turbine is connected to the same shaft as the pump, the total energy transfer efficiency is the product of the efficiency of the nozzle, the turbine and the high pressure pump [21]. A sketch of a system configuration including a turbine is provided in figure 3.3.

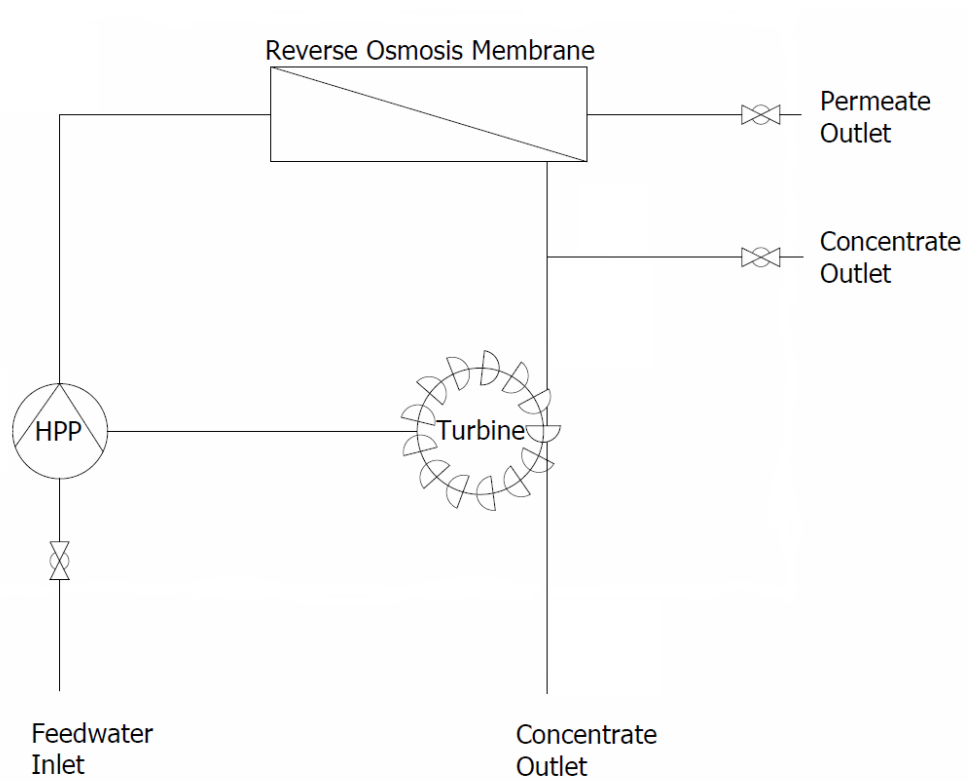


Figure 3.3: RO system configuration including a turbine. The feedwater is pressurized through a high pressure pump (HPP).

The turbocharger energy recovery device comprises a pump and a turbine combined in one housing as shown in figure 3.4. Both the pump and the turbine contain a single stage impeller or rotor. The feedwater is initially pressurized by high pressure pumps connected in series with the turbocharger to an intermediate pressure level, and then the pressure is increased to the RO inlet pressure in the turbocharger.

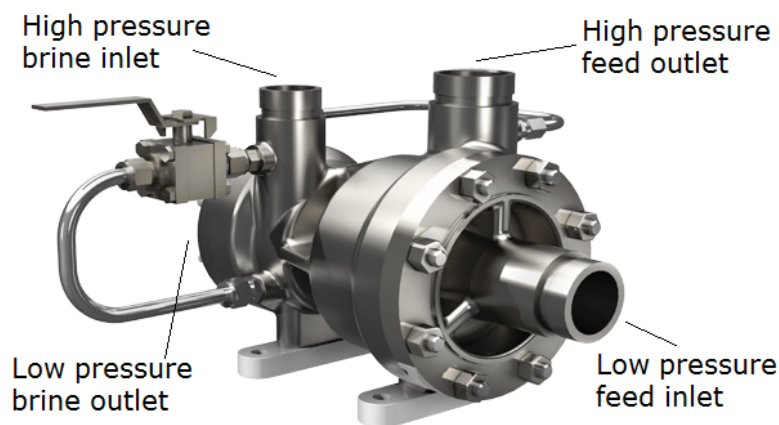


Figure 3.4: Turbocharger [17].

3.1.1.2 Positive Displacement Energy Recovery Devices

In the positive displacement energy recovery devices, the pressure energy of the concentrate is directly transferred to the feedwater. A sketch of this kind of system configuration is given in figure 3.5.

The pressure exchanger comprises a rotating cylinder with ducts parallel to the axis of rotation. The cylinder rotates within a sleeve between two end covers and is turned by the flow itself. The high pressure of the concentrate is directly transferred to the low pressure feedwater. Mixing between the concentrate and the feedwater is minimal because the exposure time is so short. The working principle is illustrated in figure 3.6.

The work exchanger is based on moving pistons in cylinders. Referring to figure 3.7, the high pressure concentrate enters the cylinder from the left and transfers energy to seawater which initially is at low pressure through the piston moving to the right. The seawater leaves the cylinder at high

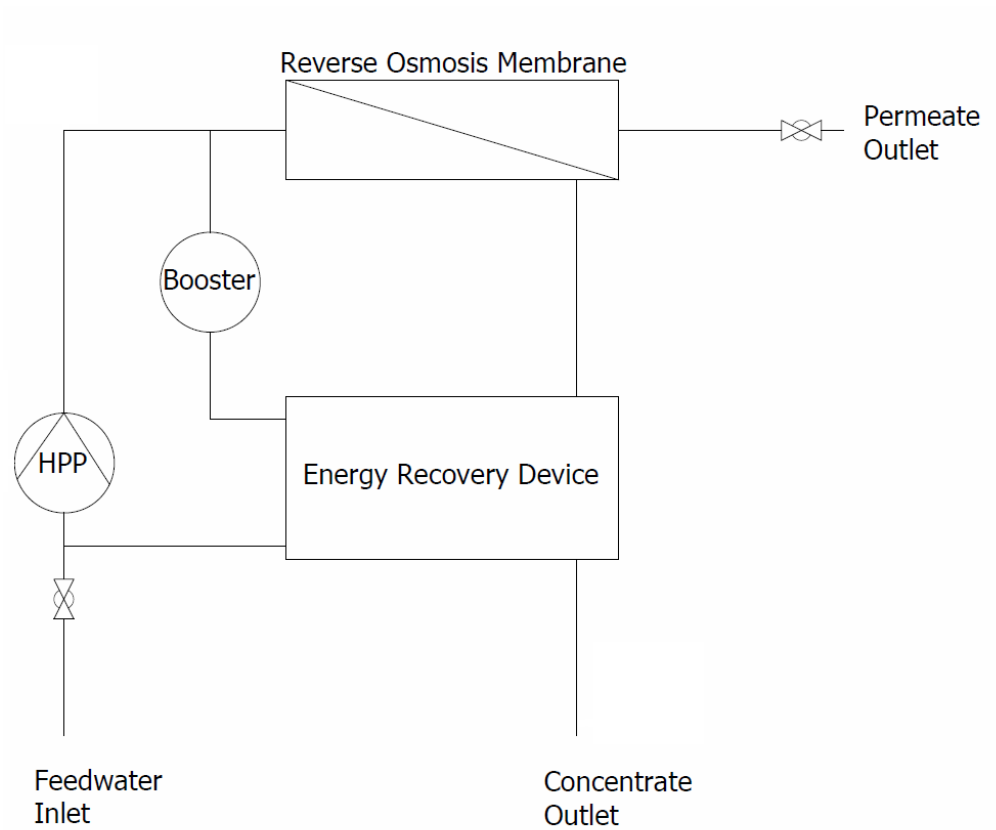


Figure 3.5: RO system configuration including positive displacement energy recovery device. Parts of the feedwater is pressurized through a high pressure pump (HPP), and the other part is pressurized in an energy recovery device and rejoins the rest of the feed stream through a booster pump (Booster).

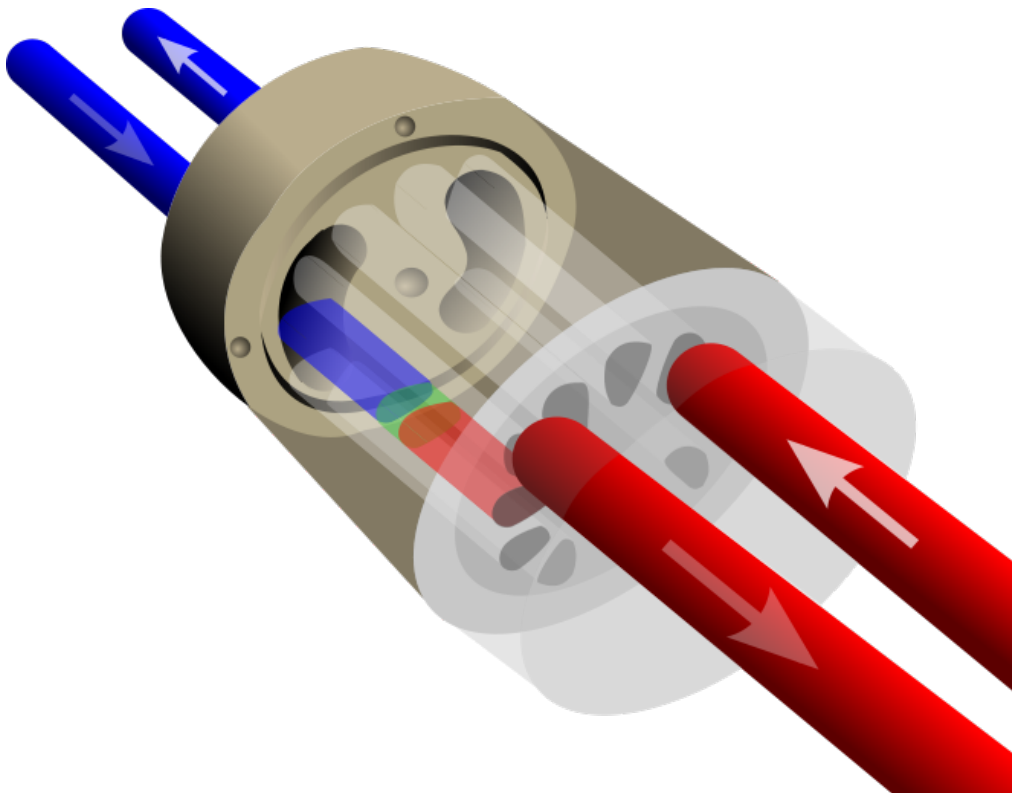


Figure 3.6: Schematics of a pressure exchanger. Arrows indicate flow direction and pressure. Red color for concentrate, blue for feedwater, high pressure white arrow, low pressure transparent arrow. [1]

pressure, and the concentrate is now at low pressure. The piston moves to the left and low pressure seawater enters from the right as seen in the bottom cylinder.

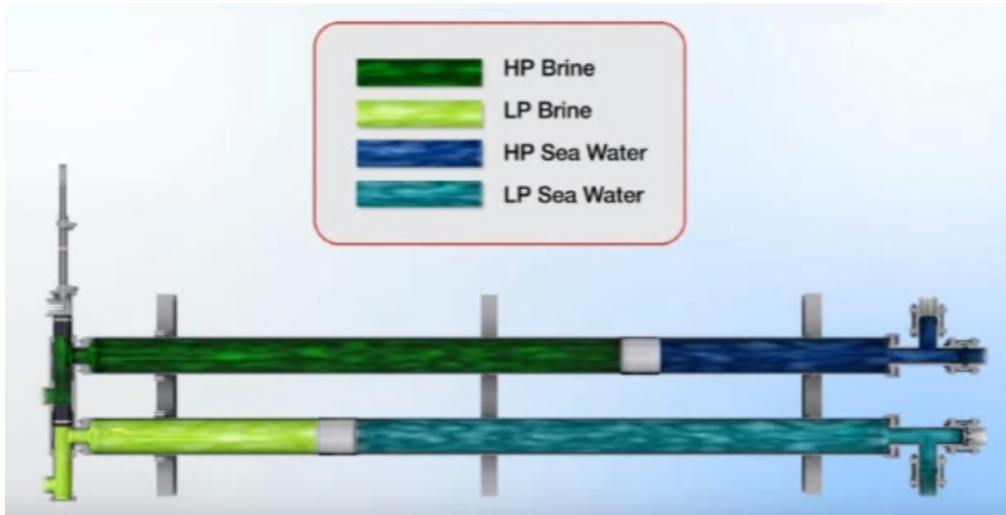


Figure 3.7: Schematics of a work exchanger [13].

The energy transfer efficiency of the the positive displacement type ERDs can exceed 95 percent [34]. Another advantage of the positive displacement ERDs compared to the centrifugal ERDs is that the efficiency varies little with operating pressure and flow rate.

3.2 The Centrifugal and the Reciprocating Pump

Parts of this section is taken from the project thesis *Desalination of Water by Reverse Osmosis* written in the fall of 2015 by Løken [26].

The objective of a pump is to lift or raise the pressure of a fluid. Common applications of pumps include the raising of fluid from a low level to a high level, the supply of high pressure fluid to some industrial process, or even the supply of fluid from a higher to a lower level. The latter may be the case in long pipelines where the hydraulic resistance is very high [25].

3.2.1 Classification of Pumps

In a pump, mechanical energy is transformed into hydraulic energy. Pumps are classified according to the way in which energy is imparted to the fluid.

Two of the basic methods are volumetric displacement and addition of kinetic energy [16].

In the positive displacement pump, energy is imparted to the fluid by means of volumetric displacement. In impeller pumps, also referred to as kinetic pumps, energy is imparted to the fluid by the addition of kinetic energy. One of the main differences between the two lies in how the fluid is transferred from the suction side to the discharge side, i.e., from the low pressure side to the high pressure side of the pump.

In a positive displacement pump, the fluid on the suction side is raised by a pressure drop created by an increasing cavity in the pump. A decreasing cavity pushes the fluid out to the discharge side. A fixed volume of fluid is displaced from the suction to the discharge.

In an impeller pump, the rotation of the impeller sets the fluid particles in motion, from the suction side to the discharge side. This motion produces a reduction in pressure at the inlet side, and the fluid flows through the suction pipe and into the pump casing. The fluid is accelerated by the motion of the impeller, and thus experiences an increase in kinetic energy. The kinetic energy is transformed into pressure energy partly in the impeller and partly in outlet elements such as diffusers and volutes, commonly termed recuperators [25].

The types of positive displacement pumps and impeller pumps can again be subdivided into different categories depending on their principle of operation. Two different pump types will be considered here. The first one is a type of impeller pump called centrifugal pump, and will be reviewed in section 3.2.2. The second, a type of displacement pump, namely the reciprocating pump, will be reviewed in section 3.2.3.

3.2.2 The Centrifugal Pump

The centrifugal pump can be classified as belonging to one of three categories depending on the flow direction through the impeller. According to this, a centrifugal pump is classified as radial, semi-axial or axial.

In the axial pump the fluid flows along the axis of rotation in a spiraling motion. In the radial pump, the fluid flows axially into the impeller eye, and radially outwards. The shape of the impeller and the casing determines the path of the flow, i.e., the shape of the impeller and casing decides whether the pump is radial, semi-axial or axial. The geometry varies continuously from the radial to the axial pump types, depending on the flow and head of the pump. More generally, the geometry varies with the specific speed of the given pump [6].

The specific speed is used to classify pumps according to the geometry of the impeller. This is useful because the performance of a given machine can be predicted by comparing it with the experimentally known performance of another geometrically similar machine [41].

The specific speed is defined as

$$n_q = n \frac{\sqrt{Q}}{H^{3/4}} \quad (3.2.1)$$

See figure 3.8 for representative impeller geometries related to different specific speeds. Note that the specific speeds given in the figure was calculated on the basis of flow and head given in gallons per minute and feet, respectively, not in SI units.

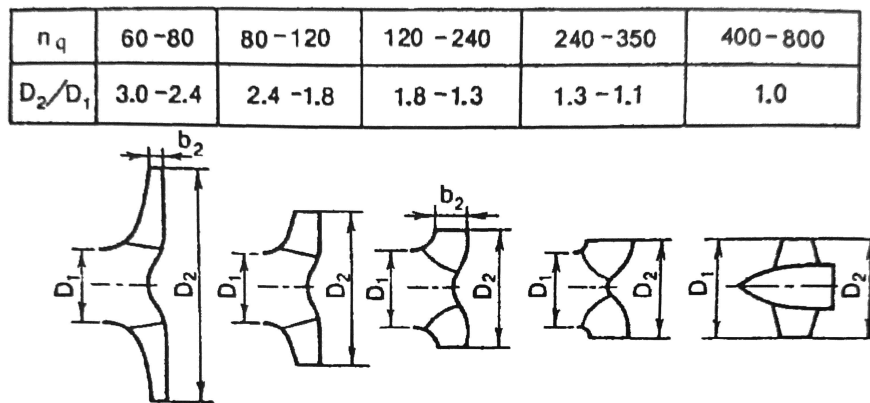


Figure 3.8: Impeller geometry as a function of flow and head [6].

The generation of head in the radial centrifugal pump is treated in section 3.2.2.1.

3.2.2.1 Energy conversion

In a centrifugal pump, the mechanical energy of the impeller or runner is transformed into hydraulic energy in the fluid. In the radial type of centrifugal pump, the total head generated is produced by the action of centrifugal forces as well as the change in absolute velocities.

A simple sketch of a radial centrifugal pump is given in figure 3.9.

The theoretical considerations for the conversion of energy in a radial centrifugal pump will be simplified with the assumption that the number of

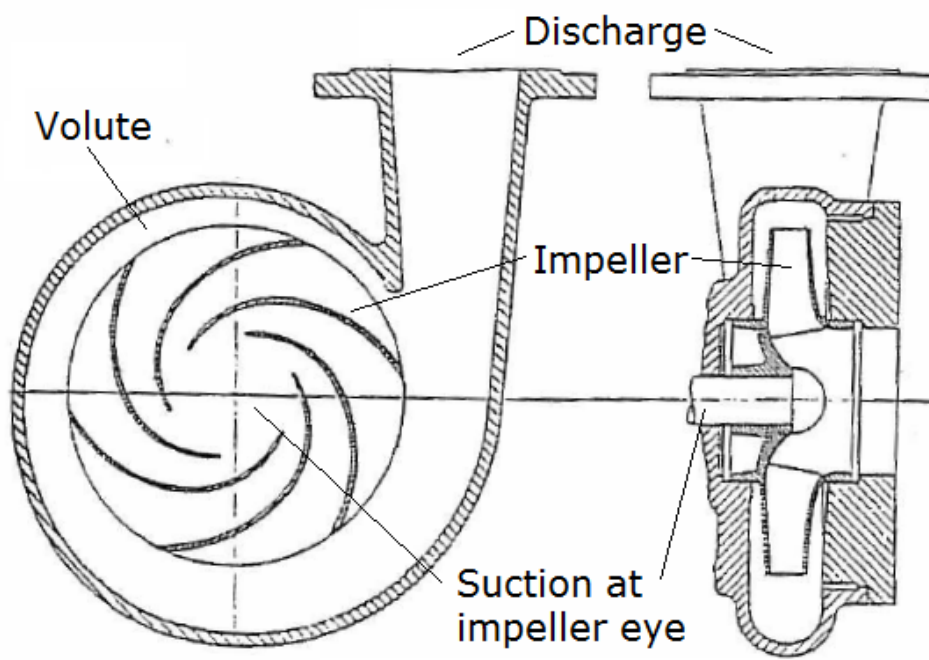


Figure 3.9: Simple sketch of a single stage centrifugal pump. Axial view to the left, and radial view to the right [5].

blades or vanes are infinite and that the blades are infinitely thin. This is equivalent with assuming perfectly axi-symmetrical flow. In a cylindrical coordinate system this means that the velocity of the flow can be described by the r and z coordinates only and is independent of θ . Further, the axi-symmetrical flow is resolved into two components, the meridional and the circumferential or tangential flow components.

The meridional velocity, denoted by subscript m , is the velocity in the axial direction at the inlet of the impeller, and at the outlet of the impeller, it is the velocity in the radial direction in the plane passing through the axis of rotation. The circumferential velocity, denoted by subscript u is the velocity in concentric circles around the axis of rotation [25].

In the following all losses are neglected, meaning that the total power output from the motor driving the impeller is assumed transformed into hydraulic energy in the fluid.

The energy conversion in the impeller can be described by considering the velocity diagrams at the inlet and outlet. See figure 3.10 for typical velocity diagrams in a radial centrifugal pump.

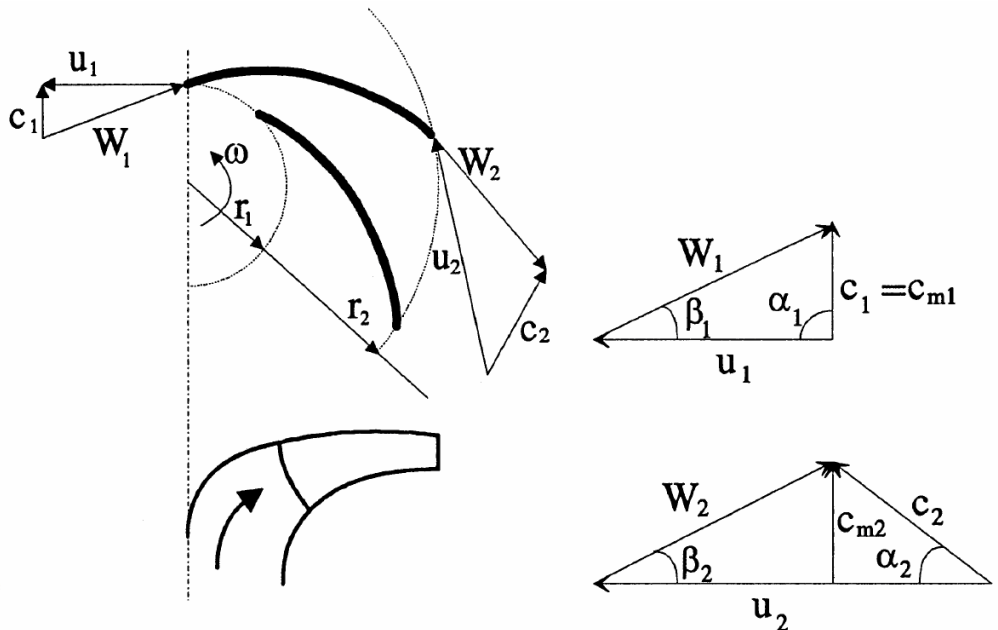


Figure 3.10: Velocity diagrams at inlet and outlet of a radial centrifugal impeller. An axial view of the impeller is given in the upper left corner and radial view of the impeller is given in the lower left corner [6].

In figure 3.10 the absolute velocity of the water is denoted by c , the relative velocity of the water to the impeller is denoted by w and the peripheral velocity of the impeller is denoted by u . The angle between the relative and

peripheral velocity is denoted by β and the angle between the absolute and peripheral velocity is denoted by α . The inlet and outlet of the impeller is denoted by the subscripts 1 and 2, respectively. The angular speed of the impeller is denoted by ω .

The force, F , exerted on the fluid by the impeller under the above mentioned assumptions is given by the product of density, ρ , flow rate, Q and the change in absolute circumferential velocity, c_u [5]

$$F = \rho Q(c_{u2\infty} - c_{u1\infty}) \quad (3.2.2)$$

The subscript ∞ indicates that the impeller has an infinite number of blades and infinitely thin blades.

The torque on the fluid is given by the product of the force and the radial distance from the axis of rotation, r [5]

$$T = \rho Q(r_2 c_{u2\infty} - r_1 c_{u1\infty}) \quad (3.2.3)$$

The power exerted on the fluid by the impeller is given by [5]

$$P = T\omega = \rho Q(u_2 c_{u2\infty} - u_1 c_{u1\infty}) \quad (3.2.4)$$

where the relationship between the angular speed ω and the peripheral velocity u of the impeller is $u = \omega r$.

The power exerted on the fluid can also be expressed as [5]

$$P = \rho Q g H_{t\infty} \quad (3.2.5)$$

where $H_{t\infty}$ denotes the theoretical head of the pump with an infinite number of infinitely thin blades. By combining equations 3.2.4 and 3.2.5 the famous Euler equation is obtained [5]

$$H_{t\infty} = \frac{u_2 c_{u2\infty} - u_1 c_{u1\infty}}{g} \quad (3.2.6)$$

This equation was introduced by Leonhard Euler in 1754, and is one of the fundamental equations in turbomachinery [25]. The Euler equation expresses that the theoretical head of the pump is dependent on the velocity changes through the impeller. From equation 3.2.6 it can be seen that a flow free of rotation at the inlet, i.e., $c_{u1} = 0$ maximizes the theoretical head.

The Euler equation can be rewritten by applying trigonometric relations found from the velocity diagrams in figure 3.10. The resulting equation shows the contribution to the theoretical head by the individual velocity components [5].

$$H_{t\infty} = \frac{u_2^2 - u_1^2}{2g} + \frac{w_{1\infty}^2 - w_{2\infty}^2}{2g} + \frac{c_{2\infty}^2 - c_{1\infty}^2}{2g} \quad (3.2.7)$$

The theoretical head is the sum of the potential head and the dynamic head. The potential head is given by the first and second term on the right hand side of equation 3.2.7, and is produced by the action of centrifugal forces and the reduction of the relative velocity. The dynamic head is given by the last term on the right hand side and is equal to the difference in the absolute velocity. The dynamic or kinetic head is transformed into pressure energy in the outlet elements of the pump, which are described in section 3.2.2.2.

Equation 3.2.7 describes the head generated by a pump with an infinite number of infinitely thin blades and no losses. In reality the head generated by a pump is influenced by the finite number of blades and hydraulic, volumetric and mechanical losses. To differentiate between theoretical and actual head, the following notation is used. $H_{t\infty}$ denotes the theoretical head of a pump with an infinite number of infinitely thin blades, H_t denotes the theoretical head of a pump where the influence of a finite number of blades is considered and H denotes the actual head of a pump with losses.

The effect of a finite number of blades leads to a phenomenon known as slip. Slip is caused by the pressure difference between the front and backside of the blades, and causes the fluid to leave the impeller at a slightly different angle than the one given by the blade outlet, β_2 . By consulting the velocity diagrams in figure 3.10, a reduction of the angle β_2 leads to a reduction in the velocity component c_{u2} and from equation 3.2.6 this means a reduction in the head generated by the pump.

The main losses in a centrifugal pump are hydraulic losses, leakage losses and mechanical friction losses [5]. These losses reduce the total head generated by the pump, and the size of these losses can be quantified by the pump efficiency. The total pump efficiency, η_p , describes the percentage of the available energy transformed to useful energy in the pump. The total efficiency is the product of the hydraulic, mechanical and volumetric efficiency

$$\eta_p = \eta_h \eta_m \eta_V \quad (3.2.8)$$

The volumetric efficiency is the ratio of the outlet flow rate to the inlet flow rate which differ because of leakage losses [25]. The leakage losses arise when the fluid travels between the different components of the pump. The essential components of a centrifugal pump are mentioned in section 3.2.2.2.

3.2.2.2 Essential components

Centrifugal pumps may be single stage or multistage, vertical or horizontal. A single stage pump comprises one impeller, a multistage pump comprises several impellers arranged in an appropriate manner, in order to increase the total head of the pump. Independent of whether the pump is single stage or multistage, the essential components of a centrifugal pumping system are; *inlet pipe, impeller (rotor), seals, shaft, bearings, casing (stator) and delivery pipe*.

In figure 3.11 a cutaway of a multistage pump is given to aid the visualization of the different components.

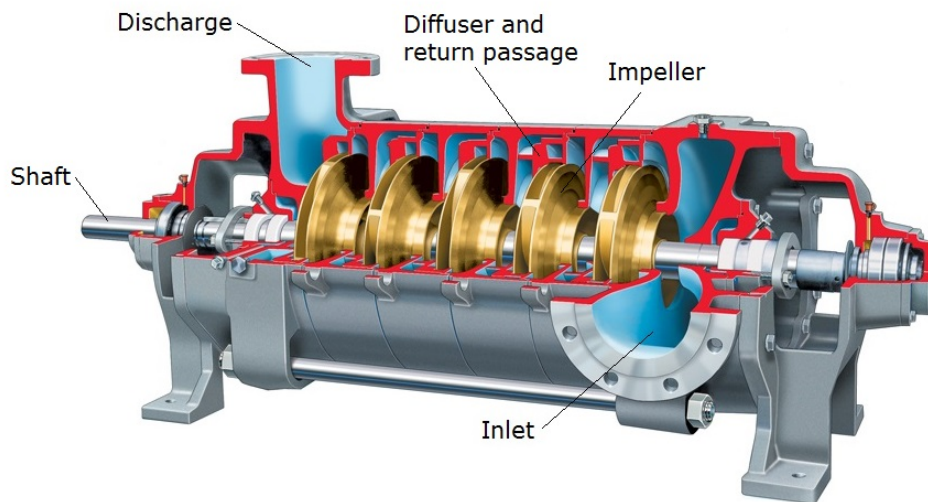


Figure 3.11: A cutaway of a multistage pump with 5 stages connected in series [14].

A pump may receive water from a sump, river, tank, reservoir or pipe, above or below the centerline of the pump [3]. The shape of the *inlet pipe* leading the fluid to the impeller is of great importance, and affect both the impeller efficiency and pump cavitation characteristics [41]. It is important that the flow into the centrifugal pump is without prerotation or prewhirl,

as seen from equation 3.2.6. To ensure this the piping should be smooth, and the cross-sectional area of the inlet pipe gradually reduced to produce a uniform velocity increase in the pipe. It is equally important to avoid air pockets in the piping, as this will reduce the efficiency of the pump. To avoid air pockets the inlet pipe should be rising at a slope from the reservoir towards the pump centerline. If the inlet pipe is horizontal, air pockets may appear.

The *impeller* is rotating at a certain angular speed and transfers mechanical energy to the fluid. The impeller often has a complex shape, and requires thorough consideration.

Seals separate the rotating and stationary parts. There will always be leakage losses through the clearance spaces.

The *shaft* connects the driver with the impeller(s). The driver is most frequently an electric motor. The shaft must be designed to withstand the torsional forces, the bending forces and the axial forces acting on the shaft. The bending forces arise from the load of the shaft itself and the parts attached to it, together with the radial thrust arising from an uneven pressure difference along the periphery of the impeller. The axial forces arise from the pressure difference between inlet and discharge and between the stages in a multistage pump.

The *bearings* transfer the radial and axial forces in the pump, and ensures that the axial movement of the shaft and radial deflection is within acceptable limits with a minimum friction loss.

The *casing* is stationary. In the casing the kinetic energy of the fluid leaving the impeller is transformed into pressure energy. This transformation takes place in elements called recuperators. The recuperators can have several different shapes, the most common ones are volutes and diffuser-rings. All recuperators have an increasing flow area in order to reduce the velocity and increase the pressure. A multistage pump also has return passages to lead the flow into the next stage.

The *delivery pipe* delivers the high pressure fluid or the discharge to the required location. The discharge may be regulated for changes in demand. Discharge regulation at constant speed is most commonly achieved by opening or closing the delivery valve [25].

3.2.2.3 Operation

Before start-up, a centrifugal pump must be primed. Priming means filling the system with fluid and driving out all air. The inlet or suction pipe,

casing and delivery pipe up until the delivery valve must be completely filled with fluid such that all air pockets are gone. At this point the delivery valve is still closed.

Priming of the centrifugal pump is essential. The pump may be started when it is filled with air, and a head will be generated. But, because of the low density of air, the suction head generated will not be enough to lift the fluid into the pump and flow can not take place [3].

When the pump is primed the motor that drives the pump may be started. The delivery valve is kept closed while starting the motor to reduce the required starting torque.

When the delivery valve is opened, the fluid flows outward in the radial direction and leaves the vanes of the impeller with high velocity and pressure.

Suction is created at the eye of the impeller due to centrifugal forces. This causes the fluid from the sump which may be at atmospheric pressure, to travel through the suction pipe and into the impeller eye.

When the fluid leaves the impeller it enters the stator. The purpose of the stator is to diffuse kinetic energy into pressure energy. This is done by gradually expanding the flow area. The fluid may travel from the impeller through the casing and to the next stage in a multistage pump, and finally the fluid travels through the delivery pipe and delivery valve.

3.2.2.4 Cavitation

Cavitation is the formation of vapor bubbles in the fluid flowing through the pump. This happens if the local static pressure falls below the vapor pressure of the fluid at the given temperature. Small vapor bubbles will form, and when reaching regions of higher pressure, they will collapse. When the bubbles collapse near a surface, a jet stream will be formed in the center which hits the surface with large impact. The collapse creates large local pressure oscillations, and because of this, fully developed cavitation can send vibrations through the whole pump and even the foundations of the pump.

In a centrifugal pump, the highest danger of cavitation is at the impeller inlet. To avoid cavitation the pressure must be above the vapor pressure of the fluid. The pressure at the inlet can be found by applying Bernoulli's equation along a streamline from the lower reservoir to the inlet of the impeller.

The required head to avoid cavitation at the inlet is called the required

Net Positive Suction Head, $NPSH_R$. It can be found from the following empirical formula

$$NPSH_R = a \frac{c_{m1}^2}{2g} + b \frac{u_1^2}{2g} \quad (3.2.9)$$

The available Net Positive Suction Head is given by

$$NPSH_A = H_{atm} - H_{va} - H_s \quad (3.2.10)$$

where H_{atm} is the atmospheric pressure, H_{va} is the vapor pressure of the water at the given temperature, and H_s is the elevation of the impeller inlet relative to the free surface of the lower reservoir as depicted in figure 3.12.

The requirement for avoiding cavitation thus becomes

$$NPSH_A > NPSH_R \quad (3.2.11)$$

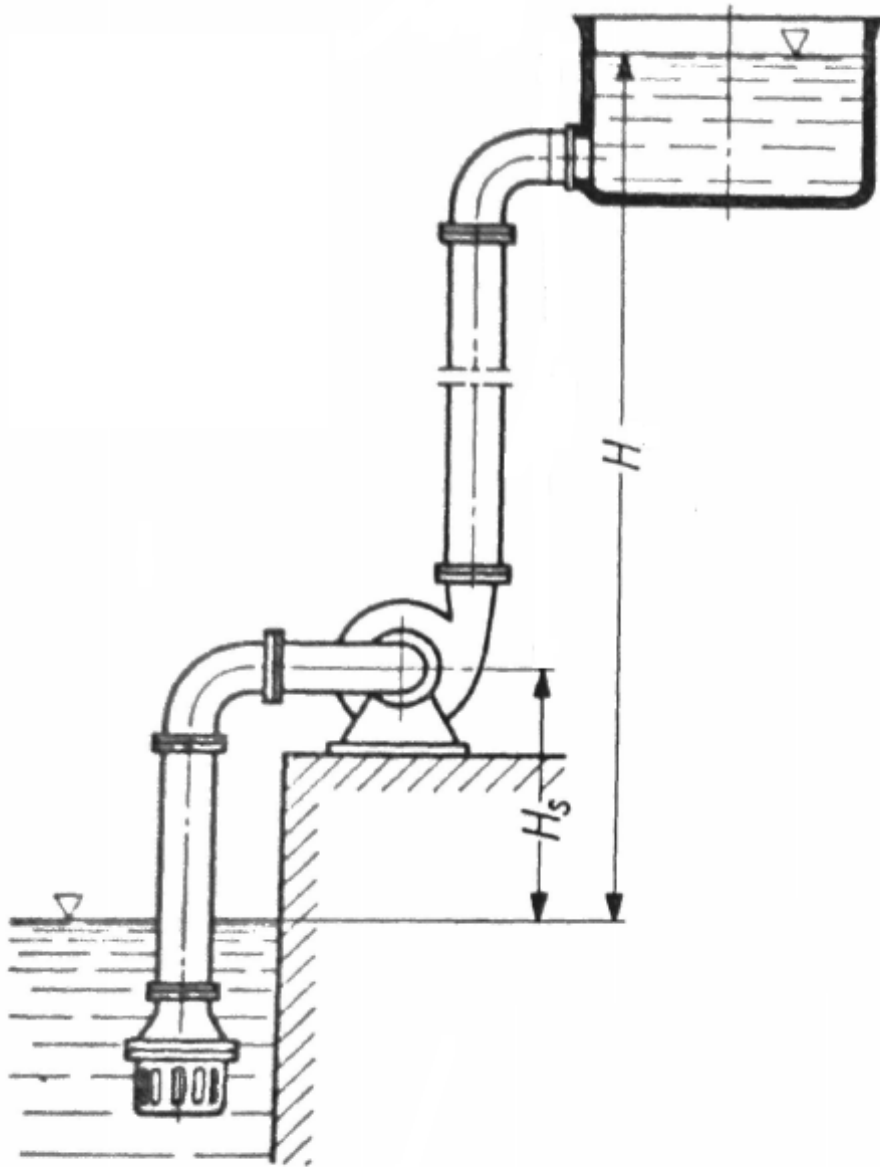


Figure 3.12: Principal sketch of a centrifugal pumping system with lower and upper reservoir [25].

3.2.3 The Reciprocating Pump

John E. Miller defines the reciprocating pump as a mechanical device used to impart a pulsating, dynamic flow to a fluid through positive displacement elements such as pistons or plungers. The displacement element moves in a linear reciprocating motion inside a stationary cylinder. The cylinder is alternately filled and emptied of fluid due to the increasing and decreasing cavity created in the cylinder by the displacement element. Check valves at the inlet and outlet of the cylinder ensure that the fluid is directed from the suction to the discharge. The piston or plunger is driven by a rotating crank and connecting rod mechanism [29].

3.2.3.1 Energy Conversion

In a reciprocating pump, the mechanical energy of the positive displacement element is transformed into hydraulic energy in the fluid. See figure 3.13, showing the basic geometry of a single-acting reciprocating piston pump.

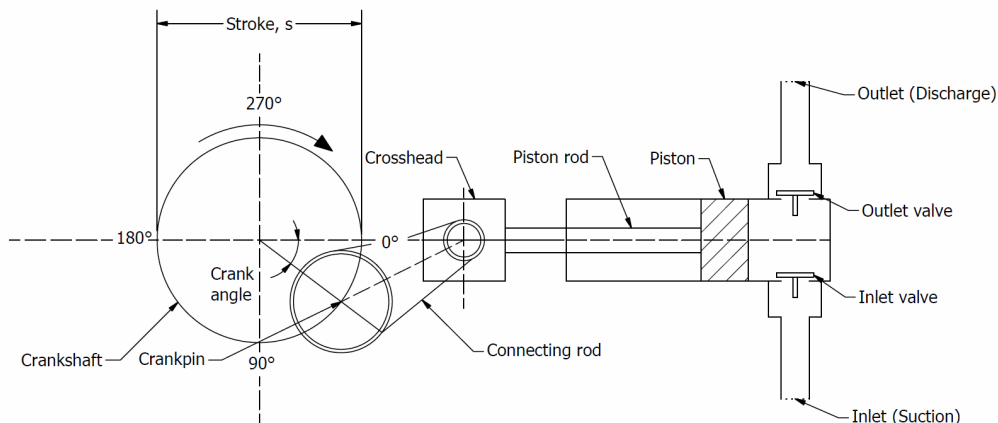


Figure 3.13: Sketch showing the basic geometry of a single-acting reciprocating piston pump.

With figure 3.13 in mind, the working principle of the reciprocating pump can be more thoroughly explained. As the crankshaft rotates, the rotating motion is transferred through the connecting rod to the crosshead. The crosshead is constrained to a linear reciprocating motion. In this manner, the rotating motion of the crankshaft is converted to linear reciprocating motion through the connecting rod and crosshead. The positive displacement element, the piston, is connected to the crosshead through the piston rod. During the rotation of the crankpin from 0° to 180° , the suction

stroke, the piston moves to the left and a cavity is created in the cylinder. The increasing cavity causes the pressure in the cylinder to drop below the pressure in the suction pipe. This allows the inlet valve to open, and fluid fills the cylinder. During the rotation of the crankpin from 180° to 360° , the discharge stroke, the piston moves to the right, the inlet valve is forced closed, and the fluid in the cylinder is compressed. When the pressure in the cylinder exceeds the pressure in the discharge pipe, the outlet valve opens, and the fluid is forced out into the discharge pipe. In this manner, mechanical energy is transformed into hydraulic energy.

The generation of pressure head in a reciprocating pump differs from the generation of pressure head in a centrifugal pump. In a centrifugal pump, the rotation of the impeller imparts kinetic energy and a centrifugal force to the fluid particles and the fluid moves radially outwards. Mechanical energy is transferred to the fluid, and at the discharge side of the impeller both the pressure and kinetic energy of the fluid rises when the impeller starts rotating. In a centrifugal pump, the flow rate is dependent on the head generated, as seen from equation 3.2.7, in section 3.2.2.1, where the absolute and relative fluid velocities, c and w , are a function of the flow rate and flow inlet and outlet area. In a reciprocating pump, the flow rate is dependent on pump rotational speed only, because a fixed volume of fluid is displaced for every rotation of the crankshaft. The pressure generated in the reciprocating pump is dependent on the system flow resistance downstream of the pump.

The main losses in a reciprocating pump are hydraulic losses, leakage losses and mechanical friction losses in bearings, seals and valves. These losses can be quantified by the pump efficiency. The total pump efficiency, η_p , describes the percentage of the available energy transformed to useful energy in the pump. The total efficiency is the product of the hydraulic, mechanical and volumetric efficiency

$$\eta_p = \eta_h \eta_m \eta_V \quad (3.2.12)$$

Volumetric efficiency is defined as the ratio between the actual displacement of fluid to the theoretical displacement calculated from pump piston diameter, stroke length and speed [29]. The delivered flow rate is always less than the theoretical flow rate given by the displacement volume, due to valve delay and leakage, and the the compressibility of the fluid.

3.2.3.2 Essential Components

Within the class of reciprocating pumps there are many possible configurations, and there are both horizontal and vertical pumps. Prior to presenting the essential components of a given reciprocating pump, the differences between some of the most important configurations will be explained. This includes the difference between a power pump and a direct-acting pump, the difference between a single-acting and a double-acting pump, the difference between a pump having one cylinder as compared to a multicylinder pump, and the difference between a piston and a plunger.

A power pump is a pump where rotary motion from an electric motor or turbine is converted into reciprocating motion through a crankshaft and connecting rod mechanism. In a direct-acting pump the reciprocating motion is caused by an integral reciprocating engine. The engine reciprocating motion is directly transferred to the positive displacement element [42].

A single-acting pump is a pump where the fluid in each cylinder is discharged only once per complete cycle or revolution. In a double-acting pump the fluid in each cylinder is discharged twice per complete cycle or revolution. To achieve this, a piston or a plunger must be situated between two sets of suction and discharge valves in a single cylinder. See figure 3.14 for a sketch showing the operating principle of a double-acting pump.

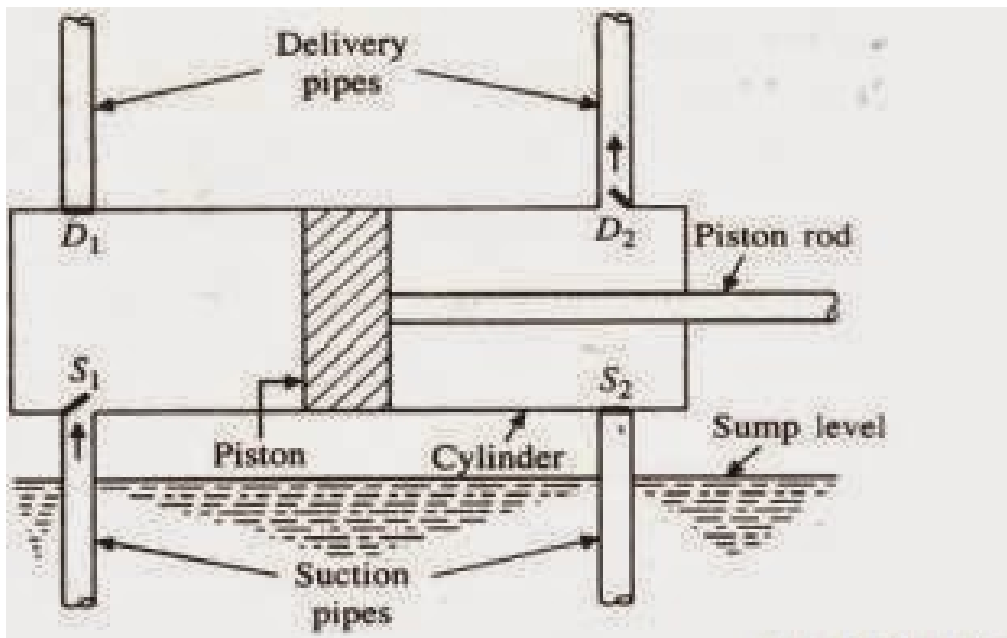


Figure 3.14: Sketch showing the basic geometry of a double-acting reciprocating pump [7].

A pump consisting of only one cylinder is often referred to as a simplex pump. A pump consisting of several cylinders is referred to as a multicylinder pump. The number of cylinders is usually emphasized in the name of the pump, like duplex for a two-cylinder pump, triplex for a three-cylinder pump, and so on. The advantages a multicylinder pump holds over a simplex pump are explained in section 3.2.3.4.

All configurations mentioned above may have either a piston or a plunger as the positive displacement element. They both impart energy to the pumped fluid and causes the pressure to rise in the cylinder. A plunger is a smooth rod moving through a stationary seal. Plungers are normally used in pumps delivering lower flow rates and higher pressures. A piston is a cylindrical disc, having a seal attached to the outer diameter. So in this case, the seal moves with the piston. Pistons are normally used in pumps delivering higher flow rates and lower pressures [42].

Having mentioned the differences between some of the most important configurations of the reciprocating pump, further discussion of the essential components will be conducted considering a power pump, namely the triplex single-acting piston pump. For illustration purposes a model of this kind of pump is given in figure 3.15.

The definitions in this section are taken from the book *The Reciprocating Pump* by John E. Miller [29]. The components of the pump belong to one of two main parts, the fluid end or the power end.

The Fluid End

Comprises all the parts that handles fluid, like the cylinder and valves.

Fluid cylinder. A chamber in which the motion of the piston is imparted to the fluid.

Cylinder liner. A replaceable liner which is placed in the cylinder of a piston pump. The piston reciprocates within the liner.

Manifold. A suction manifold is a chamber which accepts fluid from the suction port and distributes it to the suction valves. A discharge manifold is a chamber which accepts fluid from the discharge valves and directs it to the discharge port.

Valve chest cover. A cover for the valves within the cylinder.

Valve plate. A plate that contains the suction or discharge valves.

Piston. A cylindrical body which is attachable to a rod and is capable of exerting pressure upon a fluid within the fluid cylinder. A piston usually

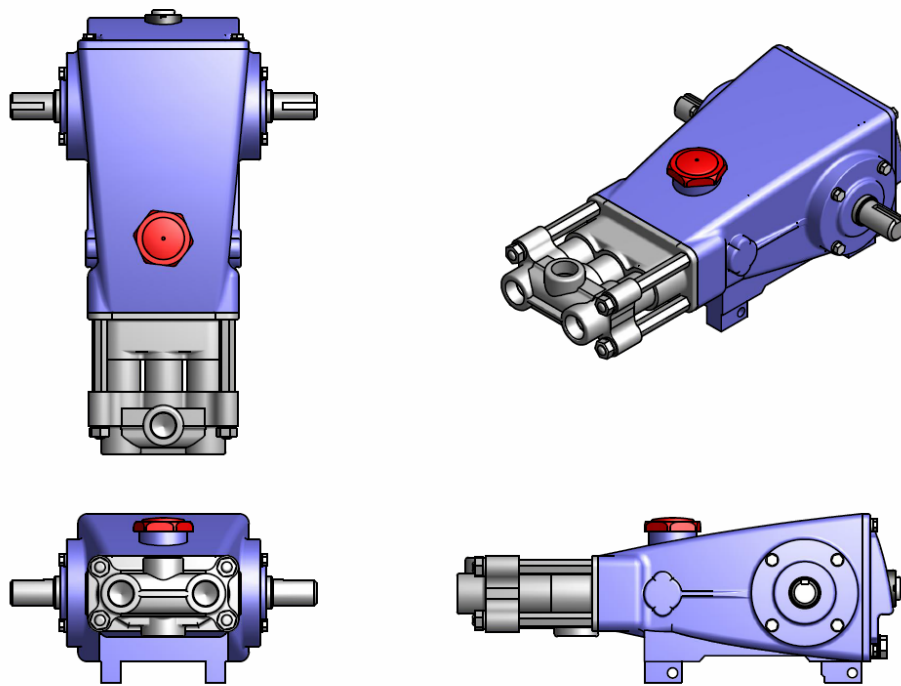


Figure 3.15: Model drawing of a triplex single-acting piston pump [35].

has grooves for containing rings which seal against the cylinder or cylinder liner.

Stuffing box. A cylindrical cavity through which the piston rod reciprocates and in which fluid leakage is controlled by means of packing.

Packing. A material used to provide a seal around the piston rod or piston.

Valve assembly. Usually consists of a seat, valve and spring. See figure 3.16, where a wing valve assembly is shown. The valve assemblies allow fluid to enter and leave each cylinder. The fluid flow through valves is associated with pressure loss. Because of this, several experimentally determined flow parameters exist for the various types of valves, describing the relationship between velocity and pressure loss [40].

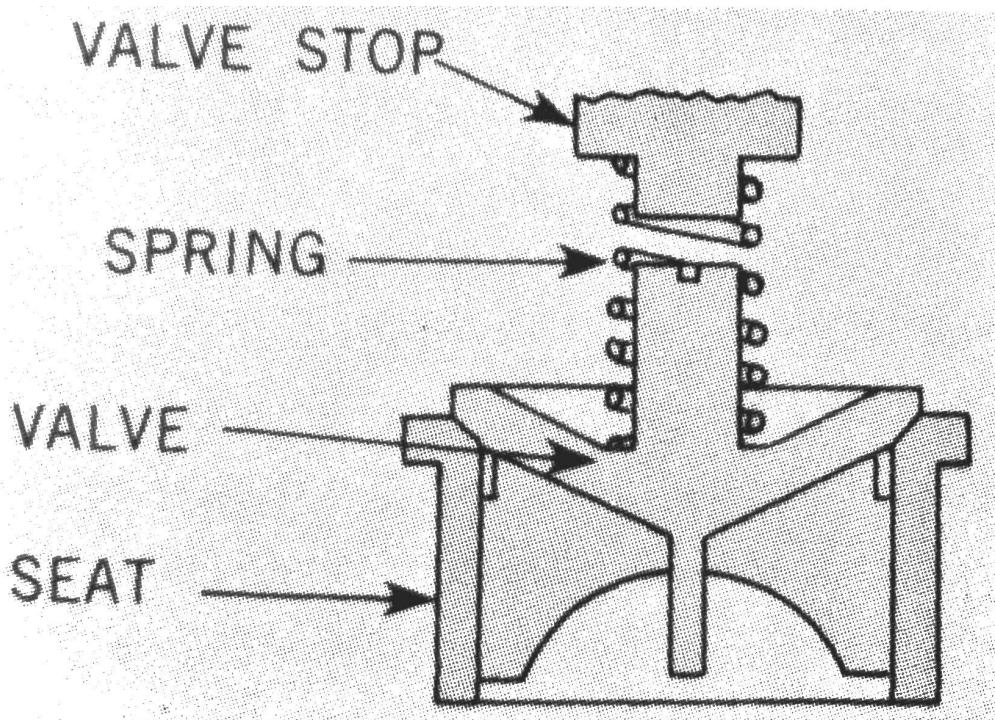


Figure 3.16: Wing valve assembly. [29]

The Power End

Comprises the parts that converts the rotating motion of the crankshaft to a reciprocating motion through the connecting rod and crosshead.

Power Frame. That portion of the power end which contains the crankshaft, connecting rods, crossheads, and bearings used to transmit power and motion to the fluid end.

Crankshaft. The shaft that transmits power and motion to the connecting rods. Main bearings and connecting rods are fitted on the crankshaft.

Main bearing. The bearing which supports the crankshaft. This bearing absorbs the fluid and inertia loads which are developed by the piston as it displaces the fluid.

Connecting rod. Transfers the motion of the crankshaft to the crosshead. Power is transmitted through compression and tension.

Crankpin. Transmits the oscillating reciprocating load transmitted by the connecting rod to the crankshaft.

Crosshead. Creates a linear reciprocating motion derived from the crankpin rotary motion through the connecting rod. The reciprocating motion of the crosshead is applied to the piston via the piston rod.

Piston rod. Connects the crosshead to the piston.

3.2.3.3 Operation

One of the advantages of the reciprocating pump is that it can be considered self-priming under the right suction conditions [42]. When the pump is started, the pump will deliver a constant, but pulsating flow rate at constant speed, because the volume displaced by the plunger with every rotation is constant. The pressure delivered by the reciprocating pump is dependent on the system flow resistance downstream of the pump. Depending on the downstream flow resistance, the pump will continue to deliver fluid and build pressure until action is taken to control the pump's work. To ensure safe operation of the pump, a safety relief valve should always be placed between the pump and the discharge pipe [42].

The pulsating flow of the reciprocating pump leads to pressure pulsations, and these pressure pulsations must be carefully considered when designing the pump, to allow safe operation, a long pump lifetime and to avoid cavitation.

3.2.3.4 Pressure Pulsations

John E. Miller defines three sources of dynamic pressure disturbances generated by the positive displacement pump: frictional pressure drop, acceleration from the fluid flow variation of the pump, and low-amplitude waterhammer-type pressure disturbances that occur each time a pump valve opens or closes [29].

3.2.3.5 Pressure Pulsations due to Friction

The pulsating flow at the suction and discharge of the reciprocating pump is caused by the variation in the piston velocity during a stroke. The velocity varies from zero at the beginning and end of each stroke, to a maximum at mid-stroke. The instantaneous piston velocity can be found by considering the geometry of the pump as depicted in figure 3.17.

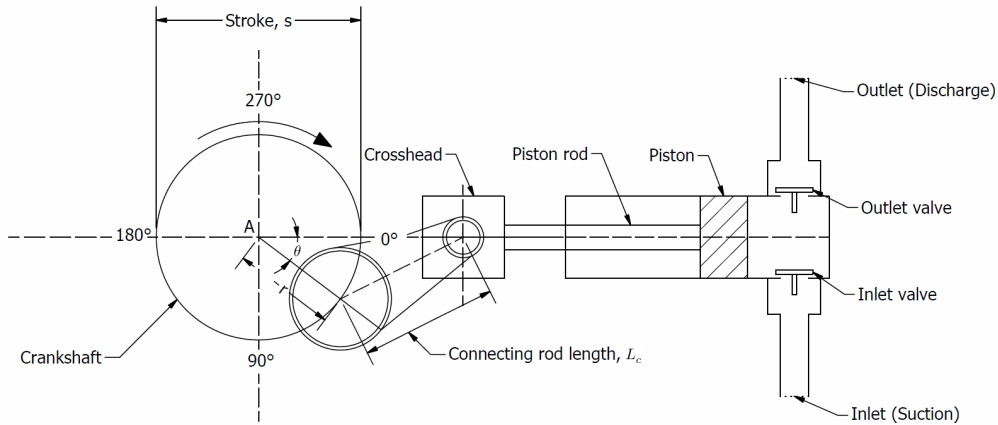


Figure 3.17: A sketch showing the geometry of one single-acting cylinder in a reciprocating pump [29].

The horizontal position of the crosshead relative to the centerline of the crankshaft, the point denoted A in figure 3.17, can be found by using trigonometry. Once the position of the crosshead is found, and therefore also the position of the piston, the velocity of the piston can easily be found by differentiation. The piston velocity, v_p , is given in equation 3.2.13.

$$v_p = r\omega \left(\sin \theta + \frac{1}{2} \frac{r \sin 2\theta}{\sqrt{L_c^2 - r^2 \sin^2 \theta}} \right) \quad (3.2.13)$$

As seen from equation 3.2.13, the piston velocity is a function of the geometry of the pump, along with the crank angle θ and the angular speed of the crankshaft ω . The shape of the piston velocity pattern during one full revolution of the crankshaft is illustrated in figure 3.18.

When the piston velocity is known, the velocities in the suction and discharge pipes can be found from mass conservation. These velocities will depend on the piston velocity v_p , the piston diameter d_p , and the suction or discharge diameter, d_s or d_d . In the case of a multicylinder pump, the suction and discharge velocities will be the summation of the contributions

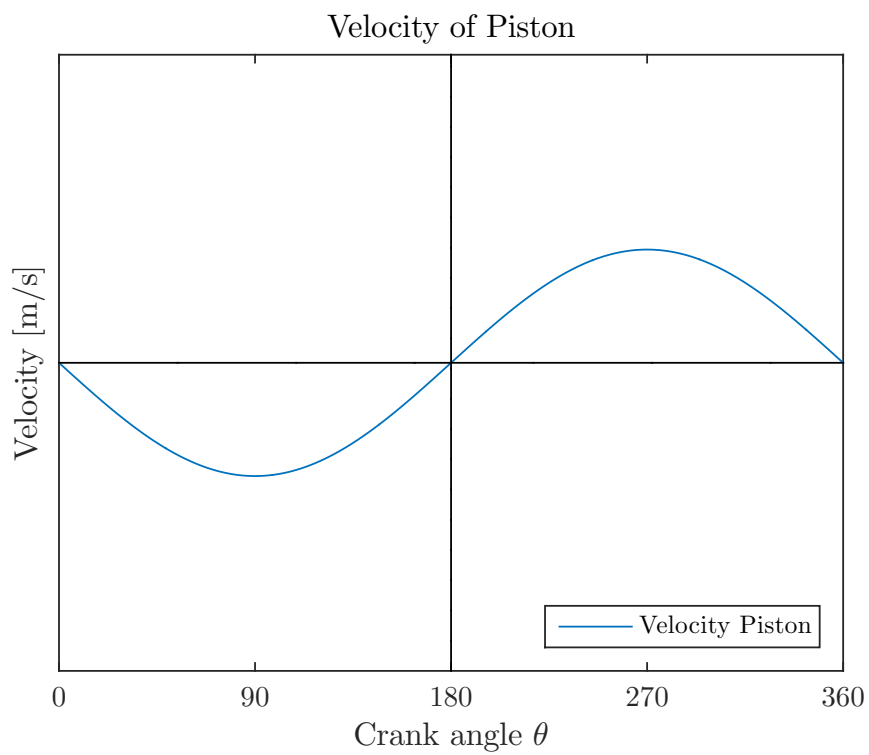


Figure 3.18: The piston velocity pattern during one full revolution of the crankshaft.

from all the cylinders, n . The respective velocities are given in equation 3.2.14 and 3.2.15.

$$v_s = \sum_{i=1}^n \frac{d_p^2}{d_s^2} v_{p_i} \quad (3.2.14)$$

$$v_d = \sum_{i=1}^n \frac{d_p^2}{d_d^2} v_{p_i} \quad (3.2.15)$$

When the velocities are known, the flow rates can be found as the product of velocity and flow area. The flow rates will therefore have the same shape and frequency as the velocity pattern. In figure 3.19, the flow in a single cylinder is illustrated.

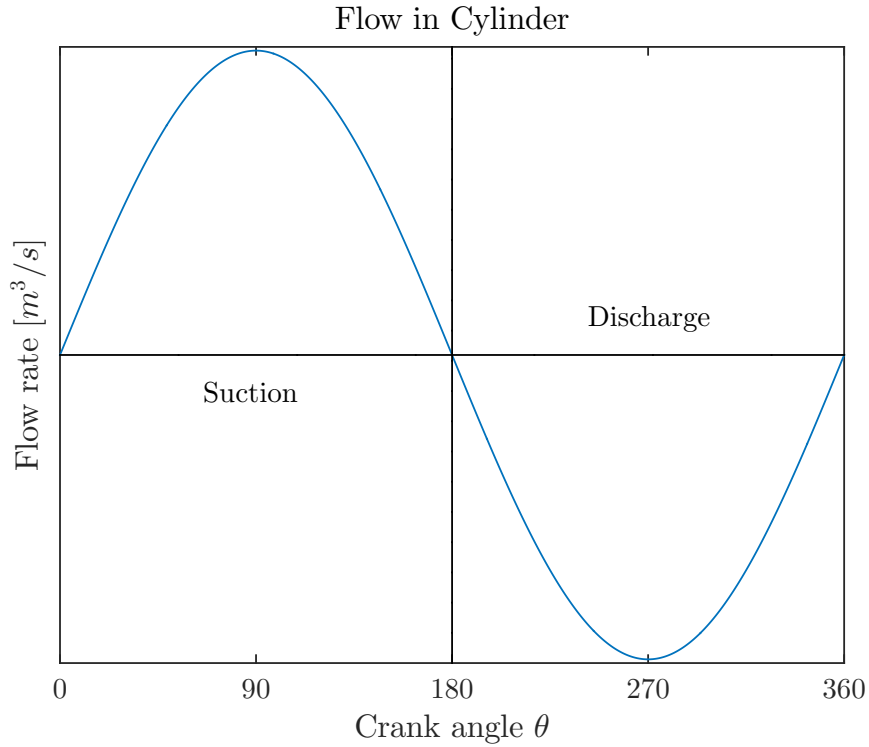


Figure 3.19: The flow rate in one cylinder of a reciprocating pump during one full revolution of the crankshaft.

As seen from figure 3.19, the flow variation in the cylinder is considerable. Large flow variation leads to varying frictional pressure drop, or in other words, pressure pulsations in the suction and discharge pipe. These pressure pulsations are illustrated in figure 3.20.

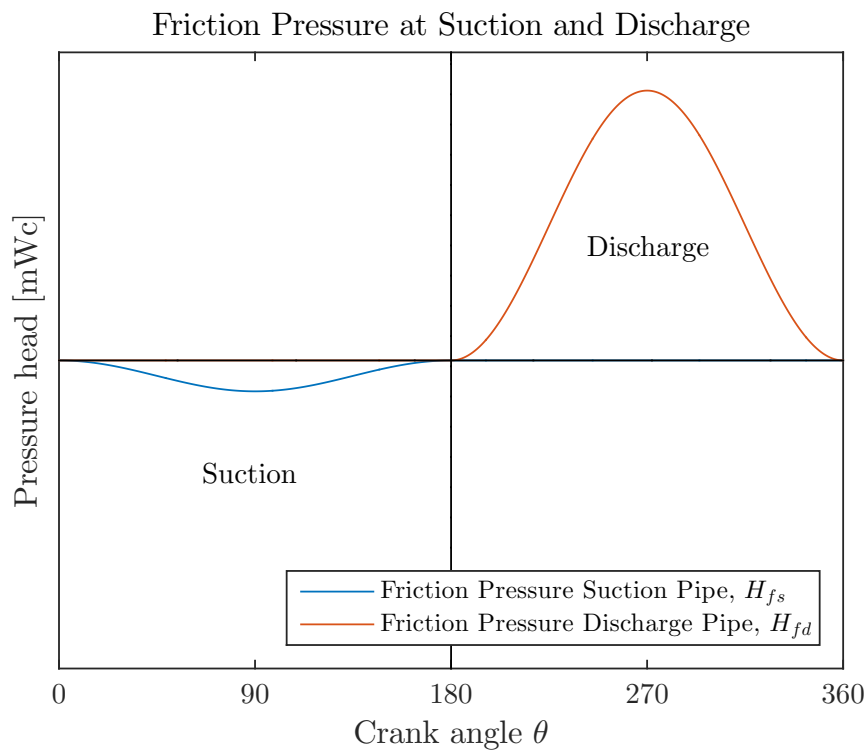


Figure 3.20: The piston velocity generates varying flow rate and thus varying frictional pressure loss or frictional pressure pulsations. Valid for a single-cylinder reciprocating pump.

From figure 3.20 it is clear that loss of pressure head because of friction is zero at the beginning and end of each stroke, and at a maximum at mid-stroke. This is not surprising, as the pressure drop is a function of the velocity of the fluid. The frictional pressure drop may be approximated by the DarcyWeissbach equation in terms of head [9]

$$H_f = f \frac{L v^2}{d 2g} \quad (3.2.16)$$

where f is Darcy's coefficient of friction. As seen from equation 3.2.16, the frictional pressure drop H_f is indeed a function of the square of the velocity v , and will lead to pressure pulsations with the same frequency as the velocity and flow. In other words, the frequency of these pulsations are exactly related to pump speed.

The large variation of flow in the single-cylinder pump is one of the main reasons to use multicylinder pumps. In a multicylinder pump the flow in the suction pipe and discharge pipe will be the sum of the contributions from all the cylinders. Having a pump with three cylinders, a triplex pump, where all the crankpins are spaced evenly, meaning 120° apart, the flow variation will be significantly reduced. See figure 3.21, where the flow in a simplex, a duplex and a triplex pump is illustrated.

As seen from figure 3.21, the variations from the average flow rate, and thus the pressure pulsations due to friction, become smaller as the number of cylinders is increased. The pressure pulsations due to friction are not however the only pressure pulsations that must be considered in the reciprocating pump. There are also pressure pulsations due to acceleration, and these will be described in section 3.2.3.6.

3.2.3.6 Pressure Pulsations due to Acceleration

The flow in a reciprocating pump is pulsating, and so the fluid is constantly accelerating and decelerating. Through one piston stroke in a reciprocating pump cylinder, the velocity varies from zero at the beginning and end of the stroke, to a maximum at mid-stroke. The piston velocity was found in equation 3.2.13, and the acceleration can thus be found by taking the derivative of the velocity with respect to time. The expression for the piston acceleration is given in equation 3.2.17.

$$a_p = r\omega^2 \left(\cos \theta + \frac{r \cos 2\theta}{\sqrt{L_c^2 - r^2 \sin^2 \theta}} + \frac{r^3 \sin^2 \theta \cos^2 \theta}{\sqrt[3]{L_c^2 - r^2 \sin^2 \theta}} \right) \quad (3.2.17)$$

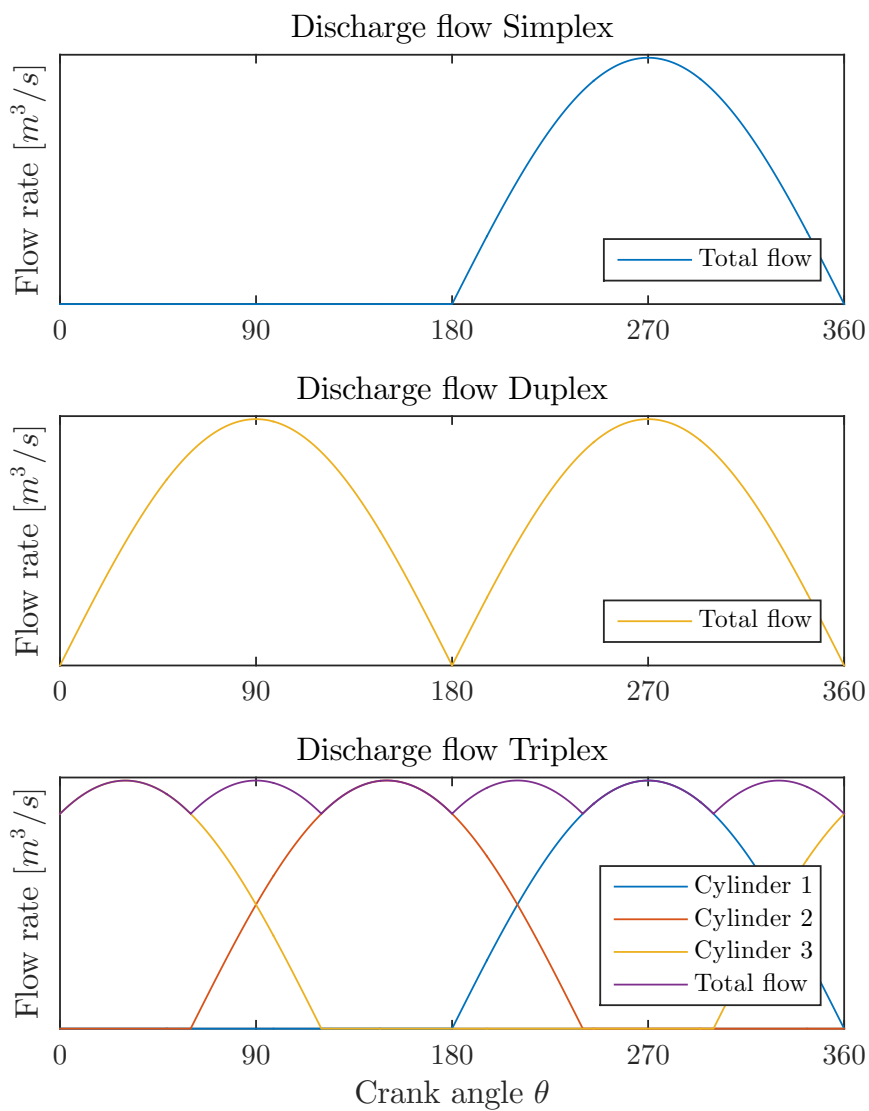


Figure 3.21: The shape of the discharge flow pattern in a triplex single-acting pump during one full revolution of the crankshaft.

As seen from equation 3.2.17, the piston acceleration is a function of the geometry of the pump, along with the crank angle θ and the square of the angular speed of the crankshaft ω . The shape of both the piston velocity and acceleration pattern during one full rotation of the crankshaft is illustrated in figure 3.22.

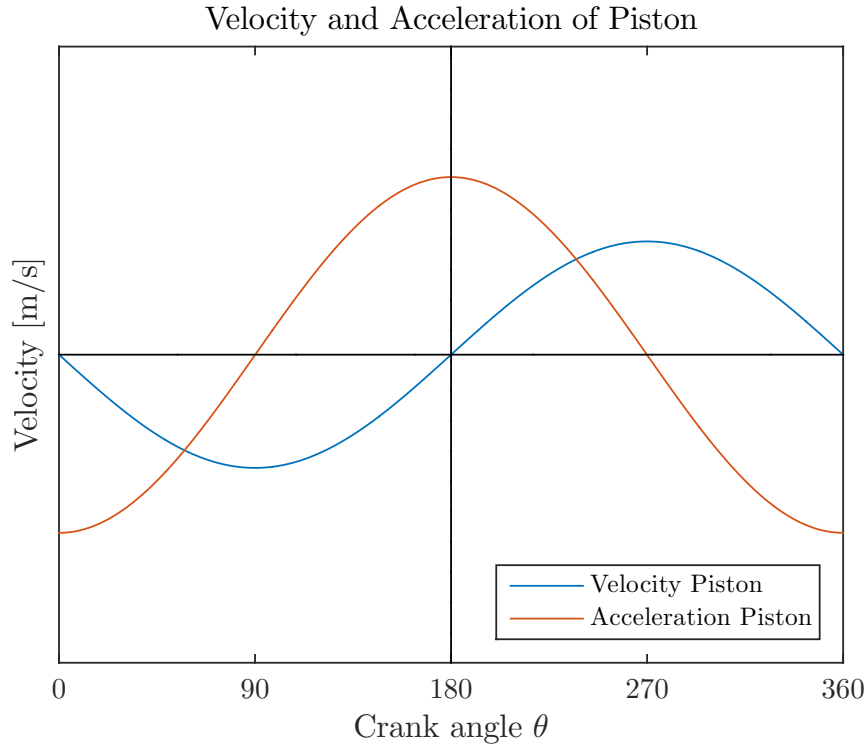


Figure 3.22: The velocity and acceleration of the piston during one stroke.

When the piston acceleration is known, the acceleration in the suction and discharge pipes can be found from mass conservation. These accelerations will depend on the piston acceleration a_p , the piston diameter d_p , and the suction or discharge diameter, d_s or d_d . In the case of a multicylinder pump, the suction and discharge accelerations will be the summation of the contributions from all the cylinders, n . The respective accelerations are given in equation 3.2.18 and 3.2.19.

$$a_s = \sum_{i=1}^n \frac{d_p^2}{d_s^2} a_{p_i} \quad (3.2.18)$$

$$a_d = \sum_{i=1}^n \frac{d_p^2}{d_d^2} a_{p_i} \quad (3.2.19)$$

The acceleration of the fluid causes pressure pulsations. This can be seen from Newton's second law, equation 3.2.20, stating that the product of mass m , and acceleration a , equals force.

$$F = ma \quad (3.2.20)$$

Equation 3.2.20 can be rewritten in terms of head, see equation 3.2.21.

$$H_a = \frac{La}{g} \quad (3.2.21)$$

As seen from equation 3.2.21, the acceleration pressure head H_a , is dependent on the acceleration a of the fluid, the length of the pipe L , and the gravitational constant g . The pattern of the friction and acceleration head in the suction and discharge pipe is illustrated in figure 3.23.

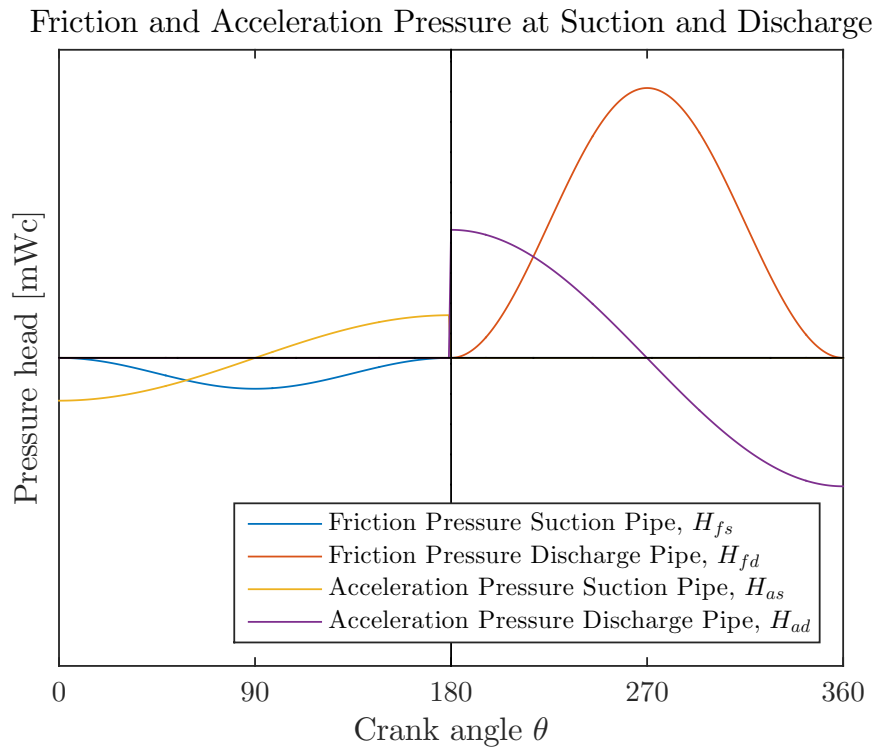


Figure 3.23: The friction and acceleration pressure in the suction and discharge pipe.

From figure 3.23, it is clear that the acceleration head is at a maximum at the beginning and end of each stroke, and zero at mid-stroke. For the pumping system illustrated in figure 3.23, it is also seen that the acceleration pressure pulsations dominates over the frictional pressure pulsations in

the suction pipe, and that the frictional pressure pulsations dominates over the acceleration pressure pulsations in the discharge pipe. This is typical for pumping systems where the suction pipe is relatively short, and the discharge pipe is relatively long, and not vertical.

The last dynamic pressure disturbance generated by the positive displacement pump is the low-amplitude waterhammer-type pressure disturbances that occur each time a pump valve opens or closes. These will be briefly described in section 3.2.3.7.

3.2.3.7 Waterhammer due to the Opening and Closing of Valves

The pulsations described in the two previous sections, 3.2.3.5 and 3.2.3.6, were due to the varying flow rate causing frictional pressure drop, and the rapid acceleration and deceleration of fluid. Waterhammer occurs when fluid is suddenly started, stopped or forced to change direction. When a valve is being opened or closed, the change in kinetic energy introduces a transient change in the static pressure in the pipe. In a pipe, this can lead to vibration and a hammering sound, and according to Smith and Zappe [40], this is the origin of the name waterhammer. The transient pressure wave travels from the valve to the end of the pipe and then reverses. This pressure wave travels at the speed of sound. The pressure rise, ΔH due to instantaneous valve closure can be found from the Joukowsky equation [30]

$$\Delta H = \frac{av}{g} \quad (3.2.22)$$

where a is the speed of sound in the fluid and v is the velocity of the flow that was stopped. This maximum pressure rise will only occur if the valve closes rapidly. If the valve closes slower than the time it takes for the pressure wave to travel the length of the pipe and back again, the returning pressure wave will dampen the outgoing waves so that the maximum pressure rise is reduced [40].

The pressure wave oscillates back and forth until it is dissipated by friction and other losses. The pressure rise due to waterhammer must be considered, because an uncontrolled pressure surges might destroy system pipes, valves and other components.

The pressure trace due to waterhammer, along with the pressure trace due to friction and acceleration is illustrated in 3.24. The figure shows the actual suction pressure trace during one full revolution a triplex single-acting pump.

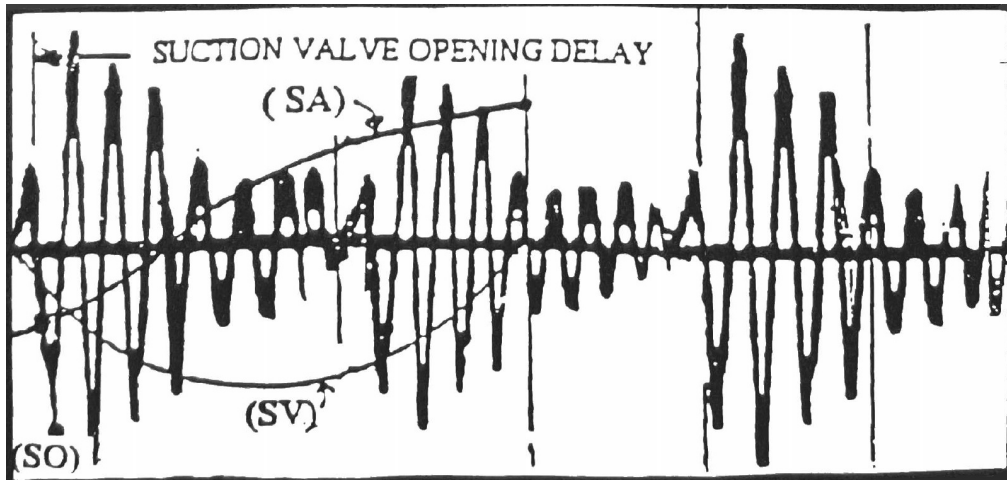


Figure 3.24: Pump inlet pressure trace. Pulsations due to acceleration are denoted SA, pulsations due to frictional pressure drop are denoted SV, and waterhammer due to the opening of the valve are denoted SO. Note how acceleration pressure overwhelms the friction pressure [29].

3.2.3.8 Cavitation

The phenomena of cavitation was explained in section 3.2.2.4. The highest danger of cavitation in the reciprocating pump is at the inlet, just like is was for the centrifugal pump. To avoid cavitation the local static pressure must be above the vapor pressure of the fluid. In figure 3.25 a sketch of a typical suction system with suction lift, z , is given. When the free water surface of the suction tank is placed lower than the inlet of the pump, the term suction lift applies. If the suction tank is placed higher than the inlet of the pump, the term suction head applies.

The absolute static pressure at the connection between the suction tank and the cylinder, H_s will be given by applying Bernoulli's equation along a streamline from the lower reservoir to the inlet of the reciprocating pump. See equation 3.2.23.

$$H_s = H_{atm} - \frac{v_s^2}{2g} - z - H_{fs} - H_{as} \quad (3.2.23)$$

The losses between the two points are accounted for as the frictional pressure drop H_{fs} and the acceleration head H_{as} .

Cavitation will start to occur when the absolute pressure H_s falls below the vapor pressure of the fluid H_{va} . This is equivalent with stating that the Net Positive Suction Head Available must not fall below the Net Positive

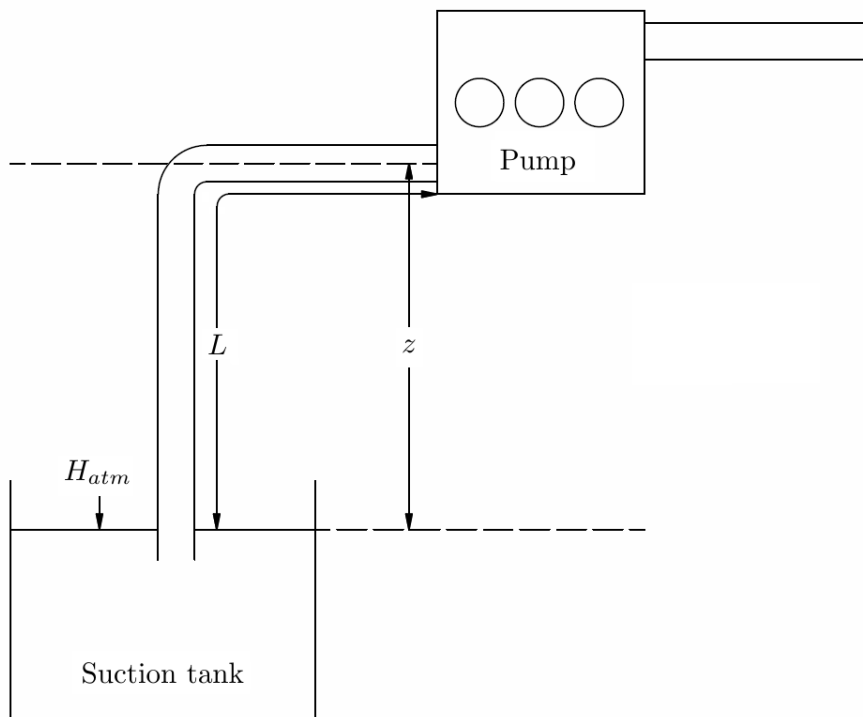


Figure 3.25: Typical suction system with suction lift, z .

Suction Head Required, as was done in section 3.2.2.4. From equation 3.2.23, it is seen that cavitation puts a limit on the suction height of the pump suction pipe, z , and the speed of the pump, because the acceleration head H_{as} is proportional to the square of the speed [38].

The upper part of figure 3.26 shows a suction pressure trace with a typical cavitation wave form. A typical cavitation waveform has sharp upward spikes and rounded bottoms. The downward spikes extend into the vapor pressure region. The spikes can not extend further because of the formation of vapor bubbles. The rounded bottoms are followed by sharp upward spikes due to the collapse of the cavitation bubbles [29].

The lower part of figure 3.26 show the suction pressure trace of the same pump with a suction stabilizer. A suction stabilizer is a pulsation dampener, and as seen from the lower trace in figure 3.26, the suction stabilizer greatly reduces the pressure pulsations in the suction of the pump. Pulsation dampeners are devices used to dampen the pressure pulsations of the reciprocating pump, and will be further discussed in section 3.2.3.9.

3.2.3.9 Pulsation Dampener

The pressure pulsations at the suction and discharge of a reciprocating pump might be damaging depending on the pressure conditions. Severe pressure pulsations might cause cavitation, vibration in pipes and inhibits safe operation of the pump. In systems where this is a problem, the pulsations can be dampened with devices called pulsation dampeners.

There are many different kinds of pulsation dampeners, and they can either dampen the pulsations or partly filter out pulsations so that they don't propagate downstream. Pulsation dampeners that dampen the actual pulsations can be described as accumulators. The accumulators are pressure vessels charged with gas having lower pressure than the system pressure at that point. This allows fluid to accumulate in the suction dampener at the closing of the suction valve, and in the discharge dampener at the opening of the discharge valve.

When the inlet valve closes, the fluid enters the inlet pulsation dampener and accumulates, and when the valve opens again we have a ready source of fluid right at the inlet of the pump. The pump then does not have to accelerate the whole string of fluid in the inlet pipe, and thus less energy is required. This inlet pulsation dampener, also referred to as suction stabilizer, ensures that less energy is required and that cavitation is avoided. The effect of the suction stabilizer is illustrated in figure 3.26, where the upper and lower curve shows the pressure trace without and with a suction

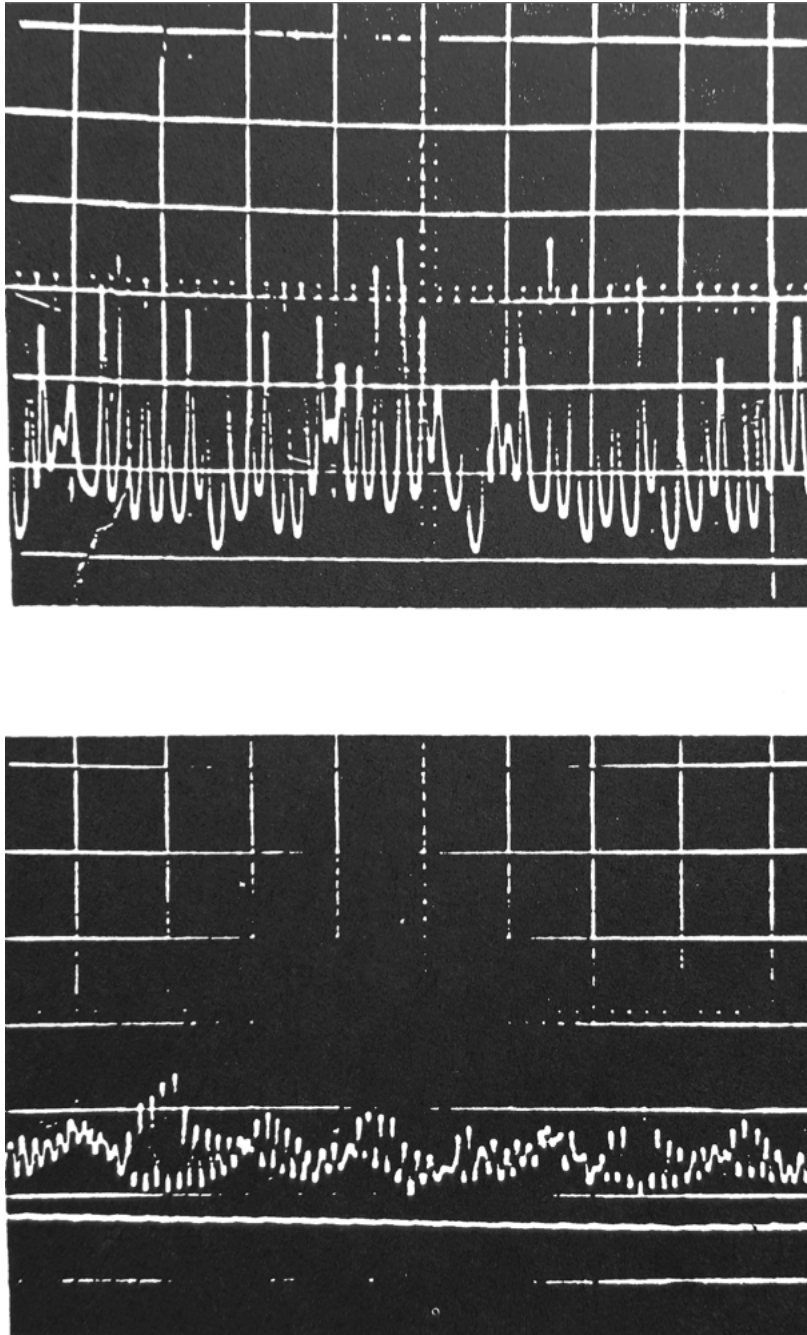


Figure 3.26: Suction pressure trace for the same pump without (upper) and with (lower) suction stabilizer. The upper pressure trace shows a typical cavitation waveform, where the downward pressure spikes have rounded bottoms. The lower pressure trace with suction stabilizer shows that the pressure spikes have lower amplitude and no rounded bottoms. The low-frequency cycles over which the high frequency is imposed, are the remnant of pump rotation-generated cycles [29].

stabilizer, respectively.

A pulsation dampener at the discharge works similarly to the suction stabilizer. On the discharge stroke of the pump, a certain amount of fluid accumulates in the dampener. When the pump starts the suction stroke, the pressure in the discharge dampener will be higher than the system pressure, and the fluid in the dampener will be pushed back into the system. In this manner we can achieve near steady-state flow in the system downstream of the pulsation dampener.

According to Cornell [12], both the discharge dampener and inlet stabilizer should be located within ten pipe diameters from the inlet or discharge.

3.2.3.10 Pump Rotational Speed

The rotational speed is one of the factors that greatly influences the performance of the pump. There is a tendency to choose a high rotational speed in order to reduce the size and weight of the pump. However, the speed of the pump can not be increased indefinitely. A higher rotational speed leads to higher piston velocity and consequently higher fluid velocity. A high fluid velocity may lead to hydraulic difficulties, especially through the valves. Another consideration is the increased friction and acceleration pressure pulsations at the pump suction and discharge. This again increases the danger of cavitation.

Finally, an excessive pump speed may not only lower the performance of the pump, but also increase parts wear and reduce the lifetime of the pump [29].

This is why pump rotational speed must be chosen with care.

3.2.4 Comparison between the Reciprocating and the Centrifugal pump

One of the main differences between the reciprocating and the centrifugal pump is that in reciprocating pumps mechanical energy is transferred periodically to the fluid, while in the centrifugal pump energy is transferred continuously. This means that in the reciprocating pump there is a periodic variation in the rate of pressure and flow with every stroke. In the centrifugal pump, the motion is uniform.

In a centrifugal pump, the flow rate is dependent on the head generated. In a reciprocating pump, the flow rate is dependent on pump rotational speed only, because a fixed volume of fluid is displaced for every rotation

of the crankshaft. The pressure generated in the reciprocating pump is dependent on the system flow resistance downstream of the pump.

The centrifugal pump is one of the most widely used pumps today [36]. It is very reliable, due to the simplicity of the moving parts, and the absence of self-acting valves. However, the efficiency of the centrifugal pump is low at small discharges and high pressures. This is because a centrifugal pump with a small discharge gives narrow flow passages, and high friction losses.

The reciprocating pump is suitable for high pressure and low flow rate applications. The advantages the reciprocating pump holds over the centrifugal pump, is a flow rate, head and speed flexibility, and an almost constant efficiency over a wide operating range. When these advantages outweighs the advantages of the centrifugal pump, being a smaller footprint, lower initial and maintenance costs, and lack of pulsations, the reciprocating pump is selected [37].

3.3 The Turgo Turbine

Parts of this section is taken from the project thesis *Desalination of Water by Reverse Osmosis* written in the fall of 2015 by Løken [26].

The objective of a turbine is to extract mechanical energy from a flowing fluid. The energy conversion in a turbine runner can be attributed to reaction and impulse forces. The change in the pressure of the fluid from the inlet to the outlet of the turbine is called the reaction part of the energy conversion. The change in the direction and magnitude of the fluid velocity is called the impulse part of the energy conversion [6].

According to the relationship between the reaction and impulse part of the energy conversion, a turbine is classified as either a reaction turbine or an impulse turbine. In a reaction turbine, the channels of the turbine runner must be completely filled with fluid in order to achieve a pressure drop. Unlike the reaction turbine, the impulse turbine has no pressure drop between the inlet and outlet of the runner, and the energy conversion is due to the impulse of the kinetic energy of the fluid hitting the turbine runner.

The science of extracting energy from water by rotating machinery has developed over hundreds of years, from the water wheel used by the Romans and Greeks [31], into the turbines seen all over the world today.

The Turgo turbine is an impulse turbine, greatly resembling the more widespread Pelton turbine. The Turgo turbine has gained renewed atten-

tion in research partly because of its potential in pico-hydropower, meaning hydropower resources of 5 kW or less. The Turgo turbine can handle higher flow rates than a Pelton turbine of the same diameter, and operate efficiently in lower head ranges than the Pelton turbine [10]. A smaller runner which is less expensive to manufacture than a Pelton wheel can lead to a lower installation cost in pico-hydropower installations. It can also be argued that the Turgo can operate for longer time periods and with less wear than Pelton turbines when the water contains sediments [2]. Another reason for the increased interest in the Turgo turbine is its applicability for energy recovery of discharged water in public water systems [19].

However, the published work on the Turgo turbine is not vast. This section aims to gather the relevant information on design of Turgo turbines, taken from published work on the Pelton turbine, as well as some sources investigating only the Turgo turbine. Firstly, because the Pelton turbine is more widespread than the Turgo turbine, this discussion will start by considering the differences between the Pelton and the Turgo turbine, and describe the flow of water in the Turgo turbine.

As seen from figure 3.27, both turbines have buckets placed along the periphery. A water jet enters the buckets through nozzles, where the available pressure energy of the water is converted into kinetic energy. The flow through the buckets of a Turgo and a Pelton is illustrated in figure 3.28.

As seen in figure 3.28, a water jet hits the buckets of both the Turgo and the Pelton with high velocity. The water jet is deflected through the surface of the buckets, and leaves the bucket with a relative velocity opposite to the inlet velocity. The pressure at both the inlet and outlet of the buckets is atmospheric, and the total available energy to be extracted by the turbine, is the kinetic energy of the water jet hitting the buckets.

The difference between the two lies in the shape of the buckets and the flow through the buckets. The water jet enters the buckets of the Turgo turbine at an angle, and does not split the water jet into two parts.

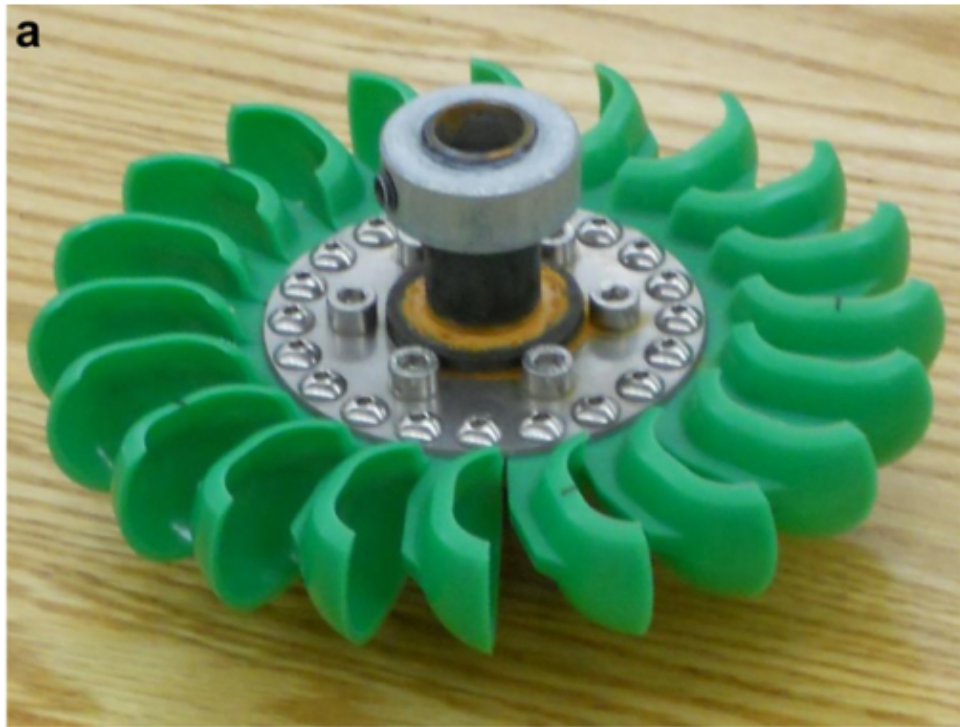


Figure 3.27: Photos of a Turgo turbine (a) and a Pelton turbine (b) [10].

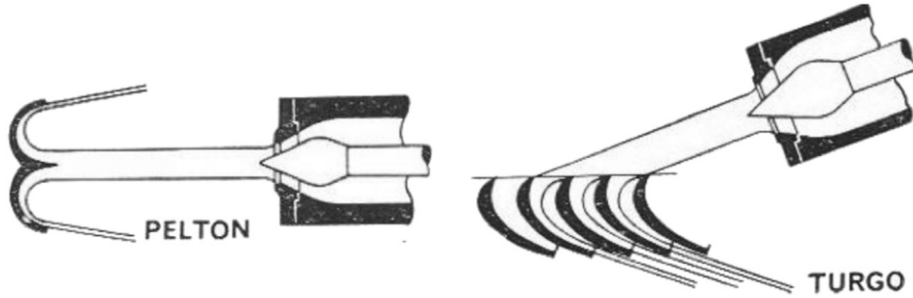


Figure 3.28: Difference in direction of water flow between the Pelton (left) and Turgo (right) turbines [19].

3.3.1 Energy Conversion

The energy conversion in the Turgo turbine can be described by considering the velocity diagrams at the inlet and outlet of the runner, in a similar manner as for the centrifugal pump in section 3.2.2.1.

The velocity diagrams at the inlet and outlet of a Turgo bucket is depicted in figure 4.8.

In section 3.2.2.1 the Euler equation 3.2.6 was introduced, expressing the theoretical head of a pump depending on the velocity changes through the impeller. The Euler equation is one of the most important equations in turbomachinery and applies to turbines as well as pumps. In a turbine, hydraulic energy in the fluid is transferred to mechanical energy in the runner, not the other way around. The Euler equation therefore expresses the hydraulic energy H transferred to the runner as

$$H = \frac{u(c_{u1} - c_{u2})}{g} \quad (3.3.1)$$

In the Turgo runner, subscript 1 denotes the inlet of the bucket and subscript 2 denotes the outlet of the bucket. The water enters and leaves the bucket at approximately the same radial distance from the axis of rotation, thus the runner peripheral velocity, u , is the same at inlet and outlet, and the subscripts are dropped. The hydraulic power transferred to the runner becomes

$$P = \rho Q u (c_{u1} - c_{u2}) \quad (3.3.2)$$

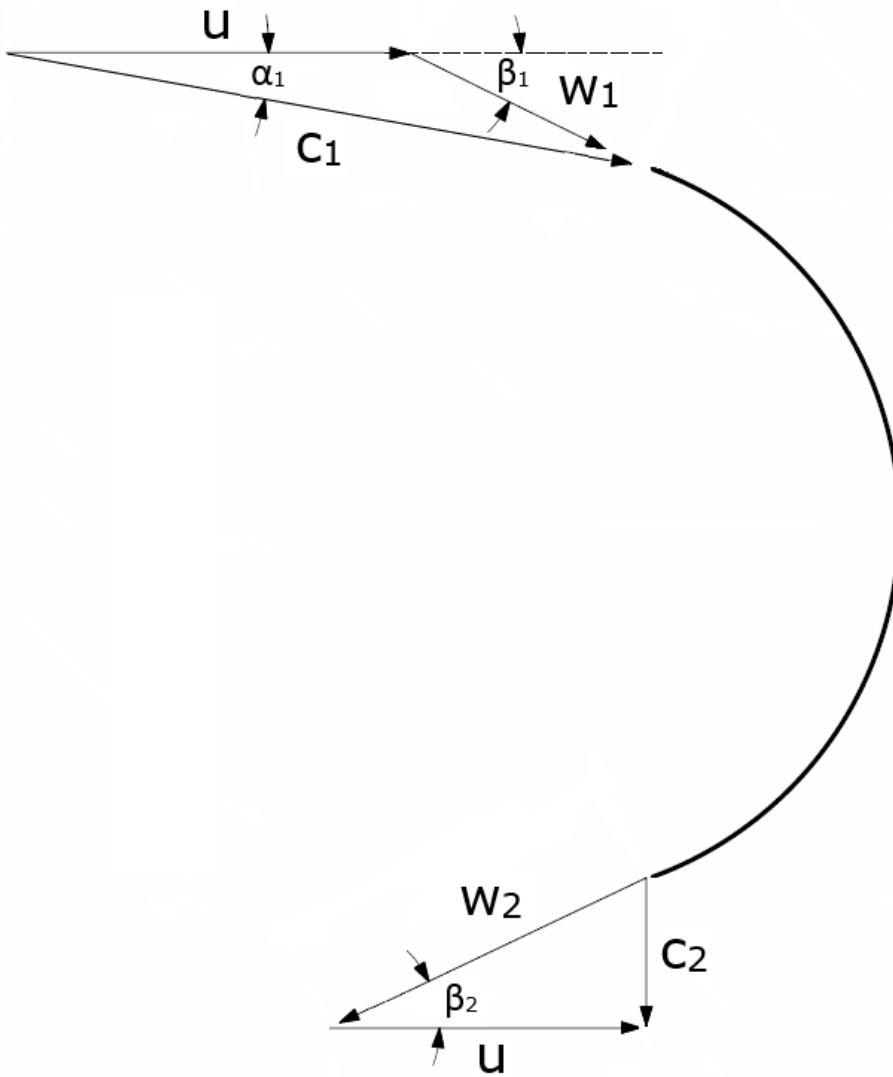


Figure 3.29: Velocity diagrams at inlet and outlet of Turgo bucket [27].

The available hydraulic power is given by

$$P = \rho g Q H_n \quad (3.3.3)$$

where H_n denotes the available head of the water before being converted to kinetic energy in the nozzle. The hydraulic efficiency is given by the ratio between the available power and the power output from the runner. By considering equations 3.3.2 and 3.3.3, the hydraulic efficiency is expressed as

$$\eta_h = \frac{u(c_{u1} - c_{u2})}{gH_n} \quad (3.3.4)$$

By assuming an absolute inlet velocity in the peripheral direction of

$$c_{u1} = c_1 \cos \alpha_1 = \sqrt{2gH_n} \cos \alpha_1 \quad (3.3.5)$$

and an absolute outlet velocity of $c_{u2} = 0$, the maximum efficiency given from equation 3.3.4 is achieved when

$$u = \frac{1}{2} \sqrt{2gH_n} \quad (3.3.6)$$

From equation 3.3.4 this would give a maximum efficiency of unity. In reality there are always losses involved, and we assume a hydraulic efficiency of $\eta_h = 0.96$. This gives an optimum peripheral velocity of

$$u = 0.48 \sqrt{2gH_n} \quad (3.3.7)$$

The total efficiency of the Turgo turbine η_t will be given as the product of the hydraulic η_h , the mechanical η_m and the volumetric efficiency η_V , as shown in equation 3.3.8.

$$\eta_t = \eta_h \eta_m \eta_V \quad (3.3.8)$$

The total efficiency η_t describes the percentage of the available energy transformed to useful energy in the turbine. The efficiency expresses the effect of losses that reduce the total energy transferred to the turbine. The volumetric efficiency quantifies the losses of the water not hitting any buckets, and the mechanical efficiency quantifies the mechanical friction losses.

3.3.2 Jet Inlet Angle

The jet inlet angle α_1 is the absolute angle of the water relative to the bucket peripheral velocity u . This angle depends on the adjustment of the nozzle. The literature does not claim one specific inlet angle to be more efficient than others. The inlet angle will also depend on the shape of the buckets. By looking at equation 3.3.4 describing the hydraulic efficiency of the runner, one can however assume that an inlet angle chosen as small as possible would maximize the efficiency. This is because the hydraulic efficiency is a function of the absolute velocity in the peripheral direction, given by $c_u = c_1 \cos \alpha$.

3.3.3 Shape of Buckets

The discussion of the Turgo turbine so far has covered the theoretical energy transfer from the water to the turbine. To achieve an energy transfer as close to the theoretical as possible, the shape of the turbine buckets are of great importance. This is the part of the Turgo turbine design that is not very well covered in the literature. There is however made certain efforts to describe design guidelines and equations. The performance and design of the Turgo turbine has been investigated with both mathematical, experimental and numerical methods.

The jet inlet angle α_1 affects the optimum angle of the bucket at the inlet. If it is assumed that the relative inlet angle of the water to the bucket β_1 is equal to the buckets inlet edge, the relative inlet angle β_1 and thus also the constructional angle of the bucket inlet can be found from trigonometry when α_1 , u and c_1 is known. The assumption that the constructional angle of the bucket inlet and the relative inlet angle of the water to the bucket is equal is according to Gaiser et al. [19] called the no-shock condition. This ensures smooth entry of the water to the bucket and reduces losses. The outlet angle of the bucket β_2 should be chosen to equal the outlet angle in order to turn the water around as much as possible, and maximize the energy transfer to the runner.

Correa et al. [28] have outlined a design procedure for the buckets of the Turgo turbine using a two-dimensional potential flow. According to Bertin and Cummings [23], one can obtain stagnation streamlines in the shape of an oval, by combining the elementary flow functions suggested by Rankine. This is known as a Rankine oval. The Rankine oval is valid for incompressible and inviscid flow fields. For this incompressible and inviscid flow field, both a velocity and a stream function can exist. Since any streamline in a potential flow can also be considered a solid surface, an

appropriate streamfunction can be chosen to simulate the bucket surface.

Correa et al. chose the inlet and outlet angles of the bucket, and then solved the streamfunction to find the desired shape of the bucket surface. An additional paper was later published by Correa, Andrade and Asuaje [27], where a CFD analysis of the flow over the buckets using ANSYS CFX was presented. This was done to find the numerical solution of the streamline's path through the bucket and compare it to the solution of the streamfunction describing the bucket surface. One of the most important findings was that the effects of the centrifugal force acting on the runner caused the streamline to deviate slightly from the centerline of the bucket to the outside. However, the mean deviation between the path of the streamline predicted by the numerical results, and the theoretical path imposed by the bucket surface was only 5.6 percent.

Correa et al. also made a theoretical consideration of the losses, such as the friction and turbulence losses and effects of water missing the buckets. They estimated the total efficiency of the turbine designed to have a mean value of 80.8 percent, where the mechanical efficiency was taken as $\eta_m = 0.97$ and the volumetric efficiency was taken as $\eta_V = 0.97$.

Finally, Correa et al. [28] suggested a useful range for the geometric parameters of the runner bucket as a function of the jet diameter d_j . The work of Correa et al. is however not validated by experiments on the turbine runner designed.

3.3.4 Number of Buckets

Gaiser et al. [19] have performed experiments on a low-cost Turgo turbine to determine the effects of different design parameters. The parameters considered were the nozzle diameter, jet inlet angle, number of blades and peripheral velocity of the runner. By adjusting these parameters and performing several experiments, they developed a second order regression model to predict the efficiency as a function of each parameter, and the interaction between each of these. Based on this they predicted the optimum value of each of these parameters through four unique design equations. These experiments were however all performed on the same turbine, and it might therefore be assumed that the results are somewhat specific for this turbine.

The number of buckets chosen in the design of the Turgo turbine in section 4.1.2, is therefore based on requiring that no water should be lost.

3.3.5 Parameters Influencing the Efficiency

The work of Gaiser et al. did however assert that the factors affecting the turbines efficiency the strongest were the nozzle diameter and the the ratio of the peripheral velocity u to the absolute peripheral velocity c_{u1} of the water entering the bucket. The strong influence of this velocity ratio is also confirmed by the expression for the hydraulic efficiency given in equation 3.3.4. Gaiser et al. also asserted that the interaction between the jet angle and the number of buckets greatly influenced the turbine efficiency. This is also demonstrated in the design of the Turgo turbine in section 4.1.2, because the requirement to not lose any water leads to an expression for the minimum number of buckets involving the jet inlet angle.

4 System Design

The motivation for this thesis was to design a reverse osmosis system that is small, lightweight, durable and easy to transport. Because of the intended application area, another important consideration was to make the system simple and robust.

In this thesis, four different system configurations have been considered. The four solutions vary according to the type of high pressure pump and energy recovery device that is utilized.

When designing the high pressure pump, the most important requirements are the capacity and pressure, or in other words, the flow rate and generated head. The pressure requirement for the high pressure pump is given by the osmotic pressure of the feedwater. Considering that the feedwater could be either brackish water or seawater, the feedwater with the highest osmotic pressure must serve as a basis for the pump pressure requirement. As mentioned in section 3.1, the osmotic pressure of brackish water is in the range of 15 to 40 bar, and the osmotic pressure of seawater is in the range of 65 to 75 bar.

The flow rate of the system could be chosen more freely. The limiting factor for the feedwater flow rate is the reverse osmosis membrane. The membrane will have a maximum capacity. For this reason, the feedwater flow rate requirement for a few of the system designs was chosen to be the one equaling the maximum flow rate of the smallest RO membranes on the market.

The first solution considered is a centrifugal pump and a Turgo turbine. Both chosen because of their robustness and mechanical simplicity. They are also suited for running at high speeds, thus reducing the necessary size of the components.

The second solution considered is a reciprocating pump and a Turgo turbine. A system very similar to this was already designed and the final parts assembled during the work with this master's thesis. The only difference is that the turbine installed in the system is a Pelton turbine and not a Turgo

turbine. The investigation of this solution therefore allowed for performing measurements on a system that was already assembled in the laboratory.

The third solution considered is a reciprocating pump without energy recovery.

The fourth and final solution considered is a reciprocating pump with integrated energy recovery.

The flow and head specifications that constituted the basis for all four system designs are given in table 4.1.

Table 4.1: Flow and head specifications.

DESIGN BASIS		Centrifugal Pump and Turgo Turbine	Reciprocating Pump and Turgo Turbine	Reciprocating Pump without Energy Recovery	Reciprocating Pump with Energy Recovery	
PUMP						
Density of water	ρ	1000	1000	1000	1000	kg/m ³
Required delivery flow rate	Q	100	40	20	20	l/min
Required delivery flow rate	Q	0.001667	0.000667	0.000333	0.000333	m ³ /s
Required delivery pressure	p	65	7-210	80	80	bar
Required delivery pressure	H	663	71 - 2141	815	815	mWc
ENERGY RECOVERY DEVICE						
Density of concentrate	ρ	1050	1050	-	1050	kg/m ³
Available flow of concentrate	Q	30	20	-	12	l/min
Available flow of concentrate	Q	0.0005	0.0003	-	0.0002	m ³ /s
Available pressure of concentrate	p	63	50	-	77	bar
Available pressure of concentrate	H	612	612	-	612	mWc

As seen from table 4.1, the flow and head specifications differ between the different solutions. The solution with the centrifugal pump and the Turgo turbine was the first to be considered. The pressure requirement for this solution is based on the assumption of a 3 percent pressure loss through the RO membrane and a membrane efficiency of 70 percent, meaning that the remaining 30 percent of the feedwater is passed to the turbine as high pressure concentrate. The flow rate was not reduced further than 100 l/min, because the centrifugal pump was already in a flow and pressure range that is well outside the traditional range for the centrifugal pump. The flow and head specifications for the system comprising a reciprocating pump and a Turgo turbine were given by the system that was already built. The flow rate constituting the basis for both the reciprocating pump designs are based on the feedwater capacity of the smallest RO membranes

on the market. This means designing the system for a feed flow rate of 20 liters per minute. The pump pressure requirement was chosen to be a maximum of 80 bar.

The rest of this section will be devoted to describing the details and the design procedures for the four solutions discussed above.

4.1 The Centrifugal Pump and the Turgo Turbine

4.1.1 Design of the Centrifugal Pump

A pump is designed to meet given requirements of capacity and pressure, or in other words, given requirements of flow rate and generated head. The design will be optimized in regard to this operating point, and it is therefore called the best efficiency point (BEP). With these parameters given the pump designer needs to choose the type and design of the pump.

The requirements for the reverse osmosis system as given in section 4 was a flow rate of $Q = 100 \text{ l/min}$ and a head of $p = 65 \text{ bar}$.

With these parameters given, the next step was to choose the rotational speed of the pump. The speed was maximized in order to reduce the size of the pump. The maximum possible speed for a pump driven by an electric motor without a gearbox, depends on the frequency of the supply current and the number of pole pairs per phase in the motor. The maximum rotational speed, n , is given by

$$n = \frac{60f}{Z_p} \quad (4.1.1)$$

where f is the frequency of the supply current given in Hz, and Z_p is the number of pole pairs per phase in the motor. With a minimum of one pole pair per phase, it is seen from equation 4.1.1 that the maximum rotational speed is $n = 3000 \text{ rpm}$ on a 50 Hz supply current. This was the rotational speed chosen for the pump.

A first approach to the design of the impeller was done by applying the equations and assumptions of section 3.2.2.1. It was found that the pump would require several stages to generate the required head, and the number of stages chosen was seven. A more detailed design approach taking the effect of a finite number of blades and losses into account was performed

next. Two different impeller designs were developed, here on out referred to as the *standard* and *adjusted* design.

4.1.1.1 Impeller

With the aid of the book *Impeller Pumps* by Łazarkiewicz and Troskoleński [25], the design procedure for the impeller was performed. Some flow parameters had to be chosen. Often times, parameters such as this can be chosen on the basis of empirical values and charts as the ones developed by Stepanoff [41]. The charts are given for certain ranges of flow and head, i.e., certain ranges of specific speed. The centrifugal pump designed for the reverse osmosis system was outside the specific speed range of the charts, and the parameters was therefore chosen within reasonable values given by empirical knowledge as found in the literature [25]. The complete design procedure for the pump is summarized here. A radial view of an impeller blade including nomenclature is given in figure 4.1.

First off, the total, hydraulic, volumetric and mechanical efficiencies were assumed to be as given in table 4.2.

Table 4.2: Assumed pump efficiencies

η_p	78 %
η_h	85 %
η_V	96 %
η_m	96 %

The total pump efficiency, η_p , is the product of the other efficiencies

$$\eta_p = \eta_h \eta_V \eta_m \quad (4.1.2)$$

The efficiencies account for the losses in the different parts of the pump as described in section 3.2.2.1.

Shaft and hub diameter

The shaft input power was found from the following equation

$$P_{sh} = \frac{\rho g Q H}{\eta_p} \quad (4.1.3)$$

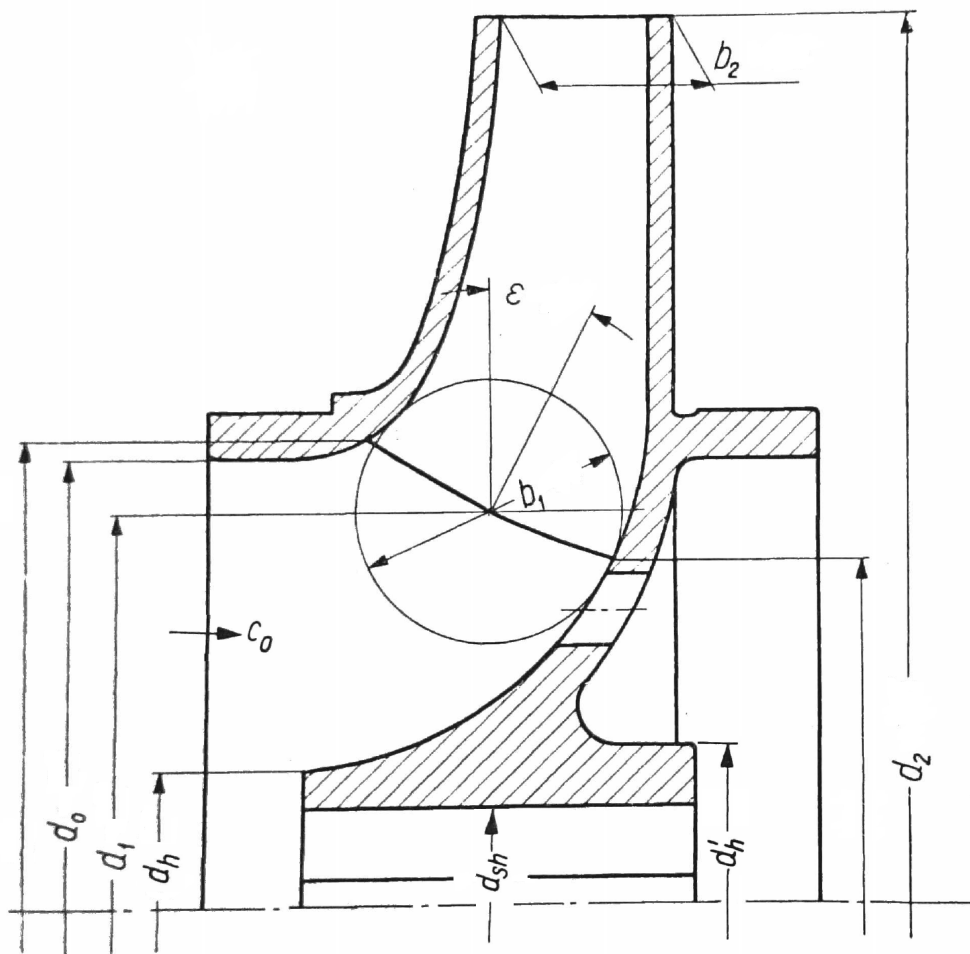


Figure 4.1: Radial view of an impeller blade of single curvature, slightly extended forward [25].

Allowing for a reserve of 17 %, the required motor power was determined as

$$P_m = 1.17P_{sh} \quad (4.1.4)$$

Assuming that the shaft is made from a material with a tensile strength of 5500×10^5 Pa, the maximum permissible torsional stress was taken as $\tau = 450 \times 10^5$ Pa.

The minimum diameter of the shaft was then found from

$$d_{sh,min} = \sqrt[3]{\frac{49P_m}{\tau n}} \quad (4.1.5)$$

Allowing for radial thrust due to non-uniformity of the pressure distribution around the impeller, the shaft diameter was taken as

$$d_{sh} = 1.14d_{sh,min} \quad (4.1.6)$$

The hub diameter on the inlet side

$$d_h = (1.3 - 1.4)d_{sh} \quad (4.1.7)$$

The hub diameter on the outlet side

$$d_h = (1.35 - 1.5)d_{sh} \quad (4.1.8)$$

Inlet diameter

Because of leakages the pump was designed for a slightly larger flow rate than the requirement at BEP

$$Q' = \frac{Q}{\eta_V} \quad (4.1.9)$$

By choosing the meridional velocity, c_{m1} , at the blade inlet, the inlet area and inlet diameter was found from continuity. The inlet velocity at the impeller eye was taken as

$$c_0 = 0.95c_{m1} \quad (4.1.10)$$

The inlet velocities were chosen below a certain limit to avoid cavitation at the inlet as described in section 3.2.2.4. See table 4.3 for the cavitation check performed for both impellers.

Table 4.3: Checking for cavitation at impeller inlet

	Standard pump design	Adjusted pump design	
a	1.8	1.8	-
b	0.23	0.23	-
c_{m1}	2.30	2.12	m/s
u_1	6.12	7.84	m/s
H_{atm}	10.32	10.32	m
H_{va}	0.32	0.32	m
H_s	1	1	m
$NPSH_R$	0.92	1.13	m
$NPSH_A$	9.00	9.00	m

As seen from table 4.3 the centerline of the pump can be raised several meters above the lower reservoir (increasing H_s), and still satisfy the condition that

$$NPSH_A > NPSH_R \quad (4.1.11)$$

The free inlet cross-sectional area at the impeller eye

$$A_0 = \frac{Q'}{c_0} \quad (4.1.12)$$

The hub inlet cross-sectional area at impeller eye

$$A_h = \frac{\pi d_h^2}{4} \quad (4.1.13)$$

The total inlet cross-sectional area at the impeller eye

$$A'_0 = A_0 + A_h \quad (4.1.14)$$

The diameter of the impeller eye inlet was finally found as

$$d_0 = \sqrt{\frac{4A'_0}{\pi}} \quad (4.1.15)$$

The blade was chosen to be slightly extended forward and for the standard design impeller the blade inlet diameter was chosen as

$$d_1 = 0.939d_0 \quad (4.1.16)$$

Blade inlet angle

The peripheral velocity at the blade inlet

$$u_1 = \frac{\pi d_1 n}{60} \quad (4.1.17)$$

Assuming that the flow into the impeller is without rotation, i.e., the velocity component c_{u1} is zero, the inlet angle $\alpha_1 = 90^\circ$, as shown in figure 3.10. The inlet angle β_1 was then given by

$$\tan \beta_1 = \frac{c_{m1}}{u_1} \quad (4.1.18)$$

Experimental measurements on centrifugal pumps have shown that the discharge at BEP is less than that corresponding to a velocity $c_{m1} = u_1 \tan \beta_1$ [25]. The blade angle was therefore increased by $\delta_1 = 3^\circ$ and

$$\beta'_1 = \beta_1 + \delta_1 \quad (4.1.19)$$

Inlet width

When finding the inlet area A_1 for the chosen velocity c_{m1} it was taken into account that the flow area found by continuity is less than the actual flow area A_1 because of the constriction of the inlet by the blades. The constriction coefficient is given by

$$\phi_1 = \frac{t_1}{t_1 - s_{u1}} \quad (4.1.20)$$

where $t_1 = \frac{\pi d_1}{Z}$ is the pitch length between the Z blades and s_{u1} is the projection of the blade thickness s_1 on the circumference.

The blade inlet area was then found as

$$A_1 = \phi_1 \frac{Q'}{c_{m1}} \quad (4.1.21)$$

Finally, the width of the impeller was given by

$$b_1 = \frac{A_1}{\pi d_1} \quad (4.1.22)$$

Impeller outlet diameter

To find the outlet diameter, d_2 , the Euler equation 3.2.6 was applied. By assuming no rotation at the inlet, $c_{u1} = 0$ and using the relations from the velocity diagram in figure 3.10, the expression for the peripheral velocity at the outlet was rewritten as

$$u_2 = \frac{c_{m2}}{2 \tan \beta_2} + \sqrt{\left(\frac{c_{m2}}{2 \tan \beta_2}\right)^2 + gH_{t\infty}} \quad (4.1.23)$$

The theoretical head with an infinite number of blades was found by applying the hydraulic efficiency η_h and Pfleiderer's correction for slip, C_p [25]

$$H_{t\infty} = H_t(1 + C_p) = \frac{H}{\eta_h}(1 + C_p) \quad (4.1.24)$$

H is the required head delivered per stage at BEP, and H_t is the theoretical head with a finite number of blades.

The velocity c_{m2} was decided as $c_{m2} = 0.7c_{m1}$. The outlet angle β_2 was chosen in the range 15° to 35° , based on experimental data [25].

Finally, the outlet diameter was found as

$$d_2 = \frac{60u_2}{\pi n} \quad (4.1.25)$$

Impeller outlet width

The impeller outlet width was found in the same manner as the impeller inlet width, by considering the constriction of the outlet by the blades.

Checking the chosen number of blades

Finally, the chosen number of blades, Z , was checked using the empirical formula

$$Z = 6.5 \frac{d_2 + d_1}{d_2 - d_1} \sin \frac{\beta'_1 + \beta_2}{2} \quad (4.1.26)$$

Calculating the shape of the blades

The shape of the blades was calculated by the point by point method as described in *Impeller Pumps* by Łazarkiewicz and Troskoleński [25]. See table 4.5 and 4.7.

The blades of the impeller were chosen to be of single curvature, with the inlet slightly extended forward as depicted in figure 4.1. With forward extended blades, the velocity c_{m1} makes an angle ϵ_1 with the radial component c_{r1} as shown in figure 4.2.

The constructional inlet angle of the blade is then given by

$$\tan \beta''_1 = \tan(\beta_1 + \delta_1) \cos \epsilon_1 \quad (4.1.27)$$

Two different impellers were designed by the procedure given above. The *standard design* was designed to have optimal dimensions by the standard procedure, and the *adjusted design* was adjusted to reduce the friction loss in the impeller channels, i.e., the width and length of the channels was maximized. The final dimensions of both impellers are given in table 4.4.

4.1.1.2 Guide-ring, U-turn and Return Passage

The casing between the impellers must transfer the kinetic energy from the outlet of the impeller to pressure energy, and remove the rotating component of the flow from the impeller outlet, such that the flow conditions into the next stage are optimal. The elements of the casing between the impellers were chosen to be a vaneless guide-ring, a vaneless U-turn and a vaned return passage.

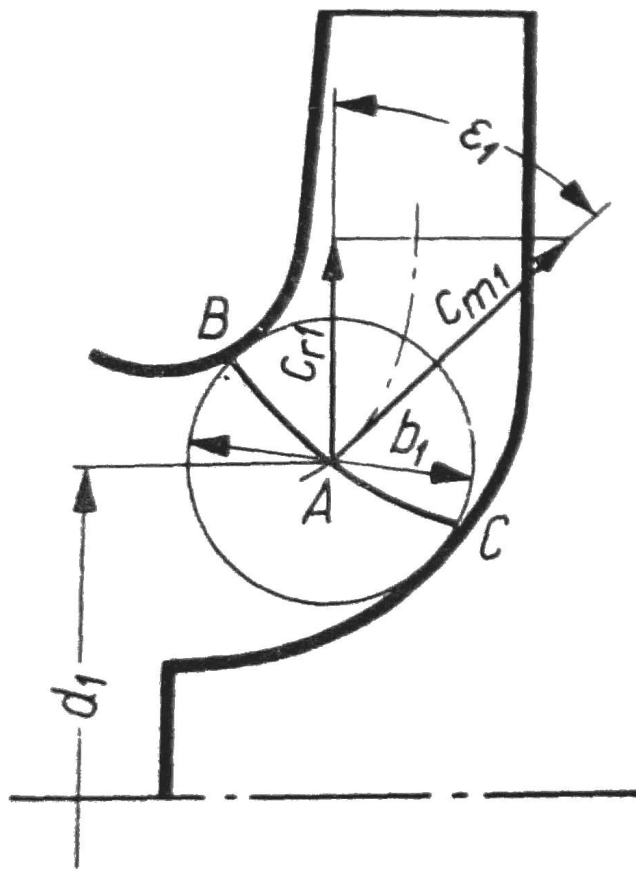


Figure 4.2: Radial view of an impeller blade of single curvature, slightly extended forward [25].

Vaned return passage

The flow in the gap between the rotating impeller and the stationary casing is a free vortex. For free vortices the following relation applies

$$c_u r = \text{constant} \quad (4.1.28)$$

The inlet diameter of the return passage was chosen to equal the outlet diameter of the impeller, so that the c_u velocity component at the inlet to the return passage could be assumed to be the same as at the outlet of the impeller.

The c_m velocity component at the inlet of the return passage was found by considering the constriction of the inlet by the blades of the return passage, as described in section 4.1.1.1.

With both velocity components known, the inlet angle of the blades in the return passage was found

$$\tan \alpha = \frac{c_m}{c_u} \quad (4.1.29)$$

The shape of the blades in the return passage was then found by the point by point method, in a similar manner as the shape of the impeller blades. See table 4.6 and 4.8 for the dimensions of the return passages for both impellers designed.

4.1.1.3 Pump Characteristic

The pump characteristic for the standard design is given in figure 4.3. The curve denoted H includes friction loss and impact losses, and is the predicted performance of the pump. The friction losses were approximated as $\Delta H_{friction} = kQ^2$, where the constant k is a friction coefficient approximated as $k = 150000$. The impact losses were approximated as $\Delta H_{impact} = j(Q - Q_{BEP})^2$, where the constant j was set to $j = 150000$ and $Q_{BEP} = 0.00167$ is the design flow rate at the best efficiency point. The values of the loss coefficients are very high, but due to narrow passages of the impeller this was considered reasonable.

4.1.1.4 Pump Dimensions

The complete specification data basis and the inlet and outlet values for the impeller and return passage for both designs are given in table 4.4.

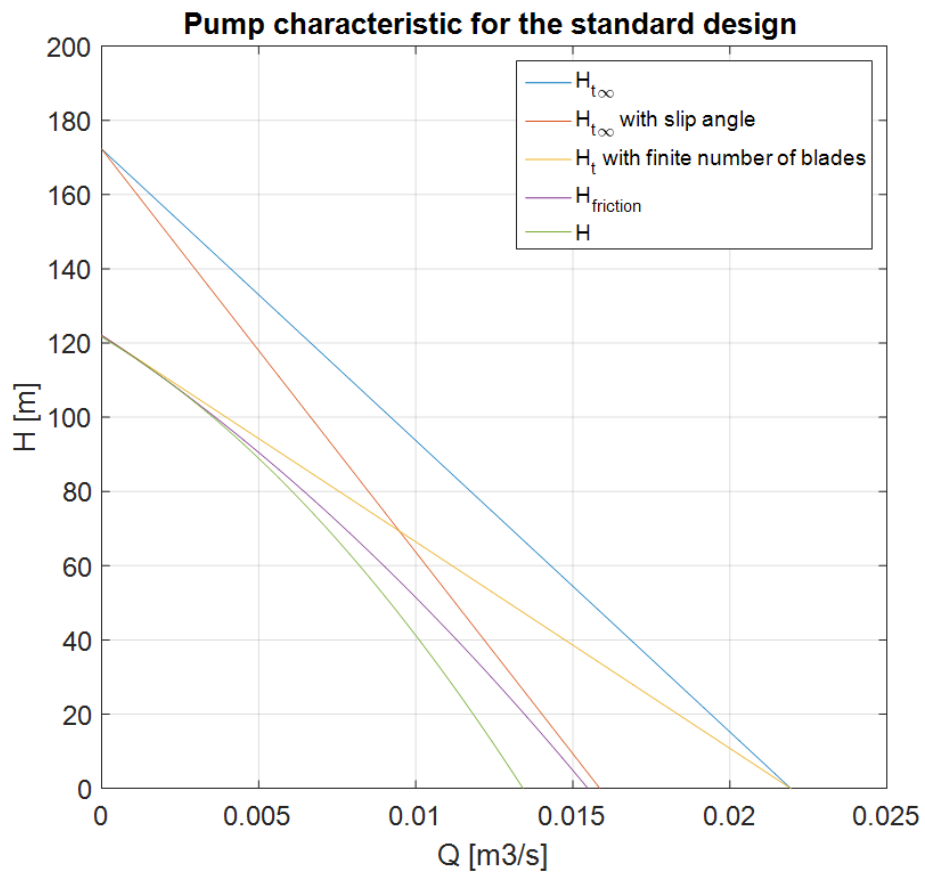


Figure 4.3: Pump characteristic for the standard design.

The shape of the blades of the impeller and return passage for both designs are given in table 4.5, 4.7, 4.6 and 4.8.

The shape of the impellers are pictured in figure 4.4 and 4.5.

Finally, a cutaway of the casing containing the seven pump stages for both impellers are shown in figure 4.6 and 4.7.

More detailed drawings are given in appendix B.

Table 4.4: Specification basis and inlet and outlet values for impeller and return passage for both pump designs

PUMP SPECIFICATIONS AND DIMENSIONS		STANDARD	ADJUSTED	
FLOW AND HEAD, CONSTANTS, EFFICIENCIES AND ROTATIONAL SPEED				
Gravitational constant	g	9.81	9.81	m/s ²
Density of water	ρ	1000	1000	kg/m ³
Required delivery flow rate	Q	100	100	l/min
Required delivery flow rate	Q	0.00167	0.00167	m ³ /s
Volumetric efficiency	η_V	0.96	0.96	-
Flow rate including leakage	Q'	0.00174	0.00174	m ³ /s
Rotational speed	n	3000	3000	rpm
Angular rotational speed	ω	314	314	rad/s
Required delivery pressure	p	65	65	bar
Required delivery pressure	p	6500000	6500000	Pa
Required delivery pressure	H	663	663	m
Total pump efficiency	η_p	78	78	%
Mechanical efficiency	η_m	96	96	%
Hydraulic efficiency	η_h	85	85	%
Shaft input power	P_{sh}	13889	13889	W
Motor power	P_m	16250	16250	W
SHAFT AND HUB				
Shaft tensile strength	$T.S.$	5.50E+08	5.50E+08	Pa
Torsional stress	τ	4.50E+07	4.50E+07	Pa
Shaft diameter	$d_{sh,min}$	0.0181	0.0181	m
Chosen shaft diameter	d_{sh}	0.0206	0.0206	m
Hub diameter inlet	d_h	0.0268	0.0268	m
Hub diameter outlet	d'_h	0.0278	0.0278	m
IMPELLER				
Number of vanes	Z_i	4	2	-
Inlet velocity	c_{m1}	2.30	2.12	m/s
Inlet velocity	c_0	2.19	1.52	m/s
Free inlet cross-sectional area	A_0	0.000795	0.004389	m ²
Cross-sectional area of hub	A_h	0.000563	0.000563	m ²
Total inlet cross-sectional area	A'_0	0.001357	0.001099	m ²
Inlet diameter impeller eye	d_0	0.0416	0.0460	m
Inlet diameter impeller blade	d_1	0.0390	0.0499	m
Inlet peripheral velocity	u_1	6.12	7.84	m/s
Blade inlet angle	β_1	20.59	15.14	
Angle of incidence	δ_1	3.00	3.00	
Increased blade inlet angle	β'_1	23.59	18.14	
Angle between c_{m1} and the radial	ϵ_1	27.00	27.00	
Constructional blade inlet angle	β''_1	21.26	0.00	

PUMP SPECIFICATIONS AND DIMENSIONS		STANDARD	ADJUSTED	
Pitch	t_1	0.0306	0.0784	m
Blade thickness	s_1	0.0050	0.0150	m
Blade thickness projected	s_{u1}	0.0125	0.0580	m
Inlet constriction coefficient	ϕ_1	1.69	3.83	-
Blade inlet area	A_1	0.001275	0.003136	m ²
Inlet width of impeller	b_1	0.0104	0.0200	m
Number of stages		7	7	-
Head per stage	H_{stage}	95	95	m
Theoretical head per stage	$H_{ts}t_{age}$	112	112	m
Outlet meridional velocity	c_{m2}	1.61	1.49	m/s
Outlet angle	β_2	25.00	20.00	
Pfleiderer's correction factor for slip	C_p	0.4109	0.7776	-
Outlet peripheral velocity	u_2	41.11	46.25	m/s
Outlet diameter	d_2	0.2617	0.2944	m
Outlet velocity circumferential component	c_{u2}	37.66	42.17	m/s
Outlet velocity corrected for slip	c_{u3}	26.69	23.72	m/s
Pitch	t_2	0.2055	0.4625	m
Blade thickness	s_2	0.0050	0.1440	m
Blade thickness projected	s_{u2}	0.0118	0.4210	m
Outlet constriction coefficient	ϕ_2	1.06	11.15	m
Outlet area	A_2	0.001144	0.01304	m ²
Outlet width of impeller	b_2	0.0014	0.0141	m
Slip angle	β'_2	6.37	3.77	
Checking calculated number of blades	Z_i	4	3	-
VANED RETURN PASSAGE				
Number of vanes return passage	Z_r	5	5	-
Inlet diameter return passage	d_7	0.2617	0.2944	m
Outlet diameter return passage	d_8	0.0456	0.0550	m
Inlet width return passage	b_7	0.0014	0.0141	m
Gap between impeller outlet and casing	$r_4 - r_2$	0.0030	0.0030	m
Pitch	t_7	0.1644	0.1850	m
Thickness of blades	s_7	0.0050	0.0050	m
Blade thickness projected	s_{u7}	0.0708	0.1656	m
Constriction coefficient	ϕ_7	1.76	9.55	-
Inlet area return passage	A_7	0.001144	0.013038	m
Inlet velocity circumferential component	c_{u7}	37.66	42.17	m/s
Inlet velocity meridional component	c_{m7}	2.66	1.27	m/s
Inlet angle return passage	α_7	4.05	1.73	
Outlet angle return passage	α_8	90	90	
Outlet width return passage	b_8	0.0060	0.0200	m
Thickness of blades	s_8	0.0050	0.0050	m
Pitch	t_8	0.0286	0.0346	m
Constriction coefficient	ϕ_8	1.21	1.17	-
Outlet area return passage	A_8	0.000857	0.003456	m ²
Outlet velocity return passage	c_{m8}	2.46	0.59	m/s

Table 4.5: Point by point method determining the blade shape for the standard design impeller [25].

Point	r	Δ_r	c_m	β	s	b	w	B	Δ_a	$\sum \Delta_a$	θ
	m	m	m/s	$^\circ$	m	m	m/s	-	-	-	$^\circ$
1	0.0195	-	2.30	21.26	0.0050	0.0104	6.8299	131.8867	0.0000	0.0000	0.00
2	0.0306	0.0111	2.23	21.64	0.0050	0.0095	3.5812	82.3257	1.1928	1.1928	68.34
3	0.0418	0.0111	2.16	22.01	0.0050	0.0086	2.5731	59.2391	0.7883	1.9811	113.51
4	0.0529	0.0111	2.09	22.39	0.0050	0.0077	2.1128	45.9026	0.5855	2.5666	147.05
5	0.0640	0.0111	2.02	22.76	0.0050	0.0068	1.8801	37.2277	0.4629	3.0295	173.58
6	0.0752	0.0111	1.96	23.13	0.0050	0.0059	1.7759	31.1413	0.3807	3.4102	195.39
7	0.0863	0.0111	1.89	23.51	0.0050	0.0050	1.7681	26.6407	0.3218	3.7320	213.83
8	0.0974	0.0111	1.82	23.88	0.0050	0.0041	1.8586	23.1814	0.2774	4.0094	229.72
9	0.1086	0.0111	1.75	24.25	0.0050	0.0032	2.0867	20.4426	0.2429	4.2523	243.64
10	0.1197	0.0111	1.68	24.63	0.0050	0.0023	2.5786	18.2227	0.2153	4.4676	255.98
11	0.1309	0.0111	1.61	25.00	0.0050	0.0014	3.8096	16.3889	0.1927	4.6603	267.02

Table 4.6: Point by point method determining the blade shape for the standard design return vane [25].

Point	r	Δ_r	c_m	α	s	b	Δ_{arc}	Δ_θ	θ
	m	m	m/s	$^\circ$	m	m	m	$^\circ$	$^\circ$
1	0.1309	0.0000	2.66	4.05	0.0050	0.0014	0.0000	0.00	0.00
2	0.1200	0.0108	2.64	12.65	0.0050	0.0019	0.0482	22.99	22.99
3	0.1092	0.0108	2.62	21.24	0.0050	0.0023	0.0278	14.58	37.57
4	0.0984	0.0108	2.60	29.84	0.0050	0.0028	0.0188	10.97	48.54
5	0.0876	0.0108	2.58	38.43	0.0050	0.0032	0.0136	8.91	57.45
6	0.0768	0.0108	2.56	47.03	0.0050	0.0037	0.0101	7.51	64.96
7	0.0660	0.0108	2.54	55.62	0.0050	0.0041	0.0074	6.42	71.37
8	0.0552	0.0108	2.52	64.22	0.0050	0.0046	0.0052	5.42	76.79
9	0.0444	0.0108	2.50	72.81	0.0050	0.0051	0.0033	4.31	81.11
10	0.0336	0.0108	2.48	81.41	0.0050	0.0055	0.0016	2.79	83.89
11	0.0228	0.0108	2.46	90.00	0.0050	0.0060	0.0000	0.00	83.89

Table 4.7: Point by point method determining the blade shape for the adjusted design impeller [25].

Point	r	Δ_r	c_m	β	s	b	w	B	Δ_a	$\sum \Delta_a$	θ
	m	m	m/s	$^\circ$	m	m	m/s	-	-	-	$^\circ$
1	0.024959	-	2.12	16.28	0.0150	0.0200	6.2231	137.2364	0.0000	0.0000	0.00
2	0.037185	0.012226	2.06	16.65	0.0279	0.0194	8.0335	89.9378	1.3887	1.3887	79.57
3	0.04941	0.012226	1.99	17.02	0.0408	0.0188	9.9483	66.1152	0.9539	2.3426	134.22
4	0.061636	0.012226	1.93	17.39	0.0537	0.0182	11.3878	51.7956	0.7208	3.0634	175.52
5	0.073862	0.012226	1.87	17.77	0.0666	0.0176	11.7148	42.2572	0.5749	3.6383	208.46
6	0.086087	0.012226	1.80	18.14	0.0795	0.0171	10.8494	35.4610	0.4751	4.1134	235.68
7	0.098313	0.012226	1.74	18.51	0.0924	0.0165	9.3242	30.3821	0.4025	4.5159	258.74
8	0.110538	0.012226	1.68	18.88	0.1053	0.0159	7.7157	26.4494	0.3474	4.8633	278.64
9	0.122764	0.012226	1.61	19.26	0.1182	0.0153	6.3187	23.3192	0.3042	5.1675	296.08
10	0.13499	0.012226	1.55	19.63	0.1311	0.0147	5.2021	20.7724	0.2695	5.4370	311.52
11	0.147215	0.012226	1.49	20.00	0.1440	0.0141	4.3376	18.6630	0.2411	5.6781	325.33

Table 4.8: Point by point method determining the blade shape for the adjusted design return vane [25].

Point	r	Δ_r	c_m	α	s	b	Δ_{arc}	Δ_θ	θ
	m	m	m/s	$^\circ$	m	m	m	$^\circ$	$^\circ$
1	0.1472	0.0000	1.27	1.73	0.0050	0.0141	0.0000	0	0
2	0.1352	0.0120	1.20	10.56	0.0050	0.0147	0.0642	27.21	27.21
3	0.1233	0.0120	1.13	19.38	0.0050	0.0153	0.0340	15.81	43.03
4	0.1113	0.0120	1.07	28.21	0.0050	0.0159	0.0223	11.49	54.52
5	0.0993	0.0120	1.00	37.04	0.0050	0.0165	0.0159	9.15	63.67
6	0.0874	0.0120	0.93	45.87	0.0050	0.0170	0.0116	7.62	71.29
7	0.0754	0.0120	0.86	54.69	0.0050	0.0176	0.0085	6.44	77.73
8	0.0634	0.0120	0.79	63.52	0.0050	0.0182	0.0060	5.39	83.12
9	0.0514	0.0120	0.72	72.35	0.0050	0.0188	0.0038	4.24	87.36
10	0.0395	0.0120	0.66	81.17	0.0050	0.0194	0.0019	2.70	90.06
11	0.0275	0.0120	0.59	90.00	0.0050	0.0200	0.0000	0.00	90.06

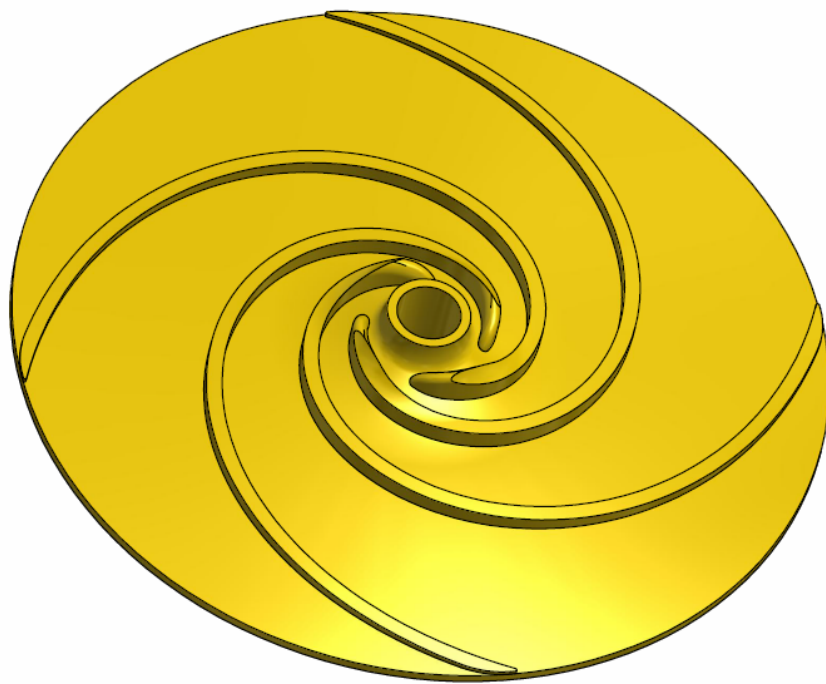


Figure 4.4: Shape of the standard impeller, model constructed in Autodesk Inventor.

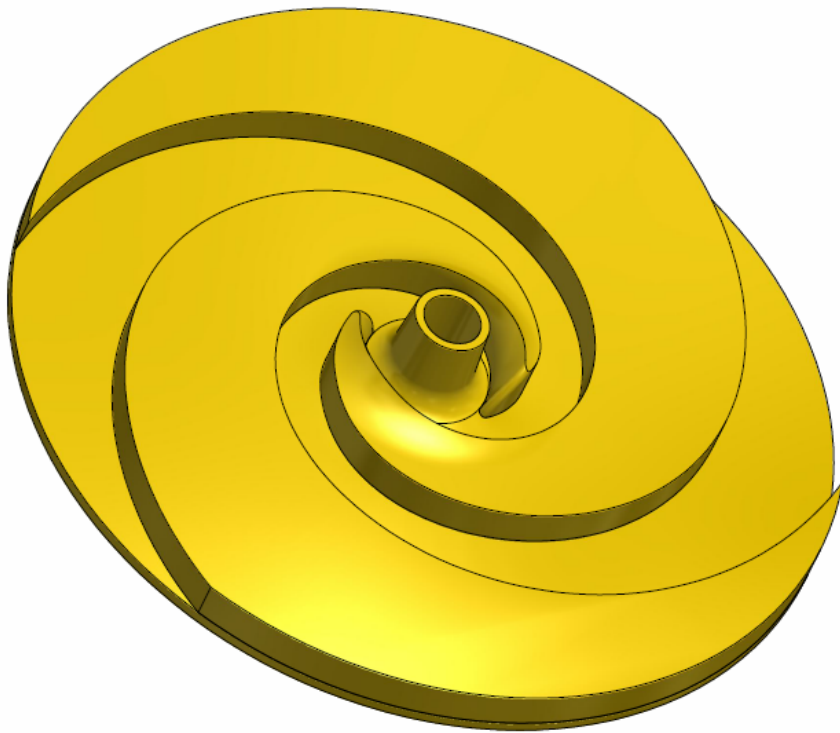


Figure 4.5: Shape of the adjusted impeller, model constructed in Autodesk Inventor.

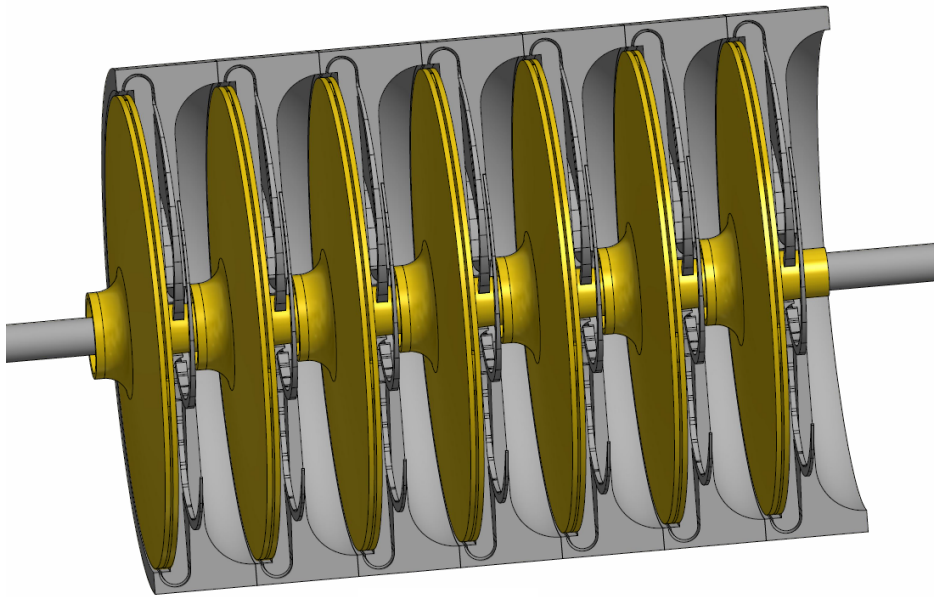


Figure 4.6: Cutaway of the casing containing the seven pump stages of the standard design, model constructed in Autodesk Inventor.

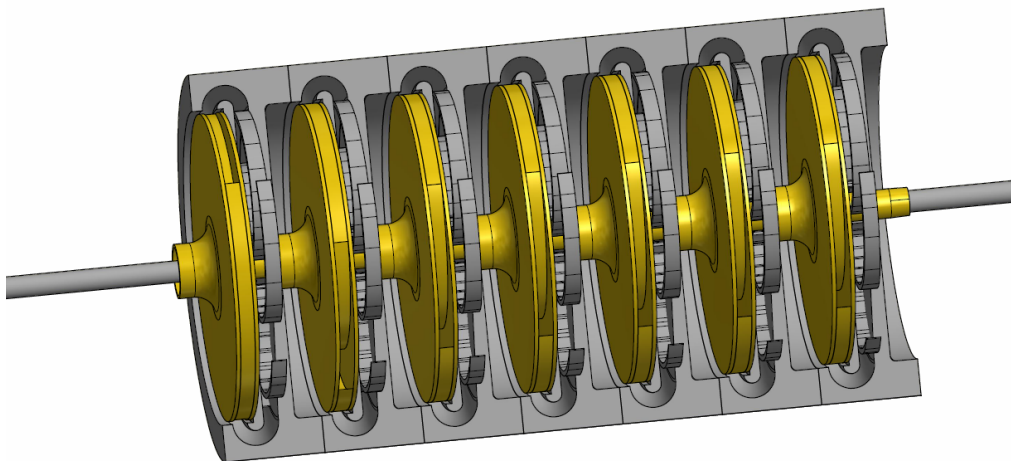


Figure 4.7: Cutaway of the casing containing the seven pump stages of the adjusted design, model constructed in Autodesk Inventor.

4.1.2 Design of the Turgo Turbine

The design of the Turgo turbine was based on hydrodynamic principles and partly on literature concerning the Pelton turbine. The work done by Anagnostopoulos [2], Gaiser [19], Cobb [10] and Correa [27] [28] has also been an inspiration.

When designing the turbine, the objective was of course to maximize the power output with the given available flow and head. The shape of the buckets was designed so that the jet would have a shockless entry and a smooth deflection, and leave the bucket with as little kinetic energy as possible. The kinetic energy of the water leaving the bucket is lost.

The rotational speed chosen for the turbine was $n = 3000$ rpm, the same as for the centrifugal pump, in order to couple them together on the same shaft without gears. By choosing the maximum rotational speed the size of the turbine was also reduced.

The energy conversion in the runner is governed by the Euler equation and the velocity diagrams at the inlet and outlet as given in figure 4.8.

The Euler equation as given in section 3.3.1.

$$\eta_h = \frac{u(c_{u1} - c_{u2})}{gH_n} \quad (4.1.30)$$

Because the water leaves and enters the Turgo bucket at approximately the same radial distance from the center of rotation, the peripheral inlet and outlet velocity is the same, as seen from figure 4.8.

In the following subsections the design strategy for the Turgo turbine will be outlined, and the resulting values for the dimensions is given in table 4.9.

4.1.2.1 Runner Diameter

The absolute inlet velocity entering the bucket from the nozzle was taken as

$$c_1 = \sqrt{2gH_n} \quad (4.1.31)$$

where H_n is the available head at the inlet of the nozzle. The optimal peripheral velocity of the runner was found from equation 3.3.7 in section

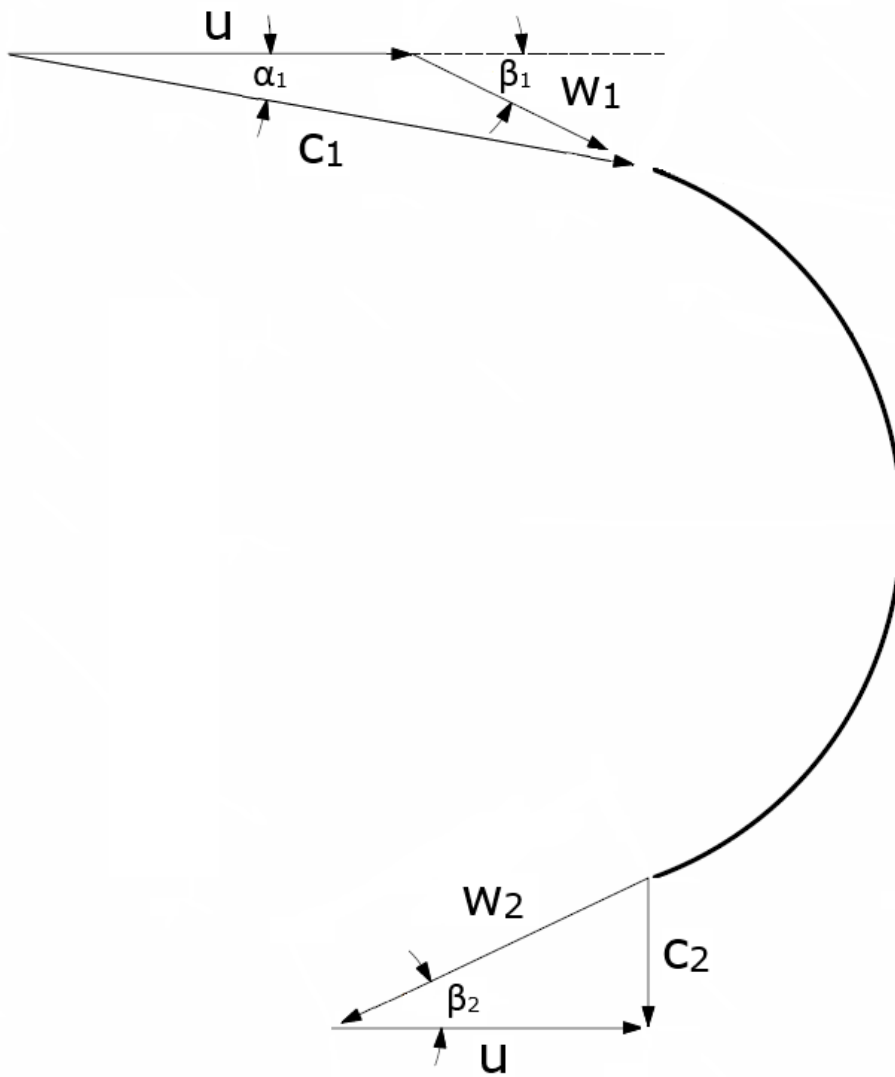


Figure 4.8: Radial view of the velocity diagrams at inlet and outlet of the Turgo bucket [2].

3.3 when assuming a hydraulic efficiency of $\eta_h = 0.96$ and an absolute outlet velocity of $c_{u2} = 0$.

$$u = 0.48\sqrt{2gH_n} \quad (4.1.32)$$

The diameter of the runner was found from

$$D = \frac{60u}{\pi n} \quad (4.1.33)$$

4.1.2.2 Jet Diameter and Number of Nozzles

The jet diameter is given by continuity

$$d_j = \sqrt{\frac{4Q}{Z_n \pi c_{u1}}} \quad (4.1.34)$$

where Z_n denotes the number of nozzles. The number of nozzles chosen for the Turgo turbine was $Z_n = 1$ due to the low flow rate.

4.1.2.3 Number of Buckets

The minimum number of buckets was found by requiring that no water should be lost. In figure 4.9 an axial view of a Turgo runner with buckets along the periphery is given.

Referring to figure 4.9, requiring that no water should be lost is the same as requiring that the water travel the distance l_w faster than the bucket travel the angular distance ψ . Mathematically this was expressed as

$$t_w < t_b \quad (4.1.35)$$

where t_w denotes the time elapsed by the water traveling the distance l_w , and t_b denotes time elapsed by the bucket traveling the angular distance ψ . If the bucket travels ψ faster than the water travels l_w , i.e., $t_b < t_w$, water will be lost because there will not always be a bucket there to catch it.

The velocity of the water, c_{u1} , is known when the jet inlet angle α_1 is chosen. The peripheral velocity at the bucket tip, u_t , can be found if the diameter at the bucket tip, D_t , is known. The diameter at the bucket tip is found by adding the diameter of the runner and the length of a bucket,

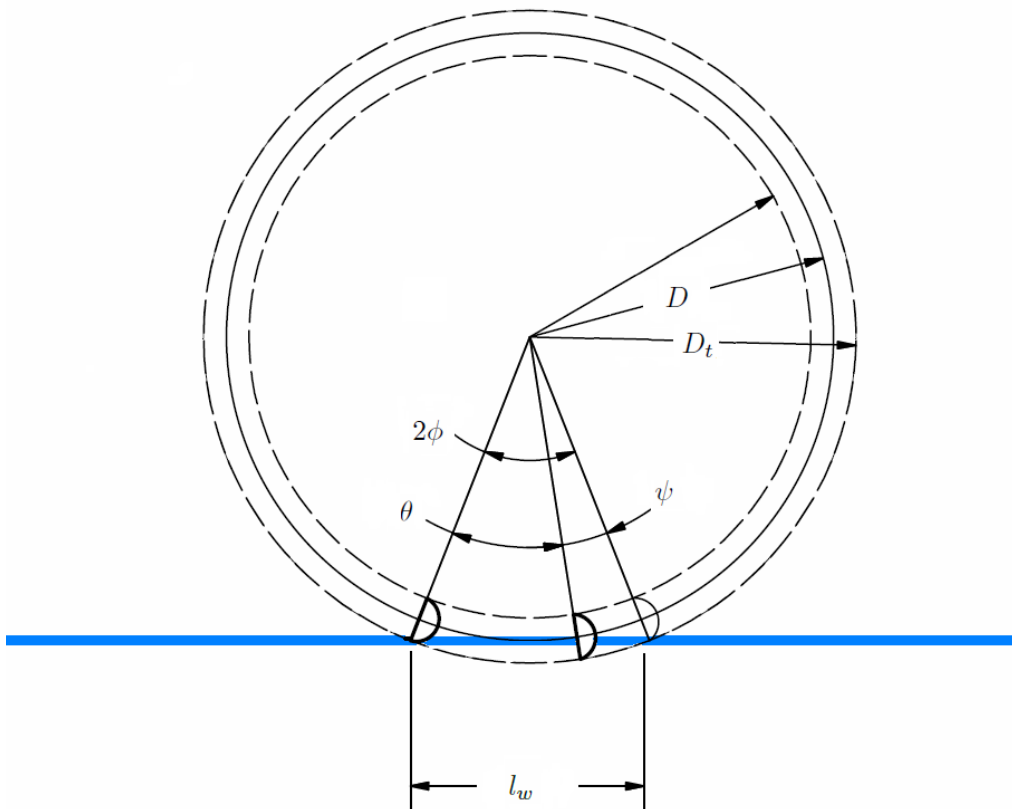


Figure 4.9: Axial view of the Turgo runner.

L . The length of the bucket will influence the required minimum number of buckets, and must be chosen with that in mind.

Equation 4.1.35 can be rewritten as

$$\frac{l_w}{c_{u1}} < \frac{\pi D_t \psi}{360 u_t} \quad (4.1.36)$$

The peripheral velocity at the bucket tip is known as $u_t = \frac{\pi n D_t}{60}$, and the distance traveled by the water is $l_w = D_t \sin \phi$, with reference to figure 4.9. The expression for ψ was then found as

$$\psi > \frac{360 n D_t \sin \phi}{60 c_{u1}} \quad (4.1.37)$$

The maximum distance between two buckets was then taken as

$$\theta = 2\phi - \psi \quad (4.1.38)$$

The minimum number of buckets is then

$$Z_b = \frac{360}{\theta} \quad (4.1.39)$$

To complete this derivation, an expression for ϕ was found from trigonometry

$$\cos \phi = \frac{D + d_j}{D_t} \quad (4.1.40)$$

By applying the above equations an expression for the minimum number of buckets was found.

The approach discussed above would also apply to Pelton turbines. However, when considering the minimum number of buckets in a Turgo turbine, the radial view of the runner must also be considered. This is because the water enters at an angle, as seen in figure 4.10.

The requirement could have been not to lose any water here as well. But, because the water enters at an angle, the relative velocity of the water will also have an angle with respect to the bucket, denoted β_1 in figure 4.8. To achieve a shockless entry of water, this angle should coincide with the constructional angle of the bucket. Thus it was required that the angle of the bucket should coincide with the angle of the water velocity relative to

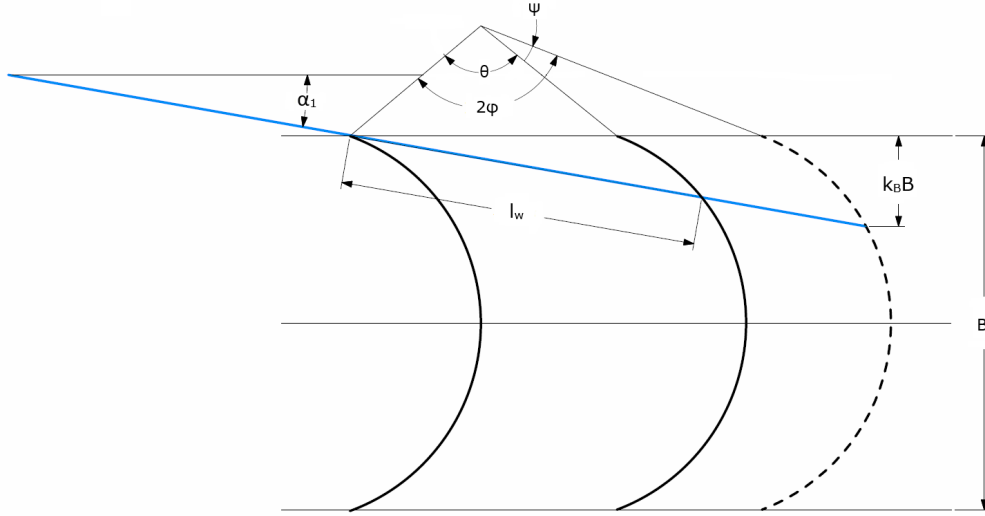


Figure 4.10: Radial view of the Turgo runner. Angles between the bucket positions from the axial view.

the bucket for the entire period of jet incidence on the bucket. The distance from the outer edge of the bucket where the first water hits to the point on the bucket where the last water hits was denoted $k_B B$, as seen in figure 4.10, where B is the width of the bucket and k_B is the constant of incidence along the width of the bucket.

By again requiring that the water travel the distance l_w faster than the bucket travel the angular distance ψ , the additional equations describing the minimum number of buckets was found as

$$\psi > \frac{k_B B \pi n}{30 c_1 \sin \alpha_1} \frac{360}{2\pi} \quad (4.1.41)$$

where α_1 denotes the angle of incidence of the water as seen from figure 4.10. The angle of incidence was chosen to be very small, but without interfering with the incoming buckets. Making the angle α_1 small, means making the velocity component c_{u1} of the water jet big, and from the Euler equation 4.1.30, this is beneficial.

$$\tan \phi = \frac{k_B B}{D \tan \alpha_1} \quad (4.1.42)$$

$$\theta < 2\phi - \psi \quad (4.1.43)$$

and finally

$$Z_b = \frac{360}{\theta} \quad (4.1.44)$$

When applying the equations for the radial view, the width B and the factor k_B must be chosen. Thus, an acceptable relationship between the bucket width B and the number of buckets must be found. Another value for the minimum number of buckets is found by considering the equations for the axial view. The final number of buckets must be the highest number of the two.

4.1.2.4 The Shape of the Buckets

The width, depth, length and angles of the bucket strongly influence the flow pattern through the bucket. The dimensions are illustrated in figure 4.11

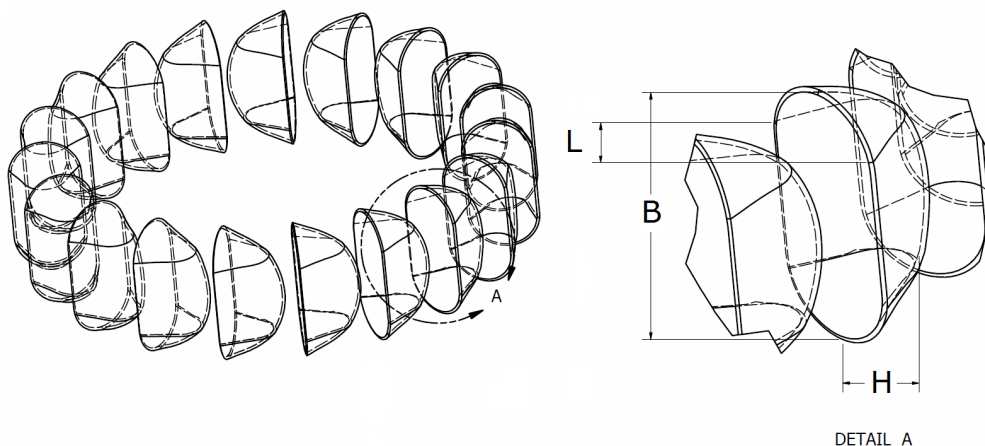


Figure 4.11: Dimensions of the Turgo bucket. Width B , length L and depth H is indicated.

The width of the bucket, B , and the length of the bucket, L , is already found from the considerations pertaining to the minimum number of buckets in the previous section.

The depth is decided by the length given by $k_B B$, see figure 4.10, and inlet and outlet angles β_2 and β_1 . The outlet angle β_1 was chosen to equal the inlet angle in order to turn the water around as much as possible and maximize the efficiency. Trigonometry provided the profiles at the inlet

and outlet, and a smooth transition was demanded. β_1 was found from trigonometry when α_1 , u and c_1 was known.

The depth was found to be considerable, and the shape was adjusted slightly to make the blade more shallow by gradually increasing the blade angle β from the inlet towards the centerline of the bucket.

Considering the axial view of the bucket it was decided that the shape should resemble an arc in this direction as well, as illustrated in figure 4.9. The blade inlet angle in this direction, denoted by β_{a1} was found from trigonometry, when the c_{u1} and u velocity components and the angle between them was known.

The relative velocity vectors at the point of the bucket where the jet is incident is shown in figure 4.12 for the Turgo design given in table 4.9.

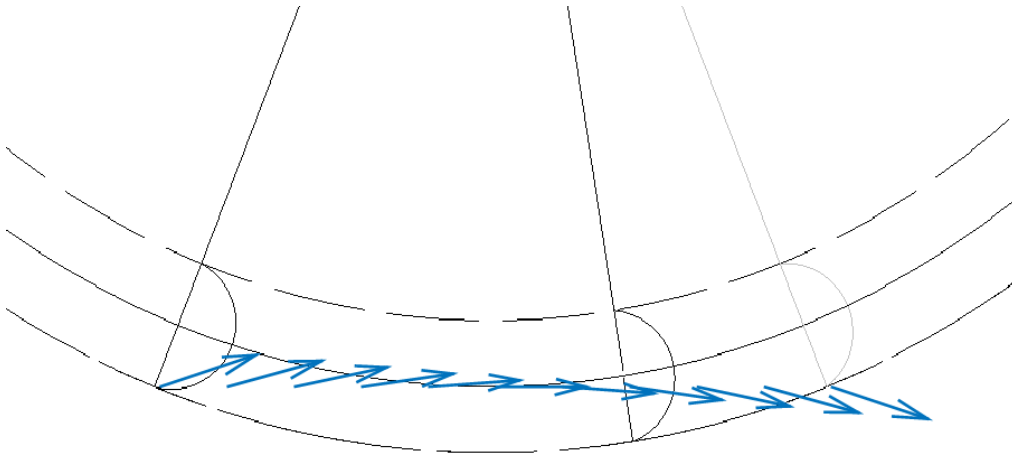


Figure 4.12: Axial view of the Turgo runner. Relative velocity vector at point of bucket where jet is incident.

The main dimensions and physical properties of the Turgo design are found in table 4.9.

A three-dimensional model of the finished design was constructed using the computer-aided design software *Autodesk Inventor*. The model is shown in figure 4.13, and additional drawings are given in appendix A.

4.1.2.5 Materials Selection

The most common construction materials for turbine runners are stainless steel alloys. The Turgo turbine designed for the reverse osmosis system

Table 4.9: Main dimensions and physical properties of the Turgo design.

TURGO DIMENSIONS AND SPECIFICATIONS			
FLOW AND HEAD, CONSTANTS AND ROTATIONAL SPEED			
Density of brine	ρ	1050	kg/m ³
Gravitational constant	g	9.81	m/s ²
Atmospheric pressure	p_{atm}	101325	Pa
Vapor pressure of water at 25C	p_v	3184	Pa
Viscosity of water	μ	0.00089	kg/(ms)
Available flow rate	Q	30	l/min
Available flow rate	Q	0.0005	m ³ /s
Pressure loss through membrane	Δp	3	%
Pressure after membrane	p	63	bar
Pressure after membrane	p	6305000	Pa
Pressure after membrane	H	612	m
Rotational speed	n	3000	rpm
Rotational speed	ω	314	rad/s
VELOCITIES, NOZZLES AND DIAMETERS			
Absolute inlet velocity	c_1	109.59	m/s
Angle of absolute inlet velocity	α_1	10.0	°
Absolute inlet velocity peripheral component	c_{u1}	107.92	m/s
Runner peripheral velocity	u	52.60	m/s
Number of nozzles	Z_n	1	-
Jet diameter	d_j	0.0024	m
Runner diameter	D	0.335	m
BUCKET SHAPE FROM CONSIDERATION OF THE RADIAL VIEW AND RELATIVE VELOCITIES			
Inlet angle	α_1	10	°
Relative inlet velocity	w_1	58.50	m/s
Inlet angle of bucket	β_1	19.0	°
Width of bucket	B	0.1	m
Factor bucket	k_B	0.2	-
Angle traveled by bucket when in contact with water	ϕ	18.7	°
Angle traveled by bucket when water travels angle 2ϕ	ψ	18.9	°
Maximum distance between buckets	θ	18.5	°
Minimum number of buckets	Z_b	19	-
Outlet angle of bucket	β_2	19.0	°
Absolute outlet velocity peripheral component	c_{u2}	0.0	m/s
Output hydraulic power	P	2980	W
Available hydraulic power	P_h	3153	W
Hydraulic efficiency	η_h	95	%
BUCKET SHAPE FROM CONSIDERATION OF THE AXIAL VIEW			
Length of buckets	L	0.05	m
Diameter at bucket tip	D_t	0.3849	m
Angle traveled by bucket when in contact with water	ϕ	28.8	°
Angle traveled by bucket when water travels angle 2ϕ	ψ	30.4	°
Maximum distance between buckets	θ	27.1	°
Minimum number of buckets	Z_b	13	-
Inlet angle between c_{u1} and u	α_{a1}	-29.5	°
Relative inlet velocity	w_1	67.35	m/s
Inlet angle between c_{u1} and w_1	β_{a1}	22.6	°
FORCES ON BUCKET			
Dimensioning force on bucket	F_R	29.32	N
Torque on root of bucket	T_b	1.47	Nm

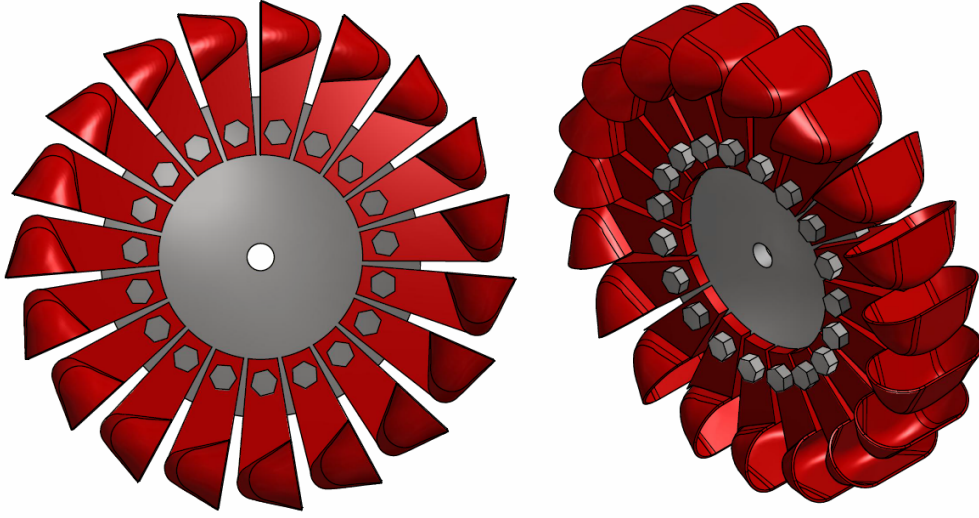


Figure 4.13: Model of the designed Turgo turbine.

will operate in a highly corrosive environment, due to the salinity of the concentrate. The material selected must therefore be very corrosion resistant. The material must also be strong enough to endure the forces and the stresses in the runner. A possible construction material apart from stainless steel is hard plastic. Then the turbine could be manufactured by injection molding. A plastic material would be beneficial because it is very light and highly corrosion resistant.

The dimensioning force acting on the turbine bucket can be approximated by the formula

$$F_R = \rho Q_R (w_{u1} - w_{u2}) = 2\rho Q_R (c_{u1} - u) \quad (4.1.45)$$

where Q_R is the relative flow rate given by

$$Q_R = \frac{\pi d_j^2}{4} (c_{u1} - u) \quad (4.1.46)$$

The torque in the root of the bucket can then be found from

$$T = F_R a \quad (4.1.47)$$

where a is the distance from the jet normal to the root of the bucket.

4.2 The Reciprocating Pump and the Turgo Turbine

During the work with this thesis, the opportunity arose to run tests on a newly built reverse osmosis system in the laboratory. This system is a prototype produced by one of the initiators of this thesis, Julia Navarsete at Waterbox4Life Norway AS.

The system has the appropriate name Waterbox, and is a system built and intended for the same application area as the systems considered in this thesis. The results from the tests on the system is therefore seen as relevant for this thesis.

4.2.1 About the System

Waterbox is a reverse osmosis system for producing clean drinking water. The feedwater is pressurized to a pressure ranging between 15 to 70 bar in a reciprocating plunger pump, and forced through the reverse osmosis membrane. The low pressure freshwater permeate and the high pressure concentrate leaves the membrane. The concentrate may leave the system directly after the membrane, or pass through a nozzle where the pressure energy is converted to a water jet with high kinetic energy. This water jet hits a Pelton turbine, and the kinetic energy is transferred to mechanical energy. The turbine is coupled directly to the shaft of the reciprocating pump and the electric motor that drives the pump. In this manner, the total power consumption of the electric motor may be reduced. See figure 4.14, where the the working principle of the system is illustrated.

The nozzle diameter in the Waterbox is 2.5 mm, and the diameter of the Pelton turbine where the water jet hits is 100 mm. The rotational speed of the system is 1500 rpm.

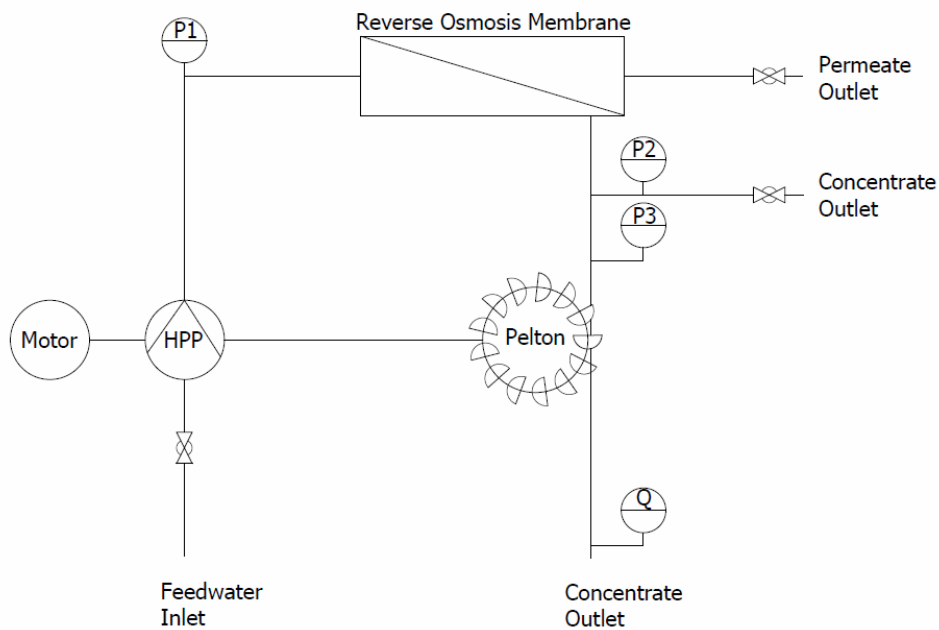


Figure 4.14: Sketch showing the working principle of the Waterbox. An electric motor drives a high pressure pump (HHP) coupled to the same shaft as a Pelton turbine. The feedwater is forced through the membrane and the products are low pressure freshwater (permeate) and high pressure concentrate. The concentrate leaves the system directly or is directed through the Pelton turbine where the hydraulic energy is converted to mechanical energy.

4.2.2 About the Measurements

The objective of the measurements was to quantify the difference in the power consumption of the electric motor when the concentrate was directed through the turbine, versus the case where it leaves the system directly after the membrane.

The system parameters that were measured are pressure, flow rate, current and voltage. See figure 4.15 for a sketch showing the system measurement setup and the locations in the system where the different parameters were measured.

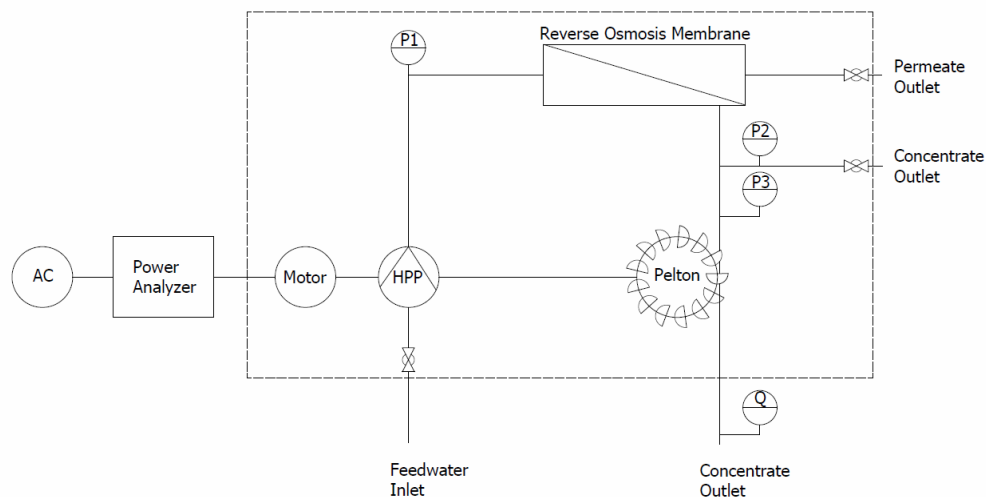


Figure 4.15: Sketch showing the measurement setup for the reverse osmosis system Waterbox. The alternating current supply is denoted AC. The current supplied to the electric motor and the voltage over the motor was measured by a power analyzer. Pressure was measured at the locations denoted P1, P2 and P3, and the flow rate was measured at the location denoted Q.

The power consumption of the motor was found by measuring the current supplied to the motor and the voltage over the motor. The system was connected to a three-phase 230 V power supply. The current and voltage was analyzed by the power analyzer *PM3000A Power Analyzer*. Details on the power analyzer and system connection are given in figure 4.16. In the figure, three phase load is referring to the electric motor, and three phase source is referring to the power supply.

The current was measured by connecting clamp-on current transformers of the type *CL1000 Current Transformer* over each of the three phases.

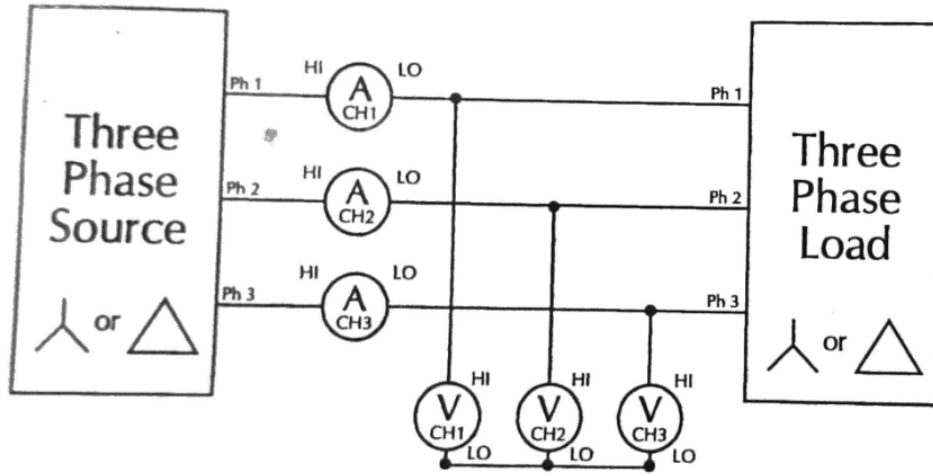


Figure 4.16: The measurement setup for the *PM3000A Power Analyzer*.

The power analyzer gave the effective values of current I_{RMS} and voltage V_{RMS} , and the power consumption P of the electric motor could therefore be found from equation 4.2.1.

$$P = V_{RMS}I_{RMS} \quad (4.2.1)$$

The pressure at the locations denoted P1, P2 and P3 in figure 4.15 was measured using manometers of the European standard EN 837-1.

The flow rate was measured at the location denoted Q in figure 4.15 by using a stopwatch to measure the time elapsed when filling a known volume with water.

4.2.3 Measurement Results

Figure 4.17, 4.18 and 4.19 present the results of the measurements performed. The total power consumption of the electric motor when the concentrate is leaving the system directly after the membrane versus the power consumption when the concentrate is passed through the Pelton turbine is shown in figure 4.17.

The total power savings when the turbine is part of the system is presented in figure 4.18. The power savings were found from equation 4.2.2.

$$Power\ savings = \frac{P_{without\ turbine} - P_{with\ turbine}}{P_{without\ turbine}} * 100 \quad (4.2.2)$$

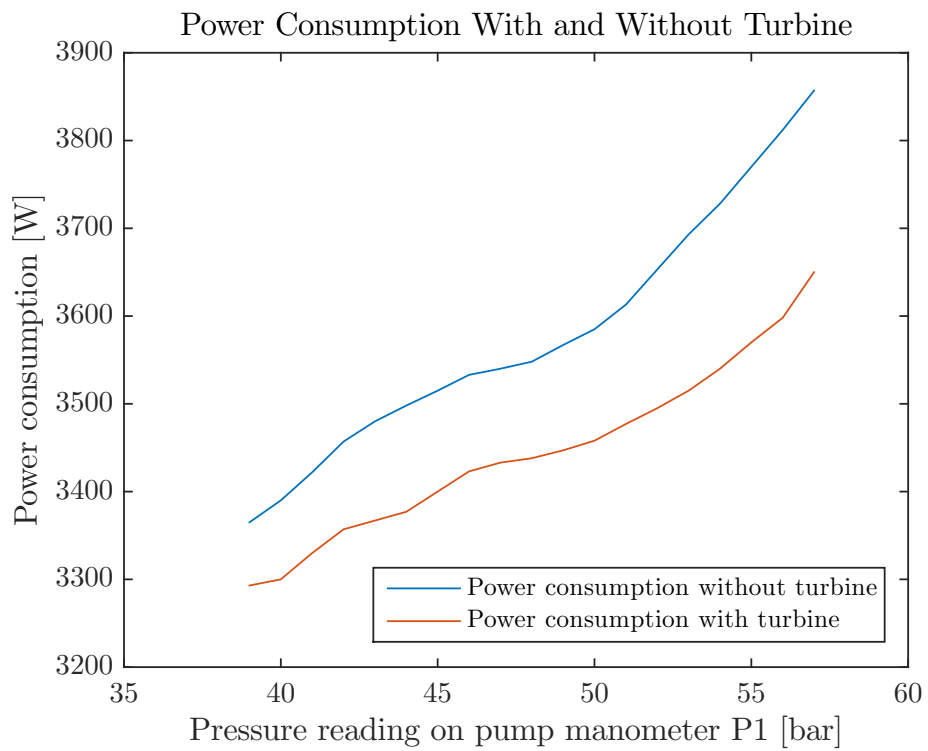


Figure 4.17: Measured power consumption with and without the turbine as part of the system. Each of the curves represent the mean value of three measurements done with continuous operation of the system.

As seen from equation 4.2.2, the difference in power consumption without the turbine $P_{without\ turbine}$ and with the turbine $P_{with\ turbine}$ is expressed as a percentage of the power consumption without the turbine $P_{without\ turbine}$.

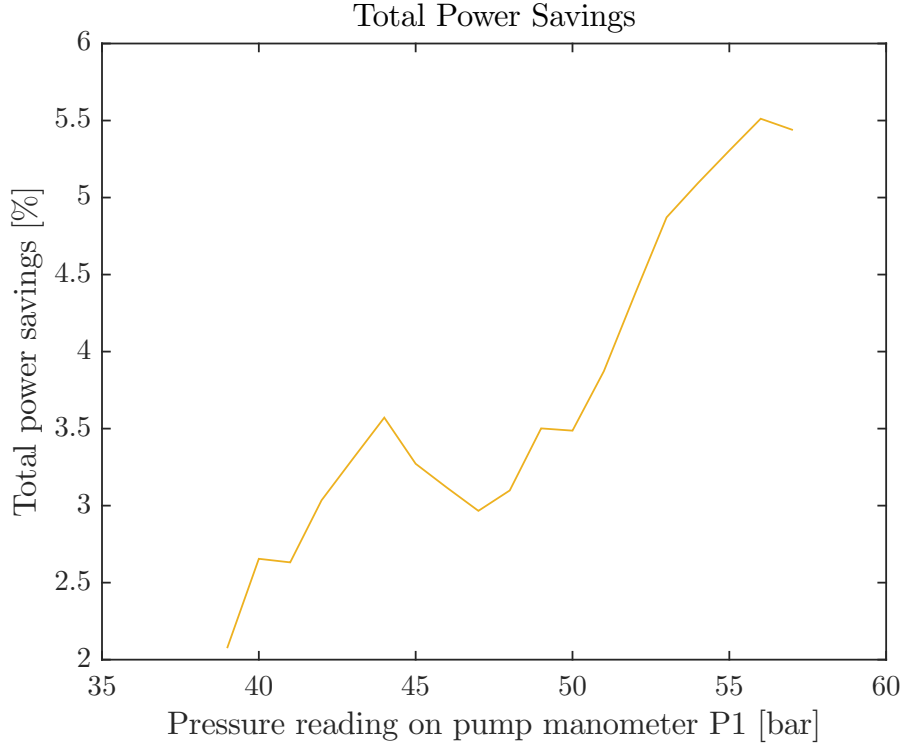


Figure 4.18: Measured power savings when operating the turbine as part of the system. The curve is based on the mean values in figure 4.17.

The measured efficiency of the turbine is presented in figure 4.19. This efficiency was found by comparing the measured difference in the mean power consumption with and without the turbine. The efficiency was found from equation 4.2.3.

$$\eta = \frac{P_{without\ turbine} - P_{with\ turbine}}{(p_3 + \frac{1}{2}\rho v_3^2 + \rho g h_3)Q} * 100 \quad (4.2.3)$$

In equation 4.2.3 η is the measured turbine efficiency, P is the power as found from equation 4.2.1, p_3 is the gauge pressure measured at manometer P3 as shown in figure 4.15, v_3 is the velocity at manometer P3, h_3 is the elevation difference between manometer P3 and the inlet to the turbine and Q is the flow rate to the turbine. ρ and g is the density of the concentrate and the gravitational constant, respectively.

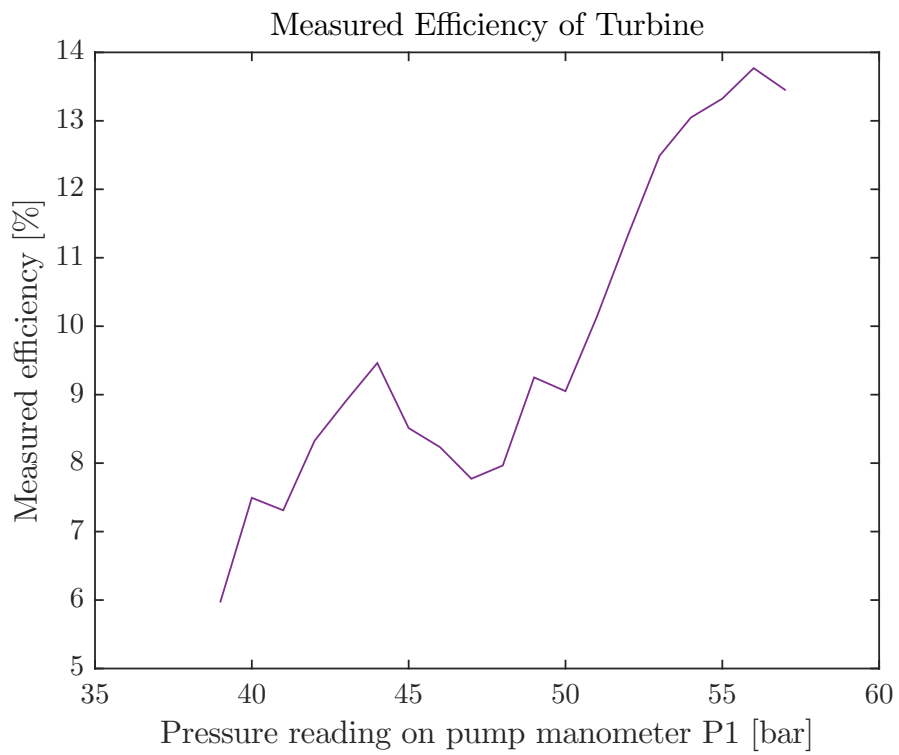


Figure 4.19: Measured efficiency for the Pelton turbine. The curve is based on the difference in the mean power consumption with and without the turbine compared to the available hydraulic power.

4.2.4 Uncertainty Analysis

All measurements are associated with some degree of uncertainty. This might be due to the measurement instruments, faulty readings or changed circumstances for the measurements. The error might be categorized as either systematic or random. Random errors are errors that varies with every measurement, and are caused by human error or changes in the circumstances of the measurements. The systematic error depends on the measurement instruments and the system, and these are errors that can not be reduced by increasing the number of measurements. The systematic error for different types of measuring instruments is often given.

By assuming that the measurements are normally distributed around the true mean value of the parameter being measured, the total uncertainty is found by taking the square of the sum of the squares of the random and the systematic uncertainty. The total uncertainty is found from equation 4.2.4.

$$\textit{Total uncertainty} = \sqrt{\textit{Random uncertainty}^2 + \textit{Systematic uncertainty}^2} \quad (4.2.4)$$

By applying equation 4.2.4, the total uncertainty will have a confidence interval of 95 percent. This means that there is a 95 percent probability that the true mean value of the measured parameter lies within the limits given by the total uncertainty.

In the same manner as the total uncertainty for one measured parameter is found, the total uncertainty for a derived value can be found by taking the square of the sum of the squares of the total uncertainties of all the variables that are part of the expression for the derived value. The total uncertainty for the power is therefore found from equation 4.2.5.

$$\textit{Uncertainty Power} = \sqrt{\textit{Uncertainty current}^2 + \textit{Uncertainty voltage}^2} \quad (4.2.5)$$

The total uncertainty for the different parameters that have been measured are given in table 4.10, and the probability of the true value lying within these limits is then 95 percent.

The uncertainty limits for power is given graphically in figure 4.20, as the vertical lines.

Table 4.10: Uncertainty analysis.

Measured parameter	Measuring equipment	Random uncertainty	Systematic uncertainty	Total uncertainty
Voltage	Voltech PM3000A	$\pm 0.05 \%$	$\pm 0.05 \%$	$\pm 0.07 \%$
Current	Voltech PM3000A	$\pm 0.05 \%$	$\pm 1.50 \%$	$\pm 1.50 \%$
Power	Voltech PM3000A	$\pm 0.07 \%$	$\pm 1.50 \%$	$\pm 1.50 \%$
Pressure	Manometer 0/100 bar EN 837	$\pm 1.00 \%$	$\pm 1.60 \%$	$\pm 1.89 \%$
Flow rate	Stopwatch and container of known volume	$\pm 0.09 \%$	$\pm 0.00 \%$	$\pm 0.09 \%$
Efficiency	Stopwatch, container of known volume, manometer 0/100 bar EN-837 and Voltech PM3000A	$\pm 1.01 \%$	$\pm 2.19 \%$	$\pm 2.41 \%$

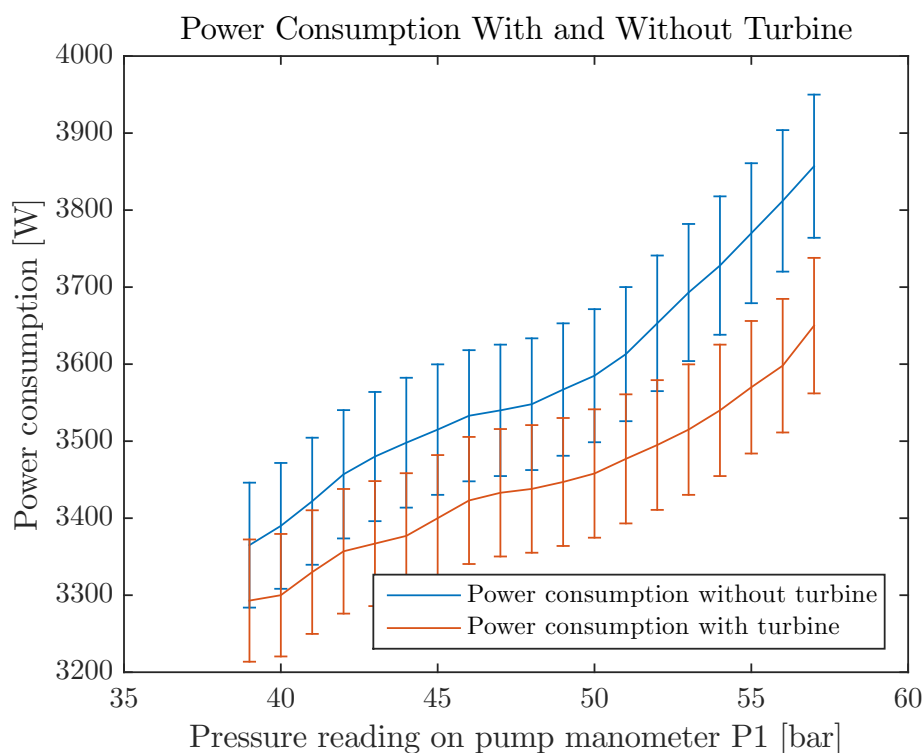


Figure 4.20: Measured power consumption with and without the turbine as part of the system. Each of the curves represents the mean value of three measurements done with continuous operation of the system. The vertical lines represent the uncertainty of the efficiency measurements.

4.2.5 Discussion of the Results

Figure 4.17 clearly shows that by passing the concentrate through the turbine, the power consumption of the electric motor will decrease. The maximum efficiency of the turbine was measured to be 14 percent as shown in figure 4.19. The maximum power savings by utilizing the turbine was measured to be 6 percent of the total power consumption without the turbine, as shown in figure 4.18. The total power savings depend on the efficiency of the turbine. A higher efficiency means higher total power savings. Suggestions on how to increase the efficiency of the turbine are given in section 4.2.6.

4.2.6 Suggestions on Improvement

To increase the total power savings in the system by passing the high pressure concentrate through a turbine, several suggestions are made. Firstly, the jet should be aligned more precisely with the runner. Secondly the Pelton turbine should be replaced with a Turgo turbine. The nozzle diameter required to obtain the necessary pressure in the membrane of the Waterbox is only 2.5 mm. It is believed that significant incident losses occur when the water jet hits the splitter of the Pelton turbine. A Turgo turbine does not have a splitter, and is therefore seen as a better solution. Thirdly, the diameter of the turbine needs to be increased. The diameter of the Pelton turbine where the water jet hits is only 100 mm.

When the pressure available upstream of the nozzle is known, the necessary turbine diameter can be found by considering the theoretical hydraulic efficiency. Much in the same way it was done in section 4.1.2 when designing the Turgo turbine for the first system solution.

The measured efficiency of the turbine in the Waterbox as given by equation 4.2.3 differs from the theoretical hydraulic efficiency in that the measured efficiency also incorporates losses in the nozzle and runner, and other mechanical losses. The theoretical hydraulic efficiency of the turbine is given by equation 4.2.6.

$$\eta_h = \frac{\rho u(c_{u1} - c_{u2})}{p_3 + \frac{1}{2}\rho v_3^2 + \rho g h_3} * 100 \quad (4.2.6)$$

In equation 4.2.6, η_h is the theoretical hydraulic turbine efficiency, c_{u1} is the absolute peripheral velocity of the water entering the turbine, and c_{u2} is the absolute peripheral velocity of the water leaving the turbine. The available hydraulic energy of the water before entering the nozzle is given by the

expression in the denominator where p_3 is the gauge pressure measured at manometer P3 as shown in figure 4.15, v_3 is the velocity at manometer P3 and h_3 is the elevation difference between manometer P3 and the inlet to the turbine. ρ and g is the density of the concentrate and the gravitational constant, respectively.

All the variables of equation 4.2.6 are given by the system upstream of the turbine, with the exception of the peripheral velocity u and the absolute peripheral water velocity c_u . By assuming that the buckets of the turbine are shaped in such a way that the absolute peripheral velocity of the buckets at the outlet c_{u2} is zero, equation 4.2.6 shows that the theoretical efficiency can be increased by increasing the peripheral velocity u of the turbine. The peripheral velocity of the turbine is given by equation 4.2.7.

$$u = \frac{2\pi nD}{120} \quad (4.2.7)$$

In equation 4.2.7, n is the rotational speed of the runner and D is the diameter of the runner where the water hits the buckets. From equation 4.2.6 and 4.2.7, it is apparent that increasing the diameter of the turbine means increasing the theoretical hydraulic efficiency of the turbine. From the previous equations and the system parameters, it is found that the optimal diameter of the turbine would be $D = 636 \text{ mm}$. The turbine in the Waterbox system has a diameter of only 120 mm .

4.2.7 Concluding Remarks on the Measurements

The measurements performed on the Waterbox indicates that passing the concentrate water through a turbine coupled to the shaft of the electric motor and reciprocating pump will give energy savings compared to the case when the concentrate water leaves the system directly after the membrane. The energy savings might be increased considerably by installing a Turgo turbine with the right dimensions as described in section 4.2.6. The total energy savings for the system might be as high as 40 percent by installing a turbine with an efficiency ranging upwards of 90 percent.

The measurements on the Waterbox has indicated that energy recovery in a reverse osmosis system is possible by coupling a turbine directly to the shaft of the electric motor driving the reciprocating pump. These measurements therefore supports the idea behind two of the four investigated solutions for the reverse osmosis system to be designed in this thesis. It also accentuates the importance of installing a properly designed turbine in such a system.

4.3 The Reciprocating Pump without Energy Recovery

4.3.1 Design of the Reciprocating Pump

Some of the most important configurations of a reciprocating pump were discussed in section 3.2.3.2. The configuration chosen for the design of the reciprocating pump for the RO system is a triplex single-acting piston pump. The triplex configuration is chosen because three cylinders is the minimum amount of cylinders required to reduce the flow variation and pressure pulsations in comparison to the simplex pump. A single-acting pump is chosen because of its simplicity. The piston is chosen over the plunger to allow the possibility of introducing pressurized fluid in the power end during the discharge stroke in order to reduce the required power input to the pump. This type of configuration will be described further in section 4.4. The crankpins of the three pistons will be spaced evenly, 120 degrees apart.

4.3.1.1 Pump Rotational Speed

The pump rotational speed greatly influences the flow and pressure pulsations in the pump. An excessive speed can be detrimental to the entire system. The advantages of high pump speed are higher flow rate with smaller pump size. The choice of rotational speed must therefore be as high as possible, without causing operational problems. Also, the speed should be synchronous with the power grid, to avoid gears between the drive and the pump, for greater mechanical efficiency. This is assuming that the drive is an electric motor.

The possible synchronous speeds depends on the frequency of the supply current and the number of pole pairs per phase in the motor. The rotational speed, n , is given by

$$n = \frac{60f}{Z_p} \quad (4.3.1)$$

where f is the frequency of the supply current given in Hz, and Z_p is the number of pole pairs per phase in the motor. With four pole pairs per phase, it is seen from equation 4.3.1 that the rotational speed becomes $n = 750$ rpm on a 50 Hz supply current. This was the rotational speed chosen for the pump.

4.3.1.2 Displacement

The displacement in one pump cylinder is the volume swept by the piston during one stroke. The total displacement of the pump is therefore the total volume swept by all three pistons.

The delivered flow rate of the pump depends on the displacement D , the rotational speed n , and the volumetric efficiency η_V , according to equation 4.3.2.

$$Q = \frac{Dn\eta_V}{60} \quad (4.3.2)$$

When the desired volume flow rate is known, the necessary displacement can be found from equation 4.3.2.

4.3.1.3 Piston Diameter and Stroke Length

When the displacement volume is known, the stroke length s and piston diameter d_p can be determined. According to Miller [29], there is no absolute rule when choosing the piston diameter and stroke length. One guideline is that the piston diameter should be no greater than the stroke length. Pumps with piston diameter equal to stroke length are called square pumps, and this configuration is chosen for the reciprocating pump designed in this section.

The stroke length s is given by dividing the cylinder displacement $D_{cylinder}$ by the piston area A_p .

$$s = \frac{D_{cylinder}}{A_p} \quad (4.3.3)$$

The piston area is given by

$$A_p = \frac{\pi}{4}d_p^2 \quad (4.3.4)$$

By combining equations 4.3.3 and 4.3.4 and requiring that the piston diameter d_p should equal the stroke length s , the following expression for the stroke length is found

$$s = \sqrt[3]{\frac{4D_{cylinder}}{\pi}} \quad (4.3.5)$$

The piston length is chosen to equal the piston diameter and stroke length. For the reciprocating pump without energy recovery, no piston rod is necessary between the piston and the crosshead. The piston can be attached directly to the crosshead.

4.3.1.4 Cylinder

The necessary pressure the cylinder must withstand can be found by considering the maximum delivery pressure required for the RO system, and add the maximum pressure rise due to pressure pulsations. From a dynamic analysis of the pressure in a system with a required delivery gauge pressure of 80 *bar* and the specifications given in table 4.12, the total maximum gauge discharge pressure is found to be $p_{d,max} = 98 \text{ bar}$.

When the pressure requirement for the cylinder is known, the necessary cylinder thickness can be found from equation 4.3.6.

$$t = \frac{p_{d,max} d_p}{2\sigma_y} S_f \quad (4.3.6)$$

4.3.1.5 Crosshead and Connecting Rod

The forces acting on the crosshead, connecting rod, and crankshaft can all be found when the geometry of the pump and the differential pressure on the piston is known. These forces will vary with the crank angle. In figure 4.21 the forces are indicated.

F_p is the force on the piston which varies between the suction stroke and the discharge stroke. F_{cr} is the force on the connecting rod, and F_{ch} is the force on the crosshead. $F_{cs,n}$ and $F_{cs,t}$ is the normal and tangential force on the crankshaft from the connecting rod.

The maximum forces on the crosshead and connecting rod occurs when $\theta = 0^\circ$. The maximum tangential force on the crankshaft occurs when $\theta = 270^\circ$, while the maximum normal load on the crankshaft occurs when $\theta = 0^\circ$. All maximum forces are given in table 4.11.

When the maximum forces are known, the connecting rod and crosshead can be designed. The necessary connecting rod area A_{cr} is found by considering the maximum stress in the connecting rod, and requiring it to be below the allowable stress in the material. The connecting rod area is found

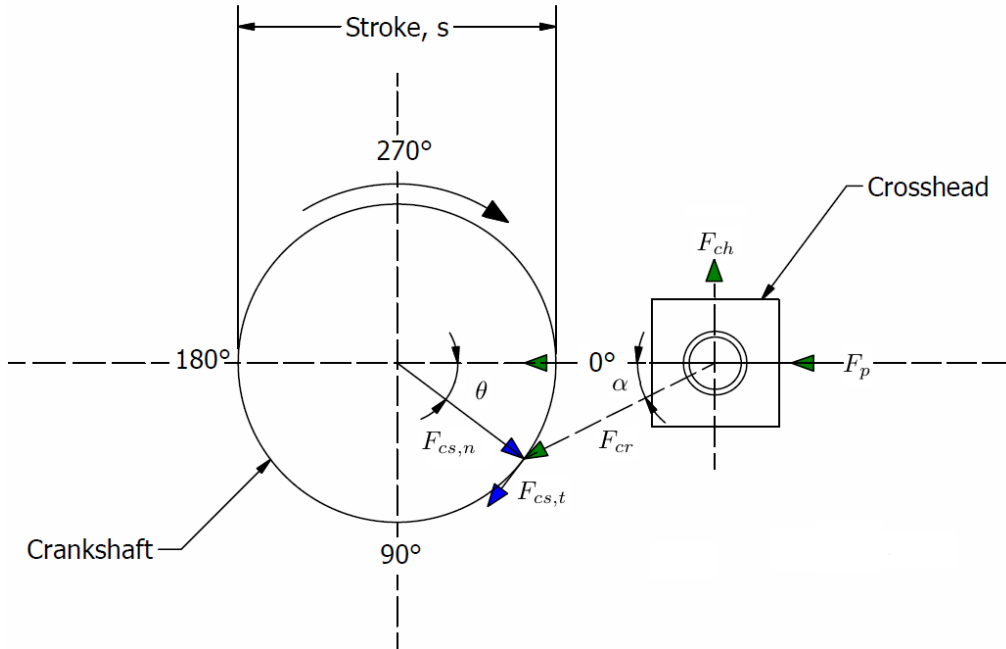


Figure 4.21: Sketch showing the connecting rod, crosshead and crankshaft forces. The force on the piston F_p is transferred to the connecting rod and crosshead. F_p is therefore the vector sum of F_{ch} and F_{cr} .

Table 4.11: Maximum forces on crosshead and connecting rod.

Maximum connecting rod load	$F_{cr,max}$	N	4263
Maximum crosshead load	$F_{ch,max}$	N	-710
Maximum crankshaft normal load	$F_{cs,n,max}$	N	4203
Maximum crankshaft tangent load	$F_{cs,t,max}$	N	-4203

from equation 4.3.7.

$$S_f F_{cr} < \sigma_f A_{cr} \quad (4.3.7)$$

The dimensions of the crosshead are chosen to equal the dimensions of the piston.

4.3.1.6 Crankshaft

The design of the crankshaft was based on a calculation of the bending moments and bending stress acting on it. The forces are transferred through the pistons and the connecting rods to the three different locations on the crankshaft where the connecting rods are fastened. The forces are absorbed by the main bearings on either side of the crankshaft. The distance between the connecting rods was decided by considering the outer diameter of each of the three pump cylinders. The forces were found from the maximum pressure acting on each piston. When the point of maximum bending moment and maximum bending stress was found, the diameter of the crankshaft was chosen so that the maximum stress at this point would not exceed the maximum allowable stress in the material. The necessary area of the crankshaft was found from equation 4.3.8.

$$S_f F_{cs} < \sigma_f A_{cs} \quad (4.3.8)$$

The calculation of the crankshaft was based on an example in the book *The Reciprocating Pump: Theory, Design and Use* by John E. Miller [29]. The results and information for the different steps of the calculation are given in table 4.12.

4.3.1.7 Check Valves

As mentioned in section 3.2.3.2, the flow through valves is associated with pressure loss. It is therefore wise to choose a valve that will minimize this pressure loss. According to Smith and Zappe [40], the resistance coefficient ζ determines the friction loss through a valve in relation to the fluid velocity through the valve. Smith and Zappe have suggested values for the resistance coefficient of different types of valves under fully turbulent flow conditions. The ball valve are among the valves having the lowest friction loss. The resistance coefficient for a ball valve is estimated to $\zeta = 0.1$, and

the head loss through the valve due to friction can therefore be approximated as [40]

$$\Delta h = \zeta \frac{v^2}{2g} \quad (4.3.9)$$

Based on the reasons given above, ball valves are chosen for the inlet and outlet valves of the reciprocating pump.

4.3.1.8 Safety Relief Valve

In order to avoid the build up of excessive pressure in the the pump and system, a safety relief valve should be placed at the discharge of the pump. This can be a spring controlled valve, which can be adjusted to different pressure levels.

The main dimensions and physical properties of the reciprocating pump without energy recovery are found in table 4.12.

A three-dimensional model of the finished design was constructed using the computer-aided design software *Autodesk Inventor*. The model is shown in figure 4.22, and additional drawings are given in appendix C.

Table 4.12: Main dimensions and physical properties of the reciprocating pump design.

RECIPROCATING PUMP SPECIFICATIONS AND DIMENSIONS			
FLOW AND HEAD, CONSTANTS, EFFICIENCIES AND ROTATIONAL SPEED			
Gravitational constant	g	9.81	m/s ²
Density of water	ρ	1000	kg/m ³
Required delivery flow rate	Q	20	l/min
Required delivery flow rate	Q	0.00033	m ³ /s
Volumetric efficiency	η_V	0.9	-
Flow rate including leakage	Q'	0.00037	m ³ /s
Rotational speed	n	750	rpm
Angular rotational speed	ω	79	rad/s
Required delivery pressure	p	80	bar
Required delivery pressure	p	8000000	Pa
Required delivery pressure	H	815	m
Total pump efficiency	η_p	78	%
Mechanical efficiency	η_m	92	%
Hydraulic efficiency	η_h	94	%
Pump power output	P_o	2667	W
Pump power input	P_i	3426	W
DISPLACEMENT, CYLINDERS, STROKE, PISTON, INLET AND OUTLET DIAMETER			
Displacement per revolution	D	30	cm ³
Number of cylinders	m	3	-
Displacement per revolution per cylinder	$D_{cylinder}$	10	cm ³
Stroke length	s	2.34	cm
Piston diameter	d_p	2.34	cm
Piston area	A_p	4.28	cm ²
Inlet diameter	d_s	2.00	cm
Outlet diameter	d_d	2.00	cm
PISTON FORCES, CYLINDER FORCES, PISTON ROD DIAMETER, CYLINDER THICKNESS			
Maximum differential pressure piston	p_{dp}	95	bar
Force on piston	F_p	4068	N
Stainless Steel Grade 310, fatigue limit in water	σ_f	100	MPa
Safety factor	S_f	3.80	-
Piston rod area	A_{pr}	1.55	cm ²
Piston rod diameter	d_{pr}	1.40	cm
Safety factor	S_f	4.50	-
Stainless Steel Grade 310, fatigue limit in water	σ_y	100	MPa
Cylinder thickness	t	0.50	cm

RECIPROCATING PUMP SPECIFICATIONS AND DIMENSIONS

FORCES ON PISTON, CROSSHEAD, CONNECTING ROD AND CRANKSHAFT

Radius from crankshaft center to crankpin	r	1.17	cm
Connecting rod length	L_c	7.01	cm

ROD 1

Crank Angle	θ_1	86	°
Angle between piston rod and connecting rod	α_1	10	°
Maximum differential suction pressure on piston	p_s	0.52	bar
Force on piston	F_p	22.23	N
Force on connecting rod	F_{cr}	22.55	N
Force on crosshead	F_{ch}	3.75	N
Normal force on crankshaft	$F_{cs,n}$	-2.19	N
Tangent force on crankshaft	$F_{cs,t}$	22.44	N

ROD 2

Crank angle	θ_2	206	°
Angle between piston rod and connecting rod	α_2	-4	°
Maximum differential discharge pressure on piston	p_d	94.99	bar
Force on piston	F_p	4067.80	N
Force on connecting rod	F_{cr}	4078.70	N
Force on crosshead	F_{ch}	-298.00	N
Normal force on crankshaft	$F_{cs,n}$	-3786.75	N
Tangent force on crankshaft	$F_{cs,t}$	-1515.37	N

ROD 3

Crank angle	θ_3	326	°
Angle between piston rod and connecting rod	α_3	-5	°
Maximum differential discharge pressure on piston	p_d	94.99	bar
Force on piston	F_p	4067.80	N
Force on connecting rod	F_{cr}	4085.58	N
Force on crosshead	F_{ch}	-380.77	N
Normal force on crankshaft	$F_{cs,n}$	3159.43	N
Tangent force on crankshaft	$F_{cs,t}$	-2590.36	N

MAXIMUM FORCES ON PISTON, CROSSHEAD, CONNECTING ROD AND CRANKSHAFT

Maximum piston load	$F_{p,max}$	4203	N
Maximum connecting rod load	$F_{cr,max}$	4263	N
Maximum crosshead load	$F_{ch,max}$	-710	N
Maximum crankshaft normal load	$F_{cs,n,max}$	4203	N
Maximum crankshaft tangent load	$F_{cs,t,max}$	-4203	N

Stainless Steel Grade 310, fatigue limit in water	σ_f	100	MPa
Safety factor	S_f	1.5	-
Connecting rod area	A_{cr}	0.63945	cm ²
Connecting rod diameter	d_{cr}	0.90231537	cm

RECIPROCATING PUMP SPECIFICATIONS AND DIMENSIONS

CRANKSHAFT BENDING MOMENTS AXIAL PLANE

Force on piston 1	F_{p1}	22.23	N
Force on piston 2	F_{p2}	4067.80	N
Force on piston 3	F_{p3}	4067.80	N
Distance from point A to line of action of F_{p1}	a_1	4.11	cm
Distance from point A to line of action of F_{p2}	a_2	4.11	cm
Distance from point A to line of action of F_{p2}	a_3	4.11	cm
Distance from point A to point B	a_4	4.11	cm
Reaction force point A	R_A	3067.52	N
Reaction force point B	R_B	5090.31	N
Moment about point A	M_A	0.00	Nm
Moment about point B	M_B	0.00	Nm
Bending moment about point 1	M_1	125.95	Nm
Bending moment about point 2	M_2	250.99	Nm
Bending moment about point 3	M_3	209.01	Nm

CRANKSHAFT BENDING MOMENTS COAXIAL PLANE

Force on crosshead 1	$F_{ch,1}$	3.75	N
Force on crosshead 2	$F_{ch,2}$	-298.00	N
Force on crosshead 3	$F_{ch,3}$	-380.77	N
Distance from point A to line of action of F_{p1}	a_1	4.11	cm
Distance from point A to line of action of F_{p2}	a_2	4.11	cm
Distance from point A to line of action of F_{p2}	a_3	4.11	cm
Distance from point A to point B	a_4	4.11	cm
Reaction force point A	R_A	241.38	N
Reaction force point B	R_B	433.64	N
Moment about point A	M_A	0.00	Nm
Moment about point B	M_B	0.00	Nm
Bending moment about point 1	M_1	9.91	Nm
Bending moment about point 2	M_2	19.98	Nm
Bending moment about point 3	M_3	17.81	Nm

CRANKSHAFT BENDING MOMENTS RESULTANT

Bending moment about point 1	M_1	126.342	Nm
Bending moment about point 2	M_2	251.786	Nm
Bending moment about point 3	M_3	209.765	Nm

CRANKSHAFT BENDING STRESS

Crankshaft diameter	d_{cs}	3.00	cm
Second moment of area cylindrical shaft	I	3.98	cm ⁴
Maximum bending stress	σ_b	94.99	MPa
Torque on shaft	T	43.62	Nm
Polar moment of area cylindrical shaft	J	7.95	cm ⁴
Torsional stress on shaft	τ	8.23	MPa
Maximum principal stress on shaft	σ_{max}	95.70	MPa
Stainless Steel Grade 310, yield limit	σ_y	310.00	MPa
Stainless Steel Grade 310, fatigue limit	σ_f	217.00	MPa
Safety factor	S_f	2.30	-
Allowable stress	$\sigma_{allowable}$	94.35	MPa

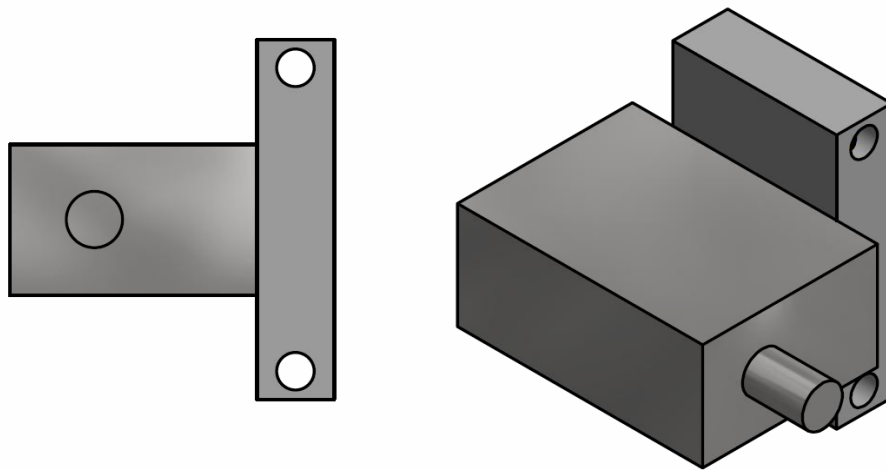


Figure 4.22: Model of the designed reciprocating pump without energy recovery.

4.4 The Reciprocating Pump with Integrated Energy Recovery

The design of the reciprocating pump with energy recovery was based on the design of the reciprocating pump without energy recovery. The reciprocating pump with energy recovery will be a solution where the reciprocating pump and a positive displacement energy recovery device is integrated. However, this solution differs from the solutions described in the theory section 3.1.1.2. All the solutions described in section 3.1.1.2 are based on transferring the high pressure energy of the concentrate stream to the feed stream prior to the feed stream entering the high pressure pump, or an additional booster pump. These solutions therefore necessitates at least two devices, an energy recovery device and a high pressure pump, or even three devices, an energy recovery device, a booster pump, and a high pressure pump.

The solution designed in this section aims to transfer the energy of the exiting high pressure concentrate directly to the pistons of the reciprocating pump. The solution suggests incorporating high pressure chambers in the power end of the reciprocating pump, directly behind the pistons. In this manner, high pressure concentrate can fill the chambers behind the piston on the discharge stroke, thereby transferring power to the piston, and ultimately, reducing the total power input to the reciprocating pump.

This solution will require check valves at the inlet and outlet of the pressure chamber behind the piston, able to control the flow of concentrate in and out. These valves can not be spring controlled check valves, seeing as the pressure of the concentrate is approximately constant, and we only want the concentrate to fill the pressure chambers at the discharge stroke of the pump. At the suction stroke of the pump, the concentrate must then be evacuated from the pressure chambers, so as not to exert an excessive force on the pistons opposite to the direction of movement. Without appropriately controlled valves, the high pressure concentrate would increase the work required of the piston on the suction stroke, and an energy recovery would not be possible. The solution chosen was therefore based on camshafts operating the check valves of the pressure chambers. The camshafts will be driven by the crankshaft. In this manner the valves can be controlled to only allow high pressure concentrate to enter the pressure chambers on the discharge stroke of the pump.

This solution will increase the size of the reciprocating pump, but not as significantly as the solutions comprising separate energy recovery devices and booster pumps.

4.4.0.9 Piston Rod Diameter

For the reciprocating pump with energy recovery, a piston rod is necessary to enable the high pressure concentrate to fill the pressure chambers behind the pistons.

The piston rod diameter must be chosen after considering the forces it must be able to withstand. During the discharge stroke the piston is in compression and during the suction stroke it is in tension.

The force acting on the piston and therefore also the piston rod during a discharge stroke is given by the product of the piston area A_p , and the differential pressure between the discharge pressure and the pressure at the power end of the piston p_{dp} , given in equation 4.4.1.

$$F_p = p_{dp}A_p \quad (4.4.1)$$

The necessary piston rod diameter can be found by requiring that the stress in the piston rod does not exceed the yield limit of the material.

When a material is subject to cyclic stresses it is possible for failure to occur at a stress level considerably lower than the yield limit of the material. Because the piston and piston rod in the reciprocating pump is clearly subjected to cyclic stresses, the maximum permissible stress in the material must be found from an S-N curve, where stress levels, S, are plotted against the number of cycles to failure, N [8]. Stainless steels exhibit a fatigue limit when cyclic stresses are applied. This means that beneath a certain stress level, the fatigue limit, failure should not occur. This limit is determined from a series of tests [4]. Data is found on the mechanical properties of stainless steel, and according to the International Nickel Company [22], the fatigue limit of stainless steel AISI type 310 in dry air is 215 MPa . The fatigue limit of a material subjected to corrosive fluid should be expected to be significantly reduced. For this reason, the piston rod is designed by requiring that the maximum stress in the piston rod should be less than 100 MPa . The necessary piston rod area can then be found from equation 4.4.3

$$S_f F_p < \sigma_f A_{pr} \quad (4.4.2)$$

where S_f is a safety factor, F_p is the force acting on the piston rod as found from equation 4.4.1, σ_f is the fatigue limit of the piston rod material and A_{pr} is the piston rod area.

The piston rod diameter can then finally be found from equation 4.4.3.

$$d_{pr} = \sqrt{\frac{4A_{pr}}{\pi}} \quad (4.4.3)$$

4.4.1 Size of Concentrate Pressure Chambers

The length of the concentrate pressure chambers will have to equal or be greater than the length of the feedwater pressure chambers. This is because the stroke of the piston is already determined, and will of course be the same on both sides of the piston. If the lengths are chosen to be equal, the volume swept in the concentrate pressure chamber will be less than the volume swept in the feedwater pressure chambers, because of the necessary volume of the piston rod. This will not be a problem, because the flow rate of the concentrate stream is lower than the flow rate of the feedwater stream. The recovery ratio of the system determines the concentrate flow rate. The recovery ratio for seawater is in the range of 40 - 70 percent [20], and thus the concentrate flow rate is not expected to exceed 60 percent of the feedwater flow rate.

4.4.2 Camshafts and Check Valves

The check valves controlling the flow in and out of the concentrate pressure chambers are driven by camshafts. Camshafts are an integral part of internal combustion engines, where they are used to operate the valves controlling the air/fuel mixture intake and exhaust gases. A camshaft is a shaft to which a cam is fastened. The shape of the cams control the timing of the opening and closing of the valves, because the translational movement of the valves follow the surface of the cams. When the camshaft is connected to the pump crankshaft through gears, the shape of the cams can be adjusted so that they open and close a valve during one half-rotation of the crankshaft, or in other words during one discharge or suction stroke. In order to be able to control the inlet and outlet valves of the concentrate pressure chamber efficiently, one camshaft will drive the inlet valves, and another will drive the outlet valves. Both camshafts will be coupled to the pump crankshaft with gears.

4.4.3 Safety Relief Valve

In order to avoid the build up of excessive pressure in the the pump and system, a safety relief valve should be placed at both the discharge of the pump and by the concentrate inlet to the pressure chambers. This can be spring controlled valves, which can be adjusted to different pressure levels.

The main dimensions and physical properties of the reciprocating pump with energy recovery are the same as for the reciprocating pump without energy recovery, and are found in table 4.12. The additional parameters in the design with energy recovery is the pressure chambers behind the pistons. These pressure chambers all have a length that equals the stroke length s in table 4.12, and a diameter that equals the piston diameter d_p in table 4.12. The inlet and outlet diameters of the pressure chambers are the same as the inlet and outlet diameters given in table 4.12, d_s and d_d .

A three-dimensional model of the finished design was constructed using the computer-aided design software *Autodesk Inventor*. The model is shown in figure 4.23, and additional drawings are given in appendix D.

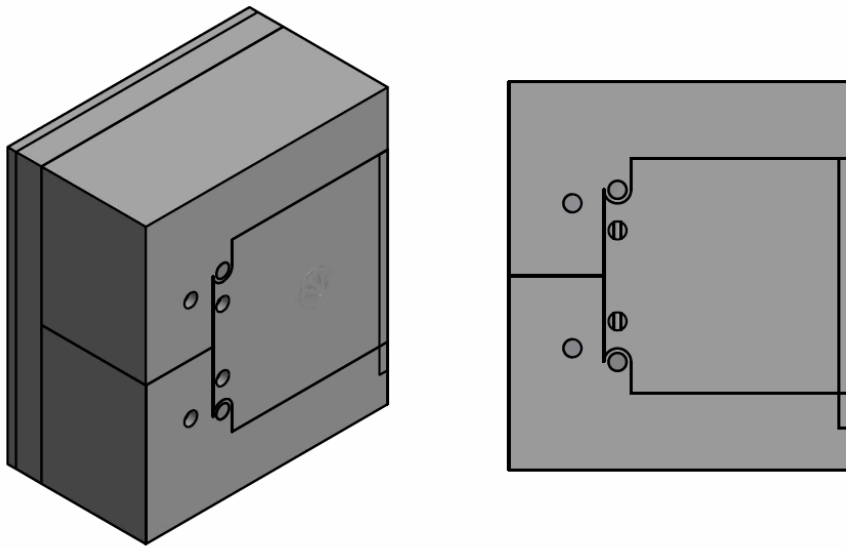


Figure 4.23: Model of the designed reciprocating pump with energy recovery.

4.5 Energy savings

Of the four solutions considered, only three of them incorporated an energy recovery device. This is of course the first and second solution with the Turgo turbine and the fourth solution with the reciprocating pump with integrated energy recovery. The objective of the first and second solution was to connect the Turgo turbine directly to the pump shaft in order to reduce the required input power to the motor. The objective of the fourth solution was to fill the pressure chambers behind the pistons with high pressure concentrate on the discharge stroke in order to reduce the required input power to the motor. An estimation of the energy savings for different membrane efficiencies or recovery ratios, i.e., permeate to feedwater ratios are given in table 4.13 for the solutions comprising a turbine and the solution comprising a reciprocating pump with integrated energy recovery. The estimated savings for the solutions comprising a turbine assumes that the turbine has the right dimensions for the given flow and head specifications.

Table 4.13: Estimated energy savings for systems with energy recovery.

Recovery ratio of RO membrane	R		40 %	70 %
Density of feed water	ρ_{feed}	kg/m ³	1000	1000
Density of concentrate	$\rho_{concentrate}$	kg/m ³	1050	1050
Gravitational constant	g	m/s ²	9.81	9.81
Flow rate of feed water	Q_{feed}	m ³ /s	0.00033	0.00033
Flow rate of permeate	$Q_{permeate}$	m ³ /s	0.00013	0.00023
Flow rate of concentrate	$Q_{concentrate}$	m ³ /s	0.00020	0.00010
Delivery pressure of feed water	H_{feed}	mWc	815	815
Assumed efficiency of pump	η_p		78 %	78 %
Maximum input power pump	P_p	kW	3.4	3.4
Available pressure energy recovery device	H_{ERD}	mWc	750	750
Assumed total efficiency of turbine	η_t		90 %	90 %
Assumed total efficiency of integrated reciprocating ERD	η_r		95 %	95 %
Maximum power output turbine	P_t	kW	1.4	0.7
Maximum power output of integrated reciprocating ERD	P_{ERD}	kW	1.5	0.7
Energy savings with turbine			41 %	20 %
Energy savings with integrated reciprocating ERD			43 %	21 %

The expected total efficiency of the energy recovery part of the reciprocating pump is somewhat higher than the expected total efficiency of the turbine. This is based on how the energy transfer occurs. The turbine transfers energy through more intermediary mechanical parts. In the reciprocating pump with integrated energy recovery, the concentrate exerts force on the pistons directly. The assumed efficiencies for the energy recovery part of the reciprocating pump and the turbine are 95 percent and 90 percent respectively. According to Gude [21], this is a reasonable assumption.

4.6 System Drive Mechanism

Seeing as all four system designs are based on relatively high rotational speeds, ranging from 750 to 3000 rpm, the optimal solution for the system drive mechanism would be an electric motor. However, because 1.4 to 1.6 billion people around the world does not have access to electricity, and another one billion people depend on unreliable electricity grids [10], the possibility of an alternative drive mechanism should be considered. One alternative would be to supply the system with a diesel driven generator, able to produce electricity to drive the electric motor. This solution will however make the system dependent on diesel instead of electricity. An optimal solution would be to make the system able to run on renewable resources such as wind, solar, or hydropower. A challenge with this solution is the unreliable nature of these resources, and the high rotational speed required for the system. The existing design of the system will therefore be based on the assumption that electricity is an available resource.

4.7 Reverse Osmosis System

A suggestion on the entire system design has been made. This design is based on the reciprocating pump with integrated energy recovery. The additional components added are an electric motor, a filtering and UV-filtration system, and the reverse osmosis membrane.

A three-dimensional model of the finished design was constructed using the computer-aided design software *Autodesk Inventor*. The model is shown in figure 4.24, and additional drawings are given in appendix E.

Additional information on the motor, filtering and UV-filtration system, and the reverse osmosis membrane are given in appendix F.

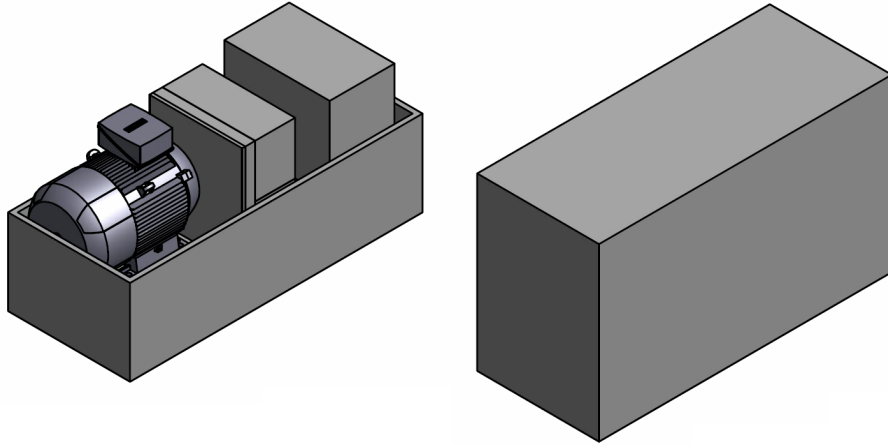


Figure 4.24: Model of the designed reciprocating pump with energy recovery.

5 Discussion and Conclusion

Parts of this section is taken from the project thesis *Desalination of Water by Reverse Osmosis* written in the fall of 2015 by Løken [26].

The intended application area of the reverse osmosis system is to secure the supply of drinking water in remote parts of the world where infrastructure is lacking, or in areas struck by natural disasters. When evaluating which high pressure pump and energy recovery device is best suited for the system, the intended application area must be kept in mind. Several parameters might be examined, such as size, weight, simplicity, durability, cost, energy requirement and efficiency. The most important parameters must be identified. Size and weight are obviously important parameters in order to have a portable system. Because the system is intended for use in areas where infrastructure is lacking, simplicity and durability become important parameters as well, seeing as the system should be easy to operate and that spare parts might be hard to come by. The energy requirement is important because the system might operate in areas where energy is a scarce resource. The four proposed solutions for the system, described in detail in the previous parts of this thesis, should be discussed in light of these parameters.

The first proposed solution was a centrifugal pump and a Turgo turbine. The design of these components were based on a required feedwater flow rate of 100 l/min and a required delivery pressure of 65 bar. The Turgo turbine was to be directly coupled to the shaft of the centrifugal pump. The rotational speed was chosen to be 3000 rpm, the highest synchronous rotational speed that can be achieved with a 50 Hz supply current. A high rotational speed reduces the necessary size of the rotating machinery. The centrifugal pump and Turgo turbine were chosen because of their robustness and simplicity. The given flow and head specifications are however well outside the range of a typical centrifugal pump. A larger flow rate would have made the centrifugal pump a more natural choice for the system. The flow rate is limited by the capacity of the RO membrane. More membranes could have been installed but this would increase the total size of the system

and the possibility was thus discarded.

Nevertheless, two different centrifugal pump designs were produced. The details of these designs are given in section 4.1.1, and in appendix B. The first design was produced by applying the governing Euler equation and using a standard procedure as outlined by Łazarkiewicz and Troskolański in the book *Impeller Pumps* [25]. It was found that the channel width at the outlet of the impeller became extremely small, only 1.4 mm. It is obvious that this standard design would lead to enormous friction losses due to the viscosity of water and the narrowness of the channels.

A second design was therefore attempted, where the channel width and height of the impeller was constrained to a lower limit of 1.4 cm. The resulting design is everything but conventional, with the thickness of the blades being many times the height of the channels. The impeller design is shown in figure 4.5. To avoid unnecessary material costs, the blades could be made hollow. The flow behavior through the impeller might however cause serious losses. At the outlet of the impeller the flow area is rapidly increasing and the flow will separate off the channel walls due to the abrupt area change. Separation causes severe disturbances in the flow, and this will lead to losses.

The design of the turbine also proved to be somewhat challenging. This was due to the scarcity of published literature on the design of such turbines. The Turgo was however designed on simple principles such as to not lose any water, and to provide a shockless entry of the water into the buckets. The shape of the buckets was also designed to give a smooth deflection of water through the bucket, making the water leave with a relative outlet velocity opposite to the relative inlet velocity, and as small kinetic energy as possible.

The design of the Turgo as seen in figure 4.13 and appendix A, is thought to be quite efficient. The size of the runner is also reasonable, and it is assumed that it can be manufactured in a light weight material such as hard plastic, by considering the dimensioning forces on the bucket. Although the theoretical considerations suggests a high efficiency for the turbine designed, this should be confirmed through Computational Fluid Dynamics (CFD), experiments or both.

The centrifugal pump would be a durable component, giving a continuous pressure rise to the water, and not requiring any valves or extra lubrication of the moving parts in contrast to the reciprocating pump. The centrifugal pump designed is however bound to give very high frictional hydraulic losses, due to the narrowness of the channels and the viscosity of water. The poor suitability of the centrifugal pump to the RO system was however

expected, because the given flow rate and head specifications are well outside the range for centrifugal pumps. Consequently, another type of pump should be considered for the RO system, a type more suitable for high head and low flow rate applications, such as the reciprocating pump.

The advantages of the reciprocating pump is the ability to generate high discharge pressure at low flow rates. The need for several stages, as in the case of the centrifugal pump, is avoided, and therefore the size and weight of a reciprocating pump will be less than that of the centrifugal pump. The complexity of a reciprocating pump is somewhat higher due to the need for valves and lubrication of the moving parts, but the advantages outweighs the disadvantages.

The second proposed solution was a reciprocating pump and a Turgo turbine. The Turgo turbine was to be directly coupled to the shaft of the reciprocating pump. The evaluation of this solution is partly based on experiments performed on a similar system, namely the Waterbox as described in section 4.2. The Waterbox is based on a feedwater flow rate of 40 l/min. The rotational speed of the system is 1500 rpm. The turbine in the Waterbox is a Pelton turbine, but the diameter of the turbine is too small for the operating range of around 60 bar. The maximum power savings by utilizing the turbine was measured to be 6 percent of the total power consumption without the turbine, as shown in figure 4.18. This was to be expected due to the small diameter of the Pelton turbine runner. The most important result of the experiments was the indication that there is a potential for saving energy when a turbine is coupled directly to the shaft of the reciprocating pump. However, the efficiency of the turbine, and therefore also the energy recovery of the system, is highly dependent on the system pressure, as was demonstrated by the low energy recovery with the small diameter turbine runner.

The third proposed solution was a reciprocating pump without energy recovery. The design of this component was based on a required feedwater flow rate of 20 l/min and a required delivery pressure of 80 bar. These specifications were adjusted from the first solution partly because the reciprocating pump allowed for a lower flow rate. At the point of designing the reciprocating pump it was also recognized that the capacity of the pump should coincide with the feedwater capacity of the smallest reverse osmosis membranes on the market, in order to reduce the size and weight of the entire system. The rotational speed chosen for this solution was 750 rpm. Although a higher rotational speed means smaller components, excessively high rotational speeds are known to cause problems in reciprocating pumps.

The design of the reciprocating pump was aided by the book *The Recipro-*

cating Pump: Theory, Design and Use by John E. Miller [29]. The design is shown in figure 4.22 and appendix C.

The solution comprising the reciprocating pump without energy recovery might be a good solution when size and weight are the most important considerations, and when energy consumption is less important.

The fourth solution considered was a reciprocating pump with integrated energy recovery. The design of this component was based on the design of the reciprocating pump without energy recovery. Pressure chambers were added behind all three pistons, allowing for the concentrate stream to fill the pressure chambers on the discharge stroke of the pistons. The design is shown in figure 4.23 and appendix D. The reciprocating pump with integrated energy recovery is the most compact solution comprising energy recovery. The energy transfer efficiency is also believed to be higher, as illustrated in table 4.13. In contrast to the Turgo turbine where the design is quite dependent on a specific pressure region, it is believed that the energy transfer efficiency of the reciprocating pump with integrated energy recovery will be high over a wide range of operating pressures.

Because it is possible to construct a reciprocating pump with integrated energy recovery of smaller size and weight than the system comprising a pump and a Turgo turbine, the fourth solution is believed to be the best solution for the reverse osmosis system.

A suggestion on the total system design including a reciprocating pump with integrated energy recovery is given in figure 4.24 and appendix E. The final size of the reverse osmosis system comprising a reciprocating pump with integrated energy recovery, a reverse osmosis membrane, a filtration and UV-system and an electric motor is $1.2\text{ m} \times 0.5\text{ m} \times 0.7\text{ m}$.

The final recommendations that can be made from the work done, are the following. A centrifugal pump seems to be a poor choice. The flow rate and head specifications of the system make a design without large hydraulic losses difficult. The recommended type of pump is the reciprocating pump, better suited for the given flow rate and head specifications. A Turgo turbine energy recovery device is a possibility, but the solution comprising the reciprocating pump with integrated energy recovery will make the system smaller in size and most likely more efficient, and this is therefore the recommended solution.

6 Further Work

Further work related to the reverse osmosis system should focus on validating the assumptions made on efficiency of the reciprocating pump with integrated energy recovery. The solution should be evaluated by doing a Computational Fluid Dynamics Analysis. The solution could also be further evaluated by building a prototype and performing experiments in a laboratory.

Another consideration is the drive mechanism for the system. The current solution is based on an electric motor supplied either from the power grid or by a diesel generator. Because the system should be able to operate in remote areas lacking infrastructure, alternative drive mechanisms should be considered. An option might be to reduce the rotational speed of the system in order to make renewable resources like wind a possibility.

To further reduce the size and weight of the system, other solutions or technologies could be considered.

Bibliography

- [1] File:PressureExchanger_3DSchematics.svg. https://commons.wikimedia.org/wiki/File:PressureExchanger_3DSchematics.svg, 2015. [Online; accessed 16-December-2015].
- [2] John S Anagnostopoulos and Dimitris E Papantonis. Optimal design and experimental validation of a Turgo model hydro turbine. *Proceedings of the ASME 2012 11th Biennial Conference on Engineering Systems Design and Analysis ESDA2012 July 2-4, 2012, Nantes, France*, pages 1–10, 2015.
- [3] H. H. Anderson. *Centrifugal Pumps and Allied Machinery*. Elsevier Advanced Technology, Oxford, UK, 4th edition, 1994. ISBN:1 85617 231 7.
- [4] British Stainless Steel Association. Fatigue properties and endurance limits of stainless steels. <http://www.bssa.org.uk/topics.php?article=104>, 2016. [Online; accessed 25-May-2016].
- [5] Professor Hermod Brekke. *Grunnkurs i hydrauliske strømningsmaskiner*. NTNU, 2000.
- [6] Professor Hermod Brekke. *Pumper og Turbiner*. NTNU, 2003.
- [7] Mechanical buzz. Reciprocating Pump (Single-acting and Double-acting reciprocating pump). <http://mechanicalbuzz.com/single-acting-double-acting-reciprocating-pump.html>, 2016. [Online; accessed 8-June-2016].
- [8] William D. Callister and David G. Rethwisch. *Failure*. John Wiley & Sons, Inc., 8th edition, 2011. ISBN:978-0-470-50586-1.
- [9] Yunus A. Cengel and John M. Cimbala. *Fluid Mechanics: Fundamentals and Applications, Chapter 8*. McGraw-Hill, 2nd edition, 2010. ISBN:978-007-128421-9.

- [10] Bryan R. Cobb and Kendra V. Sharp. Impulse (Turgo and Pelton) turbine performance characteristics and their impact on pico-hydro installations. *Renewable Energy*, 50:959–964, 2013.
- [11] The Dow Chemical Company. Filmtec Reverse Osmosis Membranes. http://msdssearch.dow.com/PublishedLiteratureDOWCOM/dh_08db/0901b803808db77d.pdf?filepath=liquidseps/pdfs/noreg/609-00071.pdf&fromPage=GetDoc, 2016. [Online; accessed 09-March-2016].
- [12] Gary L Cornell and Blacoh Fluid Control. The Necessity of Fluid Control. https://www.blacoh.com/downloads/literature/The_Necessity_of_Fluid_Control_P19E11_010.pdf, 2011. [Online; accessed 28-May-2016].
- [13] Flowserve Corporation. Calder DWEER Energy Recovery Device Animation. http://www.flowserve.com/Products/Energy-Recovery-Devices/Calder-DWEER-Energy-Recovery-Device-Animation%2Cen_US, 2015. [Online; accessed 16-December-2015].
- [14] Flowserve Corporation. NM Between Bearings, Single Case, Radially Split, Multistage, Ring Section Pump. http://www.flowserve.com/Products/Pumps/Between-Bearings/Single-Case-Radially-Split/NM-Between-Bearings,-Single-Case,-Radially-Split,-Multistage,-Ring-Section-Pump,en_US, 2015. [Online; accessed 11-December-2015].
- [15] Parker Hannifin Corporation. General Comparison of Reverse Osmosis to Vapor Compression Distillers. [http://www.villagemarine.com/images/7975_\(RO_vs_Distillation\)_TAP.pdf](http://www.villagemarine.com/images/7975_(RO_vs_Distillation)_TAP.pdf), 2012. [Online; accessed 8-June-2016].
- [16] Inc. Encyclopdia Britannica. pump. <http://academic.eb.com/EBchecked/topic/483365/pump>, 2016. [Online; accessed 23-May-2016].
- [17] Inc. Energy Recovery. Turbochargers. <http://www.energyrecovery.com/water/turbochargers/>, 2015. [Online; accessed 16-December-2015].
- [18] UCLA Engineering. First Demonstration Of Reverse Osmosis. <http://engineering.ucla.edu/first-demonstration-of-reverse-osmosis/>, 2015. [Online; accessed 29-November-2015].

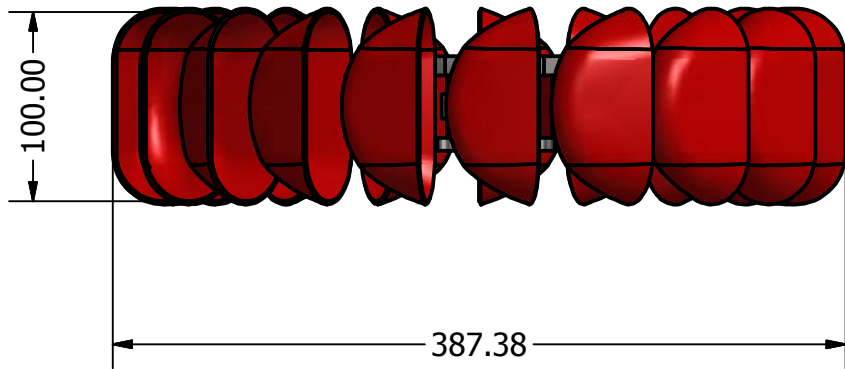
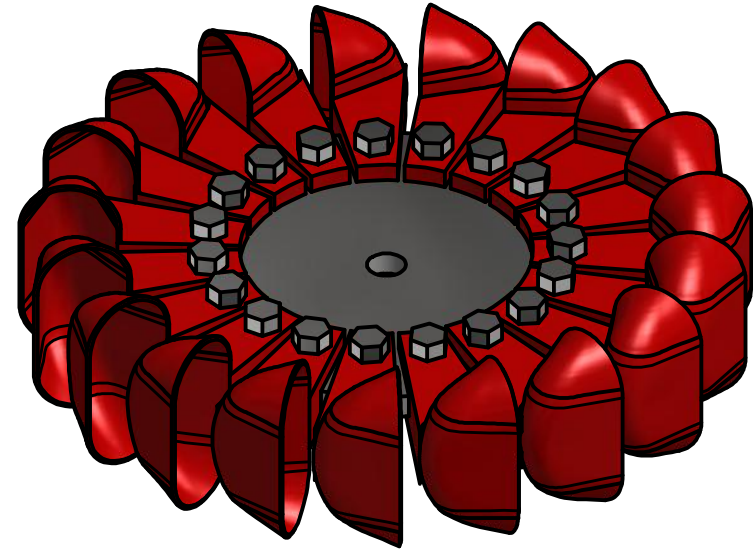
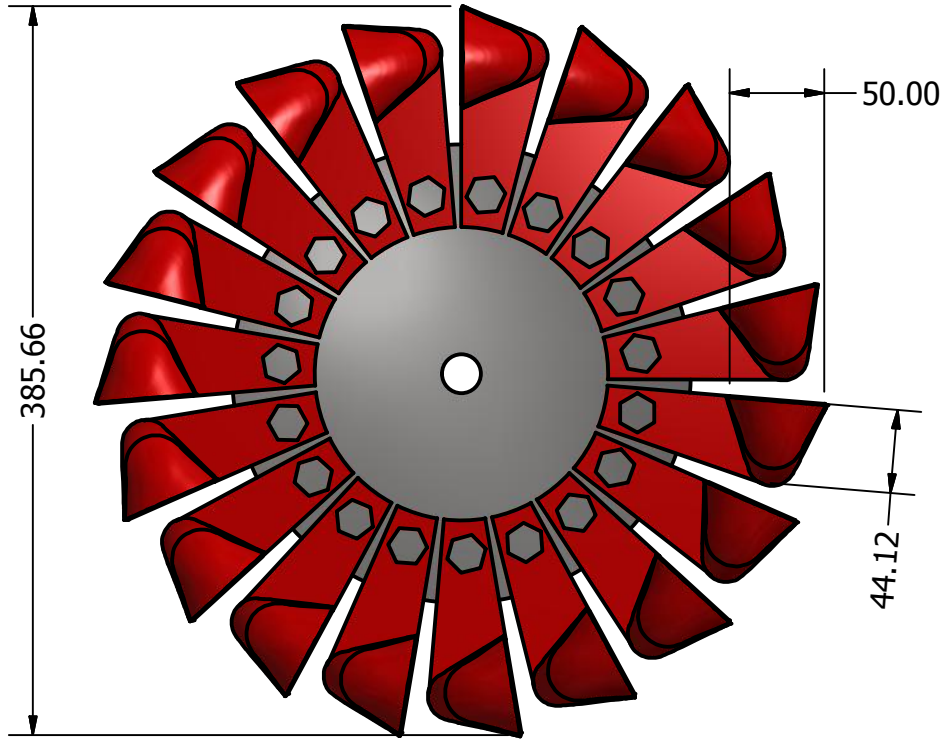
- [19] Kyle Gaiser, Paul Erickson, Pieter Stroeve, and Jean-Pierre Delplanque. An experimental investigation of design parameters for pico-hydro Turgo turbines using a response surface methodology. *Renewable Energy*, 85:406–418, 2016.
- [20] Lauren F. Greenlee, Desmond F. Lawler, Benny D. Freeman, Benoit Marrot, and Philippe Moulin. Reverse osmosis desalination: Water sources, technology, and today’s challenges. *Water Research*, 43(9):2317–2348, 2009.
- [21] Veera Gnanaswar Gude. Energy consumption and recovery in reverse osmosis. *Desalination and Water Treatment*, 36(1-3):239–260, 2011.
- [22] The International Nickel Company Inc. Mechanical and Physical Properties of austenitic chromium-nickel stainless steels at Ambient Temperatures. https://www.nickelinstitute.org/~media/Files/TechnicalLiterature/AusteniticChromium_NickelStainlessSteelsatAmbientTemperaturesMechanicalandPhysicalProperties_2978_.ashx, 1978. Publication no:2978.
- [23] Russell M. Cummings John J. Bertin. *Aerodynamics for Engineers*. Pearson Education Limited, Essex, England, 6th edition, 2014. ISBN 10:0-273-79327-6.
- [24] Dean Kamen. Pure Genius: How Dean Kamen’s Invention Could Bring Clean Water To Millions. <http://www.popsci.com/article/science/pure-genius-how-dean-kamens-invention-could-bring-clean-water-millions>, 2016. [Online; accessed 8-February-2016].
- [25] Stephen Łazarkiewicz and Adam T. Troškolański. *Impeller Pumps*. Pergamon Press Ltd., London, 1st edition, 1965.
- [26] Thea Karlsen Løken. Desalination of Water by Reverse Osmosis: Design of a High Pressure Pump and Energy Recovery Turbine, December 18th 2015. Project Thesis from the Norwegian University of Science and Technology, Faculty of Science and Technology, Department of Energy and Process Engineering.
- [27] Jorge Luis, Clarembaux Correa, and Miguel Asuaje. A Preliminary Analysis of a Turgo Type Turbine Cfd Simulation Designed With an integrated dimensional methodology. *Proceedings of the ASME 2012 Fluids Engineering Summer Meeting FEDSM2012 July 8-12, 2012, Rio Grande, Puerto Rico FEDSM2012-72018*, pages 1–11, 2015.

- [28] Jorge Luis, Clarembaux Correa, Ricardo Noguera, Sergio Croquer, Freddy Jeanty, and Miguel Asuaje. Design procedure for a turgo type turbine using a three-dimensional potential flow. *Proceedings of ASME Turbo Expo 2012 GT2012 June 11-15, 2012, Copenhagen, Denmark*, pages 1–14, 2012.
- [29] John E. Miller. *The Reciprocating Pump: Theory, Design and Use*. Krieger Publishing Company, Malabar, Florida, 2nd edition, 1995. ISBN:0-8946-4599-4.
- [30] Torbjørn K. Nielsen. *Dynamisk dimensjonering av vannkraftverk*. Sintef, 1990. ISBN:82-595-5952-8.
- [31] John Peter Oleson. *Handbook of Ancient Water Technology*. Brill, Leiden, vol 2 edition, 2000.
- [32] World Health Organization. Guidelines for Drinking-water Quality. http://apps.who.int/iris/bitstream/10665/44584/1/9789241548151_eng.pdf, 2011. ISBN:978 92 4 154815 1.
- [33] World Health Organization. Preventing diarrhoea through better water, sanitation and hygiene: exposures and impacts in low- and middle-income countries. http://www.who.int/water_sanitation_health/gbd_poor_water/en/, 2014. [Online; accessed 8-June-2016].
- [34] Baltasar Peñate and L. García-Rodríguez Lourdes. Energy optimisation of existing SWRO (seawater reverse osmosis) plants with ERT (energy recovery turbines): Technical and thermoeconomic assessment. *Energy*, 36(1):613–626, 2011.
- [35] Cat Pumps. Model: 1010, CAD Drawing: 1010.STEP. <http://www.catpumps.com/products.asp?id=124&criteria=1>, 2016. [Online; accessed 23-May-2016].
- [36] R. Rayner. Centrifugal Pump Nomenclature, Characteristics and Components. In *Pump Users Handbook*, pages 39–110. Elsevier Science, Burlington, 4th edition, 1995.
- [37] R. Rayner. Reciprocating Pumps: Nomenclature, Characteristics, Components and Types. In *Pump Users Handbook*, pages 153–170. Elsevier Science, Burlington, 4th edition, 1995.
- [38] Trinath Sahoo. Cavitation in reciprocating pumps. *World Pumps*, (472):24–27, 2006.
- [39] Hans G Scholl and Sulzer Roteq. A pump-turbine combination for seawater desalination. (February):24–25, 2000.

- [40] Peter Smith and R. W. Zappe. *Valve Selection Handbook: Engineering Fundamentals for Selecting the Right Valve Design for Every Industrial Flow Application*. Elsevier Science, Burlington, 5th edition, 2004. ISBN:0-7506-7717-1.
- [41] A. J. Stepanoff. *Centrifugal and Axial Flow Pumps*. Krieger Publishing Company, Malabar, Florida, 2nd edition, 1957. ISBN-13:978-0894647239, ISBN-10:0894647237.
- [42] Herbert H Tackett, James a Cripe, and Gary Dyson. Positive displacement reciprocating pump fundamentals- power and direct acting types. In *Proceedings of the twenty-fourth international pump user symposium*, pages 45–58, Tackett, 2008.
- [43] David J. Woodcock and I. Morgan White. The application of pelton type impulse turbines for energy recovery on sea water reverse osmosis systems. *Desalination*, 39:447–458, 1981.

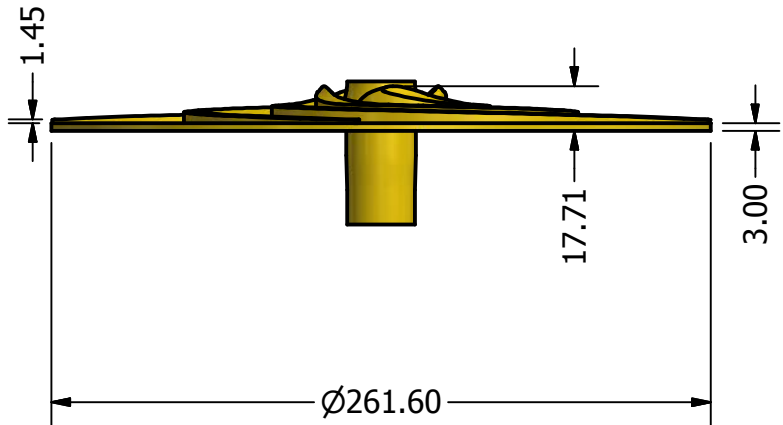
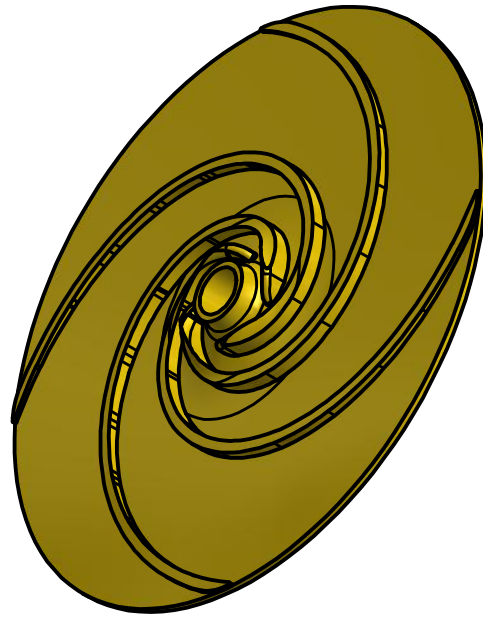
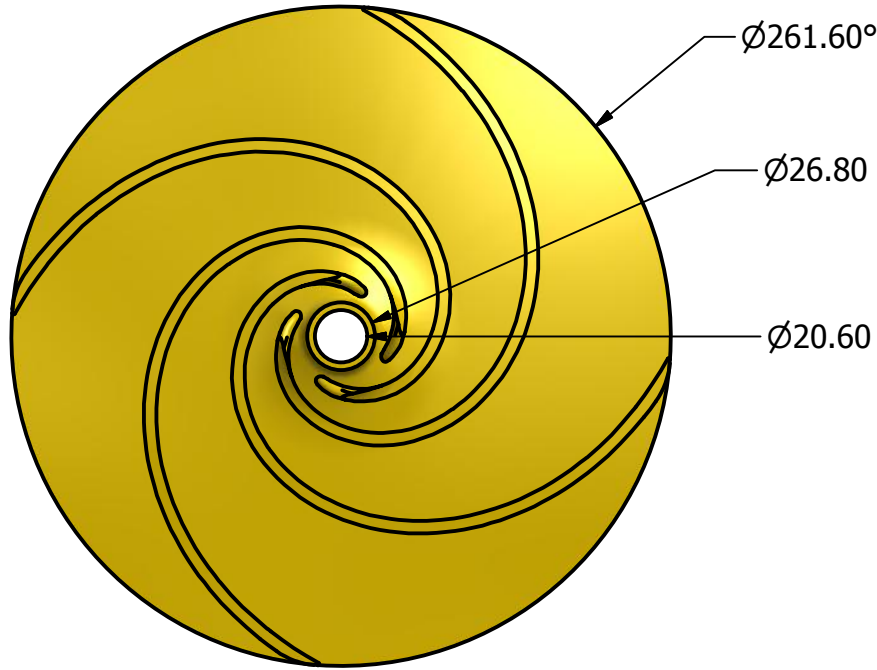
Appendices

A Turgo Drawing

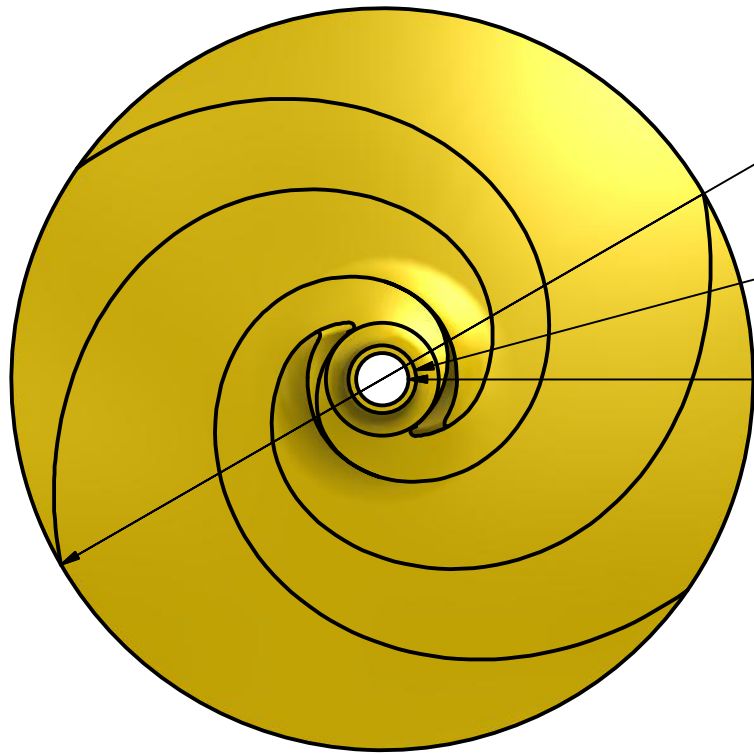


DRAWN Thea Karlsen Løken	18.12.2015	Dimensions given in mm		
CHECKED		TITLE		
QA		Turgo Turbine		
MFG		SIZE	DWG NO	REV
APPROVED		A4		
		SCALE 1/4		

B Centrifugal Pump Drawings



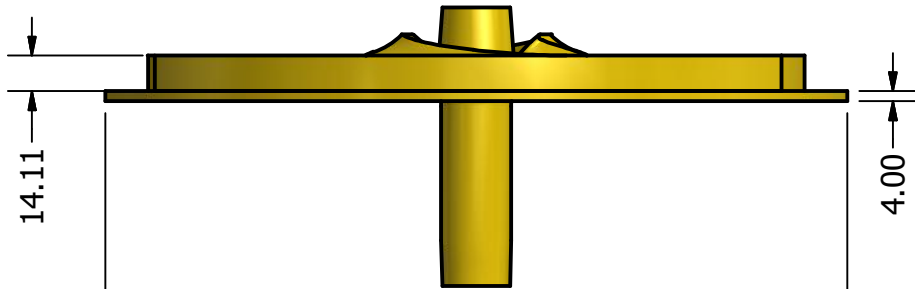
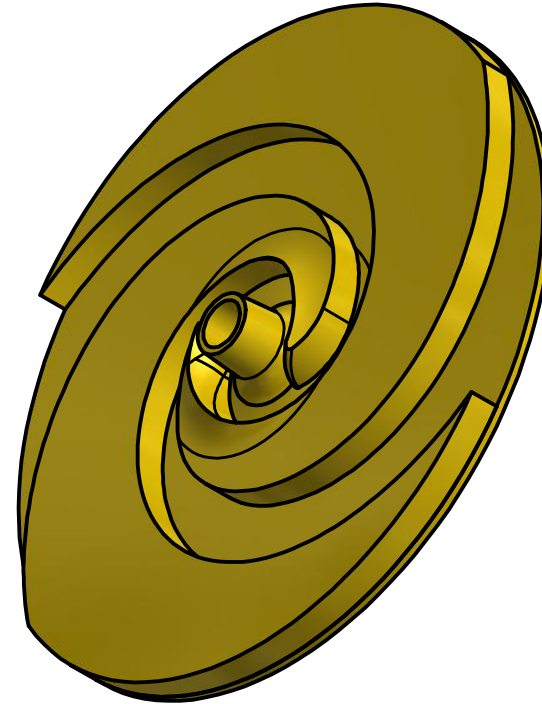
DRAWN Thea Karlsen Løken	18.12.2015	Dimensions given in mm		
CHECKED		TITLE		
QA		Impeller standard design		
MFG				
APPROVED				
		SIZE A4	DWG NO	REV
		SCALE 1/3		



Ø294.40

Ø26.80

Ø20.60

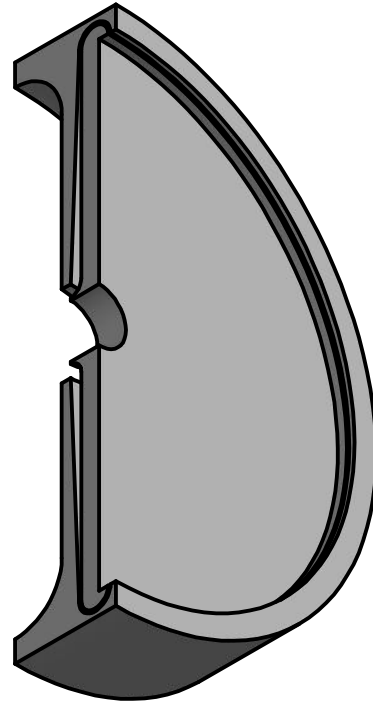
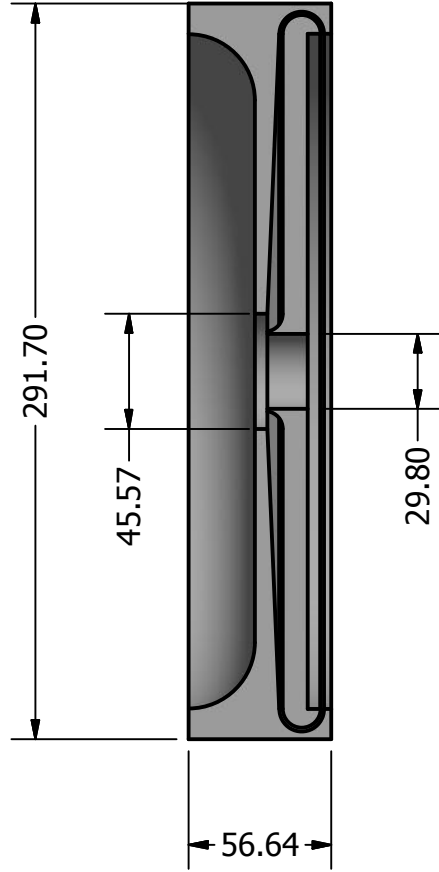
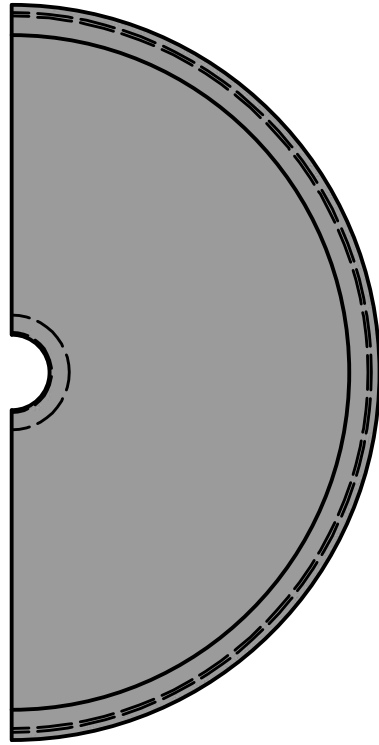


14.11

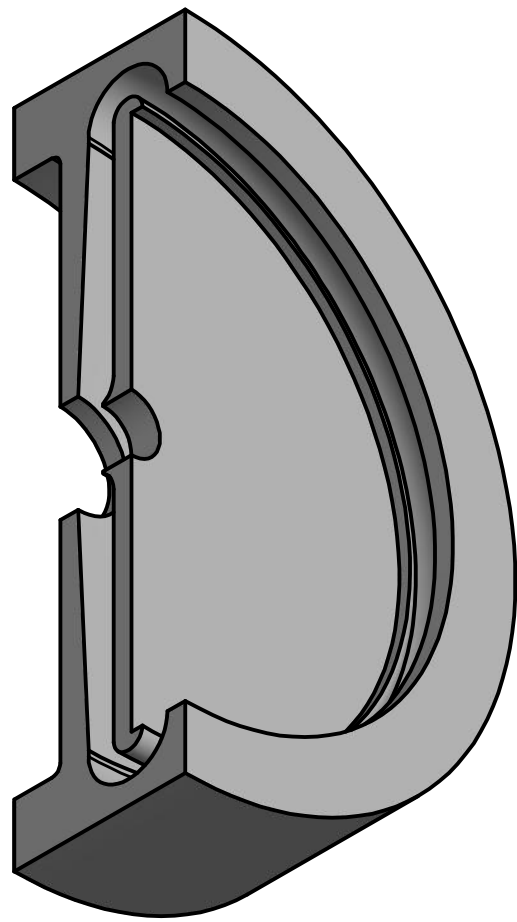
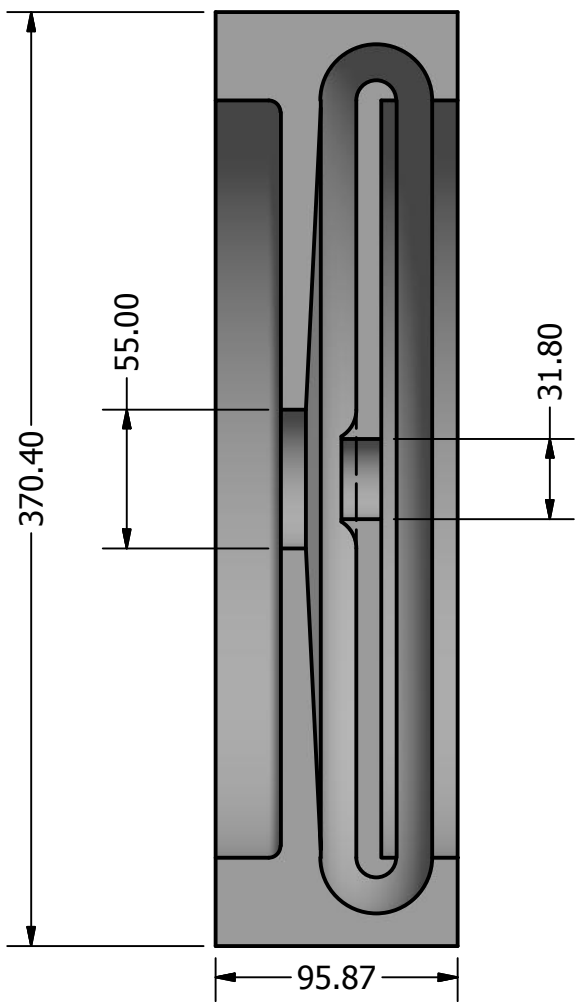
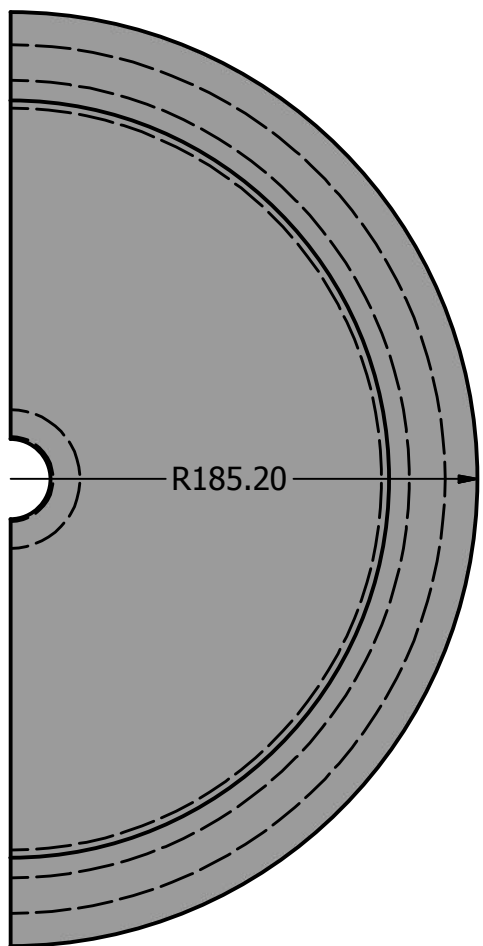
4.00

Ø294.40

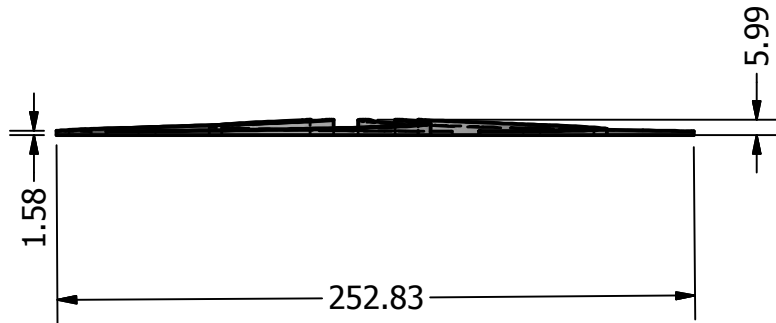
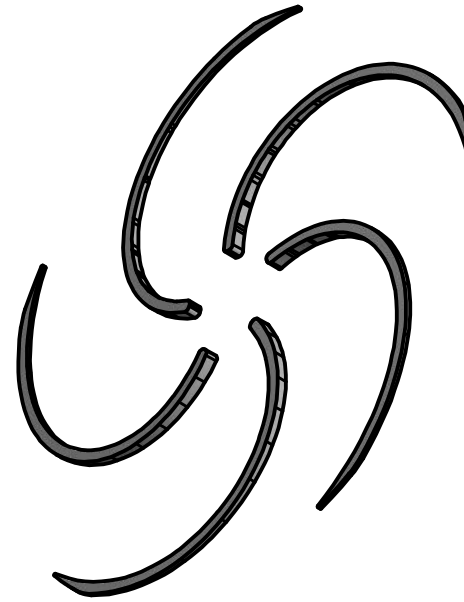
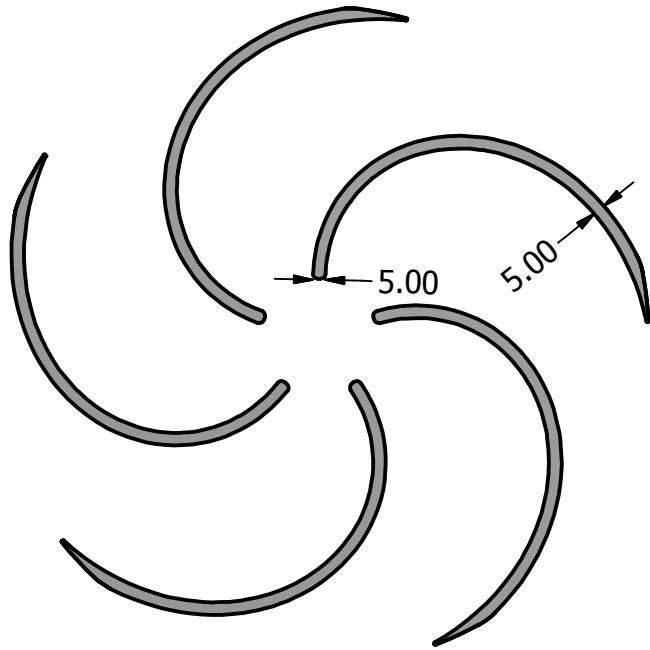
DRAWN Thea Karlsen Løken	18.12.2015	Dimensions given in mm		
CHECKED		TITLE		
QA		Impeller adjusted design		
MFG				
APPROVED				
		SIZE A4	DWG NO	REV
		SCALE 1/3		



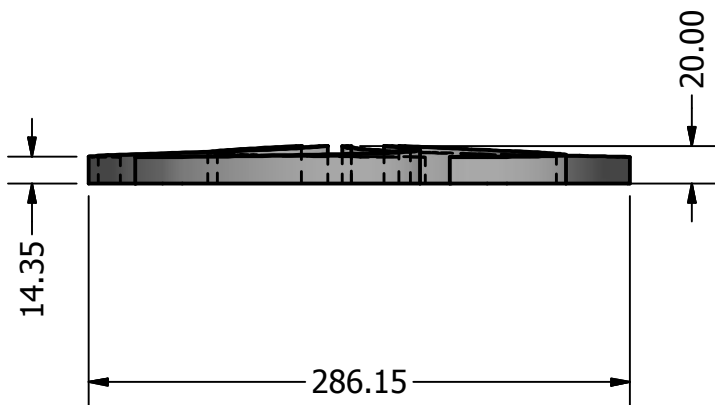
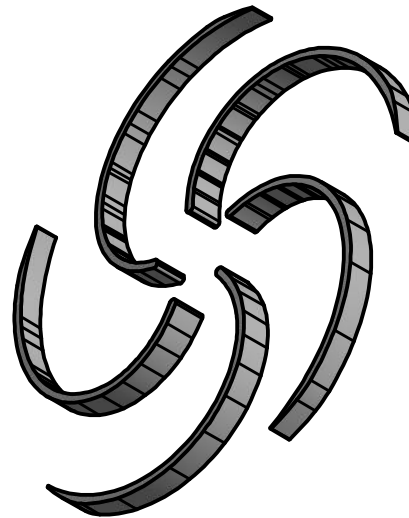
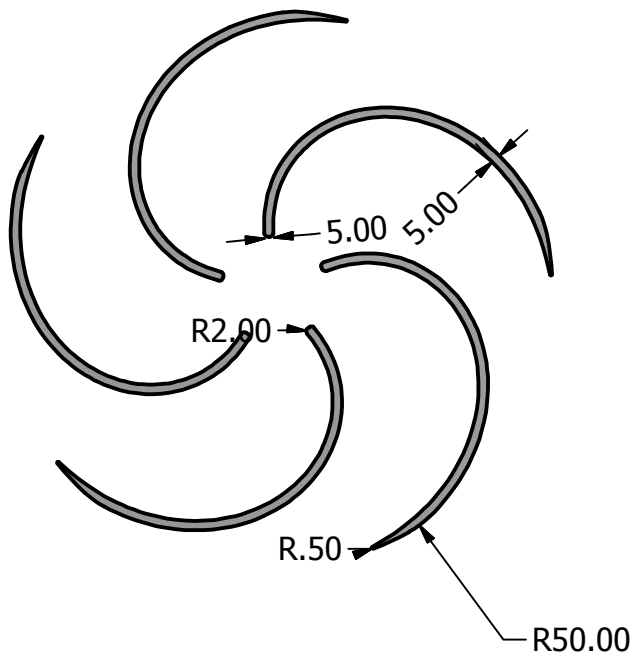
DRAWN Thea Karlsen Løken	18.12.2015	Dimensions given in mm		
CHECKED		TITLE		
QA		Casing standard design		
MFG		SIZE	DWG NO	REV
APPROVED		A4		
		SCALE 1/3		



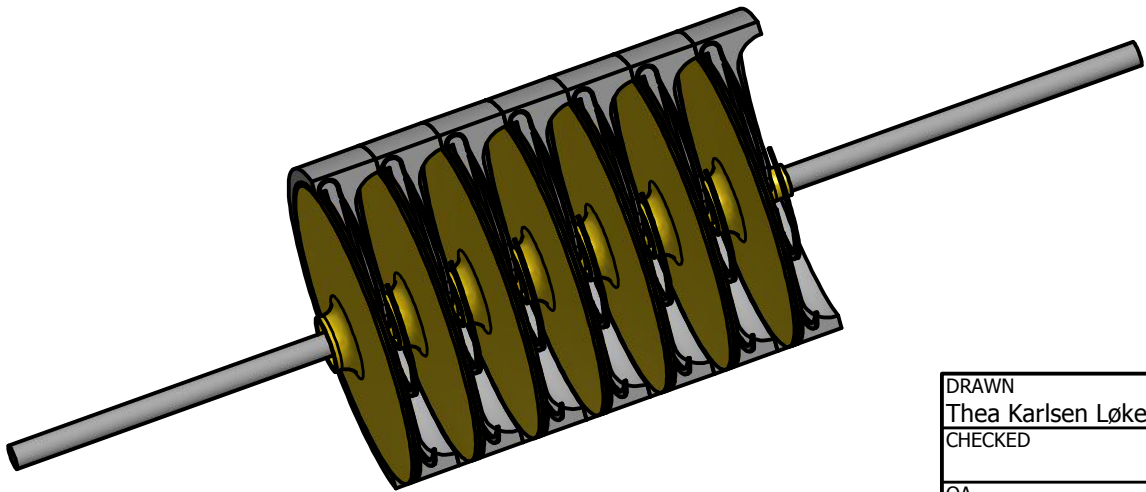
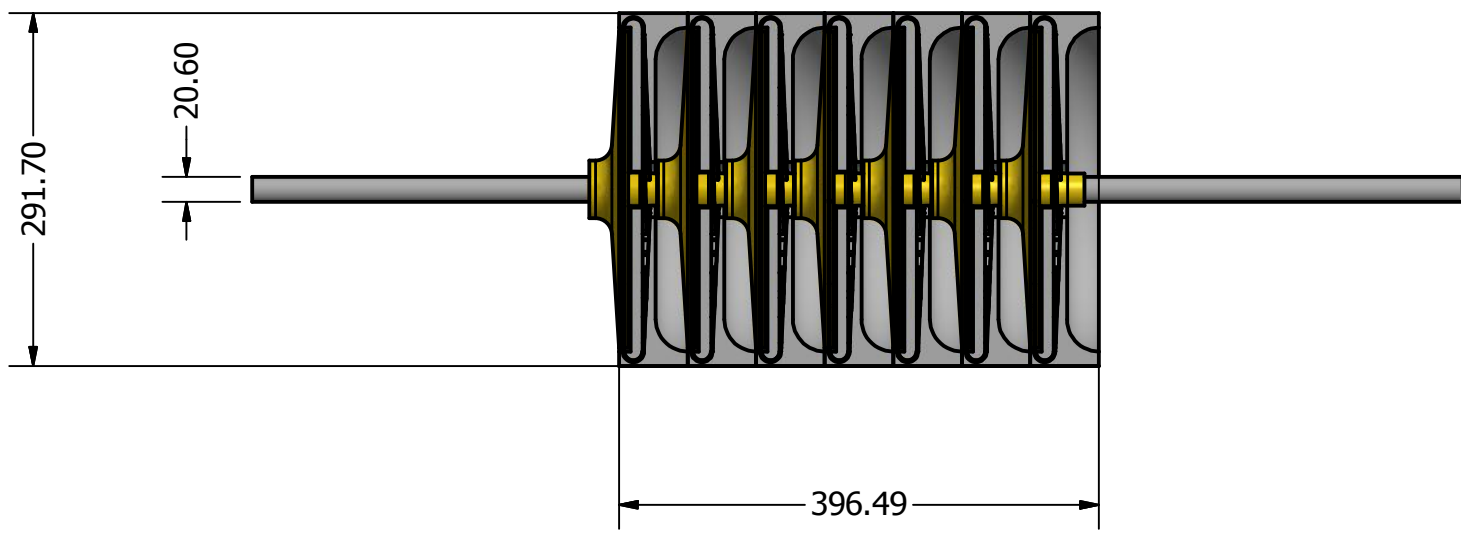
DRAWN Thea Karlsen Løken	18.12.2015	Dimensions given in mm		
CHECKED		TITLE		
QA		Casing adjusted design		
MFG		SIZE	DWG NO	REV
APPROVED		A4		
		SCALE 1/3		



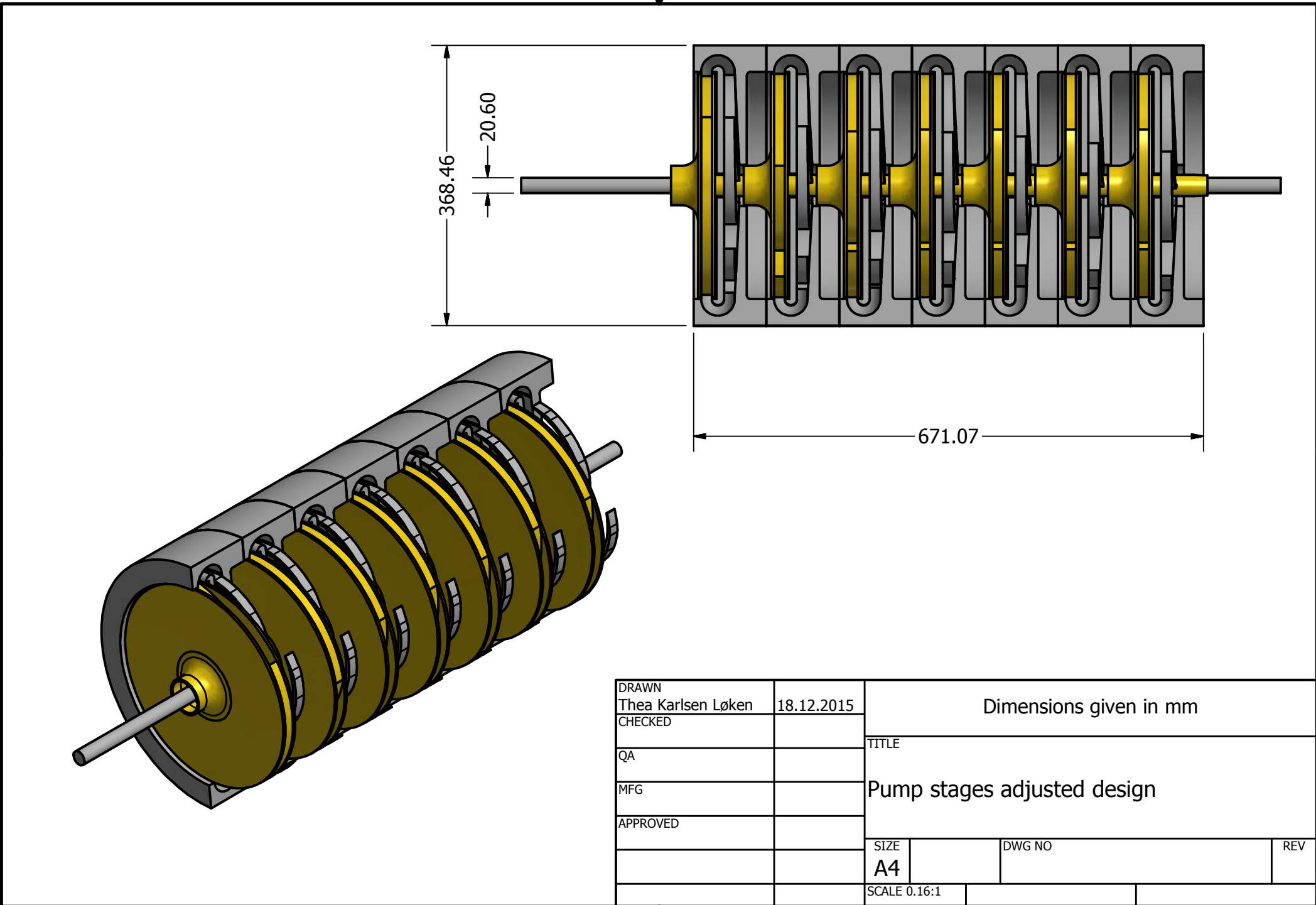
DRAWN	Thea Karlsen Løken	18.12.2015	Dimensions given in mm		
CHECKED			TITLE		
QA			Return vanes standard design		
MFG					
APPROVED					
			SIZE	DWG NO	REV
			A4		
			SCALE 1/3		



DRAWN Thea Karlsen Løken	18.12.2015	Dimensions given in mm		
CHECKED		TITLE		
QA		Return vanes adjusted design		
MFG				
APPROVED				
		SIZE A4	DWG NO	REV
		SCALE 1/3		

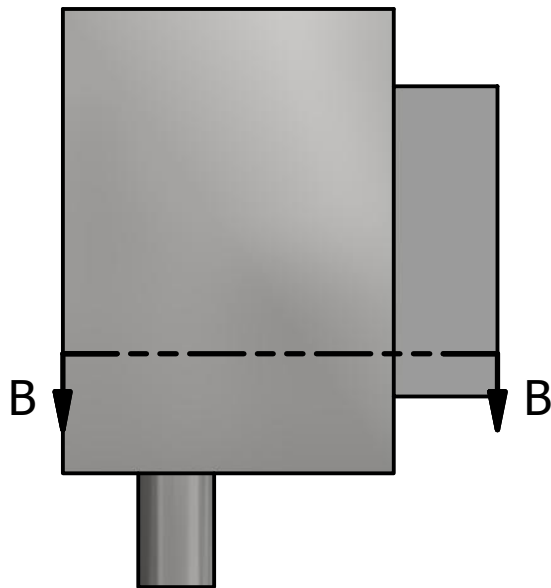


DRAWN	Thea Karlsen Løken	18.12.2015	Dimensions given in mm		
CHECKED			TITLE		
QA			Pump stages standard design		
MFG					
APPROVED					
			SIZE	DWG NO	REV
			A4		
			SCALE 0.16:1		

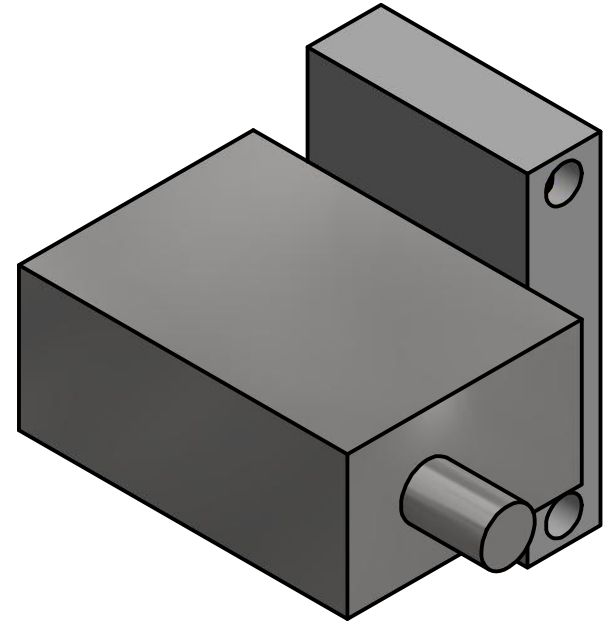
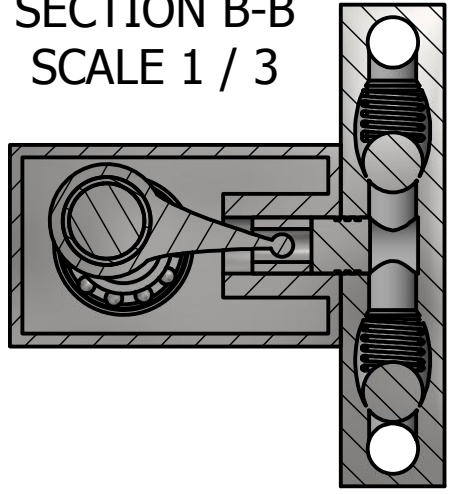


DRAWN	Thea Karlsen Løken	18.12.2015	Dimensions given in mm		
CHECKED			TITLE		
QA			Pump stages adjusted design		
MFG					
APPROVED					
			SIZE	DWG NO	REV
			A4		
			SCALE 0.16:1		

C Reciprocating Pump without Energy Recovery Drawings

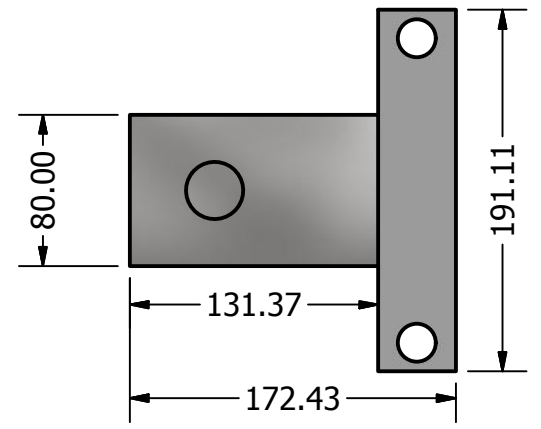
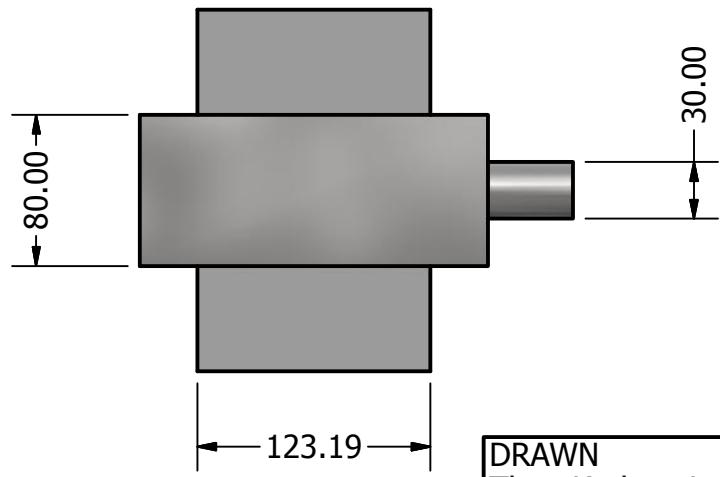
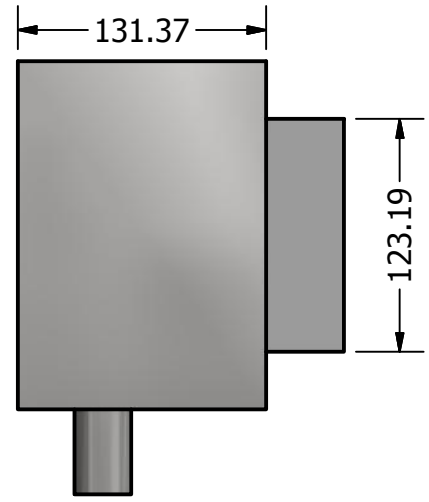
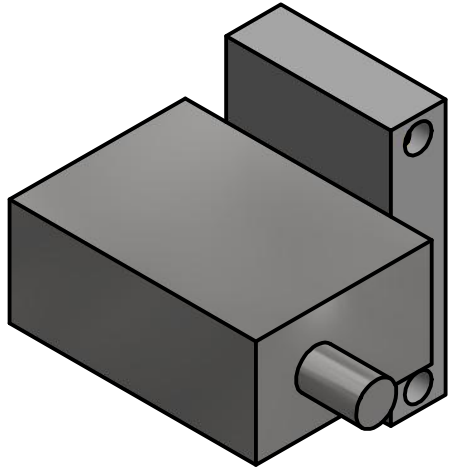


SECTION B-B
SCALE 1 / 3

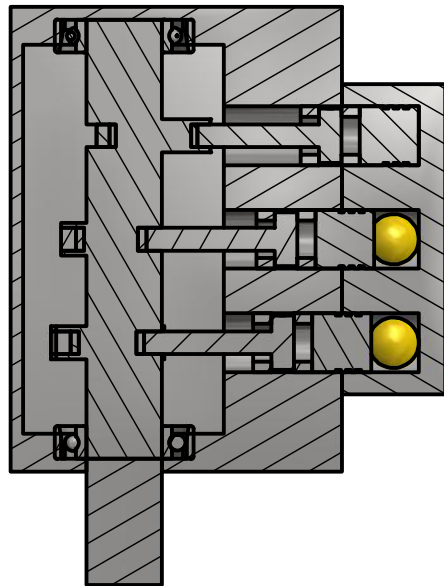
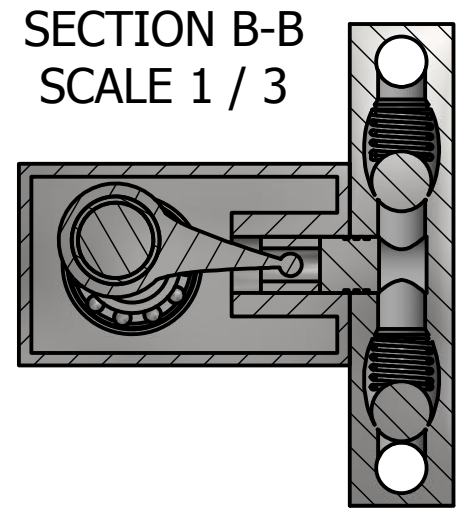
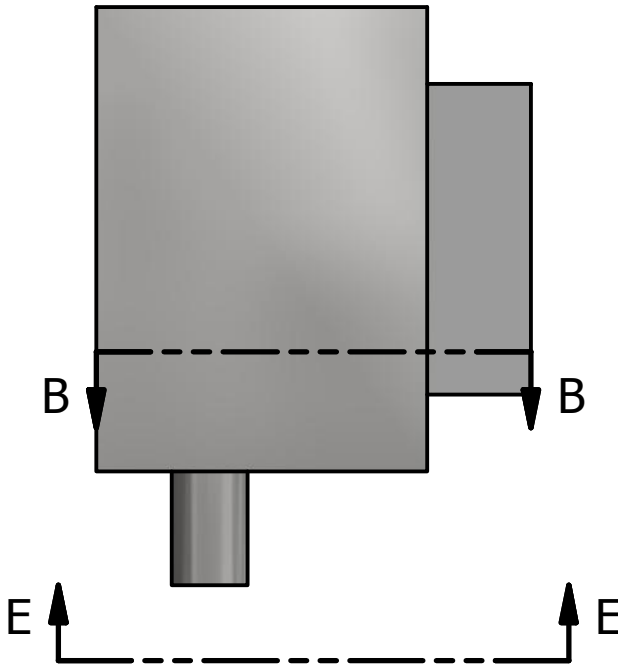
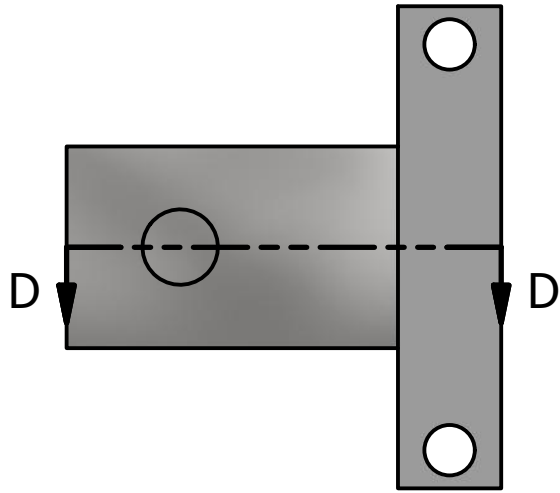


DRAWN Thea Karlsen Løken		09.06.2016		Dimensions given in mm			
				TITLE Reciprocating Pump Without Energy Recovery			
				SIZE A4		DWG NO PistonPump_Assembly-2	
				SCALE 1/3		REV	





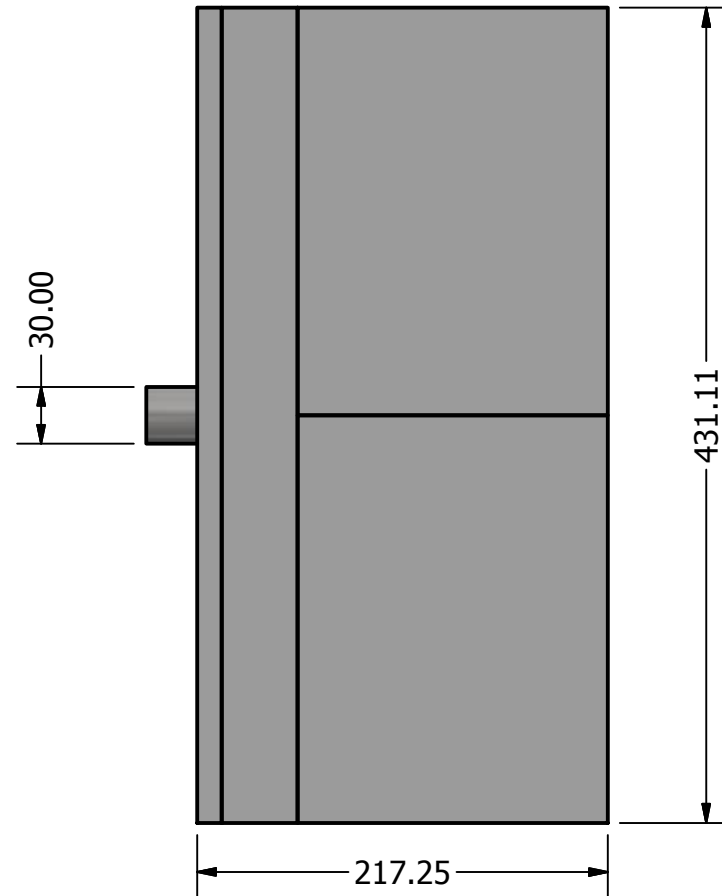
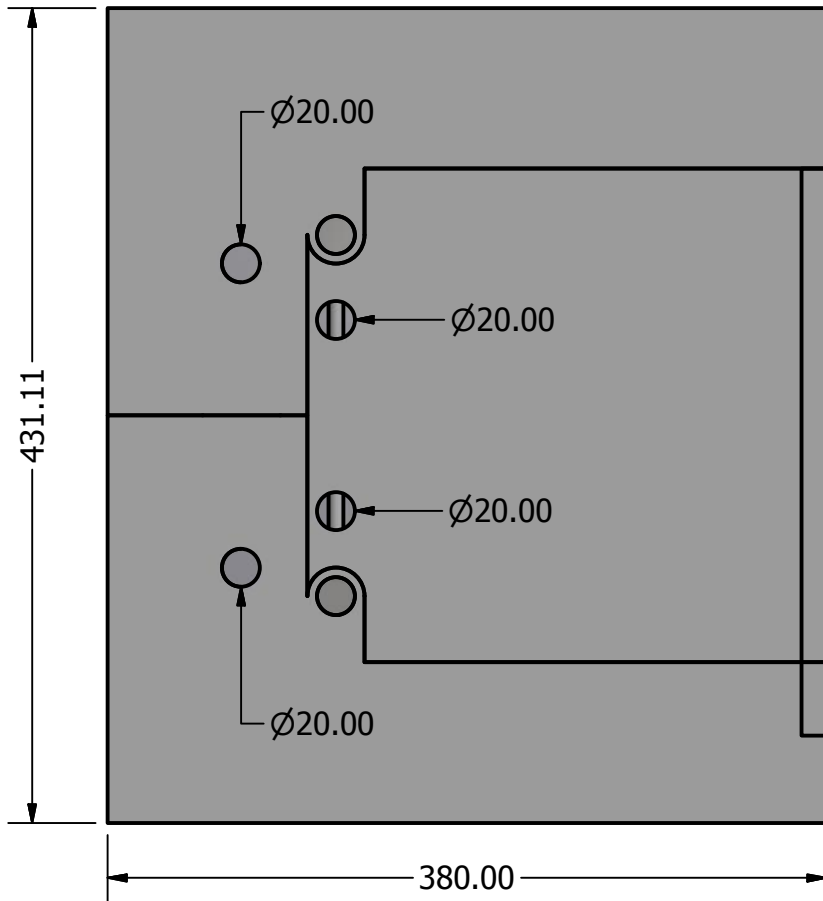
DRAWN Thea Karlsen Løken		09.06.2016		Dimensions given in mm			
				TITLE Reciprocating Pump Without Energy Recovery			
				SIZE A4	DWG NO PistonPump_Assembly-3		REV
				SCALE 1/4			



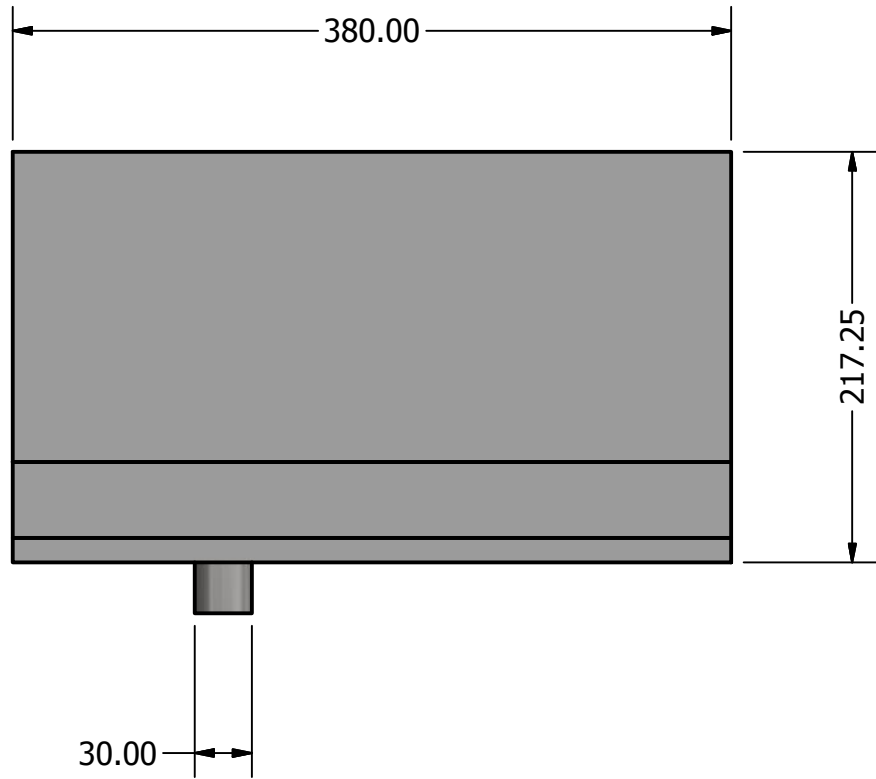
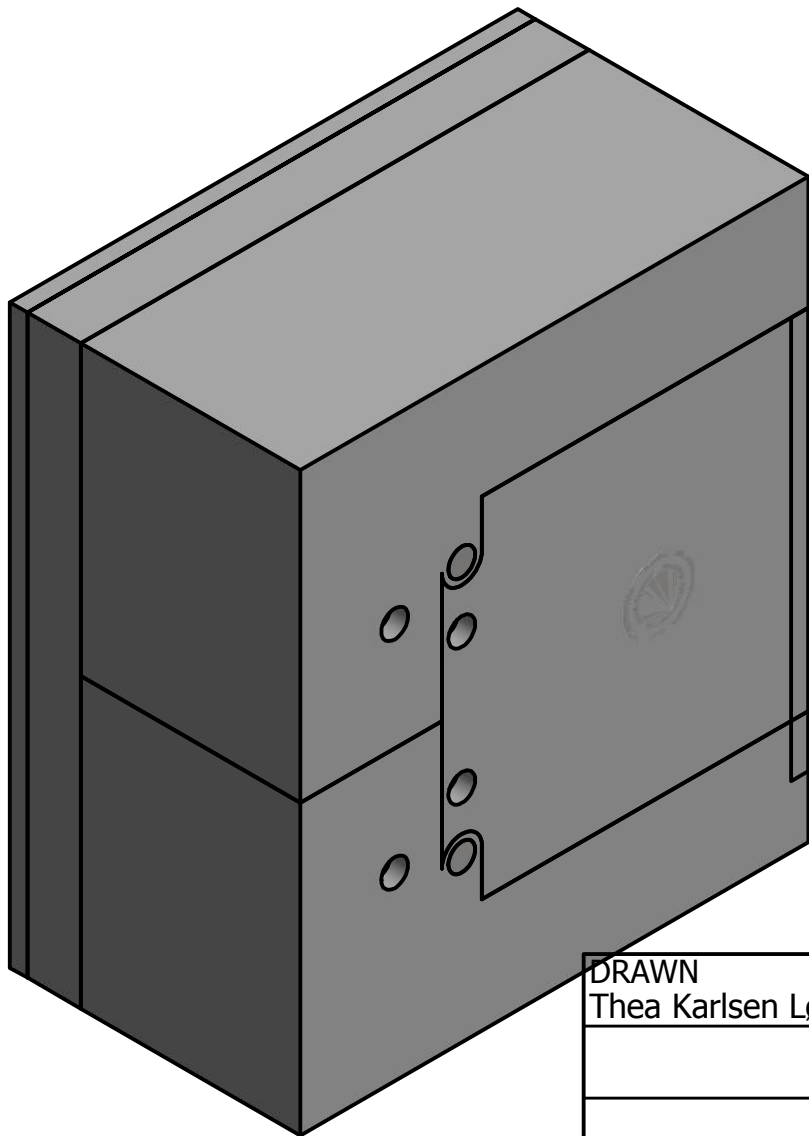
SECTION D-D
SCALE 1 / 3

DRAWN Thea Karlsen Løken		09.06.2016		Dimensions given in mm	
				TITLE Reciprocating Pump Without Energy Recovery	
				SIZE A4	
				DWG NO PistonPump_Assembly-4	
				REV	
		SCALE 1/3			

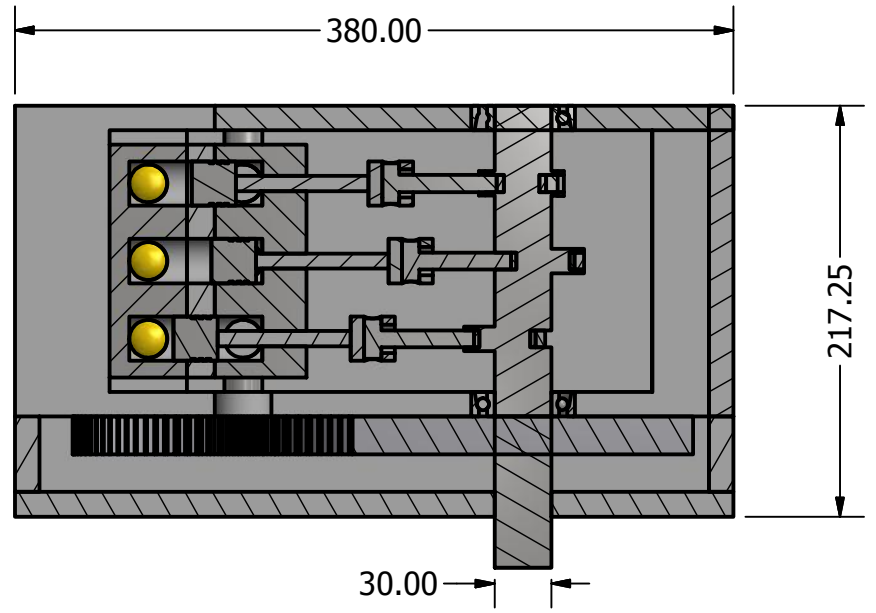
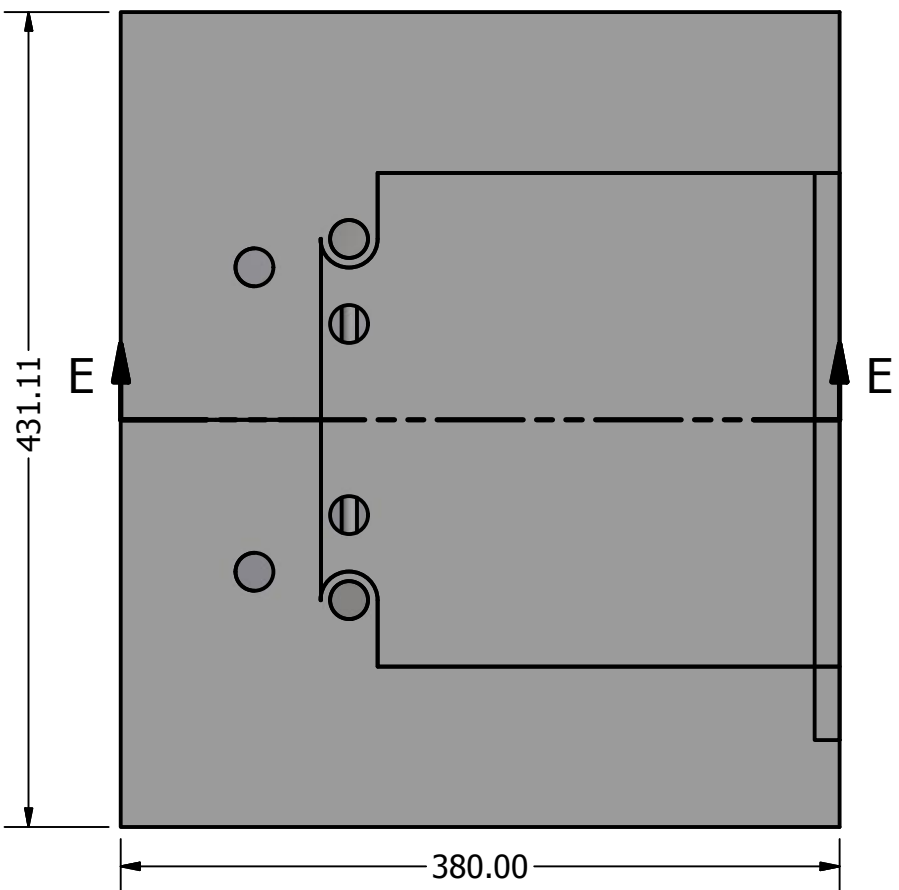
D Reciprocating Pump with Integrated Energy Recov- ery Drawings



DRAWN Thea Karlsen Løken		09.06.2016		Dimensions given in mm			
				TITLE			
				Reciprocating Pump With Integrated Energy Recovery			
				SIZE		DWG NO	
				A4		PistonPump_ER_Assembly-1	
				SCALE 1/4		REV	

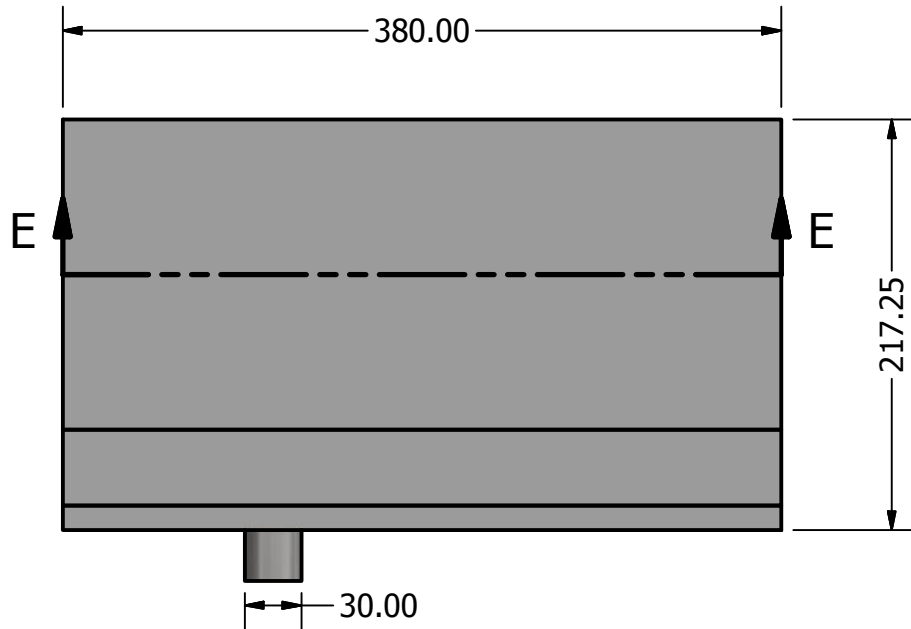
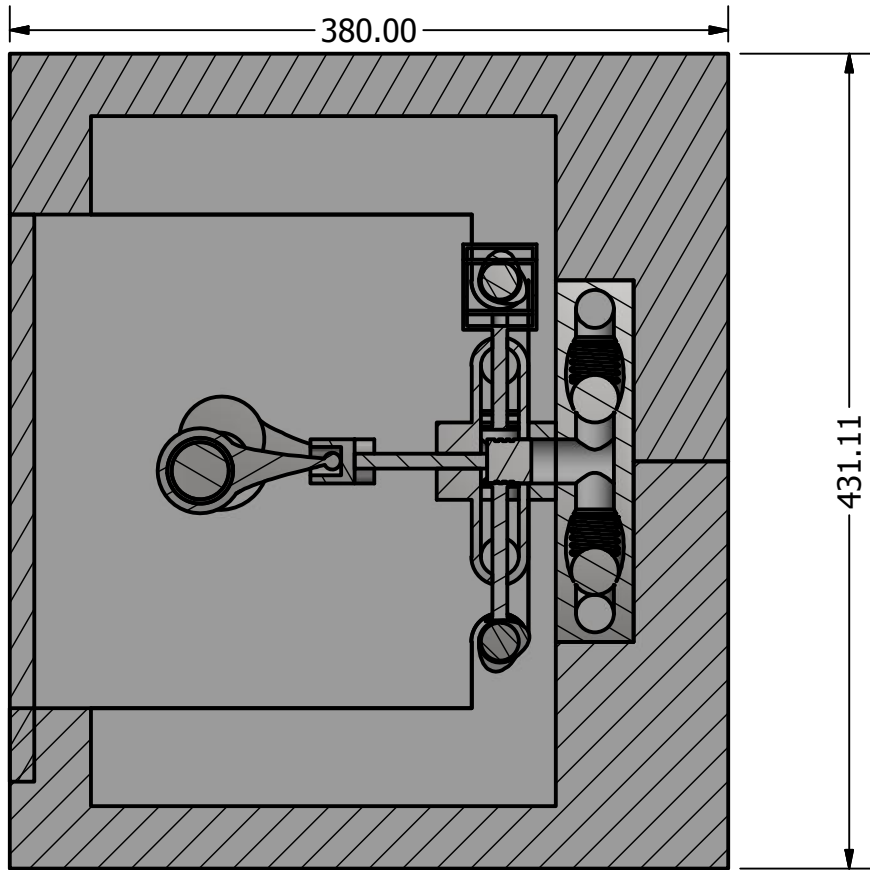


DRAWN Thea Karlsen Løken		09.06.2016		Dimensions given in mm			
				TITLE Reciprocating Pump With Integrated Energy Recovery			
				SIZE A4	DWG NO PistonPump_ER_Assembly-2		REV
				SCALE 1/4			



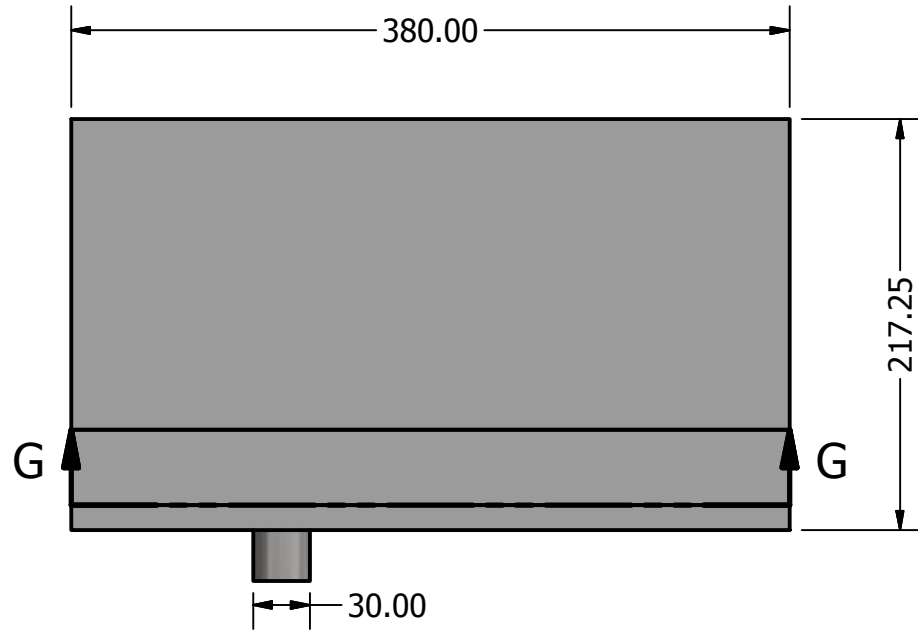
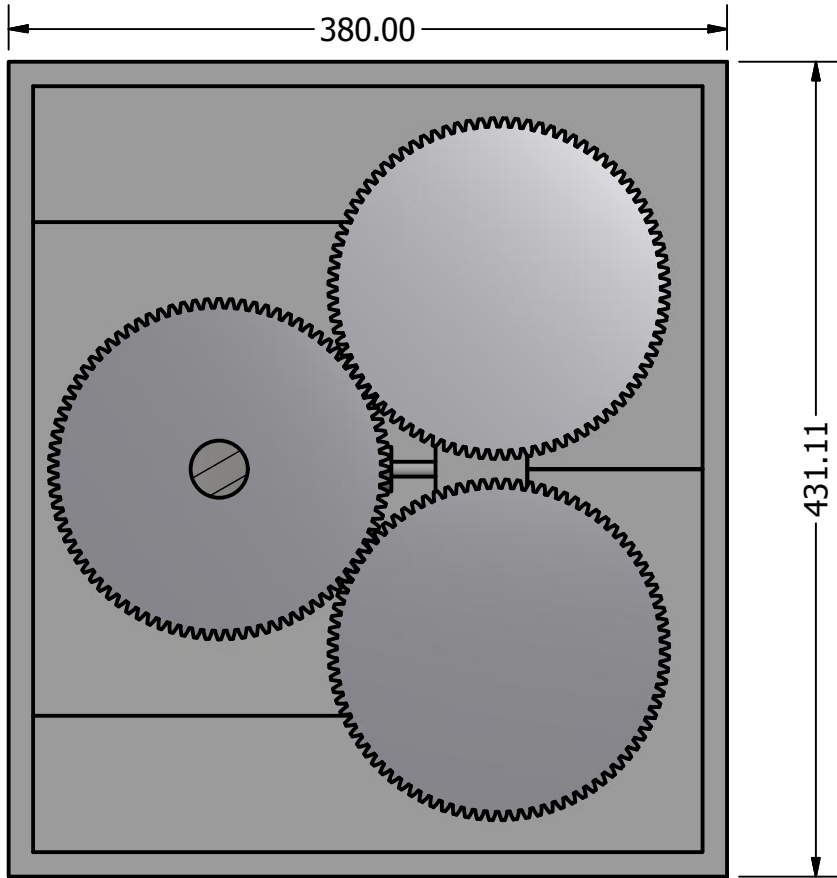
SECTION E-E
SCALE 1/4

DRAWN Thea Karlsen Løken		09.06.2016		Dimensions given in mm			
				TITLE Reciprocating Pump With Integrated Energy Recovery			
				SIZE A4		DWG NO PistonPump_ER_Assembly-3	
				SCALE 1/4		REV	



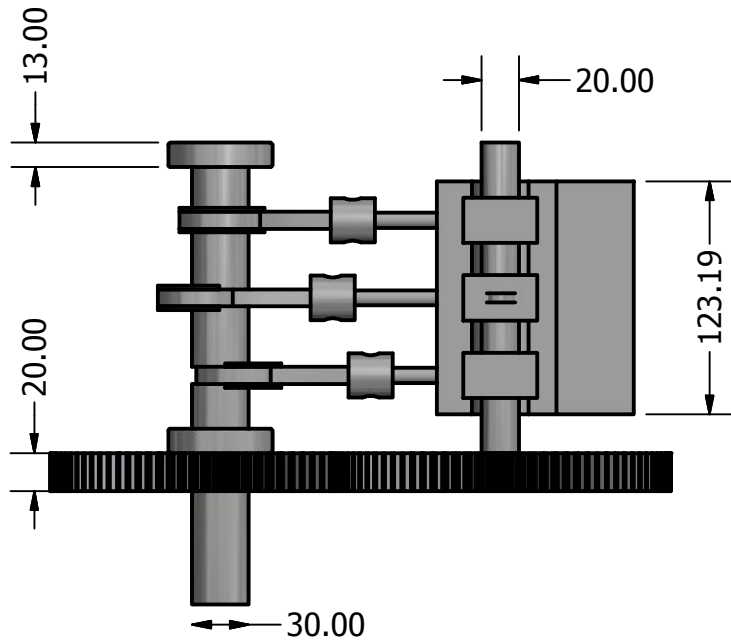
SECTION E-E
SCALE 1/4

DRAWN Thea Karlsen Løken		09.06.2016		Dimensions given in mm			
				TITLE Reciprocating Pump With Integrated Energy Recovery			
				SIZE A4		DWG NO PistonPump_ER_Assembly-4	
				SCALE 1/4		REV	

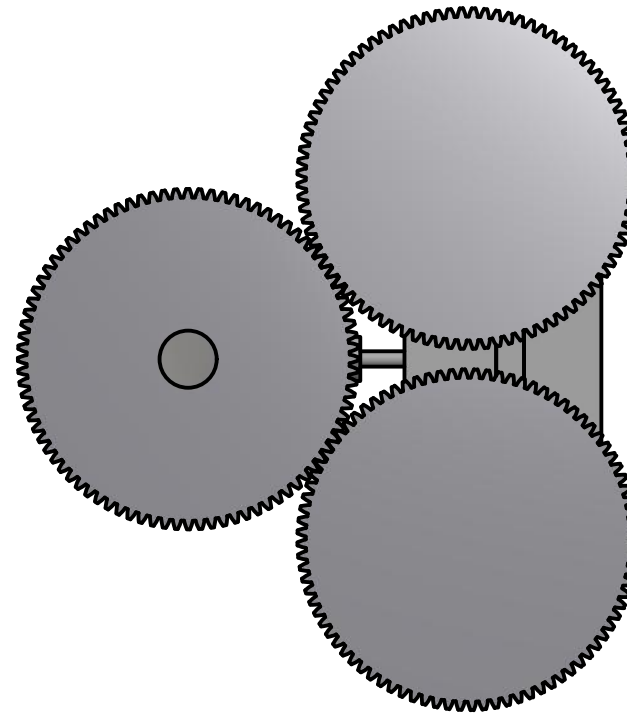
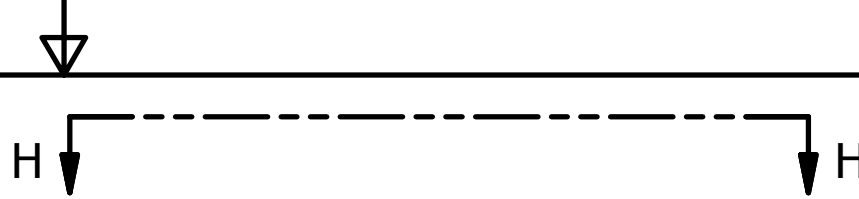


SECTION G-G
SCALE 1/4

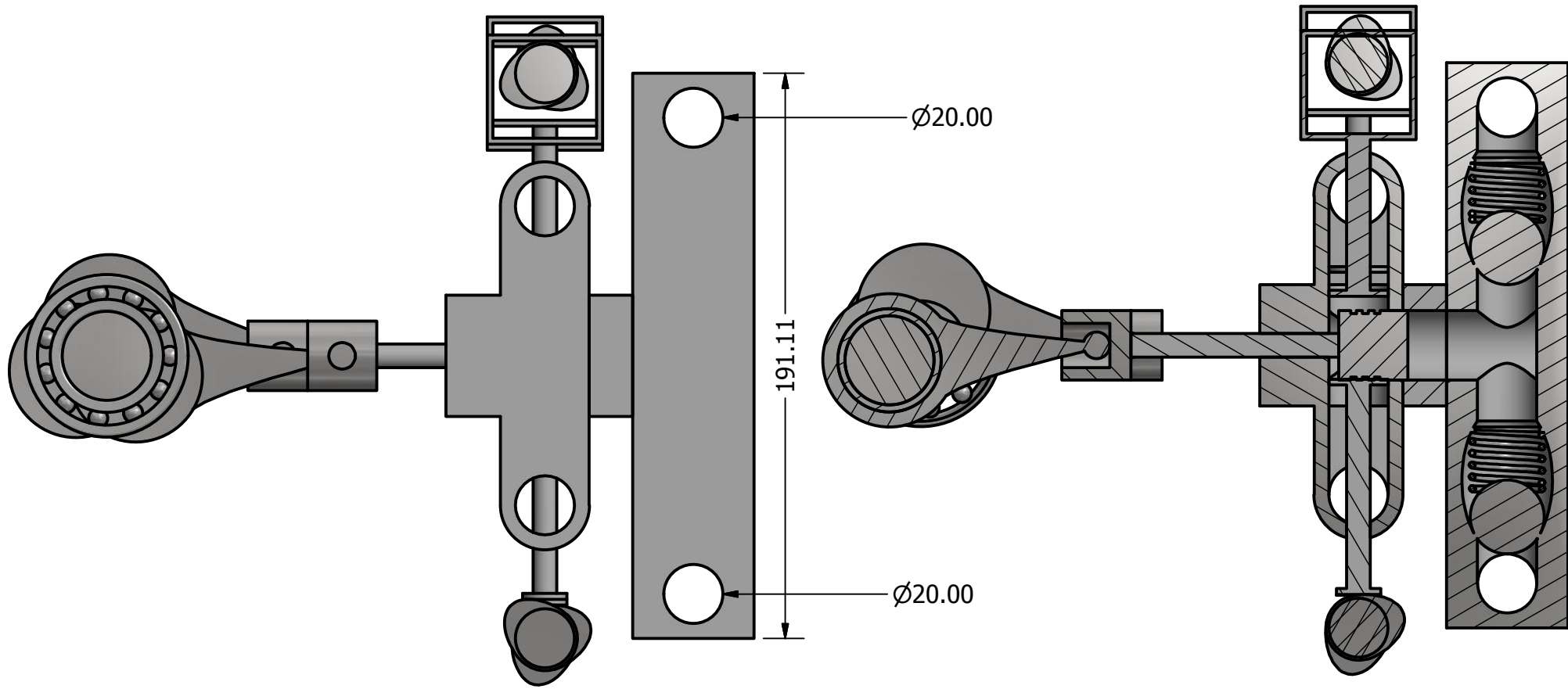
DRAWN Thea Karlsen Løken		09.06.2016		Dimensions given in mm			
				TITLE Reciprocating Pump With Integrated Energy Recovery			
				SIZE A4		DWG NO PistonPump_ER_Assembly-5	
				SCALE 1/4		REV	



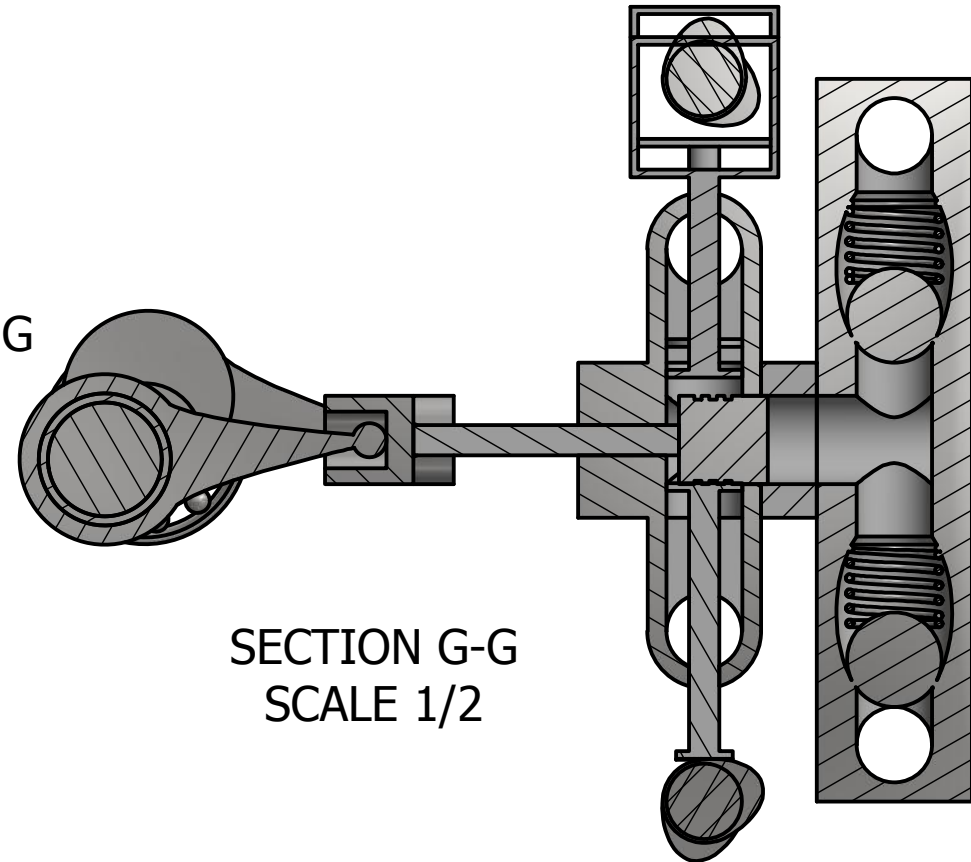
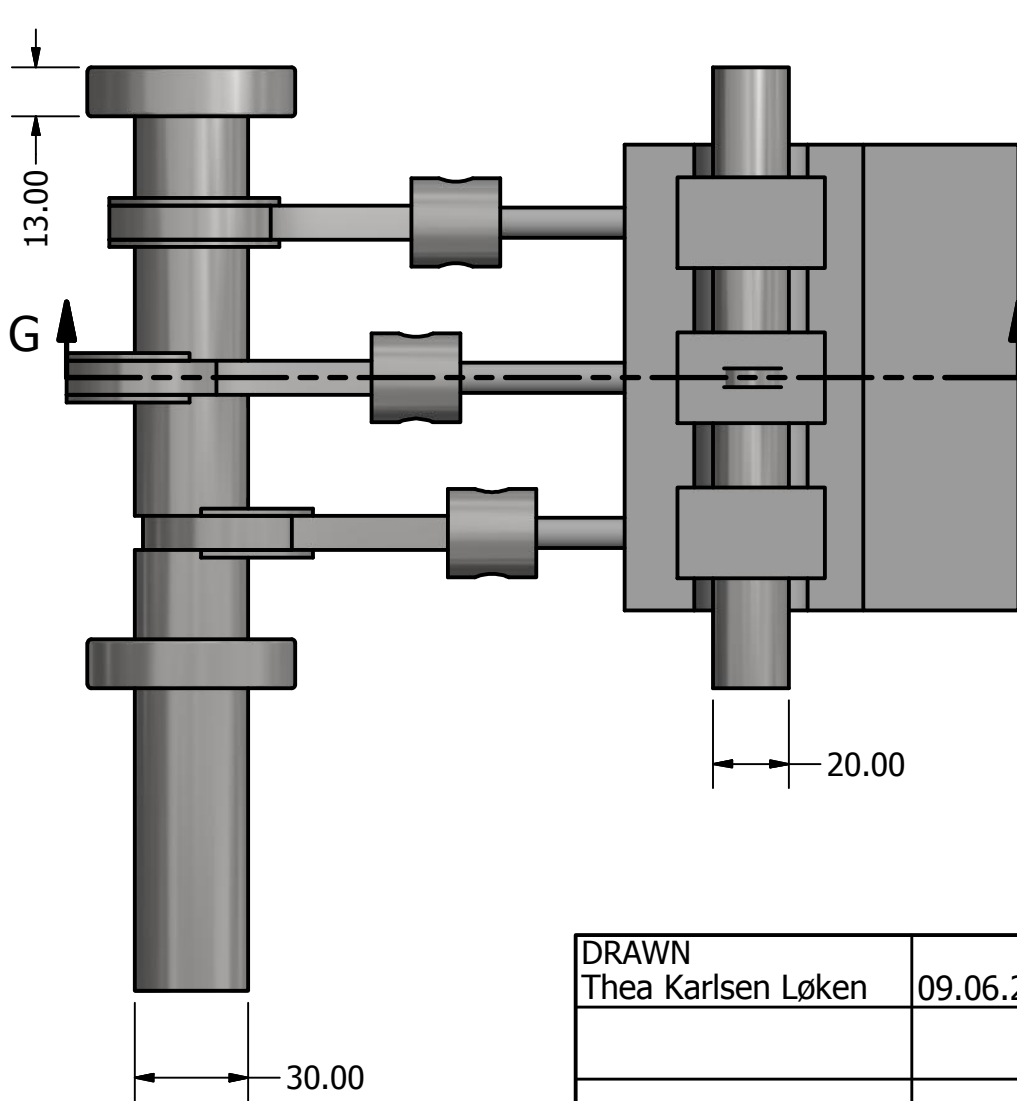
VIEW H-H
SCALE 1/4



DRAWN Thea Karlsen Løken		09.06.2016		Dimensions given in mm			
				TITLE Reciprocating Pump With Integrated Energy Recovery			
				SIZE A4		DWG NO PistonPump_ER_Assembly-6	
				SCALE 1/4		REV	



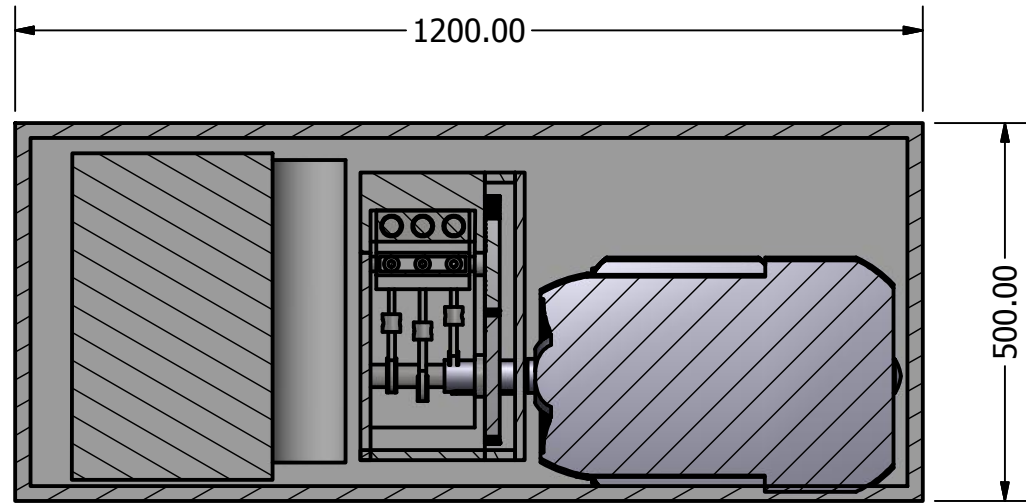
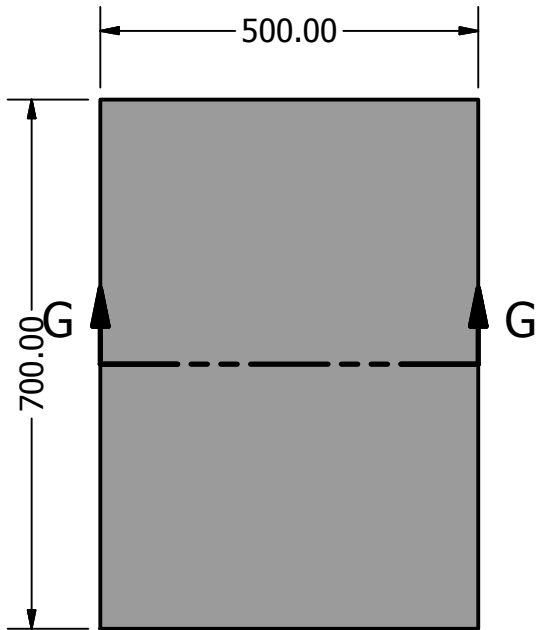
DRAWN Thea Karlsen Løken		09.06.2016		Dimensions given in mm			
				TITLE Reciprocating Pump With Integrated Energy Recovery			
				SIZE A4		DWG NO PistonPump_ER_Assembly-7	
				SCALE 1/2		REV	



SECTION G-G
SCALE 1/2

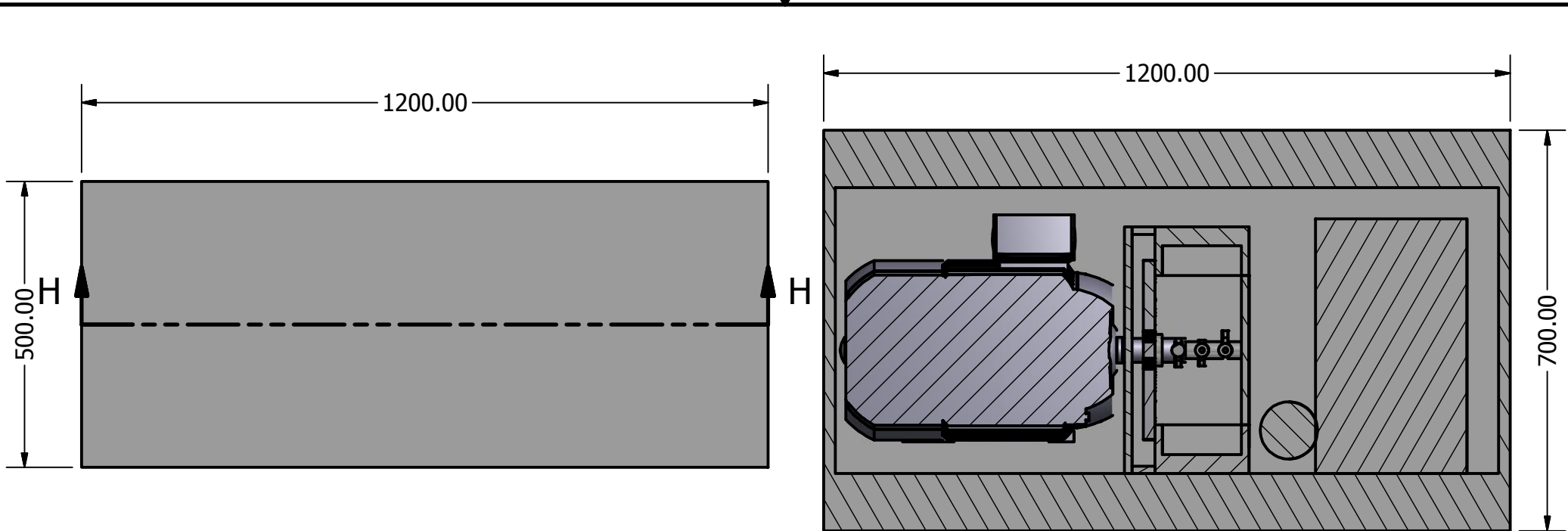
DRAWN Thea Karlsen Løken		09.06.2016		Dimensions given in mm			
				TITLE Reciprocating Pump With Integrated Energy Recovery			
				SIZE A4		DWG NO PistonPump_ER_Assembly-8	
				SCALE 1/2		REV	

E Reverse Osmosis System



SECTION G-G
SCALE 1/10

DRAWN Thea Karlsen Løken		09.06.2016		Dimensions given in mm			
				TITLE			
				Reverse osmosos system without diesel generator			
				SIZE		DWG NO	
				A4		Final2-3	
				SCALE 1/10		REV	



SECTION H-H
SCALE 1/10

DRAWN Thea Karlsen Løken		09.06.2016		Dimensions given in mm			
				TITLE			
				Reverse osmosos system without diesel generator			
				SIZE		DWG NO	
				A4		Final2-4	
				SCALE 1/10		REV	

F Reverse Osmosis System Com- ponents



Ordering data: **1LE1001-1DD22-2AA4**

Motor type: **1AV2162D**

Client order no.:

Item no.:

Order no.:

Consignment no.:

Offer no.:

Project:

Remarks:

U [V]	Δ/Y	f [Hz]	P [kW]	P [hp]	I [A]	n [1/min]	M [Nm]	NOM. EFF at ... load [%]			Power factor at ... load			I _A /I _N I _A /I _N	M _A /M _N T _A /T _N	M _K /M _N T _B /T _N	IE-CL
								4/4	3/4	2/4	4/4	3/4	2/4				
230	Δ	50	4.00	- / -	18.30	730	52.0	81.9	82.6	81.4	0.67	0.61	0.50	3.7	1.6	1.9	IE2
400	Y	50	4.00	- / -	10.50	730	52.0	81.9	82.6	81.4	0.67	0.61	0.50	3.7	1.6	1.9	IE2
460	Y	60	4.55	- / -	10.00	880	49.0	85.5	86.2	85.1	0.67	0.62	0.51	3.8	1.6	1.9	IE2
460	Y	60	4.00	- / -	8.40	885	40.0	85.5	85.3	83.2	0.65	0.59	0.47	4.6	2.0	2.2	IE2
IM B3 / IM 1001		FS 160 M		69 kg	IP55		IEC/EN 60034		IEC, DIN, ISO, VDE, EN								

These values are calculated. The final rating plate data will be calculated when the order is placed
The efficiency values and efficiency class according to EuP directive are valid for standard power ratings under standard conditions.

Mechanical data			Terminal box	
Sound pressure level 50Hz/60Hz (load)	63 dB(A)	71 dB(A)	Terminal box position	top
Moment of inertia	0.065 kg m ²		Material of terminal box	Aluminium
Bearing DE NDE	6209 2ZC3	6209 2ZC3	Type of terminal box	TB1 J00
Bearing lifetime	40000 h		Contact screw thread	M5
Lubricants	Esso Unirex N3		Max. cross-sectional area	16.0 mm ²
Regreasing device	No		Cable diameter from ... to ...	19.0 mm - 28.0 mm
Grease nipple	- / -		Cable entry	2xM40x1,5
Type of bearing	Locating bearing NDE		Cable gland	2 plugs
Condensate drainage holes	No		Special design	
External earthing terminal	No			
Vibration class	A			
Insulation	155(F) to 130(B)			
Duty type	S1			
Direction of rotation	bidirectional			
Frame material	aluminum			
Data of anti condensation heating	-/-			
Coating	Standard paint finish C2			
Color	RAL7030			
Motor protection	(A) without (Standard)			
Method of cooling	IC411 - self ventilated, surface cooled			

Environmental conditions	
Ambient temperature	-20 °C - +40 °C
Altitude above sea level	1000 m



DOW FILMTEC™ Membranes
DOW FILMTEC Seawater RO Elements for Marine Systems

Features

Improved DOW FILMTEC™ seawater reverse osmosis elements offer the highest productivity while maintaining excellent salt rejection.

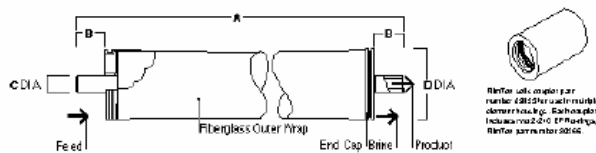
- DOW FILMTEC SW30 membrane elements have the highest flow rates available to meet the water demands of both sea-based and land-based desalinators.
- DOW FILMTEC SW30 elements may also be operated at lower pressure to reduce pump size, cost and operating expenses.
- Improved DOW FILMTEC seawater membrane combined with automated, precision element fabrication result in the most consistent product performance available.

Product Specifications

Product	Part Number	Applied Pressure psig (bar)	Permeate Flow Rate gpd (m ³ /d)	Stabilized Salt Rejection (%)
SW30-2514	80733	800 (55)	150 (0.6)	99.4
SW30-2521	80734	800 (55)	300 (1.1)	99.4
SW30-2540	80737	800 (55)	700 (2.6)	99.4
SW30-4021	80740	800 (55)	800 (3.0)	99.4
SW30-4040	80741	800 (55)	1,950 (7.4)	99.4

1. Permeate flow and salt rejection based on the following test conditions: 32,000 ppm NaCl, pressure specified above, 77°F (25°C) and the following recovery rates; SW30-2514 – 2%, SW30-2521 & SW30-4021 – 5%, SW30-2540 & SW30-4040 – 8%.
2. Permeate flows for individual elements may vary +/-20%.
3. For the purpose of improvement, specifications may be updated periodically.

Figure 1



Product	Maximum Feed Flow Rate gpm (m ³ /h)	Dimensions – Inches (mm)			
		A	B	C	D
SW30-2514	6 (1.4)	14.0 (356)	1.19 (30.2)	0.75 (19)	2.4 (61)
SW30-2521	6 (1.4)	21.0 (533)	1.19 (30.2)	0.75 (19)	2.4 (61)
SW30-2540	6 (1.4)	40.0 (1,016)	1.19 (30.2)	0.75 (19)	2.4 (61)
SW30-4021	16 (3.6)	21.0 (533)	1.05 (26.7)	0.75 (19)	3.9 (99)
SW30-4040	16 (3.6)	40.0 (1,016)	1.05 (26.7)	0.75 (19)	3.9 (99)

1. Refer to DOW FILMTEC Design Guidelines for multiple-element systems.
2. SW30-2514, SW30-2521 and SW30-2540 elements fit nominal 2.5-inch I.D. pressure vessels.
SW30-4021 and SW30-4040 elements fit nominal 4-inch I.D. pressure vessel.

Operating Limits

• Membrane Type	Polyamide Thin-Film Composite
• Maximum Operating Temperature	113°F (45°C)
• Maximum Operating Pressure	1,000 psi (69 bar)
• Maximum Pressure Drop	15 psig (1.0 bar)
• pH Range, Continuous Operation ^a	2 - 11
• pH Range, Short-Term Cleaning ^b	1 - 13
• Maximum Feed Silt Density Index	SDI 5
• Free Chlorine Tolerance ^c	<0.1 ppm

^a Maximum temperature for continuous operation above pH 10 is 95°F (35°C).

^b Refer to Cleaning Guidelines in specification sheet 609-23010.

^c Under certain conditions, the presence of free chlorine and other oxidizing agents will cause premature membrane failure. Since oxidation damage is not covered under warranty, DOW FILMTEC recommends removing residual free chlorine by pretreatment prior to membrane exposure. Please refer to technical bulletin 609-22010 for more information.

Important Information

Proper start-up of reverse osmosis water treatment systems is essential to prepare the membranes for operating service and to prevent membrane damage due to overfeeding or hydraulic shock. Following the proper start-up sequence also helps ensure that system operating parameters conform to design specifications so that system water quality and productivity goals can be achieved.

Before initiating system start-up procedures, membrane pretreatment, loading of the membrane elements, instrument calibration and other system checks should be completed.

Please refer to the application information literature entitled "Start-Up Sequence" (Form No. 609-02077) for more information.

Operation Guidelines

Avoid any abrupt pressure or cross-flow variations on the spiral elements during start-up, shutdown, cleaning or other sequences to prevent possible membrane damage. During start-up, a gradual change from a standstill to operating state is recommended as follows:

- Feed pressure should be increased gradually over a 30-60 second time frame.
- Cross-flow velocity at set operating point should be achieved gradually over 15-20 seconds.
- Permeate obtained from first hour of operation should be discarded.

General Information

- Keep elements moist at all times after initial wetting.
- If operating limits and guidelines given in this bulletin are not strictly followed, the limited warranty will be null and void.
- To prevent biological growth during prolonged system shutdowns, it is recommended that membrane elements be immersed in a preservative solution.
- The customer is fully responsible for the effects of incompatible chemicals and lubricants on elements.
- Maximum pressure drop across an entire pressure vessel (housing) is 50 psi (3.4 bar).
- Avoid static permeate-side backpressure at all times.

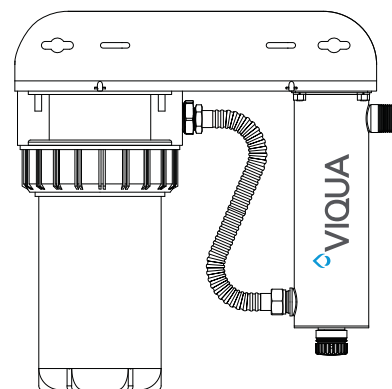
DOW FILMTEC™ Membranes
For more information about DOW FILMTEC membranes, call the Dow Water & Process Solutions business:
North America: 1-800-447-4369
Latin America: (+55) 11-5188-9222
Europe: (+32) 3-450-2240
Pacific: +60 3 7958 3392
Japan: +813 5460 2100
China: +86 21 2301 1000
www.dowwaterandprocess.com

Notice: The use of this product in and of itself does not necessarily guarantee the removal of cysts and pathogens from water. Effective cyst and pathogen reduction is dependent on the complete system design and on the operation and maintenance of the system.

Notice: No freedom from any patent owned by Dow or others is to be inferred. Because use conditions and applicable laws may differ from one location to another and may change with time, Customer is responsible for determining whether products and the information in this document are appropriate for Customer's use and for ensuring that Customer's workplace and disposal practices are in compliance with applicable laws and other government enactments. Dow assumes no obligation or liability for the information in this document. NO WARRANTIES ARE GIVEN; ALL IMPLIED WARRANTIES OF MERCHANTABILITY OR FITNESS FOR A PARTICULAR PURPOSE ARE EXPRESSLY EXCLUDED.



Owner's Manual



Models:
VH200-F10, VH410-F20

Powered by
Sterilight



425 Clair Rd. W, Guelph, Ontario, Canada N1L 1R1
t. (+1) 519.763.1032 • f. (+1) 800.265.7246 (US and Canada only)
t. (+31) 73 747 0144 (Europe only) • f. (+1) 519.763.5069
e-mail: info@viqua.com
www.viqua.com

425 Clair Rd. W, Guelph, Ontario, Canada N1L 1R1
t. (+1) 519.763.1032 • f. (+1) 800.265.7246 (US et Canada seulement)
t. (+31) 73 747 0144 (Europe seulement) • f. (+1) 519.763.5069
Courriel : info@viqua.com
www.viqua.com

425 Clair Rd. W, Guelph, Ontario, Canadá N1L 1R1
t. (+1) 519.763.1032 • f. (+1) 800.265.7246 (solo EE. UU. y Canadá)
t. (+31) 73 747 0144 (solo Europa) • f. (+1) 519.763.5069
correo electrónico: info@viqua.com
www.viqua.com

425 Clair Rd. W, Guelph, Ontario, Canada N1L 1R1
t. (+1) 519.763.1032 • f. (+1) 800.265.7246 (US and Canada only)
t. (+31) 73 747 0144 (Europe only) • f. (+1) 519.763.5069
e-mail: info@viqua.com
www.viqua.com



Congratulations on the purchase of your ultraviolet (UV) water disinfection system! This system uses the most advanced UV technology on the market and is designed to provide you with years of trouble free operation with minimal maintenance required to protect your drinking water from microbiological contaminants.

To ensure ongoing disinfection of your water, UV lamps need to be replaced annually with VIQUA factory-supplied replacements. VIQUA lamps are the result of extensive development resulting in a highly efficient disinfection platform with extremely stable UV output over the entire 9000 hour lifetime. Its success has led to a proliferation of non-genuine copies in the market.

The UV lamp is the heart of the disinfection system, and there should be no compromise when it's time for a replacement.

Why should you insist on genuine factory supplied VIQUA replacement lamps?

- Use of widely available, non-genuine, replacement lamps has been shown to damage the control module of VIQUA UV disinfection equipment.
- An increasing number of calls to VIQUA Technical Support are connected with non-genuine lamps being used (unknowingly) as replacements.
- Damage arising from the use of non-genuine lamps poses a safety risk and is not covered by equipment warranty.
- Unless the UV equipment is equipped with a UV sensor (monitor), it is not possible to verify the UV (invisible) output of replacement lamps.
- Similar appearance to the original lamp and the presence of (visible) blue light does not mean equivalent disinfection performance.
- VIQUA replacement lamps undergo rigorous performance testing and strict quality control processes to ensure that the safety and performance certifications of the original equipment are not compromised.

So, you can see that it's simply not worth the risk! Insist on genuine VIQUA replacement lamps.

Esta página está en blanco de forma intencional.

Sección 9 Garantía del fabricante

Nuestro compromiso

VIQUA se compromete a asegurar que su experiencia con nuestros productos y organización superen sus expectativas. Hemos fabricado el sistema de desinfección UV según los más altos estándares y lo valoramos como cliente. Si necesitara soporte técnico o tiene preguntas acerca de su sistema, póngase en contacto con nuestro equipo de soporte técnico en el 1.800.265.7246 o en technicalsupport@viqua.com. Estaremos encantados de ayudarle. Esperamos que disfrute de las ventajas que ofrece un agua potable limpia y segura después de la instalación del sistema de desinfección VIQUA.

Cómo realizar una reclamación bajo garantía

Nota: Para maximizar el rendimiento de desinfección y la fiabilidad de su producto VIQUA, el sistema se debe dimensionar, instalar y mantener adecuadamente. En el manual del propietario encontrará información de utilidad sobre los parámetros de calidad del agua necesarios y los requisitos de mantenimiento.

En el caso de que se necesitara una reparación o reposición de piezas cubiertas bajo esta garantía, el proceso lo gestionará el distribuidor. Si no está seguro de si un problema o fallo del sistema está cubierto por la garantía, póngase en contacto con nuestro equipo de soporte técnico en el 1.800.265.7246 o por correo electrónico en la dirección technicalsupport@viqua.com. Nuestros técnicos completamente formados le ayudarán a resolver el problema e identificar una solución. Tenga a mano el número de modelo (tipo de sistema), la fecha de compra, el nombre del distribuidor al que adquirió el producto VIQUA ("distribuidor de origen") y una descripción del problema que está experimentando. Para establecer la prueba de compra al realizar una reclamación bajo garantía, necesitará su factura original, o bien deberá haber completado y enviado su tarjeta de registro de producto por correo postal o en línea.

Cobertura específica de la garantía

La cobertura de la garantía es específica de la gama de productos de VIQUA. La cobertura de la garantía está sujeta a las condiciones y limitaciones establecidas en la sección "[Condiciones y limitaciones generales](#)".

Garantía limitada de diez años para la cámara UV de VIQUA

VIQUA garantiza que la cámara UV del producto VIQUA estará libre de defectos de material y mano de obra durante un periodo de diez (10) años desde la fecha de compra. Durante este periodo, VIQUA reparará o reemplazará, a su criterio, toda cámara UV VIQUA defectuosa. Devuelva la pieza defectuosa a su distribuidor, quién procesará su reclamación.

Garantía limitada de tres años para los componentes eléctricos y de hardware

VIQUA garantiza que los componentes eléctricos (controlador) y de hardware estarán libres de defectos de material y mano de obra durante un periodo de tres (3) años desde la fecha de compra. Durante este periodo, VIQUA reparará o reemplazará, a su criterio, toda pieza defectuosa cubierta por la garantía. Devuelva la pieza defectuosa a su distribuidor, quién procesará su reclamación.

Garantía limitada de un año para lámparas UV, vainas tubulares y sensores UV

VIQUA garantiza que las lámparas UV, las vainas tubulares y los sensores UV estarán libres de defectos de material y mano de obra durante un periodo de un (1) año desde la fecha de compra. Durante este periodo, VIQUA reparará o reemplazará, a su criterio, toda pieza defectuosa cubierta por la garantía. Su distribuidor procesará su reclamación y ofrecerá consejos sobre si el artículo defectuoso se debe devolver para realizar un análisis de fallos.

Nota: Utilice únicamente lámparas y vainas tubulares de reposición VIQUA originales en el sistema. El incumplimiento de este requisito podría poner en riesgo el rendimiento de la desinfección y afectar a la cobertura de la garantía.

Condiciones y limitaciones generales

Ninguna de las garantías anteriores cubre los daños provocados por el uso o mantenimiento inadecuados, accidentes, actos de la naturaleza o arañazos e imperfecciones menores que no afectan materialmente el funcionamiento del producto. Las garantías tampoco cubren los productos que no se han instalado según las instrucciones del manual del propietario correspondiente.

Las piezas reparadas o reemplazadas según estas garantías serán cubiertas bajo garantía hasta el final del periodo de garantía aplicable a la pieza original.

Las garantías anteriores no incluyen el coste de envío y manipulación de los artículos devueltos. Las garantías limitadas que se describen anteriormente son las únicas garantías aplicables a la gama de productos VIQUA. En estas garantías limitadas se describe el único recurso para todas las reclamaciones basadas en un fallo o defecto de cualquiera de estos productos, ya sea que la reclamación se base en contrato, agravio (incluida la negligencia), responsabilidad estricta u otro. Estas garantías reemplazan a todas las demás garantías escritas, orales, implícitas o reglamentarias. No corresponde, sin limitación, ninguna garantía de comerciabilidad o aptitud para un propósito particular a ninguno de estos productos.

VIQUA no asume ninguna responsabilidad por lesiones o daños a la propiedad causados por el uso o el mal uso de cualquiera de los productos mencionados anteriormente. VIQUA no será de ningún modo responsable de los daños especiales, incidentales, indirectos o consecuentes. La responsabilidad de VIQUA se limitará, en todos los casos, a la reparación o reposición del producto o la pieza defectuosa y esta responsabilidad finalizará al finalizar el periodo de garantía aplicable.
















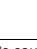
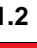
Section 1 Safety Information

Please read this entire manual before operating this equipment. Pay attention to all danger, warning, and caution statements in this manual. Failure to do so could result in serious personal injury or damage to the equipment.

Make sure that the protection provided by this equipment is not impaired. DO NOT use or install this equipment in any manner other than that specified in the installation manual.



1.1 Potential Hazards:

Read all labels and tags attached to the system. Personal injury or damage to the system could occur if not observed.

	Waste electrical and electronic equipment (WEEE). This symbol indicates that you should not discard electrical or electronic equipment (WEEE) in the trash. For proper disposal, contact your local recycling/reuse or hazardous waste center.		This symbol indicates not to store any combustible or flammable material close to the system.
	This symbol indicates there is Mercury present.		This symbol indicates that the contents of the transport package are fragile and the package should be handled with care.
	This is the safety alert symbol. Obey all safety messages that follow this symbol to avoid potential injury. When on the equipment, refer to the Operational and Maintenance manual for additional safety		This symbol indicates safety glasses with side protection is required for protection against UV exposure.
	This symbol indicates a risk of electrical shock and/or electrocution exists.		This symbol indicates gloves must be worn.
	This symbol indicates the marked equipment may contain a component that can eject forcibly. Obey all procedures to safely depressurize.		This symbol indicates safety boots must be worn.
	This symbol indicates the system is under pressure.		This symbol indicates the operator must read all available documentation to perform required procedures.
	This symbol indicates there is a potential UV hazard. Proper protection must be worn.		This symbol indicates the plumber must use copper piping.
	This symbol indicates the marked item could be hot and should not be touched without care.		This symbol indicates that the system should only be connected to a properly grounded, grounding-type receptacle that is protected by a Ground Fault Circuit Interrupter (GFCI).
	This symbol indicates there is a potential for VERY hot water when flow is started.		

Warning: This product may contain chemicals known to the State of California to cause cancer and birth defects or other reproductive harm.

1.2 Safety Precautions:

⚠ DANGER	
	<p>Failure to follow these instructions will result in serious injury or death.</p> <ul style="list-style-type: none"> Electric Shock: To avoid possible electric shock, special care should be taken since water is present near the electrical equipment. Unless a situation is encountered that is explicitly addressed by the provided maintenance and troubleshooting sections, DO NOT attempt repairs yourself, refer to an authorized service facility. GROUNDING: This product must be grounded. If it should malfunction or breakdown, grounding provides a path of least resistance for electric current to reduce the risk of electrical shock. This system is equipped with a cord having an equipment-grounding conductor and a grounding plug. The plug must be plugged into an appropriate outlet that is properly installed and grounded in accordance with all local codes and ordinances. Improper connection of the equipment-grounding conductor can result in a risk of electrocution. Check with a qualified electrician or service personnel if you are in doubt as to whether the outlet is properly grounded. DO NOT modify the plug provided with this system – if it does not fit in the outlet, have a proper outlet installed by a qualified electrician. DO NOT use any type of adapter with this system. GROUND FAULT CIRCUIT INTERRUPTER PROTECTION: To comply with the National Electrical Code (NFPA 70) and to provide additional protection from the risk of electric shock, this system should only be connected to a properly grounded, grounding-type controller receptacle that is protected by a Ground Fault Circuit Interrupter (GFCI). Inspect operation of GFCI as per manufacturer's suggested maintenance schedule. DO NOT operate the disinfection system if it has a damaged cord or plug, if it is malfunctioning or if it has been dropped or damaged in any manner. DO NOT use this disinfection system for other than intended use (potable water applications). The use of attachments not recommended or sold by the manufacturer / distributor may cause an unsafe condition. DO NOT install this disinfection system where it will be exposed to the weather or to temperatures below freezing. DO NOT store this disinfection system where it will be exposed to the weather. DO NOT store this disinfection system where it will be exposed to temperatures below freezing unless all water has been drained from it and the water supply has been disconnected.
	

Safety Information

⚠ WARNING



During extended periods of no water flow, the water in your chamber can become very hot (Approx. 60 °C) and potentially lead to scalding. It is recommended to run your water until this hot water has been purged from your chamber. Do not allow water to contact your skin during this time. To eliminate this condition, a temperature management valve can be installed at the outlet of your UV system.

⚠ CAUTION



Failure to follow these instructions could result in minor or moderate injury.

- Carefully examine the disinfection system after installation. It should not be plugged in if there is water on parts not intended to be wet such as, the controller or lamp connector.
- Due to thermal expansion concerns and potential material degradation due to UV exposure, it is recommended to use metal fittings and at least 10" of copper pipe on the outlet of your UV chamber.

NOTICE



- The UV lamp inside the disinfection system is rated at an effective life of approximately 9000 hours. To ensure continuous protection, replace the UV lamp annually.
- The UV system is not to be used or played with by children. Persons with reduced physical, sensory or mental capabilities, or lack of experience and knowledge, are also not to handle the UV system unless they have been given supervision or instruction.
- EXTENSION CORDS:** If an extension cord is necessary, use only 3-wire extension cords that have 3-prong grounding-type plugs and 3-pole cord connectors that accept the plug from this system. Use only extension cords that are intended for outdoor use. Use only extension cords having an electrical rating not less than the rating of the system. A cord rated for less amperes or watts than this system rating may overheat. Exercise caution when arranging the cord so that it will not be tripped over or pulled. DO NOT use damaged extension cords. Examine extension cord before using and replace if damaged. DO NOT abuse extension cord. Keep extension cord away from heat and sharp edges. Always disconnect the extension cord from the receptacle before disconnecting this system from the extension cord. Never yank cord to pull plug from outlet. Always grasp the plug and pull to disconnect.
- SYSTEM PROTECTION:** To protect your Controller, a UL1449 certified (or equivalent) transient voltage surge suppressor is strongly recommended.
- The UV lamp in this system conforms to the applicable provisions of the Code of Federal Regulations (CFR) requirements including, Title 21, Chapter 1, Subchapter J, Radiological Health.
- Read and understand the Owner's Manual before operating and performing any maintenance on this equipment.

1.3 Water Chemistry

Water quality is extremely important for the optimum performance of your UV system. The following levels are recommended for installation:

Water Quality and Minerals	Level
Iron	< 0.3 ppm (0.3 mg/L)
Hardness*	< 7 gpg (120 mg/L)
Turbidity	< 1 NTU
Manganese	< 0.05 ppm (0.05 mg/L)
Tannins	< 0.1 ppm (0.1 mg/L)
UV Transmittance	> 75% (call factory for recommendations on applications where UVT < 75%)

* Where total hardness is less than 7 gpg, the UV unit should operate efficiently provided the quartz sleeve is cleaned periodically. If total hardness exceeds 7 gpg, the water should be softened. If your water chemistry contains levels in excess of those mentioned above, proper pre-treatment is recommended to correct these water problems prior to the installation of your UV disinfection system. These water quality parameters can be tested by your local dealer, or by most private analytical laboratories. *Proper pre-treatment is essential for the UV disinfection system to operate as intended.*

Especificaciones

Sección 8 Especificaciones

8.1 Estándar y validado

Modelo	VH200-F10	VH410-F20	
Caudal	Servicio de Salud Pública de EE. UU. 16 mJ/cm ²	16 GPM (60 lpm) (3,6 m ³ /hr)	
	VIQUA estándar 30 mJ/cm ²	9 GPM (34 lpm) (2,0 m ³ /hr)	
	NSF/EPA 40 mJ/cm ²	7 GPM (26 lpm) (1,6 m ³ /hr)	
Dimensiones totales (ancho x profundidad x altura)	43,2 cm x 26,57 cm x 44,5 cm (17" x 10,5" x 17,8")	43,2 cm x 25,4 cm x 73,6 cm (17" x 10" x 29")	
Tamaño del puerto de entrada/salida	1"FNPT/Combo 3/4"FNPT & 1"MNPT	3/4" FNPT	
Peso del paquete	10,5 kg (23 lbs)	13,2 kg (29 lb)	
Eléctrico	Voltaje	100-240 V/50-60 Hz	100-240 V/50-60 Hz
	Consumo de energía	35 W	60 W
	Vatios de la lámpara	27 W	45 W
Presión máxima de funcionamiento	8,62 bar (125 psi)	8,62 bar (125 psi)	
Temperatura del agua	2-40 °C (36-104 °F)	2-40 °C (36-104 °F)	
Tipo de lámpara de UV	Sterilume™-HO (alta potencia)	Sterilume™-HO (alta potencia)	
Encendido visual	Sí	Sí	
Fallo de lámpara audible	Sí	Sí	
Recordatorio de reposición de la lámpara	Sí	Sí	
Indicación visual de la vida restante de la lámpara	Sí	Sí	
Tiempo total de funcionamiento	Sí	Sí	
Monitor UV 254 nm	No	No	
Salida del solenoide (solenoide no incluido)	No	No	
Materiales de la cámara	304 SS	304 SS	
Carcasa del filtro	25,4 cm (10") alto flujo	50,8 cm (20") alto flujo	

G Risk Assessment

Risikovurderingsrapport

[Waterbox]

Prosjekttittel	Test av turbin i pilot på reversert osmosesystem.
Apparatur	Waterbox
Enhet	EPT
Apparaturansvarlig	Bård Brandåstrø
Prosjektleder	Ole Gunnar Dahlhaug
HMS-koordinator	Morten Grønli
HMS-ansvarlig (linjeleder)	Olav Bolland
Plassering	Vannkraftlaboratoriet
Romnummer	11
Risikovurdering utført av	Thea Karlsen Løken

Godkjenning:

Apparatur kort (UNIT CARD) valid for:	
Forsøk pågår kort (EXPERIMENT IN PROGRESS) valid for:	

Rolle	Navn	Dato	Signatur
Prosjektleder	Ole Gunnar Dahlhaug	29/5	<i>Ole Gunnar Dahlhaug</i>
HMS koordinator	Morten Grønli		
HMS ansvarlig (linjeleder)	Olav Bolland		

INNHOLDSFORTEGNELSE

1	INNLEDNING.....	1
2	ORGANISERING	1
3	RISIKOSTYRING AV PROSJEKTET.....	1
4	TEGNINGER, FOTO, BESKRIVELSER AV FORSØKSOPPSETT.....	1
5	EVAKUERING FRA FORSØKSOPPSETNINGEN	4
6	VARSLING	4
6.1	Før forsøkskjøring.....	4
6.2	Ved uønskede hendelser.....	4
7	VURDERING AV TEKNISK SIKKERHET	5
7.1	Fareidentifikasjon, HAZOP	5
7.2	Brannfarlig, reaksjonsfarlig og trykksatt stoff og gass	5
7.3	Trykkpåkjent utstyr	5
7.4	Påvirkning av ytre miljø (utslipp til luft/vann, støy, temperatur, rystelser, lukt)	5
7.5	Stråling	6
7.6	Bruk og behandling av kjemikalier	6
7.7	El sikkerhet (behov for å avvike fra gjeldende forskrifter og normer)	6
8	VURDERING AV OPERASJONELL SIKKERHET	6
8.1	Prosedyre HAZOP	6
8.2	Drifts og nødstopps prosedyre.....	6
8.3	Opplæring av operatører	7
8.4	Tekniske modifikasjoner	7
8.5	Personlig verneutstyr	7
8.6	Generelt.....	7
8.7	Sikkerhetsutrustning	7
8.8	Spesielle tiltak	7
9	TALLFESTING AV RESTRISIKO – RISIKOMATRISSE	7
10	KONKLUSJON.....	ERROR! BOOKMARK NOT DEFINED.
11	LOVER FORSKRIFTER OG PÅLEGG SOM GJELDER.....	8
12	DOKUMENTASJON	8
13	VEILEDNING TIL RAPPORTMAL	9

1 INNLEDNING

Det skal kjøres vann gjennom et reversert osmosesystem. Hele systemet er bygd inn i en stålkasse. Vannet trykkes til ca. 65 bar i en stempelpumpe og kjøres gjennom en membran. Ved utløpet av membranen kommer rensert vann ut, i tillegg til resterende vann med fortsatt høyt trykk. Det resterende vannet sendes enten rett ut av systemet eller gjennom en turbin som omformer trykkenergi til mekanisk energi. Effektforbruket til elektrisk motor skal måles med og uten turbinen som en del av systemet. Volumstrømmen av vann inn og ut skal også måles.

2 ORGANISERING

Rolle	NTNU
Prosjektleder	Ole Gunnar Dahlhaug
Apparaturansvarlig	Bård Brandåstrø
Romansvarlig	Bård Brandåstrø
HMS koordinator	Morten Grønli
HMS ansvarlig (linjeleder):	Olav Bolland

3 RISIKOSTYRING AV PROSJEKTET

Hovedaktiviteter risikostyring	Nødvendige tiltak, dokumentasjon	DTG
Prosjekt initiering	Prosjekt initiering mal	
Veiledningsmøte	Skjema for Veiledningsmøte med pre-risikovurdering	
Innledende risikovurdering	Fareidentifikasjon – HAZID Skjema grovanalyse	
Vurdering av teknisk sikkerhet	Prosess-HAZOP Tekniske dokumentasjoner	
Vurdering av operasjonell sikkerhet	Prosedyre-HAZOP Opplæringsplan for operatører	
Sluttvurdering, kvalitetssikring	Uavhengig kontroll Utstedelse av apparaturkort Utstedelse av forsøk pågår kort	

4 BESKRIVELSER AV FORSØKSOPPSETT

Det skal kjøres vann gjennom et reversert osmosesystem. Vannet trykkes til ca. 65 bar i en stempelpumpe og kjøres gjennom en membran. Ved utløpet av membranen kommer rensert vann ut, i tillegg til resterende vann med fortsatt høyt trykk. Det resterende vannet sendes enten rett ut av systemet eller gjennom en turbin som omformer trykkenergi til mekanisk energi.

Effektforbruket til elektrisk motor skal måles med og uten turbinen som en del av systemet. Volumstrømmen av vann inn og ut skal også måles.

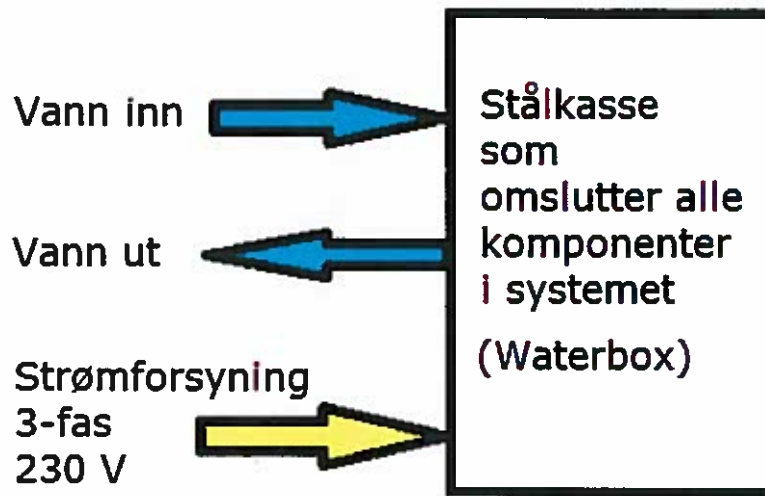


Figure 1. Skisse av enheten.

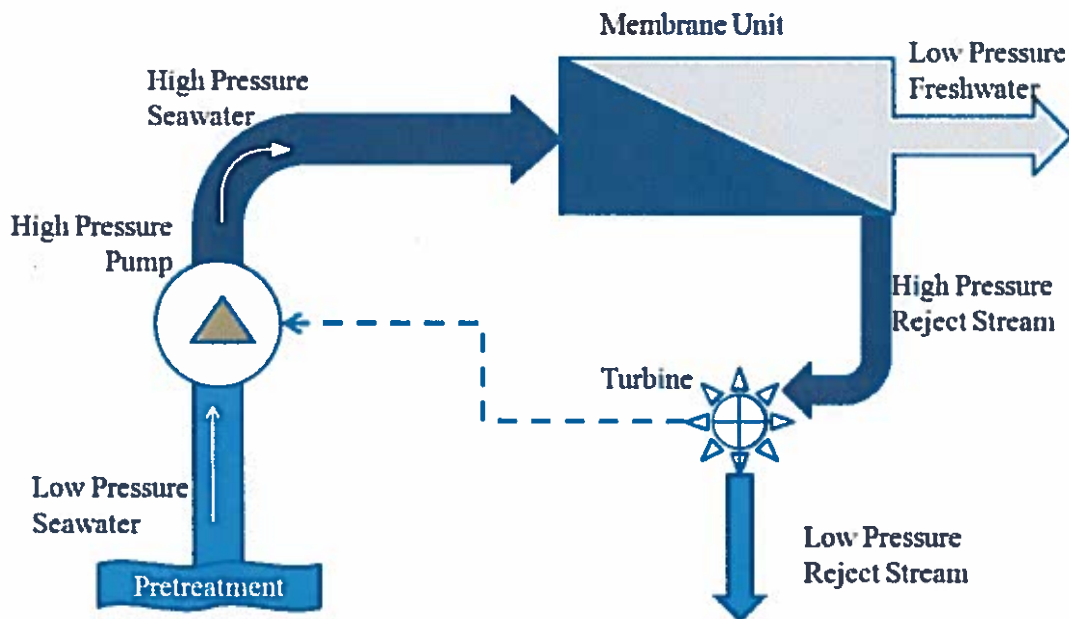


Figure 2. Skisse av hovedkomponentene inni enheten.



Figure 3. Kassen står ved nordveggen i lab. Dimensjoner er ca. 1 meter ganger 1,40 meter. Pappesker skal ryddes før igangkjøring.

5 EVAKUERING FRA FORSØKSOPPSETNINGEN

Evakuering skjer på signal fra alarmklokker eller lokale gassalarmstasjon med egen lokal varsling med lyd og lys utenfor aktuelle rom, se 6.2

Evakuering fra rigg området foregår igjennom merkede nødutganger til møteplass, (hjørnet gamle kjemi/kjelhuset eller parkeringsplass 1a-b.)

Aksjon på rigg ved evakuering:

Beskriv i hvilken tilstand riggen skal forlates ved en evakueringssituasjon (nøddavstegning, vann, gass, spenning).

6 VARSLING

6.1 Før forsøkskjøring

Varsling per e-post, til iept-experiments@ivt.ntnu.no

I e-posten skal det stå:

- Navn på forsøksleder:
- Navn på forsøksrigg:
- Tid for start: (dato og klokkeslett)
- Tid for stop: (dato og klokkeslett)

All forsøkskjøringen skal planlegges og legges inn i aktivitetskalender for lab. Forsøksleder må få bekreftelse på at forsøkene er klarert med øvrig labdrift før forsøk kan iverksettes.

6.2 Ved uønskede hendelser

BRANN

Ved brann en ikke selv er i stand til å slukke med rimelige lokalt tilgjengelige slukkemidler, skal nærmeste brannalarm utløses og arealet evakueres raskest mulig. En skal så være tilgjengelig for brannvesen/bygningsvaktmester for å påvise brannsted.

Om mulig varsles så:

NTNU	SINTEF
Morten Grønli, Mob: 918 97 515	Harald Mæhlum, Mob: 930 14 986
Olav Bolland: Mob: 918 97 209	Anne Karin T. Hemmingsen Mob: 930 19 669
NTNU – SINTEF Beredskapstelefon	800 80 388

GASSALARM

Ved gassalarm skal gassflasker stenges umiddelbart og området ventileres. Klarer man ikke innen rimelig tid å få ned nivået på gasskonsentrasjonen så utløses brannalarm og laben evakueres. Dedikert personell og eller brannvesen sjekker så lekkasjested for å fastslå om det er mulig å tette lekkasje og luften ut området på en forsvarlig måte.

Varslingsrekkefølge som i overstående punkt.

PERSONSKADE

- Førstehjelpsutstyr i Brann/førstehjelpsstasjoner,
- Rop på hjelp,
- Start livreddende førstehjelp
- **Ring 113** hvis det er eller det er tvil om det er alvorlig skade.

ANDRE UØNSKEDE HENDELSER (AVVIK)

NTNU:

Rapportering av uønskede hendelser, Innsida, avviksmeldinger
<https://innsida.ntnu.no/wiki/-/wiki/Norsk/Melde+avvik>

SINTEF:

Synergi

7 VURDERING AV TEKNISK SIKKERHET

7.1 HAZOP

Se kapittel 13 "Veiledning til rapport mal.

Forsøksoppsetningen deles inn i følgende noder:

Node 1	Waterbox
--------	----------

Vedlegg, skjema: Hazop_mal

Konklusjon: (Sikkerhet ivaretatt)

Node 1:

Forsøksprosedyren i vedlegg E følges.

7.2 Brannfarlig, reaksjonsfarlig og trykksatt stoff og gass

Se kapittel 13 "Veiledning til rapport mal.

Inneholder forsøkene brannfarlig, reaksjonsfarlig og trykksatt stoff

NEI	
-----	--

7.3 Trykkpåkjent utstyr

Inneholder forsøksoppsetningen trykkpåkjent utstyr?

JA	Komplett enhet levert av TESS. Se vedlegg H for dokumentasjon.
----	--

7.4 Påvirkning av ytre miljø (utslipp til luft/vann, støy, temperatur, rystelser, lukt)

Vil eksperimentene generere utslipp av røyk, gass, lukt eller unormalt avfall?
 Mengder/konsistens. Er det behov for utslippstillatelse, ekstraordinære tiltak?

Se kapittel 13 "Veiledning til rapport mal..

NEI	
-----	--

7.5 Stråling

Se kapittel 13 "Veiledning til rapport mal.

NEI	
-----	--

7.6 Kjemikalier

Inneholder eksperimentene bruk og behandling av kjemikalier Hvilke og hvilke mengder? Hvordan skal dette avhendes, oppbevares? Risikovurder i henhold til sikkerhetsdatablad Er det behov for beskyttelses tiltak tillegges disse i operasjonell prosedyre.

Se kapittel 13 "Veiledning til rapport mal.

NEI	
-----	--

7.7 El sikkerhet (behov for å avvike fra gjeldende forskrifter og normer)

Her forstås montasje og bruk i forhold til normer og forskrifter med tanke på berøringsfare

NEI	
-----	--

8 VURDERING AV OPERASJONELL SIKKERHET

Sikrer at etablerte prosedyrer dekker alle identifiserte risikoforhold som må håndteres gjennom operasjonelle barrierer og at peratører og teknisk utførende har tilstrekkelig kompetanse.

8.1 Prosedyre HAZOP

Se kapittel 13 "Veiledning til rapport mal.

Metoden er en undersøkelse av operasjonsprosedyrer, og identifiserer årsaker og farekilder for operasjonelle problemer.

Vedlegg: HAZOP_MAL_Proseidyre

8.2 Forsøksprosedyre og nødstopps prosedyre

Se kapittel 13 "Veiledning til rapport mal.

Driftsprosedyren er en sjekklister som skal fylles ut for hvert forsøk.

Nødstopps prosedyren skal sette forsøksoppsetningen i en harmløs tilstand ved uforutsette hendelser.

Vedlegg: Forsøksprosedyre

Nødstopps prosedyre: Se vedlegg E, Forsøksprosedyre.

8.3 Opplæring av operatører

8.4 Tekniske modifikasjoner

8.5 Personlig verneutstyr

- Det er påbudt med vernebriller i sonen anlegget er plassert i.

8.6 Generell sikkerhet

- Vann og trykklufttilførsel i slanger skal stenges/kobles fra ved nærmeste fastpunkt når riggen ikke er i bruk.
- Operatør skal være tilstede under forsøk.

8.7 Sikkerhetsutrustning

- Fare skilting, se Forskrift om Sikkerhetsskilting og signalgivning på arbeidsplassen

8.8 Spesielle tiltak

9 TALLFESTING AV RESTRISIKO – RISIKOMATRISJE

Se kapittel 13 "Veiledning til rapport mal.

Risikomatrisen vil gi en visualisering og en samlet oversikt over aktivitetens risikoforhold slik at ledelse og brukere får et mest mulig komplett bilde av risikoforhold.

IDnr	Aktivitet-hendelse	Frekv-Sans	Kons	RV
1	Roterende aksling, berøringsfare	1	D	D1
2	Lekkasje av vann under trykk	3	B	B3
3	Overoppheting av pumpe	2	C	C2
4	Luft i systemet	2	C	C2

Vurdering restrisiko: Risikoen anses å være liten. Operasjon i henhold til Forsøksprosedyre i vedlegg E reduserer risiko til et akseptabelt nivå.

10 LOVER FORSKRIFTER OG PÅLEGG SOM GJELDER

Se <http://www.arbeidstilsynet.no/regelverk/index.html>

- Lov om tilsyn med elektriske anlegg og elektrisk utstyr (1929)
- Arbeidsmiljøloven
- Forskrift om systematisk helse-, miljø- og sikkerhetsarbeid (HMS Internkontrollforskrift)
- Forskrift om sikkerhet ved arbeid og drift av elektriske anlegg (FSE 2006)
- Forskrift om elektriske forsyningsanlegg (FEF 2006)
- Forskrift om utstyr og sikkerhetssystem til bruk i eksplosjonsfarlig område NEK 420
- Forskrift om håndtering av brannfarlig, reaksjonsfarlig og trykksatt stoff samt utstyr og anlegg som benyttes ved håndteringen
- Forskrift om Håndtering av eksplosjonsfarlig stoff
- Forskrift om bruk av arbeidsutstyr.
- Forskrift om Arbeidsplasser og arbeidslokaler
- Forskrift om Bruk av personlig verneutstyr på arbeidsplassen
- Forskrift om Helse og sikkerhet i eksplosjonsfarlige atmosfærer
- Forskrift om Høytrykksspyling
- Forskrift om Maskiner
- Forskrift om Sikkerhetsskiltning og signalgivning på arbeidsplassen
- Forskrift om Stillaser, stiger og arbeid på tak m.m.
- Forskrift om Sveising, termisk skjæring, termisk sprøyting, kullbuemeisling, lodding og sliping (varmt arbeid)
- Forskrift om Tekniske innretninger
- Forskrift om Tungt og ensformig arbeid
- Forskrift om Vern mot eksponering for kjemikalier på arbeidsplassen (Kjemikalieforskriften)
- Forskrift om Vern mot kunstig optisk stråling på arbeidsplassen
- Forskrift om Vern mot mekaniske vibrasjoner
- Forskrift om Vern mot støy på arbeidsplassen

Veiledninger fra arbeidstilsynet

se: <http://www.arbeidstilsynet.no/regelverk/veiledninger.html>

11 DOKUMENTASJON

- Tegninger, foto, beskrivelser av forsøksoppsetningen
- Hazop_mal
- Sertifikat for trykkpåkjent utstyr
- Håndtering avfall i NTNU
- Sikker bruk av LASERE, retningslinje
- HAZOP_MAL_Prosedyre
- Forsøksprosedyre
- Opplæringsplan for operatører
- Skjema for sikker jobb analyse, (SJA)
- Apparatorkortet
- Forsøk pågår kort

12 VEILEDNING TIL RAPPORTMAL

Kapittel 7 Vurdering av teknisk sikkerhet

Sikre at design av apparatur er optimalisert i forhold til teknisk sikkerhet.

Identifisere risikoforhold knyttet til valgt design, og eventuelt å initiere re-design for å sikre at størst mulig andel av risiko elimineres gjennom teknisk sikkerhet.

Punktene skal beskrive hva forsøksoppsetningen faktisk er i stand til å tåle og aksept for utslipp.

7.1 Fareidentifikasjon, HAZOP

Forsøksoppsetningen deles inn i noder: (eks Motorenhet, pumpeenhet, kjøleenhet.)

Ved hjelp av ledeord identifiseres årsak, konsekvens og sikkerhetstiltak. Konkluderes det med at tiltak er nødvendig anbefales disse på bakgrunn av dette. Tiltakene lukkes når de er utført og Hazop slutføres.

(eks "No flow", årsak: rør er deformert, konsekvens: pumpe går varm, sikkerhetsforanstaltning: måling av flow med kobling opp mot nødstopp eller hvis konsekvensen ikke er kritisk benyttes manuell overvåkning og punktet legges inn i den operasjonelle prosedyren.)

7.2 Brannfarlig, reaksjonsfarlig og trykksatt stoff.

I henhold til Forskrift om håndtering av brannfarlig, reaksjonsfarlig og trykksatt stoff samt utstyr og anlegg som benyttes ved håndteringen

Brannfarlig stoff: Fast, flytende eller gassformig stoff, stoffblanding, samt stoff som forekommer i kombinasjoner av slike tilstander, som i kraft av sitt flammepunkt, kontakt med andre stoffer, trykk, temperatur eller andre kjemiske egenskaper representerer en fare for brann.

Reaksjonsfarlig stoff: Fast, flytende, eller gassformig stoff, stoffblanding, samt stoff som forekommer i kombinasjoner av slike tilstander, som ved kontakt med vann, ved sitt trykk, temperatur eller andre kjemiske forhold, representerer en fare for farlig reaksjon, eksplosjon eller utslipp av farlig gass, damp, støv eller tåke.

Trykksatt stoff: Annet fast, flytende eller gassformig stoff eller stoffblanding enn brann- eller reaksjonsfarlig stoff, som er under trykk, og som derved kan representere en fare ved ukontrollert utslipp.

Nærmere kriterier for klassifisering av brannfarlig, reaksjonsfarlig og trykksatt stoff er fastsatt i vedlegg 1 i veiledningen til forskriften "Brannfarlig, reaksjonsfarlig og trykksatt stoff"

<http://www.dsb.no/Global/Publikasjoner/2009/Veiledning/Generell%20veiledning.pdf>

http://www.dsb.no/Global/Publikasjoner/2010/Tema/Temaveiledning_bruk_av_farlig_stoff_Del_1.pdf

Rigg og areal skal gjennomgå med hensyn på vurdering av Ex sone

- Sone 0: Alltid eksplosiv atmosfære, for eksempel inne i tanker med gass, brennbar væske.
- Sone 1: Primær sone, tidvis eksplosiv atmosfære for eksempel et fylle tappe punkt

- Sone 2: Sekundært utslippssted, kan få eksplosiv atmosfære ved uhell, for eksempel ved flenser, ventiler og koblingspunkt

7.4 Påvirkning av ytre miljø

Med forurensning forstås: tilførsel av fast stoff, væske eller gass til luft, vann eller i grunnen støy og rystelser påvirkning av temperaturen som er eller kan være til skade eller ulempe for miljøet.

Regelverk: <http://www.lovddata.no/all/hl-19810313-006.html#6>

NTNU retningslinjer for avfall se: <http://www.ntnu.no/hms/retningslinjer/HMSR18B.pdf>

7.5 Stråling

Stråling defineres som

Ioniserende stråling: Elektromagnetisk stråling (i strålevernssammenheng med bølgelengde <100 nm) eller hurtige atomære partikler (f.eks alfa- og beta-partikler) som har evne til å ionisere atomer eller molekyler
Ikke-ioniserende stråling: Elektromagnetisk stråling (bølgelengde >100 nm), og ultralyd ₁ , som har liten eller ingen evne til å ionisere.
Strålekilder: Alle ioniserende og sterke ikke-ioniserende strålekilder.
Ioniserende strålekilder: Kilder som avgir ioniserende stråling, f.eks alle typer radioaktive kilder, røntgenapparater, elektronmikroskop
Sterke ikke-ioniserende strålekilder: Kilder som avgir sterk ikke-ioniserende stråling som kan skade helse og/eller ytre miljø, f.eks laser klasse 3B og 4, MR ₂ -systemer, UVC ₃ -kilder, kraftige IR-kilder ₄
<small>¹ Ultralyd er akustisk stråling ("lyd") over det hørbare frekvensområdet (>20 kHz). I strålevernforskriften er ultralyd omtalt sammen med elektromagnetisk ikke-ioniserende stråling. ² MR (eg. NMR) - kjernemagnetisk resonans, metode som nyttes til å «avbilde» indre strukturer i ulike materialer. ³ UVC er elektromagnetisk stråling i bølgelengdeområdet 100-280 nm. ⁴ IR er elektromagnetisk stråling i bølgelengdeområdet 700 nm – 1 mm.</small>

For hver laser skal det finnes en informasjonsperm(HMSRV3404B) som skal inneholde:

- Generell informasjon
- Navn på instrumentansvarlig og stedfortreder, og lokal strålevernskoordinator
- Sentrale data om apparaturen
- Instrumentspesifikk dokumentasjon
- Referanser til (evt kopier av) datablader, strålevernbestemmelser, o.l.
- Vurderinger av risikomomenter
- Instruks for brukere
- Instruks for praktisk bruk; oppstart, drift, avstenging, sikkerhetsforholdsregler, loggføring, avlåsing, evt. bruk av strålingsmåler, osv.
- Nødprosedyrer

Se ellers retningslinjen til NTNU for laser: <http://www.ntnu.no/hms/retningslinjer/HMSR34B.pdf>

7.6 Bruk og behandling av kjemikalier.

Her forstås kjemikalier som grunnstoff som kan utgjøre en fare for arbeidstakers sikkerhet og helse.

Se ellers: <http://www.lovddata.no/cgi-wift/ldles?doc=/sf/sf/sf-20010430-0443.html>

Sikkerhetsdatablar skal være i forøkenes HMS perm og kjemikaliene registrert i Stoffkartoteket.

Kapittel 8 Vurdering av operasjonell sikkerhet

Sikrer at etablerte prosedyrer dekker alle identifiserte risikoforhold som må håndteres gjennom operasjonelle barrierer og at operatører og teknisk utførende har tilstrekkelig kompetanse.

8.1 Prosedyre Hazop

Prosedyre-HAZOP gjennomføres som en systematisk gjennomgang av den aktuelle prosedyren ved hjelp av fastlagt HAZOP-metodikk og definerte ledeord. Prosedyren brytes ned i enkeltstående arbeidsoperasjoner (noder) og analyseres ved hjelp av ledeordene for å avdekke mulige avvik, uklarheter eller kilder til mangelfull gjennomføring og feil.

8.2 Drifts og nødstopps prosedyrer

Utarbeides for alle forsøksoppsetninger.

Driftsprosedyren skal stegvis beskrive gjennomføringen av et forsøk, inndelt i oppstart, under drift og avslutning. Prosedyren skal beskrive forutsetninger og tilstand for start, driftsparametere med hvor store avvik som tillates før forsøket avbrytes og hvilken tilstand riggen skal forlates.

Nødstoppsprosedyre beskriver hvordan en nødstopps skal skje, (utført av uinnvidde), hva som skjer, (strøm/gass tilførsel) og

hvilke hendelser som skal aktivere nødstopps, (brannalarm, lekkasje).

Kapittel 9 Risikomatrix Tallfesting av restrisiko

For å synliggjøre samlet risiko, jevnfør skjema for risikovurdering, plottes hver enkelt aktivitets verdi for sannsynlighet og konsekvens inn i risikomatriksen. Bruk aktivitetens IDnr. Eksempel: Hvis aktivitet med IDnr. 1 har fått en risikoverdi D3 (sannsynlighet 3 x konsekvens D) settes aktivitetens IDnr i risikomatriksens felt for 3D. Slik settes alle aktivitetenes risikoverdier (IDnr) inn i risikomatriksen.

I risikomatriksen er ulike grader av risiko merket med rød, gul eller grønn. Når en aktivitets risiko havner på rød (= uakseptabel risiko), skal risikoreduserende tiltak gjennomføres. Ny vurdering gjennomføres etter at tiltak er iverksatt for å se om risikoverdien er kommet ned på akseptabelt nivå.

KONSEKVENNS	Svært alvorlig	E1	E2	E3	E4	E5
	Alvorlig	D1	D2	D3	D4	D5
	Moderat	C1	C2	C3	C4	C5
	Liten	B1	B2	B3	B4	B5
	Svært liten	A1	A2	A3	A4	A5
		Svært liten	Liten	Middels	Stor	Svært Stor
		SANSYNLIGHET				

Prinsipp over akseptkriterium. Forklaring av fargene som er brukt i risikomatriksen.

Farge	Beskrivelse
Rød	Uakseptabel risiko. Tiltak skal gjennomføres for å redusere risikoen.
Gul	Vurderingsområde. Tiltak skal vurderes.
Grønn	Akseptabel risiko. Tiltak kan vurderes ut fra andre hensyn.

Vedlegg til Risikovurderingsrapport

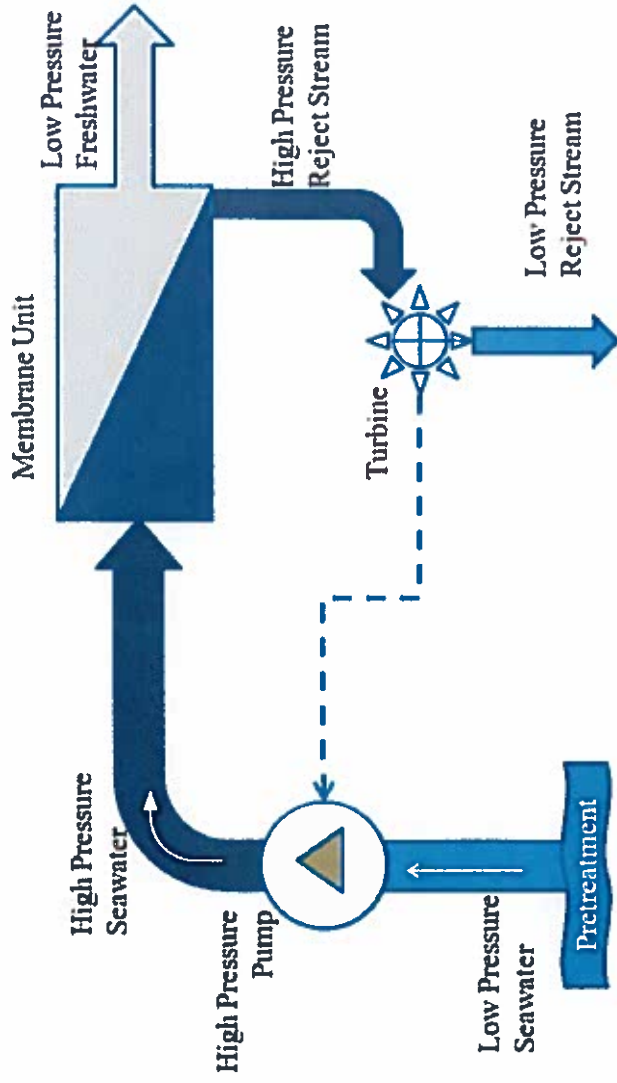
[Waterbox]

Prosjekttittel	Test av turbin i pilot på reversert osmosesystem.
Apparatur	Waterbox
Enhet	EPT
Apparaturansvarlig	Bård Brandåstrø
Prosjektleder	Ole Gunnar Dahlhaug
HMS-koordinator	Morten Grønli
HMS-ansvarlig (linjeleder)	Olav Bolland
Plassering	Vannkraftlaboratoriet
Romnummer	11
Risikovurdering utført av	Thea Karlsen Løken

INNHALDSFORTEGNELSE

VEDLEGG A: PROSESS OG INSTRUMENTERINGSDIAGRAM.....	1
VEDLEGG B: HAZOP (MAL)	2
VEDLEGG C: PRØVESERTIFIKAT FOR LOKAL TRYKKTESTING	3
VEDLEGG D: HAZOP PROSEDYRE (MAL).....	4
VEDLEGG E: FORSØKSPROSEDYRE	5
VEDLEGG F: OPPLÆRINGSPLAN FOR OPERATØRER.....	7
VEDLEGG G: SKJEMA FOR SIKKER JOBB ANALYSE.....	8
APPARATURKORT / UNITCARD	10
FORSØK PÅGÅR /EXPERIMENT IN PROGRESS.....	11

VEDLEGG A: PROSESS OG INSTRUMENTERINGSDIAGRAM



VEDLEGG B: HAZOP (MAL)

Project: Node: 1 Waterbox						Page	
Ref#	Guideword	Causes	Consequences	Safeguards	Recommendations	Action	Date/Sign
1	No flow	Main water valve not open	Overheating of pump	Make sure valve is open	Put valve check as part of startup procedure.		
2	Air in system	Air in system	Air remaining in the elements and/or in the pressure vessels may lead to excessive forces on the element in flow direction or in radial direction and causing fiberglass shell cracking, if the feed pressure is ramped up too quickly.	Flush system with water before start-up.	Make flushing a part of start-up procedure		
3	Rotating shaft	Rotating shaft, danger if touched	Personal injury	The whole shaft is enclosed in a steel-box, it is not possible to touch it without opening the box.	Keep steel box closed.		
4	Water leakage	Water under high pressure	Personal injury	The unit is enclosed in a steel-box.	Keep steel-box closed.		

VEDLEGG C: PRØVESERTIFIKAT FOR LOKAL TRYKKTESTING

Trykk testen skal utføres i følge NS-EN 13445 del 5 (Inspeksjon og prøving).
Se også prosedyre for trykktesting gjeldende for VATL lab

Trykkpåkjent utstyr:	
Benyttes i rigg:	
Design trykk for utstyr (bara):	
Maksimum tillatt trykk (bara): (i.e. burst pressure om kjent)	
Maksimum driftstrykk i denne rigg:	

Prøvetrykket skal fastlegges i følge standarden og med hensyn til maksimum tillatt trykk.

Prøvetrykk (bara):	
X maksimum driftstrykk: I følge standard	
Test medium:	
Temperatur (°C)	
Start tid:	Trykk (bara):
Slutt tid:	Trykk (bara):
Maksimum driftstrykk i denne rigg:	

Eventuelle repetisjoner fra atm. trykk til maksimum prøvetrykk:.....

Test trykket, dato for testing og maksimum tillatt driftstrykk skal markers på
(skilt eller innslått)

Sted og dato

Signatur

VEDLEGG D: HAZOP PROSEDYRE (MAL)

Project: Node: 1							Page
Ref#	Guideword	Causes	Consequences	Safeguards	Recommendations	Action	Date/Sign
	Uklar	Prosedyre er laget for ambisiøs eller preget av forvirring					
	Trinn på feil plass	Prosedyren vil lede til at handlinger blir gjennomført i feil mønster/rekkefølge					
	Feil handling	Prosedyrens handling er feil spesifisert					
	Uriktig informasjon	Informasjon som er gitt i forkant av handling er feil spesifisert					
	Trinn utelatt	Manglende trinn, eller trinn krever for mye av operatør					
	Trinn mislykket	Trinn har stor sannsynlighet for å mislykkes					
	Påvirkning og effekter fra andre	Prosedyrens prestasjoner vil trolig bli påvirket av andre kilder					


VEDLEGG E: FORSØKSPROSEDYRE

Prosjekt Test av turbin i pilot på reversert osmosesystem.		
Apparatur Waterbox		
Prosjektleder Ole Gunnar Dahlhaug	Dato 23.02.2016	Signatur <i>Ole Gunnar Dahlhaug</i>

Conditions for the experiment:	Completed
Experiments should be run in normal working hours, 08:00-16:00 during winter time and 08.00-15.00 during summer time. Experiments outside normal working hours shall be approved.	
One person must always be present while running experiments, and should be approved as an experimental leader.	
An early warning is given according to the lab rules, and accepted by authorized personnel.	
Be sure that everyone taking part of the experiment is wearing the necessary protecting equipment and is aware of the shut down procedure and escape routes.	
Preparations	Carried out
Post the "Experiment in progress" sign.	
<i>Thoroughly rinse the pretreatment section to flush out debris and other contaminants without letting the feed enter the elements.</i>	
<i>Check all valves to ensure that settings are correct. The feed pressure control and concentrate control valves should be fully open.</i>	
<i>Use low pressure water at a low flow rate to flush the air out of the elements and pressure vessels. Flush at a gauge pressure of 30 to 60 psi (0.2 - 0.4 MPa). All permeate and concentrate flows should be directed to an appropriate waste collection drain during flushing.</i>	
<i>During the flushing operation, check all pipe connections and valves for leaks. Tighten connections where necessary.</i>	
<i>After the system has been flushed for a minimum of 30 minutes, close the feed pressure control valve.</i>	
<i>Ensure that the concentrate control valve is open.</i>	
<i>Slowly crack open the feed pressure control valve (feed pressure should be less than 60 psi/0.4 MPa).</i>	
<i>Start the high pressure pump. Do not stand at either end of the pressure vessels while pressurization takes place.</i>	
<i>Slowly open the feed pressure control valve, increasing the feed pressure and feed flow rate to the membrane elements until the design concentrate flow is reached. The feed pressure increase to the elements should be less than 10 psi (0.07 MPa) per second to achieve a soft start. Continue to send all permeate and concentrate flows to an appropriate waste collection drain.</i>	
<i>Slowly close the concentrate control valve until the ratio of permeate flow to concentrate flow approaches, but does not exceed, the design ratio (recovery). Continue to check the system pressure to ensure that it does not</i>	

	<i>exceed the upper design limit.</i>	
	<i>Repeat the two previous steps until the design permeate and concentrate flows are obtained.</i>	
	During the experiment	
	<i>Control of motor power consumption</i>	
	<i>Control of permeate flow rate</i>	
	<i>Control of concentrate flow rate</i>	
	<i>Look for leakages</i>	
	End of experiment	
	<i>Slowly decrease the opening of the feed pressure control valve, decreasing the feed pressure and feed flow rate to the membrane elements, until feed pressure is less than 0.4 MPa.</i>	
	<i>Stop the high pressure pump</i>	
	<i>Fully close the feed pressure control valve.</i>	
	<i>Remove all obstructions/barriers/signs around the experiment.</i>	
	<i>Tidy up and return all tools and equipment.</i>	
	<i>Tidy and cleanup work areas.</i>	
	<i>Return equipment and systems back to their normal operation settings (fire alarm)</i>	
	To reflect on before the next experiment and experience useful for others	
	<i>Was the experiment completed as planned and on scheduled in professional terms?</i>	
	<i>Was the competence which was needed for security and completion of the experiment available to you?</i>	
	<i>Do you have any information/ knowledge from the experiment that you should document and share with fellow colleagues?</i>	
	NØDSTOPP-PROSEDYRE	
	<i>Unplug the electric motor from the power-supply.</i>	
	<i>Exit the building.</i>	

Operatører:

Navn	Dato	Signatur
Thea Karlsen Løken	23.02.2016	

VEDLEGG F: OPPLÆRINGSPLAN FOR OPERATØRER

Prosjekt Test av turbin i pilot på reversert osmosesystem.		
Apparatur Waterbox		
Prosjektleder Ole Gunnar Dahlhaug	Dato 23.02.2016	Signatur <i>Ole Gunnar Dahlhaug</i>

Kjennskap til EPT LAB generelt	
Lab	
<ul style="list-style-type: none"> • adgang • rutiner/regler • arbeidstid 	
Kjenner til evakueringsprosedyrer	
Aktivitetskalender	
Innmelding av forsøk til: iept-experiments@ivt.ntnu.no	
Kjennskap til forsøkene	
Prosedyrer for forsøkene	
Nødstop	
Nærmeste brann/førstehjelpsstasjon	

Jeg erklærer herved at jeg har gjennomgått og forstått HMS-regelverket, har fått hensiktsmessig opplæring for å kjøre dette eksperimentet og er klar over mitt personlige ansvar ved å arbeide i EPT laboratorier.

Operatører

Navn	Dato	Signatur
Thea Karlsen Løken	29/2-2016	<i>Thea</i>

VEDLEGG G: SKJEMA FOR SIKKER JOBB ANALYSE

SJA tittel:	
Dato:	Sted:
Kryss av for utfylt sjekkliste:	

Deltakere:		
SJA-ansvarlig:		

Arbeidsbeskrivelse: (Hva og hvordan?)
Risiko forbundet med arbeidet:
Beskyttelse/sikring: (tiltaksplan, se neste side)
Konklusjon/kommentar:

Anbefaling/godkjenning:	Dato/Signatur:	Anbefaling/godkjenning:	Dato/Signatur:
SJA-ansvarlig:		HMS koordinator	
Ansvarlig for utføring:		Annen (stilling):	

HMS aspekt	Ja	Nei	NA	Kommentar / tiltak	Ansv.
Dokumentasjon, erfaring, kompetanse					
Kjent arbeidsoperasjon?	X				
Kjennskap til erfaringer/uønskede hendelser fra tilsvarende operasjoner?		X			
Nødvendig personell?	X				
Kommunikasjon og koordinering					
Mulig konflikt med andre operasjoner?		X			
Håndtering av en evt. hendelse (alarm, evakuering)?		X			
Behov for ekstra vakt?		X			
Arbeidsstedet					
Uvante arbeidsstillinger?		X			
Arbeid i tanker, kummer el.lignende?		X			
Arbeid i grøfter eller sjakter?		X			
Rent og ryddig?	X				
Verneutstyr ut over det personlige?		X			
Vær, vind, sikt, belysning, ventilasjon?		X			
Bruk av stillaser/lift/seler/stropper?		X			
Arbeid i høyden?		X			
Ioniserende stråling?		X			
Rømningsveier OK?	X				
Kjemiske farer					
Bruk av helseskadelige/giftige/etsende kjemikalier?		X			
Bruk av brannfarlige eller eksplosjonsfarlige kjemikalier?		X			
Er broken risikovurdert?	X				
Biologisk materiale?		X			
Støv/asbest/isolasjonsmateriale?		X			
Mekaniske farer					
Stabilitet/styrke/spenning?		X			
Klem/kutt/slag?		X			
Støy/trykk/temperatur?		X			
Behandling av avfall?		X			
Behov for spesialverktøy?		X			
Elektriske farer					
Strøm/spenning/over 1000V?		X			
Støt/krypstrøm?		X			
Tap av strømtilførsel?		X			
Området					
Behov for befarings?	X				
Merking/skilting/avsperring?	X				
Miljømessige konsekvenser?		X			
Sentrale fysiske sikkerhetssystemer					
Arbeid på sikkerhetssystemer?		X			
Frakobling av sikkerhetssystemer?		X			
Annet					

APPARATURKORT / UNITCARD

Dette kortet SKAL henges godt synlig på apparaturen!
This card MUST be posted on a visible place on the unit!

Apparatur (Unit) Waterbox	
Prosjektleder (Project Leader) Ole Gunnar Dahlhaug	Telefon mobil/privat (Phone no. mobile/private) +47 918 97 609
Apparaturansvarlig (Unit Responsible) Bård Brandåstrø	Telefon mobil/privat (Phone no. mobile/private) +47 918 97 257
Sikkerhetsrisikoer (Safety hazards) Pressurized components	
Sikkerhetsregler (Safety rules) Operate unit according to procedures. Manually inspect the unit for leakages while in operation.	
Nødstopprosedyre (Emergency shutdown) Turn off the high pressure pump	

Her finner du (Here you will find):

Prosedyrer (Procedures)	Tapet fast til stålkassen som inneholder systemet
Bruksanvisning (Users manual)	Tapet fast til stålkassen som inneholder systemet

Nærmeste (Nearest)

Brannslukningsapparat (fire extinguisher)	Vestveggen i Lab
Førstehjelpsskap (first aid cabinet)	Vestveggen i Lab

NTNU
Institutt for energi og prosessteknikk

SINTEF Energi
Avdeling energiprosesser

Dato

Dato

Signert

Signert

FORSØK PÅGÅR / EXPERIMENT IN PROGRESS

Dette kortet SKAL henges opp før forsøk kan starte!
This card MUST be posted on the unit before the experiment startup!

Apparatur (Unit) Waterbox	
Prosjektleder (Project Leader) Ole Gunnar Dahlhaug	Telefon mobil/privat (Phone no. mobile/private) +47 918 97 609
Apparaturansvarlig (Unit Responsible) Bård Brandåstrø	Telefon mobil/privat (Phone no. mobile/private) +47 918 97 257
Godkjente operatører (Approved Operators) Thea Karlsen Løken	Telefon mobil/privat (Phone no. mobile/private) +47 40 32 71 30
Prosjekt (Project) Test av turbin i pilot på reversert osmosesystem.	
Forsøksstid / Experimental time (start - stop) 24.02.2016 – 11.03.2016	
Kort beskrivelse av forsøket og relaterte farer (Short description of the experiment and related hazards) Måling av effekt og volumstrøm. Vann under høyt trykk.	

NTNU
Institutt for energi og prosessteknikk

SINTEF Energi
Avdeling energiprosesser

Dato

Dato

Signert

Signert

